

SELF-AWARE SELF-ASSEMBLY for SPACE ARCHITECTURE:
Growth Paradigms for In-Space Manufacturing

by

Ariel Ekblaw

B.S., Yale University (2014)

M.S., Massachusetts Institute of Technology (2017)

Submitted to the Program in Media Arts and Sciences, School of Architecture and Planning, in partial fulfillment of the requirements for the degree of

Doctor of Philosophy

at the

MASSACHUSETTS INSTITUTE OF TECHNOLOGY

September 2020

© Massachusetts Institute of Technology, 2020. All rights reserved

Author

.....

Ariel Ekblaw
Program in Media Arts and Sciences
August 17, 2020

Certified by

.....

Joseph Paradiso
Alexander W. Dreyfoos (1954) Professor of Media Arts and Sciences
Thesis Supervisor

Accepted by

.....

Tod Machover
Academic Head, Program in Media Arts and Sciences

SELF-AWARE SELF-ASSEMBLY for SPACE ARCHITECTURE:
Growth Paradigms for In-Space Manufacturing

by

Ariel Ekblaw

Submitted to the Program in Media Arts and Sciences, School of Architecture and Planning, on August 17th, 2020 in partial fulfillment of the requirements for the degree of Doctor of Philosophy

Abstract

Humanity stands on the cusp of interplanetary civilization. As we prepare to venture into deep space, we face what appears to be an irreconcilable conundrum: at once a majestic domain for human exploration, while also a domain of unrelenting challenges, posing dangers that are fundamentally at odds with our evolved biology. The field of space architecture struggles with not only these environmental challenges, but also constrained physical dimensions (e.g., rocket payload fairings), risky astronaut space-walks and limited robotic mobility for assembly, and capricious budgets as political whims change. How might we incorporate the robustness principles and incremental additions of indeterminate-growth living systems into the habitats that will sustain us over time? We begin by exploring how to enable dynamic, self-assembling space structures that are informed by both inorganic and organic growth processes from complex Earth systems.

How can we design, induce, and scale *self-aware self-assembly* to grow space architecture, natively, in orbit?

We answer this call, for space architecture that builds itself, through transformative *self-aware self-assembly*—adaptive, responsive “living structures” that follow principles of tessellation and self-similarity to scale elegantly from common base units to modular space stations to future mega-structures. In an orbiting context, freed from the constraints of Earth’s gravity, we can redefine how space architecture is conceived, designed, assembled, and lived within.

These principles are applied across all four areas of thesis contributions: a novel design theory for space architecture realized in a portfolio of space structure concepts; systems engineering mission architecture and feasibility analyses for contextualizing proposed space structures in realistic aerospace deployments; physics simulation modeling for habitat-scale self-assembly dynamics in microgravity; and quasi-stochastic self-assembling tile hardware creation and evaluation across four space environment missions, culminating in a successful 30-day International Space Station experiment in March 2020. The thesis contributions center on the TESSERAE (Tessellated Electromagnetic Space Structures for the Exploration of Reconfigurable, Adaptive Environments) platform.

Thesis Supervisor: Joseph Paradiso

Title: Alexander W. Dreyfoos (1954) Professor of Media Arts and Sciences, MIT Media Lab

SELF-AWARE SELF-ASSEMBLY for SPACE ARCHITECTURE:
Growth Paradigms for In-Space Manufacturing

by

Ariel Ekblaw

This thesis has been reviewed and approved by the following committee members:

Thesis Supervisor

.....

Joe Paradiso
Alexander W. Dreyfoos (1954) Professor of Media Arts and Sciences
MIT Media Lab

Thesis Reader

.....

Dava Newman
Apollo Program Professor of Aeronautics and Astronautics
MIT AeroAstro

Thesis Reader

.....

Neri Oxman
Associate Professor of Media Arts and Sciences
MIT Media Lab

Thesis Reader

.....

Danny Hillis
Visiting Professor of Media Arts and Sciences
MIT Media Lab

Acknowledgements

This PhD is the outgrowth of many a romantic notion about space exploration—from the intrinsic beauty found in the search for new knowledge of our cosmos, to the grand adventures, quests, and missions awaiting humanity as we venture into the far reaches of our solar system and eventually our galaxy. I am profoundly fortunate to have been guided, encouraged, and supported in this work by many an exceptional human. This is the least exhaustive section of the thesis, as I have so many more to thank, and so much to be thankful for.

To my Committee—

To Joe, I owe so much. You have my deepest gratitude for shaping my formative years as a researcher and builder, for providing insightful mentorship across a range of technical areas, and for so enthusiastically sharing your love of science fiction. You gave me freedom—freedom to combine the technical rigor of the Responsive Environments group approach with far-future design creativity. This propelled my explorations as I took the PhD into uncharted territory for our future lives in space. We shared a way of thinking from the world of Particle Physics in past lives and yet you also introduced me to a new mode of scientific and engineering inquiry through the promise of ubiquitous sensing and iterative prototyping. It has been my distinct pleasure to build a “responsive space environment” in your honor. On top of all of this, you supported me unwaveringly in my parallel endeavor at the Lab, as I founded and led the growing MIT Space Exploration Initiative. I am so grateful for your open-mindedness and belief in me as I pursued an unorthodox path through graduate school.

Dava, you inspire me. I have learned so much from how you approach human spaceflight and how you lead innovative research—across academia, government, and industry—to realize our space exploration future. You helped me take this thesis from a set of unusual, provocative ideas to an aerospace platform with a roadmap of flight tests that have and will continue to prepare the work for deployment at scale, in orbit. Thank you for your research insight and your encouragement. I am so grateful for your mentorship.

Neri, you open my eyes. From teaching the course that provoked my first inklings of the thesis research, to every one of our research conversations, you show me a way of thinking about the world that fascinates and intrigues me. I aspire to develop a *taste in thinking* worthy of your use of the term, guiding the next decade of my work in space architecture. Thank you for always pushing me to explore a realm of creativity, design rigor, and expansive vision—you have so enriched my work.

Danny, you motivate me—to follow in your footsteps and build systems at scale that can last for centuries. I am grateful for the depth of your technical advising for this thesis, the wisdom you bring from so many different disciplines, and the infectious, mischievous mindset that working with you inevitably cultivates for solving problems and applying technological paradigms.

To my mentors and research collaborators—

First and foremost, thank you, Joi Ito, for introducing me to the magic of the Media Lab. You gave me space to grow, to build an ecosystem of space exploration endeavors in a new pocket of MIT. This powered the PhD and set me on an entirely new trajectory. Thank you for this transformative opportunity and for your friendship. Thank you, Maria Zuber, for championing both the Space Exploration Initiative and my PhD, guiding me throughout the last four years. Radhika Nagpal, while a trick of fate led me to a different lab as an undergraduate REU, I am so lucky to have found my way back to you! I have so greatly enjoyed every minute of our conversations and am grateful for your expertise and mentorship. To Neil Gershenfeld and the entire CBA, thank you for the How to Make Almost Anything course where the first TESSERA prototype was born and for the intellectual heritage behind programmable matter (with a special thanks to Zach Fredin for the EPM winding tutorial!). Thank you, Neil, for introducing me to Ara Knaian. Ara, thank you for your incredible

generosity in teaching me the finer points of COMSOL and for the particularly fruitful collaboration around the ISS flight. Thank you, Aswin Karthik Ramachandran Venkatapathy, for your dedication to our electronics collaboration over several years and for so many fantastic conversations. Please extend my thanks to the TU Dortmund Fraunhofer institute for sharing your time and their research resources with us. My thanks also go out to the Cyberbotics team and their superb software and engineers, particularly David Mansolino, with whom I had the pleasure of working closely for the TESSERAE physics simulation. Thank you to visiting student Anastasia Prosina for a summer rich in architectural exploration and for your contributions to the TESSERAE interior design. Thank you, MIT UROPs Elisheva Shuter and Peter Williams, for your early prototyping efforts. Thank you Vince Tolentino, Edward Oo, and Marlena Fauer, for enlightening conversations on the broader cultural, art, and architectural influences that humanity would yearn for in space architecture.

To my colleagues and friends at the Media Lab, MIT, and beyond—

Thank you, Andy Lippman, for bringing me to the Media Lab in the first place! Thank you to all the wonderful members and fellow graduate students of the Responsive Environments group for creating an intensely passionate, while also friendly, easygoing, and welcoming community—that combination is so rare in graduate school and is a testament to the people in the group. I'm lucky to have worked alongside you all. Thank you, Travis Rich and Gershon Dublon, for showing me what it means to do a PhD in this unique place and for serving so compellingly as the community members that I looked up to.

Thank you to the gurus of the Media Lab for all you did to support this PhD—from machine shop maestros John DiFrancesco and Tom Lutz, to electronics wizards Brian Mayton and Mark Feldmeier, to Joost Bensen, Peter Rombult, and all of ML Facilities and NeCSys. Thank you to the dedicated staff of the Director's Office and Finance who keep the place running and supported so many of my endeavors, with special thanks to Janine Liberty, Jess Sousa, Ryan McCarthy, Nicole Degnan, and Rebecca Reid, for their incredible help and friendship. Thank you, Habib Haddad, for guiding my decisions on next steps and providing the infrastructure for so much opportunity coming out of the Lab. Thank you to the two goddesses of MAS, from my early days to now—Monica Orta and Keira Horowitz—for all your kindness and advice.

Thank you to my amazing, dedicated staff at the Space Exploration Initiative who inspire me each day with their contributions to our collective Starfleet Academy. Thank you, Maggie Coblenz, for keeping the ship afloat while I wrapped up this thesis and for being such a fantastic partner in crime, and thank you, Xin Liu, Sands Fish, Mehak Sarang, Sean Auffinger, Che-Wei Wang, Peter Dilworth, Jamie Milliken, Sana Sharma, Avery Normandin, Amna Carreiro, our many volunteers (Devora Najjar! Pat Pataranutaporn!), and broader community members for your passion. Knowing that we might all live together in a TESSERAE space habitat “baugruppen” one day keeps me going strong!

Thank you to the best cast and crew of friends a space cadet could ever hope for! You brought joy and mirth to my days at the Lab, always in the wings, sharing yourselves, your own inspiring work, and your kind hearts as I progressed through the PhD. Thank you Caroline Jaffe, Jifei Ou, Bianca Datta, Sunanda Sharma, Matt Carney, Nicole & Juan & Luna, Nick Barry, Juliana Cherston, Ani Liu, Chelsea Barabas, Pip Mothersill, Amanda & Michael Sherman, Ben Green & Salome Viljoen, Danny Howe, Renate Roehl, and Megan Perley.

To Levi, you are my partner in the truest sense of the word—PhD applications really should come with a warning label for all they require of a couple—and through it all you supported me, shared ideas and skills with me, and loved me with such grace. Thank you.

To my parents, you gave me the best gifts one ever gives a being—life, a loving family, profound inspiration, and an amazing childhood on which I built my aspirations (two US Air Force pilots set a high bar!). But most importantly, you gave me my binar. Ian, I look forward to every moment of our lives together. Here's to the first planet we explored in tandem, and on to another!

Table of Contents

Acknowledgements	4
Table of Contents	6
Table of Figures	9
1. Introduction	14
Chapter 1	14
1.1 Thesis Approach.....	15
1.1.1 Design Theory.....	18
1.1.2 TESSERAE Hardware Platform.....	18
1.1.3 Space Environment Deployments.....	21
1.1.4 Simulation and Mathematical Modeling.....	21
1.1.5 Mission Architectures and Concept of Operations.....	22
1.2 In Summary: Why Self Assembly?.....	22
2. Literature Review	23
Chapter 2	23
2.1 Science and Application of Self-Assembly.....	24
2.2. Engineering Precedents.....	26
2.2.1 Sensing.....	26
2.2.2 Magnets.....	26
2.2.3 Engineering Building Blocks and Direct Aerospace Applications.....	26
2.3 Terrestrial and Space Architecture Precedents.....	27
2.3.1 Terrestrial Precedents.....	27
2.3.2 Space Architecture Precedents.....	29
2.4 Theoretical Underpinnings: Mathematics, Philosophy, Literature, and Art.....	37
3. Growing Space Architecture: A New Design Theory	38
Chapter 3	38
3.1 A Biomimetic Framework.....	39
3.1.1 Accretion Over Construction.....	40
3.1.2 Seeding Over Erecting.....	40
3.1.3 Cascades Over Dams.....	41
3.2 Indeterminate Growth.....	42
3.3. Designing in Concert with the Space Environment.....	43
3.4 Parameter Space for Microgravity Space Architecture.....	44

3.5 An Aside: Aesthetics worthy of Life in Space, and a Life in Space Worthy of the Patterns of Nature .	47
3.5.1 Informing Form	48
3.5.2 Shaping Surfaces: Tilings and Tessellations	51
3.5.3 Choosing Cladding.....	54
3.6 Summary.....	55
4. TESSERAE Hardware: Space Environment Experiments and Results	56
Chapter 4.....	56
4.1 TESSERAE Shell Prototypes and Testing	58
4.1.1 Generation 1: Tested via Parabolic Flight.....	62
4.1.2 Generation 2: Tested via Suborbital Launch and Parabolic Flight	70
4.1.3 Generation 3: Tested via ISS Mission.....	82
4.1.4 Generation 4: Autodesk Architectural Scale.....	113
4.1.5 TESSERAE Shell Hardware Contributions Summary and Next Steps.....	116
4.2 TESSERAE Cell Prototypes.....	119
4.2.1 Generation 1: Tested via Parabolic Flight.....	120
4.2.2 Generation 2: Hardware Maturity Next Steps and “Cell” Extensibility to Other Shapes.....	126
5. TESSERAE Modeling and Simulation.....	129
Chapter 5.....	129
5.1 TESSERAE Shell Robotics Simulation	129
5.1.1 Preliminary Models: Unity and Simulink.....	131
5.1.2 Full Behavioral Model and Characterization Results	133
5.1.3 Physics Simulation Conclusions and Next Steps	149
5.2 TESSERAE Cell Genetic Algorithm and Generative Design Model.....	150
5.2.1 Modeling Approach and Assumptions.....	150
5.2.2. User Interface Features	152
5.2.3 Output.....	154
5.2.4 Generative Simulation Conclusion and Next Steps.....	155
6. TESSERAE Aerospace Mission Architectures	156
Chapter 6.....	156
6.1 TESSERAE Shell ConOps:	158
6.1.1 TESSERAE Mission Concept.....	161
6.1.2 Deployment Feasibility Analysis – At Habitat Scale	175
6.1.3 Comparison with Alternative Habitation Module Concepts	179
6.1.4 Alternative Shell ConOps: Origami Assembly.....	183
6.1.5 Extensibility to other Geometries	184

6.1.6 Summary: TESSERAE Shell ConOps.....	186
6.2 TESSERAE Cell ConOps.....	187
6.2.1 Plesiohedrons and Packing: Crystalline Space Station Mega-Structures	189
6.2.2 Defining the Cell MVU: From “Minimum Viable Unit” to Station.....	190
6.2.3 Extensibility to Other Geometries	197
6.2.4 Summary: TESSERAE Cell ConOps	199
6.3 Integration with NASA mission priorities.....	200
6.3.1 TESSERAE Alignment with NASA Strategic Objectives and Roadmaps.....	200
6.3.2 Extensibility and Wider Benefits	200
6.4 Applications Beyond Habitats	201
6.4.1 Storage Chambers, Space Ports & Logistics Depos	201
6.4.2. Parabolic Mirrors.....	202
6.4.3 Satellites	203
6.5 Extensions of the TESSERAE Paradigm: From Modularity to Continuity	204
6.5.1 Extrusion & the Space Cocoon	204
6.6 Aerospace Mission Architectures Conclusion.....	205
7. Conclusion	207
Chapter 7.....	207
Appendix: the MIT Space Exploration Initiative	209
Bibliography	217

Table of Figures

Figure 1-1. TESSERAE Space-Time map.....	17
Figure 1-2. TESSERAE Shell deployment sequence.....	20
Figure 1-3. TESSERAE Cell packing approach.	21
Figure 2-1. Bucky Fuller’s 1965 patent	27
Figure 2-2. Dutch Structuralists.....	28
Figure 2-3 Konstantin Tsiolkovsky 1895 spherical spaceship.....	29
Figure 2-4. Left: Salyut Station; Right: Model of Tiangong	31
Figure 2-5. Left: Skylab; Right: Mir.....	31
Figure 2-6. International Space Station.. ..	32
Figure 2-7. Comparison matrix for Salyut, SkyLab, Mir and ISS.....	33
Figure 2-8. Stanford Torus, 1975 NASA Summer Study.....	34
Figure 2-9. Bernal Sphere	34
Figure 2-10. Prospective Model of Orion spacecraft.....	35
Figure 2-11. Prospective model of Gateway Station.....	35
Figure 2-12. Comparison matrix for Stanford Torus (conceptual), Bernal Sphere (conceptual), Orion (planned), and Gateway (planned).....	36
Figure 3-1. Design theory examples: mussels, crystals, cascades	41
Figure 3-2. Companion charts showing Function vs. Structure (left) and Form vs. Status (right)	46
Figure 3-3. TESSERAE 3D Parameter Space design tool.....	47
Figure 3-4. Parastichy and Voronoi	48
Figure 3-5. Phyllotaxis.....	49
Figure 3-6. Pages from the <i>Divina Proportione</i>	49
Figure 3-7. Étienne-Louis Boullée’s Cenotaph to Newton.....	50
Figure 3-8. Fractal examples	50
Figure 3-9. Radiolarians and Sponge Spicules.....	51
Figure 3-10. Persian architecture	52
Figure 3-11. Tessellation in nature.....	53
Figure 3-12. Tilings in 3D.	53
Figure 3-13. Truncated icosahedron and truncated octahedron	54
Figure 3-14. Solar Egg.....	54
Figure 4-1. Dihedral bonding angle diagram	58
Figure 4-2. Polarity map for pentagon and hexagon tiles (Left). Application to 3D joints (Right).	59
Figure 4-3. TESSERAE tile housing and constitute components.....	60
Figure 4-4. TESSERAE bonding control and correction algorithm.....	60
Figure 4-5. Self-Assembly hypotheses and research variables.....	61
Figure 4-6. TESSERAE prototype progression	62
Figure 4-7. TESSERAE prototype through course development.....	63
Figure 4-8. TESSERAE next stage prototype through further course development.....	63
Figure 4-9. Table of major PCB components for TESSERAE Gen 1 boards.....	64
Figure 4-10. Simplified schematic for TESSERAE Gen 1 PCBs.	65
Figure 4-11. Performance curves for the KXOB22-01X8F PV cells.....	65
Figure 4-12. Current draw by operating mode for major Gen 1 PCB components.....	66
Figure 4-13. Communication protocol comparison chart.....	67
Figure 4-14. PCB layout in Altium and built PCB	68
Figure 4-15. Parabolic flight experiment apparatus.....	69

Figure 4-16. Generation 2 tiles	71
Figure 4-17. Table of key components on peripherals and motherboard for TESSERAE Gen 2 hardware. ..	72
Figure 4-18. Generation 2 preliminary control algorithm.....	73
Figure 4-19. Final control logic plan for TESSERAE Gen 2.....	73
Figure 4-20. Magnetometer data (uT) for TESSERAE tile bonding thresholding (1).....	73
Figure 4-21. Magnetometer data (uT) for TESSERAE tile bonding thresholding (2).....	74
Figure 4-22. Magnetometer data (uT) for TESSERAE tile bonding thresholding (3).....	74
Figure 4-23. Communications architecture for suborbital launch test.....	74
Figure 4-24. TESSERAE Generation 2 bill of materials.....	75
Figure 4-25. Final experiment integration and check-out at Blue Origin’s West Texas Launch Facility.	76
Figure 4-26. TESSERAE tiles for 2019 suborbital launch test, situated inside Blue Origin Single Payload Locker experiment chamber.	76
Figure 4-27. Suborbital launch latching mechanism.	77
Figure 4-28. Suborbital launch: tiles latched, released, bonded.....	78
Figure 4-29. Experiment operation timetable, with power consumption from Blue Origin onboard system..	79
Figure 4-30. Liftoff for the NS-11 mission (Blue Origin Suborbital).	80
Figure 4-31. Initial arrangement of TESSERAE tiles for 2019 parabolic flight.....	81
Figure 4-32. TESSERAE tiles in formation flight, parabolic flight test.	82
Figure 4-33. Gen 2 tiles on Suborbital Flight.....	83
Figure 4-34. Inverted error mode for TESSERAE tiles.....	83
Figure 4-35. Gen 3 tile mechanical features.	86
Figure 4-36. Gen 3 tile holsters	87
Figure 4-37. Gen 3 tile attachment mechanisms.	87
Figure 4-38. Sensor and communications component table for Gen 3, ISS hardware.	88
Figure 4-39. Gen 3 Power Circuitry Component Table.....	89
Figure 4-40. Supercapacitor discharge testing.....	89
Figure 4-41. Overview system diagram for TESSERAE PCBs, showing pentagon configuration.	90
Figure 4-42. COMSOL EPM model (1)	91
Figure 4-43. Lab testing of EPMs.	92
Figure 4-44. COMSOL EPM model (2).	93
Figure 4-45. Design parameter sweep (Pareto frontier) for COMSOL EPMs.....	93
Figure 4-46. EPM manufacturing drawing.....	94
Figure 4-47. EPM performance details and prototypes.....	94
Figure 4-48. Gen 3 control algorithm phase 1	97
Figure 4-49. Gen 3 control algorithm phase 2.....	98
Figure 4-50. Gen 3 control algorithm (RGB exchange inset).....	99
Figure 4-51. ISS mission tile integration and testing.....	100
Figure 4-52. ISS mission development schedule	101
Figure 4-53. ISS mission experiment apparatus, integration, and testing.....	102
Figure 4-54. ISS step by step flight plan.	104
Figure 4-55. ISS launch and on-orbit install.....	105
Figure 4-56. Gen 3 hardware on-orbit, prior to experiment start.....	106
Figure 4-57. Gen 3 tile behavior on-orbit, experiment results (1)	107
Figure 4-58. Gen 3 tile behavior on-orbit, experiment results (2)	108
Figure 4-59. Gen 3 tile behavior on-orbit, experiment results (3)	109
Figure 4-60. Gen 3 tile behavior on-orbit, experiment results (4)	110
Figure 4-61. Gen 3 tile behavior on-orbit, experiment results (5)	111
Figure 4-62. Gen 3 tile behavior on-orbit, experiment results (6)	112

Figure 4-63. ISS mission experiment summary performance table.....	112
Figure 4-64. Autodesk BUILD Space in Boston, MA.....	113
Figure 4-65. Tile clamp mechanical approaches (1).....	114
Figure 4-66. Tile clamp mechanical approaches (2).....	114
Figure 4-67. Comparison of two tile latch ideas.....	115
Figure 4-68. Summary of TESSERAE large-scale clamp principles.....	115
Figure 4-69. Summary of TESSERAE Generation 1 through Generation 3 hardware features.....	117
Figure 4-70. TESSERAE tile metastable error mode.....	118
Figure 4-71. TESSERAE Shell and Cell habitat style comparison.....	119
Figure 4-72. TESSERAE Cell prototype design matrix with varying magnet joints.....	121
Figure 4-73. TESSERAE Cell prototype units.....	122
Figure 4-74. Pre-flight documentation for TESSERAE Cell units.....	122
Figure 4-75. Parabolic flight TESSERAE Cell experiment plan.....	123
Figure 4-76. TESSERAE Cell unit behavior during flight, experiment results (1).....	124
Figure 4-77. TESSERAE Cell unit behavior during flight, experiment results (2).....	124
Figure 4-78. TESSERAE Cell unit behavior during flight, experiment results (3).....	125
Figure 4-79. Extension of TESSERAE Cell concept to fractal patterns.....	126
Figure 4-80. Extension of TESSERAE Cell concept to triply periodic gyroids.....	127
Figure 4-81. Greg Lynn modular “Blob Wall”.....	128
Figure 4-82. Sea shells and space stations.....	128
Figure 5-1. TESSERAE error modes for correction in-flight and in-simulation.....	130
Figure 5-2. Unity model output.....	131
Figure 5-3. Close-up of Unity modeling environment, with TESSERAE stochastic tiles.....	132
Figure 5-4. Close-up of Simulink modeling environment, with TESSERAE active tiles.....	133
Figure 5-5. TESSERAE Shell WeBots simulation screenshots.....	134
Figure 5-6. Cylindrical magnet behavior as a function of length and radius.....	135
Figure 5-7. TESSERAE Shell WeBots simulation code parameters.....	141
Figure 5-8. TESSERAE Shell WeBots simulation trail run, initial variables.....	143
Figure 5-9. TESSERAE Shell WeBots simulation intra-trial results (1).....	143
Figure 5-10. TESSERAE Shell WeBots simulation intra-trial results (2).....	144
Figure 5-11. TESSERAE Shell WeBots simulation intra-trial results (3).....	144
Figure 5-12. TESSERAE Shell WeBots simulation intra-trial results (4).....	145
Figure 5-13. TESSERAE Shell WeBots simulation intra-trial results (5).....	145
Figure 5-14. TESSERAE Shell WeBots simulation intra-trial results (6).....	146
Figure 5-15. TESSERAE Shell WeBots simulation intra-trial results (7).....	146
Figure 5-16. TESSERAE Shell WeBots simulation intra-trial results (8).....	147
Figure 5-17. TESSERAE Shell WeBots simulation inter-trial results comparison (1).....	148
Figure 5-18. TESSERAE Shell WeBots simulation inter-trial results comparison (2).....	148
Figure 5-19. TESSERAE Cell prototypes showing range of configuration shapes.....	150
Figure 5-20. Core elements of the TESSERAE Cell generative algorithm codebase implementation.....	151
Figure 5-21. TESSERAE Cell generative design GUI (1).....	152
Figure 5-22. TESSERAE Cell generative design GUI (2).....	153
Figure 5-23. TESSERAE Cell generative design GUI (3).....	153
Figure 5-24. TESSERAE Cell generative design output results (1).....	154
Figure 5-25. TESSERAE Cell generative design output results (2).....	155
Figure 6-1. Truncated icosahedron and truncated octahedron.....	157
Figure 6-2. Evolution from TESSERAE flat-pack for launch to a multi-chamber station.....	159
Figure 6-3. TESSERAE mission concept.....	161

Figure 6-4. TESSERAE docking with the Lunar Gateway.....	161
Figure 6-5. Ashby Chart.....	163
Figure 6-6. Flow chart tracking step-by-step deployment for TESSERAE Shell system.....	164
Figure 6-7. TESSERAE packed for launch.....	165
Figure 6-8. TESSERAE tile insertion order.....	167
Figure 6-9. Artists render of TESSERAE tile deployment holster in orbit.....	167
Figure 6-10. TESSERAE mixed-use module size increase.....	169
Figure 6-11. TESSERAE interior habitation core.....	170
Figure 6-12. Exploded view of TESSERAE multi-functional interior design.....	171
Figure 6-13. Speculative TESSERAE interior	172
Figure 6-14. Integration with robotic swarms and “Rovables”.....	173
Figure 6-15. Dual use for surface habitation.....	174
Figure 6-16. Stuffed Whipple Shield specifications.....	175
Figure 6-17. Force analysis for pressurization clamps.....	176
Figure 6-18. Mass comparison between TESSERAE and ISS modules.....	179
Figure 6-19. Functionality comparison between TESSERAE and BEAM (inflatables).....	179
Figure 6-20. ISS module specifications drawn from Columbus, Destiny, BEAM.....	180
Figure 6-21. Space architecture comparison quad charts.....	181
Figure 6-22. Hoberman Sphere patent.....	182
Figure 6-23. TESSERAE origami, hinged deployment approach.....	184
Figure 6-24. Extensibility to other tessellations and geometries.....	185
Figure 6-25. Extensibility to other base unit shapes.....	185
Figure 6-26. TESSERAE Cell base module with an indefinite configuration possibilities.....	188
Figure 6-27. Examples of truncated octahedron (truncated octahedron) packing and branching structures.....	189
Figure 6-28. Detailed listing of ISS subsystems for selective inclusion in TESSERAE MVU definition.....	191
Figure 6-29. Use of cellular comparisons for informing TESSERAE Cell MVU.....	192
Figure 6-30. Umbrella mushrooms: start small, grow organically, with modest resources.....	193
Figure 6-31. TESSERAE Cell space station.....	194
Figure 6-32. Functional zone definition from generative algorithm results for TESSERAE Cell.....	195
Figure 6-33. TESSERAE Cell exponential growth estimates (1).....	196
Figure 6-34. TESSERAE Cell exponential growth estimates (2).....	197
Figure 6-35. A range of forms showing potential focus areas for TESSERAE Cell architecture next steps.....	198
Figure 6-36. Parastichy in the Star Wars universe.....	198
Figure 6-37. TESSERAE as a logistics and storage chamber in-orbit.....	201
Figure 6-38. Application of self-assembly to parabolic mirrors.....	202
Figure 6-39. Robotic on-orbit self-assembly of satellites.....	203
Figure 6-40. TESSERAE Space Cocoon extrusion design.....	204
Figure 6-41. TESSERAE Space Cocoon extrusion process.....	204
Figure 0-1. The SEI’s first parabolic flight in 2017.....	210
Figure 0-2. SEI 2017 and 2019 Parabolic flight highlights.....	210
Figure 0-3. SEI 2019 Blue Origin Suborbital flight.....	211
Figure 0-4. SEI November 2019 Research Showcase.....	211
Figure 0-5. SEI March 2020 ISS mission.....	212
Figure 0-6. SEI on the cover of WIRED.....	212
Figure 0-7. SEI coordinating with MIT MOU and Blue Origin for a lunar lander mission.....	213
Figure 0-8. Beyond the Cradle event.....	214
Figure 0-9. SEI team through the years.....	215
Figure 0-10. Reminders of our inspiration and responsibility. We stand on the shoulders of giants.....	216

Intentionally left blank

1. Introduction

Chapter 1

“Everything was so new—the whole idea of going into space was new and daring. There were no textbooks, so we had to write them.”

—Katherine Johnson

Despite three centuries of space architecture science fiction storytelling, we have yet to realize the enlightening, inspiring structures so fondly envisioned. Where are our space hotels, our sprawling ringworlds, our space cathedrals?

To a first degree, we still require core technological development in the obvious three gatekeepers: heavy lift rockets (making the transportation of our creations from Earth to space more feasible), in-space material sourcing and manufacturing, and environmental control and life-support systems. Sustainable human life in space at the architectural scales we are discussing—from outposts, to colonies, to space cities—will also require advances in the sourcing of power and energy storage densities. Yet even with renewed and expanded commitment to these technical goals, we still face archetypal barriers to space architecture and systematic scaling.

Space architecture has traditionally been hampered by capricious political whims, where one generation’s investment in lofty space exploration goals can be swiftly washed away. This might be crystallized into a single observation: the infeasibility of deploying and maintaining cost-sink behemoths. To address this, we can fundamentally change the paradigm of how space architecture is conceived: instead of summoning resources for a pre-determined megastructure, let us start small and grow iteratively and organically (a “spiral” theory of development). A fully formed tree does not burst forth from the ground, nor is the precise final form of the tree known at the seed stage; the tree evolves over decades, responsive to its environment, in an indeterminate pattern of growth requiring only modest resources at any one moment in time. So too, have our cities traditionally grown, by fits and starts with incremental additions that add to the “fractal density.”¹

As humans make progress in the gatekeeper technical areas, we will need a means of scaling habitation in low Earth orbit and beyond. Our Earth-based approach, heavily dependent on manual labor and human design oversight, simply cannot be extrapolated to the space environment. The risk of astronaut extra-vehicular activities (EVAs) and limitations of single-design, single-use architecture would continue to unnecessarily rate-limit progress. We strive to answer this call for space architecture that builds itself through transformative *self-aware self-assembly*—adaptive “living structures” that follow principles of fractal self-similarity² to scale elegantly

from common base units to modest multi-part and modular space stations to, ultimately, a family of mega-structures.

Finally, the domain of space presents us with grand—and as currently known to our models of physics, unyielding—time and spatial scales. Our future space architecture must commune with these scales, designed as a complementary feature of its environment, rather than in opposition to it. This suggests we should think of space architecture not as a temporary, technological artifact of its time, but as a fully embodied, sentient, and self-aware complex system in symbiosis with its human designers and inhabitants—as an organism in its own right, responsive and robust, accreting and evolving over the long time horizons native to traversing the expanses of our cosmos. The noble mission of space architecture is to answer our yearning to experience and investigate the cosmos while we retain our current human form.

This leads us to the research question that guides the contributions of this thesis:

How can we design, induce, and scale self-aware¹ self-assembly to grow² space architecture, natively, in orbit?

1.1 Thesis Approach

As habitation and operational needs evolve around new commercial space stations in LEO (low Earth orbit) and exploration missions to the Moon and Mars, space architecture must adapt to address new use cases and deployment contexts. Rather than relying on fixed, rigid shell or fixed, inflatable modules, a new paradigm for *self-aware, self-assembly* can offer adaptive, reconfigurable, and re-usable outer shells built on biomimetic principles. A self-assembly approach divides the final structure into many constituent, complementary parts that join together under certain rules and constraints.

This thesis offers a design theory, produces prototypes, models at-scale dynamics, evaluates space environment tests and develops a technology roadmap template for a multi-year research effort around the TESSERAE (Tessellated Electromagnetic Space Structures for the Exploration of Reconfigurable, Adaptive Environments) Platform. This platform explores two different models for self-assembly in orbit, two different sets of “rules and constraints”—the TESSERAE Shell and the TESSERAE Cell.

The TESSERAE Shell model comprises a complementary set of self-assembling hexagonal and pentagonal panels, outfitted with an array of magnetic field, inertial, and proximity sensors to diagnose and actuate bonding via controllable electro-permanent magnets (EPMs) at their interface surfaces. The target structure for the self-assembling TESSERAE Shell is an open chamber buckminsterfullerene (or truncated icosahedron), with 20 hexagons and 12 pentagons.

The TESSERAE Cell model arises from a volumetric node, designed as a plesiohedron (or space-filling solid) with self-aligning magnetic joints such that many Cell nodes can accrete together into a densely packed,

¹ In this context, we use “self-aware” to mean sensor-mediated and responsive to the local environment (e.g., proximity sensing and neighbor-neighbor mesh communications), with both local and global system knowledge of the final target structure. The self-aware constituents of a TESSERAE module, the tiles or nodes, use this self-awareness for swarm-like agency—to diagnose and separate if needed for assembly error correction. We are not using “self-aware” to imply a sense of habitat-scale consciousness in the tradition of Strong AI—though perhaps advancements in neural networks, deep learning, and applied artificial intelligence will bring us closer to the latter vision, long predicted by science fiction.

² We focus here on models of growth to emphasize that space architecture, particularly structures in microgravity, might be constructed in energy-favorable pathways that mimic growth patterns in nature.

crystalline-like structure. We chose the truncated octahedron (14 sides: 8 hexagons, 6 squares) as the initial base geometry to test for the Cell units.

This thesis follows an arc from theory, to prototype realization, to testing, to modeling projections for extensibility to the space environment, to planning for near-term space missions. A broad set of space structure concepts and associated self-aware growth patterns are proposed and analyzed, emerging from the space architecture design theory. A subset of these concepts is then realized in two particular prototype platforms (TESSERAE Shell and Cell), which are executed and tested across several physical scales (from desktop prototypes for parabolic flights to early stage designs for a human-scale model). These prototypes are evaluated across a gradient of ground testing, space simulation environments, and space-deployed contexts, including two parabolic flights, one suborbital launch, and a 30-day International Space Station (ISS) mission. The two concepts are modeled (via both architectural renders and dynamics simulation modeling with embedded control algorithms) and taken through prospective mission architecture flows. With this multi-pronged approach, we hope to enable a clear path to the realization of a concrete, new space architecture technology within the scope of a PhD, while also laying the intellectual groundwork for a space architecture “chaconne”: many further explorations and variations on a “self-aware” theme.

The TESSERAE platform aims to contribute space architecture construction approaches across all three spatial scales and across varying time-constraints, from near-instantaneous assembly for rapid-deploy use cases to the long-duration use considerations described by an indeterminate growth paradigm. Beginning with the obvious three-dimensional case and working backwards, we present the TESSERAE Cell, the TESSERAE Shell, and the TESSERAE Cocoon (a one-dimensional filament of extruded material used to self-assemble a coiled structure, discussed more briefly in 6.5.1). In this case, we define the filament as “1D” extrusion, owing to the fact that its diameter will be sufficiently small in comparison to the one axis that dominates its description—the length. To this mix, we add one hybrid concept, an origami-inspired approach for unfolding hinged stacks of TESSERAE Shell tiles into a connected spiral arm that immediately coils into the buckyball target geometry due to the magnet polarity map of its joints. We label this approach as 1.5D, due to the cross-over between a single length dimension that coils into a final structure and the individual tiles of this spiral arm that define a predominantly 2D plane (before assembly into a 3D form). Drawings, prototypes, simulations, and aerospace mission considerations for all four concepts are discussed in Chapters 3, 4, 5 and 6, respectively.

Due to the unique prototyping and deployment considerations of each approach, they yield a variety of timescales for assembly. In Figure 1-1, we present the Space-Time chart, a self-assembly map to the TESSERAE portfolio. From our modeling, the origami approach completes fastest, as its completion is more deterministically driven than the others. Individual TESSERAE Cells (the “nodes”) also self-assemble quickly and directly, through the self-aligning magnetic joints designed and tested in Chapter 4. The time range extends further for the Cells than it does for the origami-inspired approach, however, as they can continue to grow indefinitely and may take time to quasi-stochastically self-assemble into a desired target topology (if specific boundary conditions have been set). The extrusion approach for the TESSERAE cocoon is expected to follow a comparable time trajectory to that of the Cell nodes, with a relatively fixed time per incremental addition (the time to add one full ring to the coil can be reliably, consistently predicted—both nodes and coils scale linearly with respect to unit additions). In contrast, the TESSERAE Shell tiles witness the greatest variability in time to assemble, as a quasi-stochastic process drives the bonding error detection and correction. This wait time comes with a significant advantage, however: TESSERAE Shell tiles can autonomously build large, unconstrained open volumes that are modular and fully reconfigurable—no other of the three models offers all three benefits. While the bulk of the thesis and spaceflight experiments have therefore focused on the TESSERAE Shell hardware, all four models offer intriguing functionality for different scenarios. This map presents the trade-off space for comparisons within the TESSERAE portfolio and charts the thesis contributions across spatial scales (1D, 1.5D, 2D, and 3D) and across anticipated time to completion by model.

Shading of each figure represents how quickly the structures proceed from an initial state, where many final configurations are possible, to the final annealed state. While the Shell tiles may take the longest to complete assembly, the point where the final annealed state is known is quite early—logic in the control algorithm for the autonomous self-assembly ensures that as soon as a “seed” of two bonded tiles is formed, the rest of the tiles must accrete to that proto-group, forming a buckyball as determined by the dihedral angles and magnet polarity of the tile-tile bonding joints. In contrast, both the Cell nodes and Cocoon extrusion approaches can maintain variability and achieve any number of final structures throughout the assembly trajectory (i.e., nodes can accrete indefinitely in a space-filling solid, and the radius of coils can be dynamically widened, constricted, and added to).

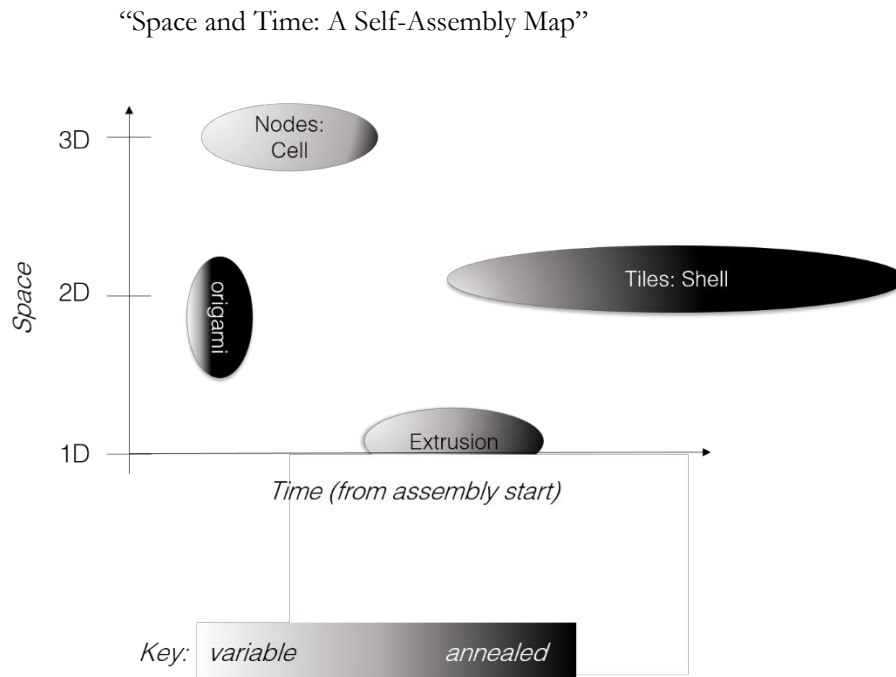


Figure 1-1. TESSERAE Space-Time Map, showing the relationship between 1D, 2D, and 3D spatial scales of the prototypes and the time they take to anneal, or self-assemble.

In this thesis, each chapter develops key insights that directly feed into the next. The design theory (Chapter 3) shaped the motivation for the design and creation of biomimetic self-assembling hardware platforms (Chapter 4). Results from the hardware tests in space environments (Chapter 4) informed and validated the behavior of the simulation environment (Chapter 5) that models the assembly dynamics of TESSERAE at scale, in orbit. The modeling chapter then informed our expectations for TESSERAE assembly for a realistically posed and scoped aerospace mission, for which we have developed extensive systems engineering plans and concepts of operations (Chapter 6). Each chapter draws heavily on text published in our academic papers, noted by paper and venue at the beginning of each Chapter for reference. All together, the thesis contributions include: development of a novel design theory for space architecture; four generations of the Shell experimental hardware platform culminating in a 30-day ISS mission and an additional generation of the Cell experimental platform tested on a parabolic flight; physics simulation modeling to assess these prototypes and their assembly dynamics at scale; and aerospace systems engineering to design mission architectures and concepts of operation that could be realized within five to ten years. Videos documenting the flight tests, live TESSERAE behavior, simulations, and on-orbit deployment sequence can be found at: arielekblaw.com/tesseract.

1.1.1 Design Theory

Humanity stands on the cusp of interplanetary civilization. As we prepare to venture into deep space, we owe our origins a thoughtful nod—how might we bring the essence of Earth and organic life with us? We begin by exploring how to free space architecture from static, survivalist designs and instead enable dynamic, self-aware space structures that are informed by both inorganic and organic growth processes in complex Earth systems. The future of human habitation in outer space lies in “living structures”—self-assembling and adaptive, following principles of self-similarity to scale elegantly from common base units to a relatively unrestricted family of mega-structures. In an orbiting context, freed from the constraints of Earth’s gravity, we can redefine how space architecture is conceived, designed, built, and lived within. The future of human habitation in space, from LEO to planetary exploration far beyond, also lies in self-assembling, adaptive, and autonomously reconfigurable structures. Rather than relying on astronaut EVAs and deploying solely fixed hard-shell or fixed inflatable structures, we can lower payload weight for a given volume, reduce assembly complexity, and introduce transformative space-structure modularity by implementing quasi-stochastic, “self-aware” assembly for aerospace structures. This paradigm shift will enable entirely new mission architectures for in-space construction, from LEGO-like interchangeability of structural components, to ease of autonomous repair and servicing, to re-use and re-purposing of a single, “minimum viable unit” (MVU) of cellular architecture for multiple aerospace habitation mission contexts.

This thesis explores three core design principles for growth paradigms in space architecture. The first two explore the physical features and topologies of growing systems (both inorganic and organic) and the third bears on energy flows and non-equilibrium phase transitions that govern how such growth is induced and guided:

Accretion over Construction | Seeding over Erecting | Cascades over Dams.

These principles are applied across all four areas of thesis contributions (design theory, hardware, simulation, and mission planning) and build into an expansive “Indeterminate Growth Theory” for space architecture, drawing extensively on the behavior of plants to guide iterative, self-aware accretion where the “whole,” or space station, can be more than the sum of its parts.

1.1.2 TESSERAE Hardware Platform

How will we build the coming generations of space architecture—the modules, spaceships, and space stations that will ensconce our space-faring species? Can we move beyond the 20th century paradigm of cylindrical tubes in orbit to geodesic dome habitats, microgravity concert halls, and space cathedrals? The next generation of space architecture should delight, inspire, and protect humanity for our future in the near and far reaches of space. The space industry’s habitation and operations needs are rapidly evolving around new commercial space stations in LEO and exploration missions to the Moon and Mars. Space architecture must adapt to address new use cases like influxes in crew sizes, space tourism, and new agile deployment contexts.

Through this thesis, we have developed a hardware platform that demonstrates autonomous self-assembly with dynamic error correction. Habitats based on fundamental, repeating units of the TESSERAE systems (both Shell and Cell models) will be able to better serve the breadth of future in-orbit needs and the unpredictability of exploratory life in space as we move beyond heavily scoped, meticulously planned ISS missions. Self-assembling architectures will be based on fundamental assembly units, or tiles, that provide enough degrees of freedom for multiple structural arrangements while retaining the required specificity to generate a predictable

suite of desired shapes. In the design of such a self-assembling hardware system, we consider four key parameters: the base-unit tiles, the jointing method, the assembly protocol, and the holistic function of the structure.

For predictability of the assembly, the tiles or nodes must be standardized to certain sizes and geometries that assemble to create desired macro-shapes. This generally calls for tiles in the form of “regular” (equiangular and equilateral) geometric building blocks, such as triangles or other simple polygons. The needs of a particular structure will determine the resolution of the assembly—a mesh of many small tiles for an approximation of a smoother surface, or a polyhedron composed of only a few, larger tiles for a coarser shape. In concert with this notion of prefabricated modularity lies an opportunity for optimizing the functional properties of different tiles for the aerospace structures context. Certain tiles can serve as sensor nodes, while others are augmented with imaging capabilities built in for remote-sensing or life-support system monitoring. While aerospace deployments will likely require heavy customization inside the structures (to meet the needs of occupants, storage, power generation, etc.), the exoskeleton of a self-assembling structure should rely on a standard suite of tiles with augmented functionality. Though we focus initially on regular, geometric building blocks for near-term manufacturing feasibility, we are keenly interested to expand into organic-inspired base units. The thesis explores this extensibility in the design theory (Chapter 3) and in cellular architecture applications (Chapter 6).

Beyond the properties and functional purpose of any individual base-unit tile, we must design a way for tiles and nodes to securely and reliably mate with neighbors. This definition of jointing could take many forms, including magnetic joints that rely on aligned polarities and proximity for the magnetic forces to draw pieces together, unique lock-and-key joints where compatible pairs snap in place, interleaved edges where tabs slide into slots, and specially activated adhesives that bond matching tiles edges (or some combination of these and other methods). In the TESSERA hardware examples for this thesis, we have focused on magnetic joints for their potential to draw tiles towards each other in microgravity, extensively leveraging EPMS for tunable control and bonding behavior error correction (more on this in Chapter 4).

Intimately related to the jointing mechanism is the self-assembly protocol. Options include: passive self-assembly, where tiles float around each other and assemble in a stochastic process; a tile dispenser that releases one tile at a time for a predictable feed of parts that accrue to a growing structure; a robot-mediated control algorithm that directs tiles toward each other at the optimum time and place; and more. These self-assembly protocols must be matched with jointing methods that correspond to the anticipated amount of time tiles would need to spend near each other, how much kinetic disturbance the system requires to circulate tiles past each other in assembly-favorable positions, the desired level of automation, etc. Appropriate pairs of assembly protocols and joint fittings (i.e., magnetic joints with stochastic tile dynamics or lock-and-key joints with robot-mediated assembly) will yield varying efficiencies in the time it takes for the full structure to assemble and the likelihood of incorrect bonding into local-minima structures.

Finally, the holistic function, or end purpose, of the assembled structure also drives key elements of the design. Will the resulting capsule need to be airtight to support human inhabitants (in which case the assembly jointing must be supplemented with additional sealing or an inner pressurized layer)? Will the self-assembled structure serve as a docking bay for larger, more customized modules and thus require special interface tiles? If some of the tiles are bulkier than others to accommodate this docking, how does the variance in mass distribution affect the dynamics of the assembly process? The requirements for the holistic function therefore shape design decisions for the individual tiles, jointing method, and assembly protocol.

This thesis explores these four parameters for a self-assembling system across a multi-year research deployment schedule of space-environment tests. We scaled the research down to lab-bench size to fit within the available space environment testing apparatus (parabolic flight box, ISS experiment racks, etc.), with the clear intent and extensibility, however, to extrapolate the research to habitation structure scale. The idea was first conceived in

Neri Oxman’s Design Across Scales course in the spring of 2016. The first Shell prototype (both physical tiles and sensor board) was created in Neil Gershenfeld’s How to Make Almost Anything course, with the first major PCB revisions and maturity to a space-sensing platform undertaken in Kerri Cahoy’s Spacecraft Sensors course in the MIT AeroAstro Department. From here, the development continued across three more generations of hardware and several flight tests, culminating in a March 2020 launch to the International Space Station for a 30-day mission. Through all the hardware development, we held to one overarching principle: do as much with stochasticity as possible. Save energy, work elegantly, design a process within the flow of energy favorability, define individual objects within which the logic and blueprint for the final target shape was already reflected—and by doing so, prove the more difficult theory that quasi-stochastic self-assembly *can* successfully produce closed topologies and future habitat structures in a reasonable time duration. Having proved the viability of the core concept—that space docking need not always be the highly choreographed and excruciatingly constrained process used thus far, but rather that we could build on autonomous, stochastic processes—the thesis then also explores modifications and optimizations for a gradation of stochastic to deterministic assembly, all within the TESSERAE hardware platform.

TESSERAE Shells

Our tessellated shell structure approach proposes multifunctional tiles that assemble autonomously via magnetically mediated bonding along regular geometric edges. We present an extensible paradigm for in-orbit space habitat construction via quasi-stochastic self-assembly in microgravity, with extensive hardware development and space environment testing (Chapter 4, Section 4.1). Using the Cyberbotics robotic simulation platform, we have modeled the dynamics of self-assembly for the TESSERAE Shell set at scale, in orbit (Chapter 5, Section 5.1). TESSERAE Shells (Figure 1-2) are designed towards a blue-sky vision of multi-use, interchangeable, and “stackable,” cost-effective orbiting modules that can convert to surface habitats. We aim to supply transformational, practical space infrastructure for the next generation of microgravity habitats that can convert efficiently into staging bases for on-surface exploration (Chapter 6). Unlike large-scale habitats proposed for entire space settlements, the TESSERAE Shell models should be thought of as flexible and reconfigurable modules to aid in agile mission operations.

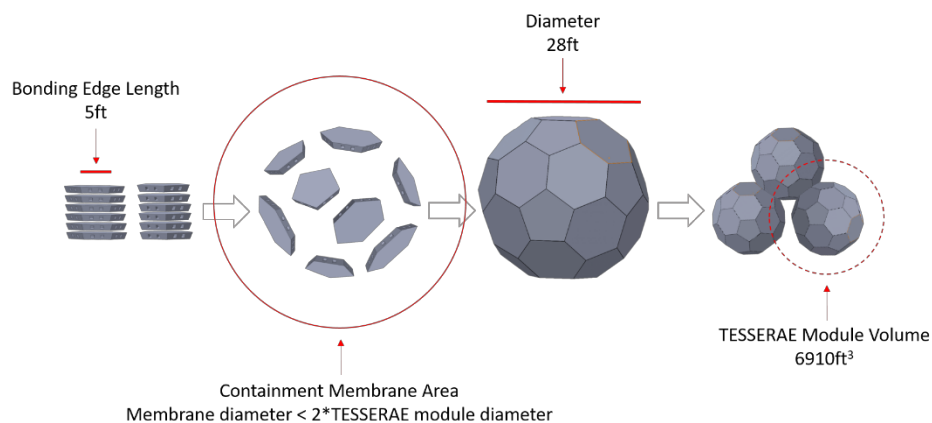


Figure 1-2. Left to Right: TESSERAE tiles packed flat for launch; circulating for self-assembly inside a containment membrane; tiles assembled into a single buckyball; TESSERAE modules docked for larger space station configuration.

TESSERAE Cells

Our volumetric nodes, modeled in the shape of truncated octahedrons for their space-filling properties (Figure 1-3), allow us to take the design theory visions of “growth” patterns and extend this directly to defining a cellular unit of space architecture. From this base unit, or cell, we can define many different functional “tissues” or accretions, thus exploring the application of plesiohedrons to large multi-unit space stations (and perhaps even eventually, to the beloved megastructures of science fiction). Section 4.2.1 discusses the first generation prototype, tested on a 2019 parabolic flight. Section 4.2.2 discusses extension to shapes other than the truncated octahedron and next steps for scaling hardware development of this model. Chapter 5 further explores this Cell model in simulation, using generative algorithms to apply generational fitness constraints and “grow” Cell-based space stations as many individual nodes accrete into bounded shapes. Chapter 6, Section 6.2 discusses how we integrate the requirements for human habitation and aerospace missions into a sample Cell module (docking ports, interchangeability of airlocks, functional zone use by astronauts, environmental control and life support systems, etc.), thus defining an MVU for cellular space architecture.

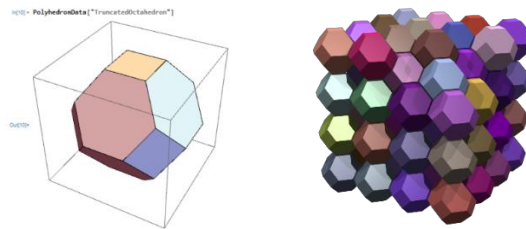


Figure 1-3. From a single TESSERAE Cell base unit, or truncated octahedron, we can form many crystalline-like, densely packed structures.

1.1.3 Space Environment Deployments

We deployed early Technology Readiness Level (TRL – per NASA) miniaturized proof of concept prototypes on parabolic flights (2017, 2019), one suborbital launch (2019), and one 30-day ISS mission (2020). Our November 2017 parabolic flight successfully validated the stochastic magnet-based assembly, with subsets of tiles drawn together over 20-30cm in a matter of seconds. This flight established tile assembly behavior and error modes that we then incorporated into our error-correction control algorithm and used to inform our simulation modeling. Our 2019 zero-g flight and 2019 suborbital launch validated a larger tile set with full sensing, EPM actuation, and control code. The ISS mission tested the largest number of electronics-mediated tiles to date (seven) to assess tile swarm dynamics, a custom EPM design, and holster deployment optimization. This flight successfully demonstrated entirely autonomous error detection and correction, with several correctly diagnosed bonding events in microgravity. These results further calibrate our simulation modeling for on-orbit deployments.

1.1.4 Simulation and Mathematical Modeling

To further assess and connect the hardware proof of concept development to habitat construction at human scale in orbit, we undertook extensive robotics simulation modeling. Working with the Cyberbotics platform for the TESSERAE Shell set, we incorporated rigid body collisions, magnetostatics, friction, Earth’s magnetic field, variable boundary conditions, and input parameters (all in microgravity) to establish a holistic, rigorous physics simulation of the system (Chapter 5, Section 5.2). This simulation yielded particularly impactful

results—optimizing the containment volume (cutting time to full assembly in orbit by half in some cases) and informing the on-orbit power requirements based on records of how many joint corrections (i.e., EPM pulse-off events) go into each successful assembly, among others.

For the TESSERAE Cell nodes, we built a generative design algorithm that automatically generates a matrix of multi-unit space stations, driven by “evolutionary” fitness constraints like maximizing surface area (for solar panel application) or minimizing branches (to keep habitats condensed for radiation protection). The results from these generative runs inform our mission architecture concept of operations (ConOps) for the Cells in Chapter 6 and demonstrate the potential for creativity and non-deterministic assembly in space architecture.

1.1.5 Mission Architectures and Concept of Operations

The self-assembling TESSERAE modules can be autonomously and sustainably constructed and reconfigured as needed in orbit, without astronaut intervention (saving crew costs and time), and without propulsion (saving non-renewable resources and payload mass). Our mission design ConOps proposes a standard suite of modular tiles (Shell model) or nodes (Cell model), including structural units, airlocks, docking ports, windows, etc. These are meant to be interchangeable in LEGO-like style to allow for many permutations and custom mission designs at low “iteration cost” in both microgravity and on-surface contexts. The closed TESSERAE Shell modules, once assembled from tiles, can be joined together to form compound structures of several buckyballs. The volumetric TESSERAE Cell modules, after several units have docked together, can create decentralized space stations of varying geometries. When realized in an orbiting context, this would enable numerous architectural and spatial arrangements (Chapter 6), and could dramatically improve safety (ease of escape pod release in orbit) and robustness (avoiding single point of failure via many modular components to a larger space station).

We aim for TESSERAE to support NASA’s strategic plan for both returning to the Moon and pushing out to Mars. We note a natural extensibility to other microgravity self-assembly contexts, including re-purposing the key technical contributions for autonomous self-assembly of satellites, telescopes or parabolic mirrors, and other in-space infrastructure for space exploration (Chapter 6, Section 6.4); for the purpose of this thesis, however, we remain primarily focused on the habitat application.

1.2 In Summary: Why Self Assembly?

Throughout this thesis, we trace a core idea that informs contributions from the hardware prototype level to the space architecture systems level: the application and generalizability of quasi-stochastic, self-aware self-assembly. This can be *agentless* self-assembly, as seen in nature from protein folding to planetary accretion, but with local and global knowledge of the target structure contained within the tiles. We argue that self-assembly offers a process for in-space manufacturing that saves energy and reduces cost by avoiding consumption of non-renewable propulsion resources. Self-assembly can provide a step-function change in agility and adaptability for the space architect (building on principles of biomimicry and variation), thus offering a path towards scaling and deploying space architecture that does not rely on the capricious political whims that have hampered us for the five decades since Apollo. By starting small and growing sustainably and organically towards the monumental space architecture we yearn for, we may finally achieve the megastructures of science fiction. We have proven that agentless self-assembly need not be chaotic nor entirely random—through the careful definition of base units, jointing, and energy favorable assembly dynamics, we can converge structures into volume-enclosing chambers and multi-module stations. The following chapters chart an interdisciplinary path towards that discovery, in the spirit of the MIT Media Lab, uniting science, engineering, design, and art.

2. Literature Review

Chapter 2

*“As an artist, I got constraints, gravity is one of them.
But within all those constraints I have 15 percent of freedom to make my art.”*

– Frank Gehry

Imagine what Frank Gehry could do without gravity. In this section, we look at the precedents and prior art building up to our ability to conceive of and deploy space architecture in such an environment, and the unique biological and engineering heritage behind self-assembly as our construction mechanism. In addition, we consider the intellectual traditions that inform and inspire our big questions about how to architect life in space.

This thesis attempts to marry two domains for self-aware self-assembly: growth mechanisms across inorganic and organic subjects, and extraterrestrial space structures. Due to the vastness of the former domain, we focus here on the most relevant subset, with particular attention shown to growth mechanisms (e.g. self-assembly, accretion, crystal nucleation; Section 2.1) and engineering building blocks and scaling paradigms that can be intentionally employed as structural design tools (Section 2.2). For the latter domain, we build on both previously realized aerospace habitats (the three to four landmark space stations achieved since the 1970s in LEO, depending on definitions) and theorized aerospace structures (from historical NASA studies to science fiction). Architectural examples are analyzed from a site-based perspective—how modules are constructed (form), docked (growth), and reconfigured (self-awareness). Adding to this analysis, we also consider terrestrial precedents that inform our design theory for TESSERAE, both those that we are pushing back against and those we are leaning towards, from the Structuralists to Buckminster Fuller (Section 2.3). Section 2.4 concludes with a 30,000-foot look at core influences on this work from philosophy, art, literature, and mathematics—because while we may be preparing for life in the vacuum, we’re certainly not designing in one.

2.1 Science and Application of Self-Assembly

To inform a new design theory for space architecture, one built on self-aware and iteratively scalable growth, we build on a mathematical grounding that can tie “organic transformations” together across vast scales—from minute organisms to a metropolis. D’Arcy Thompson’s application of the physical laws of nature to describe biological growth, form, and evolution³ help us extrapolate these same concepts into an entirely new environment and architectural context. Bringing this framing into conversation with Geoffrey West’s arguments for the approximate universality of certain scaling relationships,¹ we can rigorously describe a model for dynamic, self-aware space structures that are informed by both inorganic and organic growth processes in complex, Earth systems. Our goal is to realize “indeterminate growth” space architecture, an entanglement between both natural and artificial processes,⁴ across a time horizon that is both immediately present and long enduring—aspiring to the Long Now⁵ view for vessels of our Space Exploration future.

This thesis builds on research in the emerging coupling of biology and architecture^{6, 7} and biomimetic approaches for material design and fabrication.^{8, 9} However, the inspiration drawn from nature and biology for this thesis lies primarily in the evolution and responsiveness of structural form—a new genetic code for the assembly of space architecture—rather than in literal biological material choice (as the latter would not survive against outgassing in the vacuum).

At the smallest scales, we draw on self-assembly processes from chemistry, DNA molecular assembly, and protein folding. Noting the voluminous work of George Whitesides, Sr., on this topic, we take inspiration from his micro¹⁰, meso¹¹, and macro^{12, 13} scale endeavors. Even at larger scales, self-assembly processes are still modeled after DNA molecular assembly and use an “annealing ramp” approach.^{14, 15} We note additional work in macro and meso scale self-assembly out of the MIT Self-Assembly Lab, where the geometry of each sub-part is tuned to induce accretion into the desired whole, such as lock and key physical joints or magnet bonding pairs.^{16, 17} This involves tuning inputs or “stirring energy” (e.g., vibration and shaking) to circulate units and converge a multi-part system into a cohesive whole. The Lab’s work also explores self-assembly in a bio-inspired context, with plastic “chiral assemblies” that are shaken stochastically into final form to simulate biomolecular processes. In collaboration with Autodesk, their results show potential for embedding logic in many small parts, that when brought into contact with sufficient randomness and circulation, can dynamically self-assemble into predicted shapes. In a different approach, their work on self-folding surfaces uses built-in restoring forces and spring forces to actuate a final shape after an initial perturbation. Without the need to counteract the force of gravity, we have shown that similarly-jointed base units (in our case, polygon tiles with magnet joints) will assemble in shorter time-scales.

In addition to motion-driven or stochastic self-assembly, the MIT Self-Assembly Lab explores fundamental units where the final-state configuration logic is embedded in the fabrication of the constituent parts. In “Biased Chains,” a connected chain of plastic nodes can be held at the end and shaken into a desired sequence of folds.¹⁸ Though the individual nodes are still connected manually, subsequent configuration states of the chain are encoded via the “biased direction” introduced in each base unit. Many further examples abound in other fields, using clever geometries to bias self-assembly, folding, or accretion towards a desired end state.^{19, 20, 21} We take a similar approach in our work and push this further by translating these principles into 3D, macroscale objects and by removing manual construction steps. By carefully designing the tile geometry (e.g., size, dihedral bonding-edge bevel) and the magnet polarity jointing, we embed physical logic in the assembly protocol and can constrain the assembly to a buckminsterfullerene, for example, for the TESSERAE Shells.

The self-assembling sample prototype system for this thesis, TESSERAE, combines these various approaches, as we design the tiles’ physical geometry, the magnet polarity arrangement along tile bonding faces, and a quasi-stochastic annealing ramp via sensor-mediated EPM actuation to direct the self-assembly process into the desired configurations. Additive and subtractive modes of assembly have been previously explored in 2D, water-supported systems²² and 3D “pebble” rearrangement, respectively.²³ TESSERAE uniquely combines the additive, self-assembly and subtractive, self-disassembly approaches with a new polarity map (additional degrees of freedom with more magnet attachment points) and a quasi-stochastic actuation approach in 3D microgravity spaces. The combined function of our custom EPMS affords us this flexibility for both accretion and on-demand separation of the nodes.

TESSERAE also builds on prior research in control algorithms for self-assembling swarms that exchange data between members.^{24, 25} Tiles in our system are augmented with custom sensor Printed Circuit Boards (PCBs) that facilitate data exchange between neighbors as well as globally, across the system. We note prior art in scalable communication and data architectures for swarm dynamics, coming out of Radhika Nagpal’s Self-Organizing Systems Research Group at Harvard University, and their work on “Kilobots”—a bio-inspired robotic swarm²⁶. Their work explores self-assembly in a different context, with a focus not on bonding assembly but rather the data architecture, algorithmic development, and start-up tasks (i.e., power charging) required for a swarm of over a thousand small robots to perform tasks, move, and communicate as a collective. The Kilobots are currently restricted to a 2D plane but nevertheless offer an enlightening example of how to scale communication and power-management tasks across many nodes.

TESSERAE inherits its coded self-assembly from a long line of research into “Programmable Matter”²⁷ including EPM actuators developed by Ara Knaian²⁸ (with whom we had the pleasure of collaborating for the EPMS on the ISS mission; Chapter 4, Section 4.1.3), Neil Gershenfeld’s broad application to functional surfaces,²⁹ and Wood et al.’s inquiries into programmable folding.³⁰ We have seen the science fiction desire for truly nano-scale, programmable matter grow considerably from early provocations by Richard Feynman³¹ to the work of K. Eric Drexler that later became known as Molecular Nanotechnology (MNT) and assemblers.³² This is evidenced in aspirational science fiction as different as Neal Stephenson’s cyberpunk³³ and popularized swarms of “microbots” that take shape and assemble in the Oscar-winning animated feature *Big Hero 6* (which credits Gershenfeld and MIT’s Center for Bits and Atoms). Recent work in infrared mediated interactivity between modular PCB-augmented tiles, “AutomaTiles” (now Blinks) by Jonathan Bobrow,³⁴ also contributes ideas in this area via a 2D plane for programmable matter. Bobrow’s work influenced our sensor node design, and while we ultimately settled on Bluetooth Low Energy and a different communication architecture, we note the infrared emitters approach (also used in Nagpal’s Kilobots) as an additional functionality to consider for future work. All together, the promise of programmable matter is vast—we take this notion into the microgravity and space environment context, where individual nodes are freed to circulate and accrete in new ways, to create programmable matter at the space scale.

While prior art has extensively analyzed 2D self-assembly in normal gravity environments and limited 3D self-assembly without active control, we believe TESSERAE to be the first microgravity-based, three-dimensional self-assembly system with error detection and self-correction; we are thus interested in modeling and simulation to fully characterize both desirable and undesirable assembly states as we tune parameters that affect quasi-stochastic, self-aware behavior in three dimensions and explore this extensively in the simulation modeling (Chapter 5).

2.2. Engineering Precedents

2.2.1 Sensing

The sensor suite acting in the TESSERAE tiles is core to the entire operation. In the spirit of truly “responsive environments,”³⁵ we aim to facilitate space architecture that can support informative, environmental data exchange and structural status between tiles before, during, and after self-assembly. This functionality relies on pervasive sensing and builds on work in multi-modal, sensor-mediated units^{36, 37} and augmented “skin” surfaces that can be employed as the technical basis for “self-aware” interactivity.³⁸ Our early circuit designs drew directly on environmental sensing nodes from the Paradiso Lab, deployed in nature and optimized for low power consumption.³⁹ By expanding and translating this work to the space environment, and varying the particular suite of sensors to match our data needs while retaining the theory and pervasive sensing approach, we can enable sensing across scales.

2.2.2 Magnets

Development of novel magnets in recent years has greatly expanded the palette available to engineers and designers looking to passive and active magnetic fields for actuation purposes. While we ultimately decided to design and fabricate our own custom electro-permanent magnets (EPMs) for the capstone hardware work of this thesis, owing to the particular features required in our deployment context, we did consider several off-the-shelf options and tested APW EPMs⁴⁰ extensively in our suborbital hardware platform. Similar magnets exist at much larger dimensions and field strengths,^{41, 42} off of which we base our feasibility review for actuating EPMs for much larger, habitat-scale tiles (Chapter 6). While not immediately necessary for the TESSERAE technology roadmap (as we benefit currently from simplifying magnet joints to reduce the total complexity of the system rather than making them into lock-and-key joints), we do note the potential of Polymagnets⁴³ with their pixel-level control and unique, non-traditional polarity maps for future work.

2.2.3 Engineering Building Blocks and Direct Aerospace Applications

MIT’s Center for Bits and Atoms (CBA) has demonstrated innovative assembly and reversibility protocols for lattice structures, notably carbon fiber-reinforced units that feature reversible shear clip joints.⁴⁴ We consider a similar principle, relying instead on magnets to provide joint connection and subsequent detachment flexibility. Langford and Ghassaei, also of the CBA, demonstrate a pattern of interlocking tabs for 3D circuits that could be extrapolated to other assembly protocols.⁴⁵ We may later begin to integrate the EPMs of the TESSERAE bonding joints more directly into modular circuits, building on further CBA work by Nadya Peek.⁴⁶ In recent work with NASA Ames’ Kenny Cheung and through Ben Jennet’s PhD thesis work, the CBA has explored agent-based hierarchical assembly of spacecraft⁴⁷ and other space structures.⁴⁸ While TESSERAE builds on certain of these engineering building block concepts, we diverge to focus on *agentless*, swarm-inspired self-assembly and embrace a quasi-stochastic assembly paradigm.

The TESSERAE assembly plan uniquely combines several existing aerospace technologies. In the aerospace engineering context, the most informative precedents for in-space mobility, self-assembly, and magnetic docking come from work in the MIT Space Systems Laboratory (SSL)—nearly two decades of development engineering and ISS time for SPHERES (Synchronized Position Hold Engage Reorient Experimental

Satellites).⁴⁹ We note related work by NASA⁵⁰ and Weber et al.⁵¹ in this area for demonstrating feasibility of magnetic docking approaches, and we build on electromagnetic formation flight out of the MIT SSL, including the Kong⁵² and Getliffe⁵³ PhD theses, for our magnet-mediated self-assembly. Recent work out of the European Space Agency (ESA) has generated a theoretic model for the behavior of EPMS for self-assembly of satellites and miniature spacecraft like PocketCube,⁵⁴ building on a tradition from Dario Izzo’s prior work on swarm, formation flight, and inter-satellite coulomb forces.⁵⁵ While not deployed in an aerospace environment, the concept of magnet-jointed frames self-assembling via drone work has been previously explored as a teaching tool for mechatronics and integrated control at ETH Zurich.⁵⁶

Beyond direct assembly, the TESSERAE in-orbit deployment steps require a temporary, flexible membrane to encapsulate payload elements and undergo autonomous inflation (building on various previously explored concepts for balloon inflation in aerospace contexts^{57, 58}) upon reaching the intended deployment orbit. This ensures that the component tiles are kept in relatively close proximity when released into the microgravity environment, to improve the likelihood of finding neighbors (ensuring that magnets need only act over short ranges, per the $1/r^2 - 1/r^4$ drop off in magnetic force depending on magnet geometry).

2.3 Terrestrial and Space Architecture Precedents

2.3.1 Terrestrial Precedents

Inorganic

The impact that Buckminster Fuller has had on this thesis cannot be overstated. While we ultimately envision the TESSERAE platform moving far beyond just geodesic domes (Figure 2-1),⁵⁹ the architectural father of the later-discovered (and named in his honor) buckminsterfullerene⁶⁰ provided not only the initial architectural inspiration but also a philosophical one. From the self-sustaining principles of his Dymaxion house⁶¹ to the moral and ethical framing of an *Operating Manual for Spaceship Earth*,⁶² Bucky Fuller laid the intellectual groundwork for sustainable, self-assembling space architecture. In his honor, we discuss our dedication to extending the principles of TESSERAE to robust shelter for resource-constrained human communities on Earth at the close of Chapter 6 (Mission Architectures).

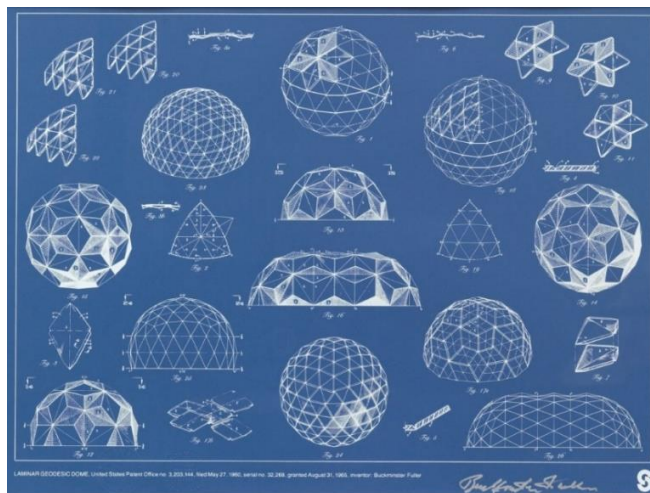


Figure 2-1. A figure from Bucky Fuller’s 1965 patent for laminar, geodesic domes. ⁶³

Moving from geodesic domes to other modular, nesting, and serial structures, we note the influence of the Structuralists.⁶⁴ While we hope to free future space architecture from the rectilinear forms and almost excessive regularity that dominated much of their realized architecture (e.g., the Amsterdam Orphanage of the Dutch Structuralists, shown in Figure 2-2), their focus on the interplay between social and cultural aspects⁶⁵ and the way in which architecture should be responsive to these forces encourages us to consider the same. In Chapter 3, we explore ways to design in concert with the space environment, rather than in opposition to it. The modularity of these structures still incorporated a certain playfulness and we hope to infuse the modular TESSERAE stations with the same potential. The Metabolist's integration of modular building parts with an organic-inspired architectural philosophy⁶⁶ influences the TESSERAE design theory as well; we also juxtapose a vision for biomimetic growth and expandability of our structures against a near-term reality of regular building units to meet the practical requirements of aerospace manufacturing and deployment. We diverge from both these movements however, in more explicitly facilitating unplanned, non-deterministic growth of structures through stochastic processes and designing towards a future where the base-units themselves can be curvilinear, soft, organic and inviting.

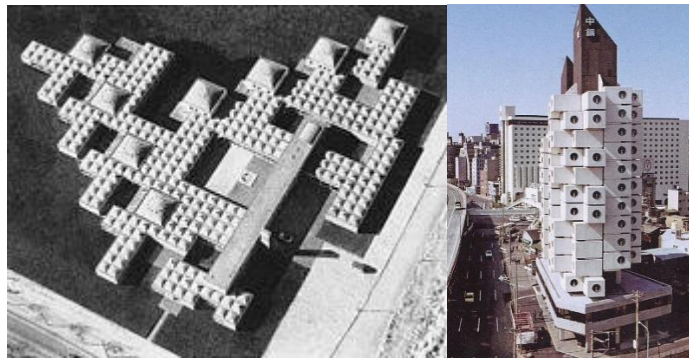


Figure 2-2. Dutch Structuralists and the Amsterdam Orphanage (Left), juxtaposed with the Metabolist Nagakin Capsule Tower (Right).

To combine the practicality of the seriality and nesting of structuralism with a more heartfelt homage to the botanical, we look to parastichy in the natural world. While explored in more detail in Chapter 3, we find examples of this type of phyllotaxis in Persian architecture, particularly through the introduction of the muqarnas⁶⁷ in Safavid buildings. As Arthur Pope notes, the rich tiling and architectural features of Persian buildings give “a marked feeling for form and scale; structural inventiveness, especially in vault and dome construction; [and] a genius for decoration with a freedom and success not rivaled in any other architecture.”⁶⁸

In the context of space architecture, where for the last two decades on the ISS every choice has been carefully and meticulously planned for co-living, we take the Schindler House experiment as a warning.⁶⁹ While beautifully designed in a configuration to support collaborative living, and now considered a hallmark of California architecture and architectural elegance, the architectural choices did not guarantee peaceful habitation (nor marital bliss) for its original inhabitants. Human activity cannot be entirely programmed by physical space. In the spirit of Umberto Eco, in our architectural planning we should decide to “leave arrangements of some constituents of a work to the public or to chance”⁷⁰—or perhaps to the future astronauts and space tourists who will join us there.

Organic

While the design theory (Chapter 3) deals extensively with Nature’s prior art, we focus here on a selection of the bio-inspired architecture most relevant for direct precedent. Building on the work of Lorna Gibson and the notion of cellular solids,⁷¹ we define a “cellular” unit of space architecture. While our prototyped forms have yet to achieve the same organic curves and smooth definitions found in foams and other cellular solids as defined by material science (though our future work points us in this direction), we establish the technical basis on which to build scaffolds of multi-unit, densely packed space architecture based on these cellular solid concepts. Some architects have explored speculative application of cellular solids—in the more traditional sense—directly to space architecture, including Greg Lynn⁷² and Julia Koerner.⁷³

Neri Oxman’s notion of material ecology⁷⁴ grounds our work in a metaphorical way—while we are severely constrained to non-outgassing materials for exoskeletons that will operate in the vacuum of space, we still take inspiration from the possibility that material could take a driving role in the nature of space architecture. Our “materials,” in this case, are not the raw materials likely to be found in space habitats (e.g., aluminum, carbon fiber, and Kevlar) but rather the TESSERAE nodes themselves that should accrete and join together like cells of a macro-structure joining together into a functional tissue. These are materials that self-assemble and define the nature of a structure through the density or porosity of their accretion (i.e., whether we create bulky, globular space stations for radiation protection, or branching, fractal space stations for maximizing surface area and power generation). As many have before, we draw inspiration from E.O. Wilson’s focus on the promise of biophilia in design,⁷⁵ and note prior work from T. McNulty in building the frameworks^{76, 8} that would enable us to realize this in aerospace materials and aerospace structural engineering.

2.3.2 Space Architecture Precedents

Often touted as one of the fathers of modern rocketry, Konstantin Tsiolkovsky was speculating on spherical spaceships (Figure 2-3), generating artificial gravity and how to best arrange the interior divisions of a spacecraft in 1895.⁷⁷ Fast forward just over 100 years, and humanity sees off the first of many launches to construct the ISS in 1998.⁷⁸ NASA has long relied on astronauts and careful robotic arm maneuvers to attach new modules and components in space,⁷⁹ and in recent years, has begun to explore modular building blocks for space stations.⁸⁰

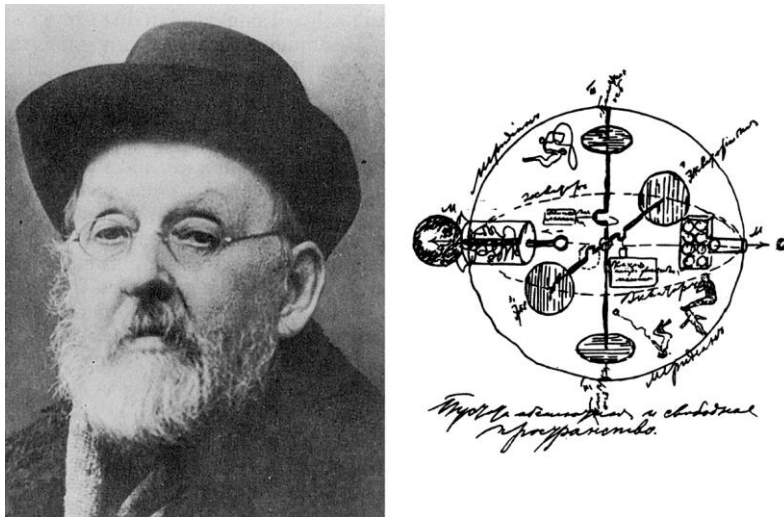


Figure 2-3 Konstantin Tsiolkovsky with his 1895 drawing of a spherical spaceship.⁷⁷

We note the BEAM inflatable habitat⁸¹ and Bigelow's next generation B330, an autonomous, stand-alone space station,⁸² as fellow examples of architecture that can be condensed for launch via flat-packing in a rocket payload fairing. Our modular approach yields the additional benefit of modularity and re-configurability at the shell level, which the BEAM model does not include (one cannot easily remove and change out segments of the BEAM inflatable walls, as is possible with TESSERAE base-unit tiles; Chapter 6, Section 6.1.3). Beyond inflatable module concepts, we also note prior work in essentially self-deploying, origami-inspired space structures (currently for open form, unfurling surfaces like James Webb,⁸³ Starshade,⁸⁴ and tensioned arrays⁸⁵). Notions of expandability and growth in space architecture can be found going back to the 1970s, including Gui Trotti's study at Rice University.⁸⁶ Modular assembly of space habitats has been explored by de Weck et al., including use of the truncated octahedron for its space-filling properties that TESSERAE also employs for the Cell nodes.⁸⁷ The literature review in de Weck's 2005 analysis point us to a rich history of standardization, interoperability design, and modularity in space structures. We present a condensed version of their review here, including Frisina's work on densely packing space structures for launch based on triangular faces,^{88, 89} and the interoperability and interchangeability with other models from the early work of Baily et al.,⁹⁰ Harwood et al.,⁹¹ and Abbot et al.,⁹² for standardization of interfaces, docking systems and reconfigurable spacecraft, respectively. Newman et al., further discuss how to incorporate principles of flexibility into aerospace system design.⁹³ Finally, we draw on the trenchant observation that cost, rather than strictly performance or engineering ingenuity, now drives the space program⁹⁴ after the geopolitical motivators of the Apollo era waned and the calculus of political budget planners changed. We intentionally offer TESSERAE as a platform for iterative, incremental growth with only modest resources required for each additional Shell set or Cell node module, in an explicit attempt to jumpstart progress on sustainable expansion of human activity in space that does not depend on political whims.

Recent developments out of Silicon Valley startup Made in Space lead us to envision a future where our self-assembling tiles are even fabricated in-situ, via advances in zero-gravity 3D printing and in-orbit material recycling.⁹⁵ While other pre-constructed geodesic dome objects have been sent into orbit for artistic or demonstration purposes, we believe the TESSERAE Shells to be the first proposal for an operational, reticulated shell space habitat, and the first proposal for a buckyball form factor to be constructed via self-assembly in orbit. We find no direct precursor for the organic, tissue-like accretion plan for multiple TESSERAE Cells, with most modular space stations instead depending on pre-planned, axis-based arrays of modules (like the proposed Gateway⁹⁶ and Axiom⁹⁷ Stations).

At the multi-module scale, when planning for the aesthetic, radiation shielding, and interior-use considerations that must come into play for a functional space habitat, we note Constance Adams' focus on designing the human domain for long-duration space facilities,⁹⁸ and Sherwood's analysis on the reality of how such structures will be used in lunar urbanism contexts: "they will be densely populated, hermetic, shielded and interior but kinesthetically expansive and visually lightweight."⁹⁹ We take this guidance to shape our architectural interior design for both microgravity and surface-based applications of TESSERAE. As the domain of space architects widens, many other creative voices are joining this community as well, reviewed in 2014 by Neil Leach.¹⁰⁰

For the future exterior cladding, we look to recent advances in aerospace-grade fabrics and "space skins" that, while originally designed for astronaut suits, could also serve a dual role as self-aware, sensor-mediated surfaces that detect micrometeoroid impacts, gas leaks and other dangers in orbit. We build on the extensive work of Dava Newman in this area,^{101, 102, 103, 104} and emerging work in the Paradiso Lab for woven fibers with embedded piezoelectric functionality.¹⁰⁵ Olga Bannova's analysis of resource-constrained analogs on Earth,¹⁰⁶ Darlene Lim's work on BASALT,¹⁰⁷ and Gui Trotti's design of self-sustaining environments for Earth, space and sea,¹⁰⁸ all inform our understanding of a space architect's responsibility: to consider how our technology for modular, robust, easy-to-assemble architecture could be used to help populations on Earth.

To further guide TESSERAE development, we undertook a detailed review and comparison between the four core examples of realized space architecture (combining the Salyut and Tiangong approaches for their structural similarities) and four core examples of near-term, theorized, or prospective space architecture. We compare features from the Salyut (1971–1986, Figure 2-4)¹⁰⁹ and related Tiangong series,¹¹⁰ SkyLab (1973–1974, Figure 2-5),¹¹¹ Mir (1986–2001, Figure 2-5),¹¹² and ISS (1998–present, Figure 2-6)⁷⁸ to establish a gradient of already-explored technologies and architectural paradigms. While countless imaginative examples abound, we identify the Stanford Torus (Figure 2-8),¹¹³ Gerry O’Neill’s Bernal Sphere (Figure 2-9),¹¹⁴ the Orion spacecraft (Figure 2-10),¹¹⁵ and the Lunar Orbital Platform Gateway (Figure 2-11)⁹⁶ as the most rigorously envisioned and relevant theorized or under-development space structures for additional prior art. While this particular chart set does not include the prospective Axiom station, Bigelow’s B330, nor the NanoRacks Outpost, we do examine these examples in a more exhaustive “design space” comparison in Chapter 3.

A note on the terms used below:

- The definition of “self-awareness” in this context centers on the structure’s perception (embedded sensing and responsivity), independent actuation ability (autonomous actuation, robotics, self-healing, etc.), and knowledge of both local and global information aiming towards a target structure.
- Re-configurability is granted to a space architecture example at two levels: (a) if the shell material constituting a module can be removed, replaced or remixed and (b) if the module itself can be moved around to accommodate changing macro structures.

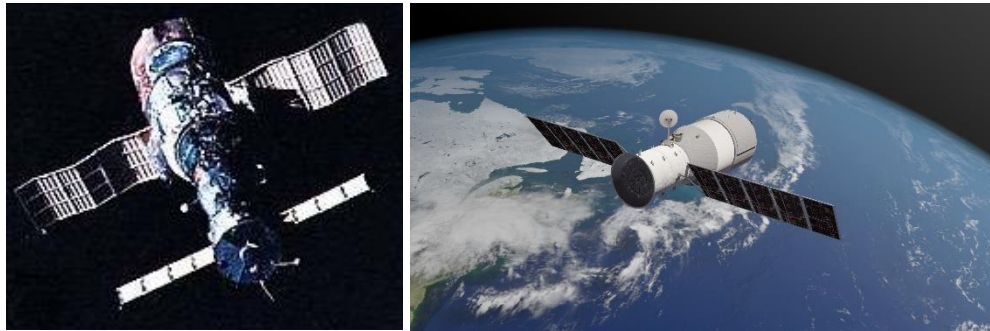


Figure 2-4. Left: Salyut Station; Right: Model of Tiangong. Image credit: Creative Commons.

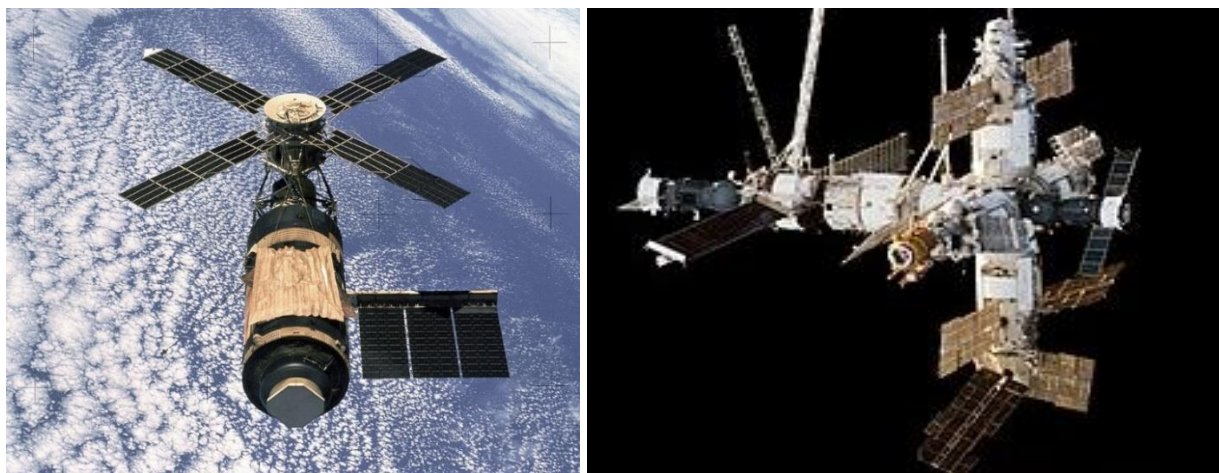


Figure 2-5. Left: Skylab; Right: Mir. Image credit: NASA and Creative Commons, respectively.

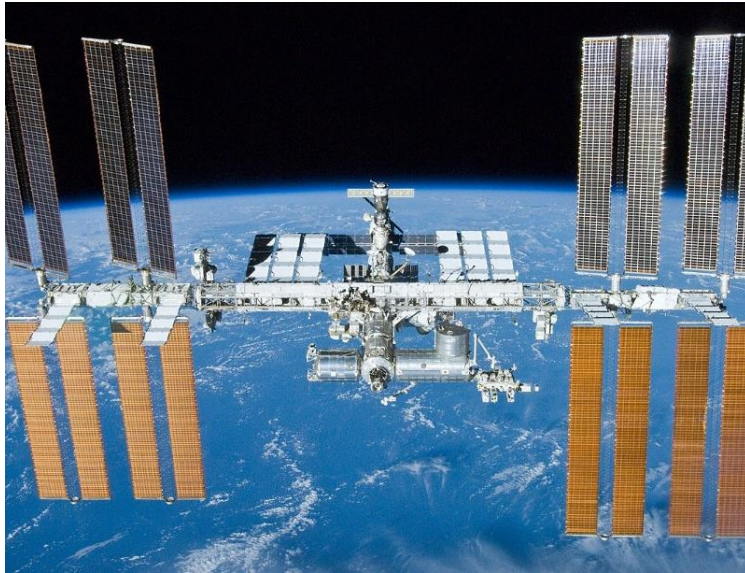


Figure 2-6. International Space Station. Image credit: NASA.

	Salyut/Tiangong	Skylab	Mir	ISS
Assembly Construction Steps	<p>Overview: Discussed for Salyut 1 (first human space station in orbit). Launched in single payload, but part of a further series launched subsequently.</p> <p>Launch count for full assembly, per Salyut station entity: 1 (7 generations total)</p> <p>Docking ports: 1</p> <p>Pressurized volume: 90m³</p>	<p>Overview: Launched via Saturn V (last mission to do so), suffered major assembly damage including full loss of one solar panel array.</p> <p>Launch count for full assembly: 1</p> <p>Docking ports: 2</p> <p>Pressurized volume: 352m³</p>	<p>Overview: Launched via Proton rockets and one U.S. Space Shuttle mission. First multi-module, with n>1 primary spacecraft. Dawn of “Space Architecture.”</p> <p>Launch count for full assembly: 7</p> <p>Docking ports: 1 aft; 5 in spherical docking module at forward end</p> <p>Pressurized volume: 350m³</p>	<p>Overview: Launched via U.S. Shuttle and Russian Proton and Soyuz rockets, continually adapted and added to from inaugural module in 1998 to 2016 (BEAM), to prospective NanoRacks Bishop Airlock.</p> <p>Launch count for full assembly: 27 (counting only major modules and structural changes)</p> <p>Docking ports: 8, including cargo berths</p> <p>Pressurized volume: 931m³</p>
Growth Approach	<p>Overview: None in Salyut 1. Salyut 6 and 7 feature 2 docking ports, allowing influx in crew size and resource exchange via Soyuz craft. Proposed models for next two Salyut generations became Mir Core Module, and Zarya Module for ISS.</p>	<p>Overview: None undertaken due to short lifecycle.</p>	<p>Overview: Staged growth over 9 years, incremental addition of self-contained modules via docking ports. Growth plan evolved to meet changing mission needs.</p>	<p>Overview: Staged growth over 22 years and counting, incremental addition of self-contained modules via docking ports. Growth plan evolved to meet changing mission needs.</p>
Structure & Function	<p>Geometry: Monolithic; expansion along single linear axis</p> <p>Shape: Cylinder</p> <p>Config: Single unit</p> <p>Use: Passive – shielding & containment</p>	<p>Geometry: Monolithic; expansion along single linear axis</p> <p>Shape: Cylinder</p> <p>Config: multi-part design, single core unit</p> <p>Use: Passive – shielding & containment</p>	<p>Geometry: Polyolithic; three-dimensional, linear growth along X, Y, and Z axes</p> <p>Shape: Cylinder</p> <p>Config: seven distinct pressurized modules</p> <p>Use: Passive – shielding & containment</p>	<p>Geometry: Polyolithic; three-dimensional, linear growth along X, Y, and Z axes</p> <p>Shape: Cylinder</p> <p>Config: 16 distinct pressurized modules</p> <p>Use: Passive – shielding & containment</p>
Self-Aware Assembly?	<p>Overall: No</p> <p>Docking: Autonomous + Manned</p> <p>Re-configurability: None</p>	<p>Overall: No</p> <p>Docking: Manual (astronaut mediated)</p> <p>Re-configurability: Emergency repair undertaken via EVA</p>	<p>Overall: No</p> <p>Docking: Autonomous + Manned, drogue-assisted EVA (astronaut mediated)</p> <p>Re-configurability: rudimentary ability to shift Kristall module to accommodate Shuttle Atlantis</p>	<p>Overall: Partial</p> <p>Docking: Russian modules docked robotically, others docked manually via Canadarm2 and EVAs</p> <p>Re-configurability: Reconfigured from Space Shuttle-optimized configuration, to commercial crew and cargo vehicles</p>

Figure 2-7. Comparison matrix for Salyut, SkyLab, Mir and ISS.

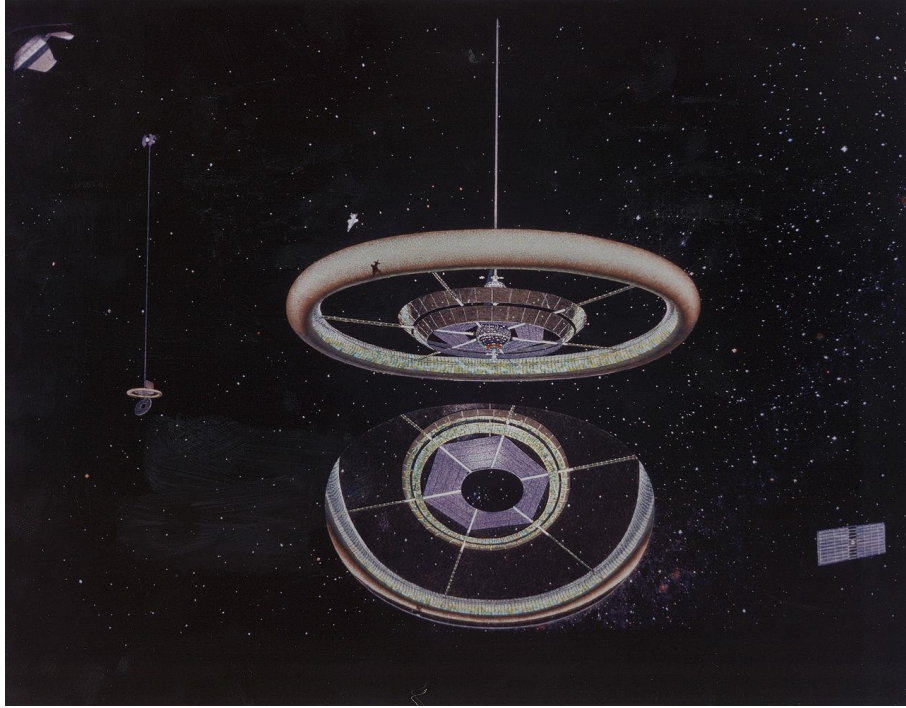


Figure 2-8. Stanford Torus, 1975 NASA Summer Study. Image credit: Creative Commons.

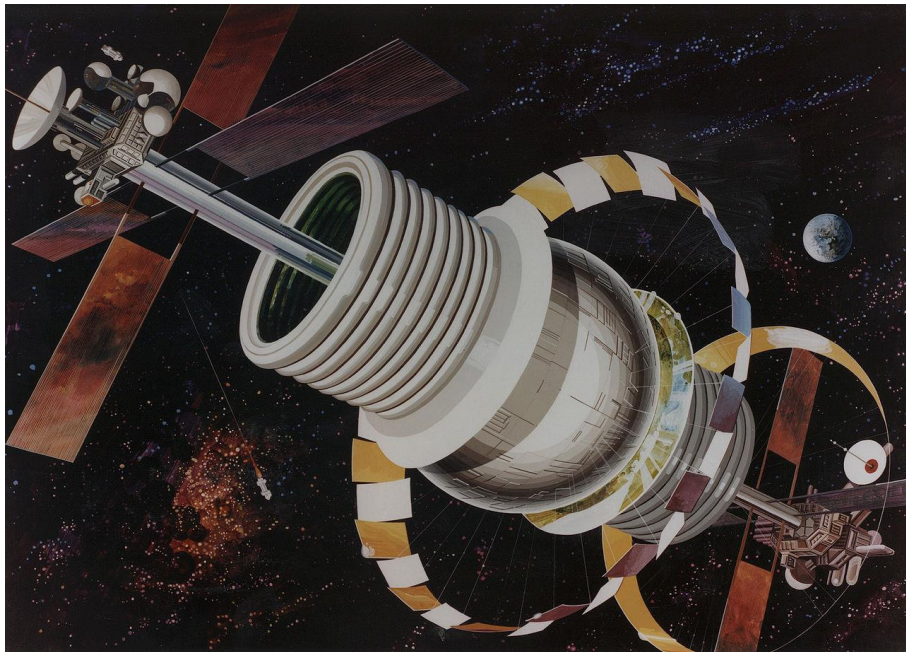


Figure 2-9. Bernal Sphere. Image credit: Creative Commons.



Figure 2-10. Prospective Model of Orion spacecraft. Image credit: NASA.

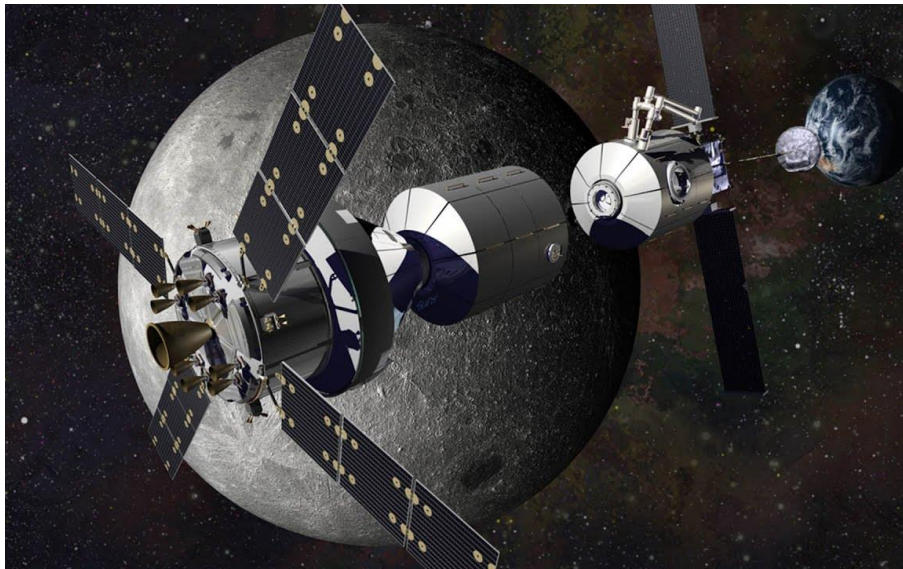


Figure 2-11. Prospective model of Gateway Station. Image credit: Lockheed Martin.

	Stanford Torus	Bernal Sphere	Orion	Gateway
Assembly Construction Steps	<p>Overview: Concept design studied by NASA in 1975; Ring based super-structure to house 10,000–140,000 permanent space residents; 1.8 km in diameter</p> <p>Launch: moon extraction for materials, launched to L2 via mass-driver, transported to L5; custom materials from Earth</p> <p>Docking ports: inner disk docking bay (minimal rotation)</p> <p>Pressurized volume: 6.9x10⁷m³</p>	<p>Overview: Concept proposed in 1929, revamped by Gerry O’Neill in 1975–1976; hollow spherical shell to house 10,000 people; 500m in diameter (O’Neill)</p> <p>Launch: comparable to Stanford Torus</p> <p>Docking ports: at both ends of axial extension</p> <p>Pressurized volume: ~6.54 x 10⁷ m³</p>	<p>Overview: Exploration travel spacecraft concept under active development by Lockheed Martin/Airbus for NASA & ESA (not to be confused with 1958 Orion)</p> <p>Launch: Single launch (tested on Delta IV); to be deployed via SLS</p> <p>Docking ports: available for crew transfers</p> <p>Pressurized volume: 19.6m³</p>	<p>Overview: Exploration staging-base spacecraft for lunar orbiting missions, under NASA review</p> <p>Launch: To be deployed via SLS, likely multi-launch</p> <p>Docking ports: available for crew transfers & influx in crew size</p> <p>Pressurized volume: ~125m³</p>
Growth Approach	<p>Overview: Continuous fabrication of the ring super-structure, with colonization taking place as sections are completed. No proposals for later add-ons.</p>	<p>Overview: Limited plans known; construction of the sphere was primary concern</p>	<p>Overview: None; intended for transit akin to Apollo module</p>	<p>Overview: Likely staged growth over various launches, evolving to meet lunar mission needs</p>
Structure & Function	<p>Geometry: Monolithic; closed topology, no expansion planned</p> <p>Shape: Torus</p> <p>Config: Single ring super-structure, with central hub and spokes</p> <p>Use: Active – ring interior supports life systems directly; rotates to provide partial gravity</p>	<p>Geometry: Monolithic; closed topology, no expansion planned; likely expansion along single linear axis if needed</p> <p>Shape: Sphere</p> <p>Config: Single module super-structure</p> <p>Use: Active – shell interior supports life systems directly; rotates to provide partial gravity</p>	<p>Geometry: Monolithic; likely expansion along single linear axis if needed</p> <p>Shape: Conical</p> <p>Config: multi-part design, single core unit</p> <p>Use: Passive – shielding & containment</p>	<p>Geometry: Polyolithic; expansion along single linear axis</p> <p>Shape: Cylinder</p> <p>Config: proposal for at least seven distinct modules</p> <p>Use: Passive – shielding & containment</p>
Self-Aware Assembly?	<p>Overall: Partial</p> <p>Docking: Supported via central hub, no explicitly provisions for autonomy</p> <p>Re-configurability: None; outside scope [major limitation] **could have considered stackable rings, or nested rings like atom model</p>	<p>Overall: No</p> <p>Docking: Supported via axial endpoints</p> <p>Re-configurability: None; outside scope</p>	<p>Overall: No</p> <p>Docking: Supported via single adaptor point</p> <p>Re-configurability: None; outside scope</p>	<p>Overall: Partial</p> <p>Docking: Supported via single adaptor point</p> <p>Re-configurability: to be determined by mission needs</p>

Figure 2-12. Comparison matrix for Stanford Torus (conceptual), Bernal Sphere (conceptual), Orion (planned), and Gateway (planned).

Our research builds on the prior art discussed above to both (a) offer a technically rigorous engineering approach to realize self-assembly of space structures and (b) adapt best practices in space architecture design and ConOps to make TESSERAE a feasible near-term solution for space habitats. We have combined the distinct fields of self-assembly and space architecture to propose an extensible construction paradigm in orbit.

2.4 Theoretical Underpinnings: Mathematics, Philosophy, Literature, and Art

The TESSERAE paradigm for scaling growth draws extensively on Geoffrey West’s *Scale: The Universal Laws of Growth, Innovation, Sustainability, and the Pace of Life in Organisms, Cities, Economies, and Companies*¹ and Eric Smith’s transformative *The Origin and Nature of Life on Earth*.¹¹⁶ We leverage Smith’s focus on the centrality of non-equilibrium phase transitions in the evolution of life from the planet’s early geochemistry to inform how we think about energy favorability. How can we drive or converge the TESSERAE tiles towards a convergent assembly? Specific influences from D’arcy Thompson’s *On Growth and Form*³ have been presented previously, but we include the work again here to honor the extent to which Thompson’s approach integrates the organic with principles from mathematics—we strive to do the same with TESSERAE. To this point (while discussed in greater detail in the design theory in Chapter 3), we note the considerable impact that Mandelbrot’s² and Michael Frame’s¹¹⁷ work in fractals has had on the shape and form choices, juxtaposed with a biomimetic growth framework, in this thesis.

The thesis also draws on the philosophical principles of the Long Now foundation⁵ and Japan’s Ise Shrine,¹¹⁸ planning ahead for the rebuilding and regeneration of spacecraft over the time scales inherent to our expansive cosmos. While we try to avoid an overly utopian vision of this, keeping the technology contributions focused on practical, realizable achievements, we still take inspiration from optimistic, far futuristic visions for humanity and the space environment from literature and science fiction.³ And finally, the Mori Building 2016–2017 Universe and Art Exhibit, led by Nanjo Fumio, provided an unparalleled view into the scientific, engineering and design visual history of space exploration—from Galileo’s earliest drawings to the stunning Super-Kamiokande neutrino detector to the Mars Ice House—and in doing so, profoundly inspired our desire for TESSERAE to be one day worthy of that tradition.

³ Including formative ideas from Thomas Moore’s Utopia, Gerry O’Neill, Neal Stephenson, Larry Niven, Arthur C. Clark and Gregory Benford, Asimov, and of course, Gene Rodenberry’s Star Trek (particularly The Next Generation with Picard), among others.

3. Growing Space Architecture: A New Design Theory

Chapter 3

“The clearest way into the universe is through a forest wilderness.”

–John Muir

As humanity prepares for the commercialization of LEO and interplanetary civilization, we face an opportunity for a renaissance in space habitat design. Realized space architecture, to this point in history, has been dominated by just a few prominent examples: Salyut, SkyLab, Mir, Tiangong, and the International Space Station (ISS). These structures nearly universally rely on pre-fabricated, cylindrical modules with bespoke module-to-module interfaces. Given the anticipated rise in orbital space travel (“space tourism”), the renewed focus on crewed, martian exploration missions, and NASA’s transition plan for space habitats from government-run to independently-managed, we expect a proliferation of orbiting space stations in the next decade (Axiom, Lunar Gateway, Tiangong-3, and several others). This beckons for a holistic evaluation of space architecture. How can we build safer, more efficient, reconfigurable, and adaptable—but also profoundly inspiring or enlightening—space structures?

As we prepare to venture into deep space, we face an inflection point for self-aware space structures. Can we free space architecture from static, single-use module design and a survivalist design aesthetic, and instead enable dynamic, abundant space structures that “grow” and evolve over the course of a mission and even generations of use?

This chapter presents the design theory contributions for the thesis, focusing on a biomimetic design framework to ground the growth paradigm for self-assembly in orbit. We discuss the unique applicability of indeterminate growth to the space environment (Section 3.2) and consider how we can design in concert with the particular affordances of microgravity, unabated incident solar energy, and the vacuum (Section 3.3). Section 3.4 introduces a design tool for exploring the parameter space of microgravity space architecture, comparing the TESSERA Shell and Cell models to all known real and prospective space habitats and a selection of the most compelling mega-structures from science fiction. While primarily occupied with the structure, form, and function of a new generation of space architecture, we are keenly interested in evoking wonder and provoking curiosity for future inhabitants as well, and have included an aside (Section 3.5) on aesthetics “worthy of life in space,” and a life in space worthy of the patterns of nature. We conclude in Section 3.6 with a summary motivating the focus on biomimicry-inspired self-assembly for this thesis. This chapter draws heavily from text in our 2019 IAC Space Architecture paper.¹¹⁹

3.1 A Biomimetic Framework

Humanity faces the dawn of interplanetary civilization, emerging from a domain rich in the complexity of life into a great expanse which, while it may ultimately reveal life, presents for now mostly inorganic matter. The extreme challenges of surviving in this environment have pushed our attempts thus far into the realm of the artificial, the “man-made,” the heavily engineered, and the unyieldingly practical—without much room for whimsy. As we prepare to venture into deep space and establish habitats, we can consider ways to enhance this survivalist strategy with structural techniques that build on the millennia of precedent in robustness, adaptation, self-healing, and indeterminate growth from the flora (and to a lesser extent, the fauna⁴) of Earth. As stated in the introduction, we begin by exploring how to enable dynamic, self-aware space structures that are informed by both inorganic and organic growth processes from complex Earth systems. We explore self-aware growth as an architectural paradigm for space that can still deliver on the survival requirements to support human life in space while also entertaining room for the wonder and delight we humans find in nature.

*How can we design, induce, and scale self-aware self-assembly
to grow space architecture,
natively, in orbit?*

To unpack these terms, the self-assembling “awareness” and adaptivity depend on pervasive sensing built into interior and exterior shells of the architectural base units—from proximity sensing, to environmental sensing (e.g., light, radiation), to nearest-neighbor mesh networking and swarm-inspired communication protocols. We see examples of such systems in nature—self-organizing animals with collective intelligence, or swarms, where intentional, targeted macro-configurations can evolve from embedded behavior and local interactions among constituent members of the group.^{24, 26} This dynamic, multi-agent responsive sensing facilitates actuators that tune self-assembly from a purely stochastic process as found in nature (say, the accretion of small particles into a clump through Brownian motion), into guided, convergent assembly managed by certain global rules and local interactions between neighbors. Principles of tessellation and self-similarity, drawn from the mathematics of fractals,² help us select base-unit geometries for modules. We seek module geometries that will dock in energy-favorable assemblies for modular space stations that can continue to grow larger and adapt beyond the designer’s original conception.

This approach yields immense practical benefit in the reduction of traditional control mechanisms—less need for propulsion and thrusters for path-planning; less planning for guidance, navigation and control (GNC); and less human or robot-mediated “agent-based” construction. In addition, this self-assembling and adaptive paradigm inherently supports redundancy and repair—when damaged modules can be reliably jettisoned, with interlocking modules added in their place, we can achieve on-demand, in-situ repair of space assets. In this context, we draw on biomimetic inspiration from the repair of nucleic acids. DNA exists in a veritable soup of G, T, A, and C nucleotides and when the strands of DNA are damaged, these base pairs can be slotted in to match the bonding site in question.¹²⁰ We envision a similar definition of space architecture modules that be slotted into standard macro-geometries of space stations for ease of reconfigurability and repair.

Finally, this paradigm of adaptive, self-assembling, modular space architecture also provides decentralized control and modest part-by-part growth; this may free us from the constraints of fickle funding and political whims that limit long-term, consistent progress towards megastructures. If the modularity and interchangeability of the architectural base units is preserved for backwards compatibility (even as hardware iterations and tech maturity inevitably lead to new versions), then the ability to expand the structure to house more humans depends on small, iterative resource allocation rather than a large budget for an entirely new

⁴ Animals often stop growth at “maturity,” whereas many plant species can grow throughout their entire lifespan.

station. Instead of needing to build an entirely new structure from scratch, we simply add a new wing onto our house. We are now facing such a challenge with the ISS, as plans for its retirement or transition to private ownership are discussed.¹²¹ This example of space architecture—a monumental achievement in its own right—cannot scale and grow indefinitely. In preparation for space tourism and a democratization of the countries and citizens involved in space exploration, we are already facing needs for larger space stations built anew. A major effort in our research centers on designing a proof of concept minimum viable unit (MVU) for modular, reconfigurable space architecture. While many different candidate geometries and concepts of operations exist, and ultimately we hope to see a rich ecosystem of MVUs, we must start by analyzing the feasibility and architectural lifecycle of at least one candidate. Our TESSERAE prototypes, experiment launches, and aerospace mission architectures toward this goal are discussed in Chapters 4 and 6.

Our design theory for growth paradigms in space architecture relies on three core principles, phrased as dichotomy priorities. The first two explore the physical features and topologies of growing systems (both inorganic and organic); the third bears on energy flows and non-equilibrium phase transitions that govern how such growth is induced and guided. Together, they fall under an “indeterminate” growth philosophy (best known to us in botanical examples, where growth continues throughout the lifetime of an organism rather than stopping at “maturity”). This provides an opportunity to grow and adapt space structures⁵ over timescales more suited to space travel and the vast distances we may one day cross. Can we build space architecture that keeps on growing?

1. Accretion over Construction
2. Seeding over Erecting
3. Cascades over Dams

3.1.1 Accretion Over Construction

Let us start small, with the MVUs of space architecture (e.g., the cells of a larger structure) and grow organically. Like mussels accreting to a pier or proto-planetary mass accreting into planets, we can start with feasible base units, impose form constraints to enable a reasonable level of deterministic outcome, and allow the structures to self-assemble and evolve into these boundary conditions. This principle recurs throughout the thesis contributions, from hardware designed with specially-tuned magnetic joints to accrete over mere seconds in microgravity, to generative design algorithms exploring the design space of accreting, three-dimensional TESSERAE nodes under certain fitness constraints.

3.1.2 Seeding Over Erecting

Traditional “erecting” modes of architecture yield smooth (at macro scale) outer shells. A seeding process allows greater variation to evolve without all detail requiring individual manual execution, while still being responsive to certain initial conditions that govern the nucleation period and surrounding environment. We pull from the formal definition of “fractal dimension” as a mathematical framing for condensed, highly-textured, branching structures. Fractal “self-similarity across scales” can be used as a guiding concept for self-replication and continuous growth of the structure without extensive human/agent intervention. A single base unit can be replicated, can bond to an ever-growing structure, and can continue expanding in a seeded-pattern (i.e., self-aware) through open “bonding sites” that continue the self-similar pattern at a larger scale. Self-similarity and fractal branching structures are also shown to increase resiliency of certain systems.¹ This can be

⁵ Building on growth notions, though not the exact aesthetics, from the space station in *Valerian and the City of a Thousand Planets*.

combined with our poly lithic, reconfigurable systems approach (decentralized, multi-part structures), for robust, life-like space craft that are self-aware, self-healing, and easily dispersed for independent function.

Both seeding and accretion processes require in-situ resources—while this can be achieved in the short term by adding redundant base units to our enclosed self-assembling systems (e.g., a “swarm” of generalizable, re-mixable units to draw from with LEGO-like interchangeability), we also consider the merging of our research work with in-situ resource utilization technology development in the future.

3.1.3 Cascades Over Dams

Drawing on Eric Smith’s hypothesis for the earliest origins of life on Earth,¹¹⁶ we are interested in finding the non-equilibrium phase transitions or energy-driven processes that would govern elegant evolution of space architecture structures. As he notes in *The Origin and Nature of Life on Earth*:

“Our thesis in this book is that the emergence of life should be understood as a cascade of dynamical phase transitions, as matter in an energetically stressed young planet was rearranged into conduits for energy flow.”

This means identifying and designing *with* the flows of available energy (cascades) rather than designing against them (dams). In designing and building space architecture, we should take explicit advantage of the physics of microgravity and the “native” environment of the vacuum—capitalize on swirling circulation dynamics for quasi-stochastic self-assembly (no gravity, no air drag to counteract); explore radial space structures (building on Thompson’s radial coordinates projections³) where we can build outward in all directions; or energy-actuated systems based on inflation (air pressure leads membranes to expand out into the vacuum) and solar radiation (solar sails and panels for energy capture from incident rays unabated by an atmosphere). These choices are akin to the “native” growth paradigms of the Earth and sea, to clearly motivate “design by and for” the unique affordances of the space environment.



Figure 3-1. Left to Right: Mussels accreting, crystal growth, and a waterfall serve as organic and inorganic examples of growth paradigms and energy-favorable processes after which we can model aspects of space architecture. Image credit: Creative Commons.

Ultimately, we aim to define cellular space architecture, or minimum viable *architectural* units, that can be assembled into complex structures through the application of the three design principles (accretion, seeding, and harnessing cascading energy flows—see Figure 3-1), tying the biological base-unit scale to the space urbanism scale.

3.2 Indeterminate Growth

Merriam-Webster defines Indeterminate Growth as “plant growth in which the main stem continues to elongate indefinitely without being limited by a terminal inflorescence or other reproductive structure.”¹²² To this, we add a conception of radial growth in three dimensions across many “stems”—beyond simply that of the main stem—as structures in space need not worry about directing growth resources to a single main stem to hold up other parts. Indeterminate growth serves plants particularly well, helping them become the perennials of their environment—the Mother Fir that watches multiple generations of a human family grow beneath it. The resiliency of their matter long after the “living” period has waned contributes longevity to a second order—the stunning paneling of a gothic cathedral or the beams and joists of a centuries-old tavern. We hope to design space architecture in this twofold paradigm, with growth potential in the structure that can sustain evolving additions well beyond those of the original builder and designer, and also the quality and permanence that allows the inhabitants to rely on them for generations. Given the input resources and the nature of space-travel, it is no wonder that authors from Heinlein to Niven to Asimov have imagined spaceships and habitats that are thousands of years old.⁶ Newman et al. have explicitly considered the “spacecraft design lifetime” in scoping the aerospace technology needs for future life in space.¹²³ In this growth-defined context, we can ask: what does “birth” entail for a fractal or crystalline-packed, self-aware space ship? For us, this starts at the moment of first accretion. And what does “death” entail? Hopefully decades or centuries of continued use even in passive form, when the self-aware, self-assembling systems have faded.⁷

To progress towards indeterminate growth, we model the base units of our space architecture on the cell—a constituent part that is both self-sustaining in certain regards, and yet most effective when joined in a tissue with other cells for a holistic function that is greater than the sum of its parts. We are interested in both the base unit and the super-structure scale. The design choices made in the unit (i.e., what shape or functionality a particular cell has) inherently affect the superstructure outcome (the global work of a particular tissue or organism). The DNA in a tree’s early cells, say the fusiform initials, carries much of the logic for the overall form of the tree, but certainly does not specify the location of every branch, nor even the exact final height—these are left to develop responsive to the environment and to the lived experience of the tree.¹²⁴ This models a compelling balance of deterministic and indeterminate growth—incorporating just enough logic in the early constituent parts to guide, but not overly constrain, the final assembly. Architects and engineers have long looked to DNA and nature for such examples of coded growth and even molecularly-engineered buildings;^{6, 32, 125, 126} we take this inspiration into the space environment to achieve longer-lasting, more robust and resilient space architecture worthy of the vast scales inherent to space travel.

Beyond the definition of a base-unit TESSERA Cell, the process of morphogenesis, by which groups of cells differentiate into tissues, guides the growth and zoning of our near-term space habitat proposal (Section 6.2.2). The process by which stirring energy forms an “annealing ramp” for DNA^{10, 14} informs our approach to tuning kinetic perturbances, initial velocity, and circulation of the TESSERA Shell tiles to anneal or converge the buckyball for completed self-assembly. The simplicity in definition and optimization of the TESSERA Shell parts (only two tiles types, with only two types of bonding joints—Hexagon: Pentagon and Hexagon: Hexagon) not only helps to improve the likelihood that proximate tiles can bond, but also builds on Peter Pearce’s

⁶ Drawing here, from Heinlein’s *Universe*, Niven’s *Ringworld*, Asimov’s *Foundation Trilogy*, and Clarke and Benford’s *Beyond the Fall of Night*.

⁷ A brief aside—studies of elephant health show they do not suffer from cancer at the rate that might otherwise be expected (larger organism, more cells, more divisions, more chance of mutation would presumably lead to more cancer). Instead, they have adopted a mechanism by which cancer-fighting genes remove the threat from mutated cells before they form a tumor. While we’re just at the beginning of this self-assembling space architecture journey, it’s worth considering early how we might design a comparable self-correcting mechanism into large masses of accreting space structures. What principles can we draw from the elephant morphology and genetic code that could help us maintain and self-heal large space stations? Relevant paper: Vazquez, Juan Manuel, et al. “A zombie LIF gene in elephants is upregulated by TP53 to induce apoptosis in response to DNA damage.” *Cell reports* 24, no. 7 (2018): 1765-1776.

principle of “minimum inventory, maximum diversity,”¹²⁷ for a sustainable, nature-inspired construction paradigm. The self-healing surface repair found across the living world (from plants to shark skin¹²⁸) inspires our approach for this same model, where tiles not only self-assemble but can also dynamically detach for repair, servicing, and replacement. Within this realm of indeterminate growth and biomimetic approaches, our space architecture design theory enjoys a wealth of precedent on which to draw.

3.3. Designing in Concert with the Space Environment

Much as contemporary architecture now aims to integrate into the local setting, embracing sustainability and the native environment as a Latourian “matter of concern,”¹²⁹ we should aim as well to design *with* the flows of energy and unique affordances of the space environment, rather than in opposition to them. This is the principle of Cascades over Dams, returning. Building upon the focus on indeterminacy, we have a responsibility to consider the long time horizons inherent to space travel and design patterns of growth and in-situ operation for space habitats that can be self-sustaining and stably integrated into their environment. Long time horizon forethought is sometimes lost in the quick pace of modern life, but not entirely forgotten—from the rebuilding of the Ise shrine every 20 years as part of Shikinen Sengu¹¹⁸ (and the careful planting of parallel generations of trees to support the iterative rebuilding) to an organization like the LongNow Foundation, dedicated in its mission to “foster long-term thinking and responsibility in the framework of the next 10,000 years.”⁵ In this spirit, we consider the features of the space environment that would uniquely shape space architecture, empower new approaches to life in orbit, and prepare us for a harmonious co-existence in new pockets of the cosmos.

With the freedom of microgravity, we derive an interest in growing radially. Space stations can and should expand in three dimensions, making use of the apparent absence of gravity⁸ to expand into new forms. Even the ISS, the pinnacle of humanity’s space structure achievements, still primarily expands along an xy-plane of modules, with only the solar panel and radiator arrays allowed in the z-axis. We can instead explore spherical and radial symmetry—not just of platonic solids, but structures like spore pods, spirals, and helices. Microgravity also furnishes an opportunity for swirling circulation dynamics, much like those seen at microscales on Earth (plankton in swaths of ocean water or the small particles of Brownian motion), to bring objects together for stochastic and quasi-stochastic exchanges. It is this property that motivates magnetic joints for the TESSERAE tiles and so effectively supports quasi-stochastic assembly—without gravity to counteract the movement, magnetic forces can elegantly draw objects together in microgravity and exploit circulation dynamics to find bonding partners. Once masses increase significantly enough, we even begin to see gravity-driven accretion—the process by which planets form¹³⁰ at massive scale.

In orbit, well beyond the protective boundary layers of Earth’s inner atmosphere, we can also harness relatively unabated solar energy—both for energy storage (e.g., solar panels) and also for motion. Space habitats are often referred to as “ships” for a reason—but instead of relying so extensively on propulsion (albeit necessary for large delta-V orbit transfers over short timescales), we should design habitats that leverage sails, solar sails, that capture the energy of photons. Motion can be a greater part of everyday life in space, from rotating space habitats that generate artificial gravity through centripetal forces to solar sails that propel habitats on certain journeys; in comparison, we have seen limited attempts¹³¹ at integrating motion into habitats on Earth, due to the great costs of overcoming gravity and the related friction.

⁸ Note, gravity is always present—a force defined between all bodies of matter in the universe. Being in orbit, however, provides a sensation of continuous free-fall around a planet or celestial body.

The downside, of course, of existing further out beyond the near-Earth protective cocoon, becomes immediately apparent when combatting radiation. Without Earth's magnetic field to deflect solar wind and other sources of radiation, we will need to explore new models for protecting fragile human biology. Comprehensive proposals for this rely on a combination of passive (i.e., shielding material) and active (generating magnetic fields in orbit from superconducting magnets, like those at CERN, are already under consideration for aerospace adaptation¹³²) approaches. D'Arcy Thompson asks us to consider the "trammels"³ or natural lines of constraint at work within an organism—at the space ship or space urbanism scale, the trammel might be the shadowed, safe area from a radiation shield deployed via such magnets, or even placed further out at a Lagrange point.

Out of the many challenges that living in a grand but menacing vacuum presents (from outgassing and freezing of exposed organic materials, to the extreme risks of depressurization), we also gain an affordance—the ease with which we can inflate structures into a low or no pressure environment, offering opportunities that the TESSERAE platform leverages to define temporary containment membranes for quasi-stochastic self-assembly (Chapter 6).

Finally, Geoffrey West's work¹ encourages us to ask, as he does for cities: what is the "natural scale" for a space ship? In the same way that mammals can only be so small (before fluid mechanics limitations are reached for circulatory systems) and so large (before being crushed by their own weight, or oxygen deprived due to capillary distance separation, per West), what are the inherent bounds on space ship size? This is a large source of motivation for focusing on microgravity habitats in particular, rather than reduced gravity bodies (i.e., Moon and Mars settlement architecture). Much as we find the largest Earth animals in the ocean, avoiding being crushed or immobilized due to the full weight of their own bodies, the greatest opportunity for innovation and creativity in architecture lies in this serene, floating domain.

3.4 Parameter Space for Microgravity Space Architecture

As we forge a new approach for space architecture, we first catalog and characterize the current state of the field. Beyond the literature review presented in Chapter 2, this section presents a design tool created to assess space architecture precedents along form, function, structure, and self-aware "status." We stand on the shoulders of giants here, from master engineers and teams of hundreds of people who have realized space habitats like Mir and the ISS, to the paragons of science fiction inspiring our conception of the possible.

For **structure**, we examine a gradient from monolithic to polyolithic. Monolithic structures are conceived or built to achieve a single, often monumental, open chamber or geometry. While perhaps constructed in pieces, the ultimate result is a recognizable, single "monolith"—often (though not always) definable by a globally convex topology. In contrast, polyolithic structures are by definition multitudinous. They, too, can form large structures, but the resulting morphology is more that of a tissue made of many cells or an accretion out of many distinct parts.

For **form**, we consider a range from idealized geometries (e.g., platonic solids, perfect rings) to organic and irregular examples (based on cellular solids or unpredictable groupings of base units), with amalgams of these models in between. In Figure 3-2, note how many of the previously built and near-term prospective space stations rely on exactly the same form—cylinders with end caps, linked together like a sausage or a rock cairn. This is not for trivial reasons—the distribution of pressurization forces around a cylinder has its advantages and they nest well into cylindrical rocket payload fairings—but surely we can expand into other forms!

With regard to **function**, we choose a single dyad out of many possible functions that might have been considered. For the purposes of this thesis, we are most interested in the tradeoff between entirely static habitats (their function is simply to statically “contain and house” as they did from even before their deployment into space) and reconfigurable habitats (with a mandate, mission, and capability to dynamically adapt in function to serve evolving goals). This notion of reconfigurability includes several factors, among them the ability of the structure to self-assemble and disassemble, to change dynamically in size or dimensions, and to serve changing ConOps (e.g., planning for the Lunar Gateway’s autonomous adaptation to “seasonal” activity).

Finally, we define “**status**” as relating to the degree of self-awareness in the structure. Here, we do not measure against full sentience (as we might for the human definition of “self-aware” beings), nor do we refer to artificial intelligence and HAL.⁹ Rather, we are measuring space architecture against our incarnation of self-awareness as defined in Section 3.1—an “awareness” and adaptivity that depends on pervasive sensing, collective intelligence-inspired communication, and physical responsiveness and receptiveness to new “growth” or accretion of modules through clever geometry and self-similar bonding sites. In many ways, this builds on the mindfulness notions of self-awareness, in being observant, aware, and receptive,¹³³ which we extend to the space surroundings. While this category of status, ranging from “passive to self-aware” may at first seem to overlap with the function-defined range from “static to reconfigurable,” a module could in theory be both static (does not change in morphology itself) and still self-aware (supports extensive interaction between itself with others).

To determine inclusion in the charts below, we relied on the following selection procedure:

- All examples of realized, built space architecture are included, even if only a single-module. Where a class of related modules all share a particular form or structure (e.g., the Soviet Salyut series or Chinese Tiangong series), we group them under one name.
- For prospective space stations, we selected based on near-term viability (i.e., whether the concept for deployment is feasible within five to ten years) and seriousness of the current implementation endeavor (i.e., whether NASA contracts are at play in supporting the concept, hardware is already in development, etc.).
- In the realm of imagined habitats, where so many concepts abound from both science fiction and the 1975 NASA Summer Study,¹³⁴ we did have to make a more severe cut based on ultimate feasibility of the concept. Realization may still be far in the future, but the concept should not itself be entirely fanciful. The organic spaceship from Beyond the Fall of Night (BTFoN)¹³⁵ pushes hardest against this boundary and lies just at the extremities of what should be included. It is included to show the trifecta of a reconfigurable, self-aware, organic form.

⁹ A reference to HAL 9000 from Stanley Kubrick’s “2001: A Space Odyssey.”

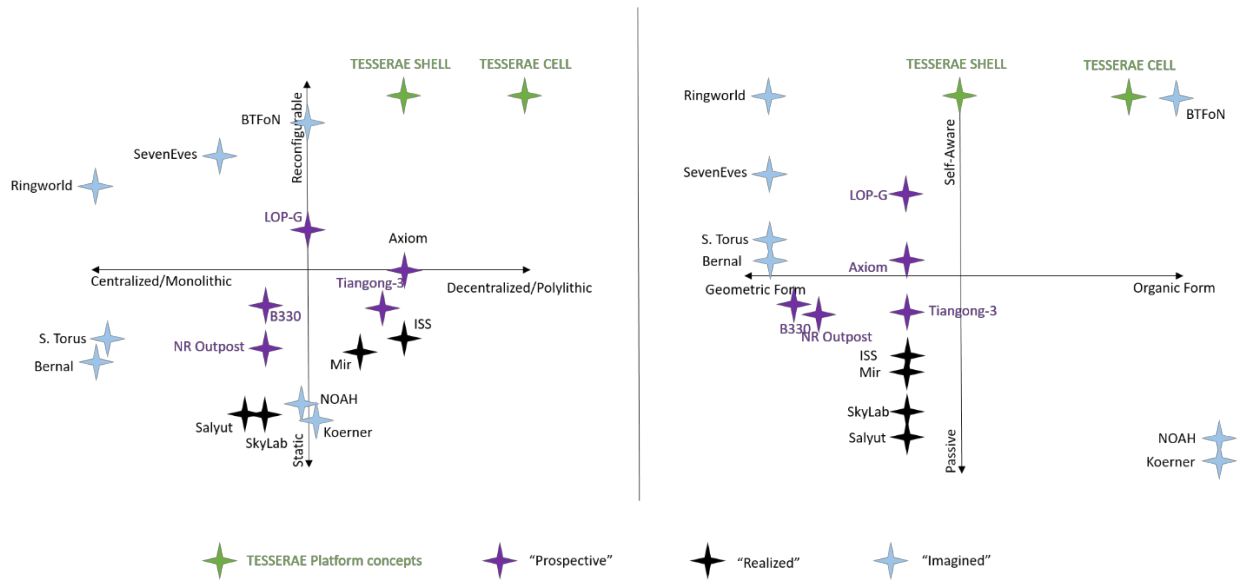


Figure 3-2. Companion charts showing Function vs. Structure (left) and Form vs. Status (right), where these terms are defined as Function: static to reconfigurable; Structure: monolithic to polyolithic; Form: geometric to organic; Status: passive to reconfigurable.

With these charts as a baseline, we scored each example of space architecture on a 10-point scale (-5, to 5) along each axis dimension described above (structure, function, form, and status). Importantly, no connotations of “worthiness” are ascribed to these positive and negative values used for plotting—equally inspirational structures are found on either extreme (e.g., the Stanford Torus and Greg Lynn’s NOAH). The result is a 3D map that helps us both explore the current “parameter space” of space architecture and also identify areas of open opportunity—unpopulated regions on the map. Some open areas present conundrums or obvious incompatibilities—there are very few to no entirely static and fully polyolithic examples, implying that a fully throated commitment to supporting many individual modules often lends itself naturally to reconfiguration of said units. Similarly, monoliths do not tend to be associated with reconfigurability. Figure 3-3 shows several screenshots from this tool.

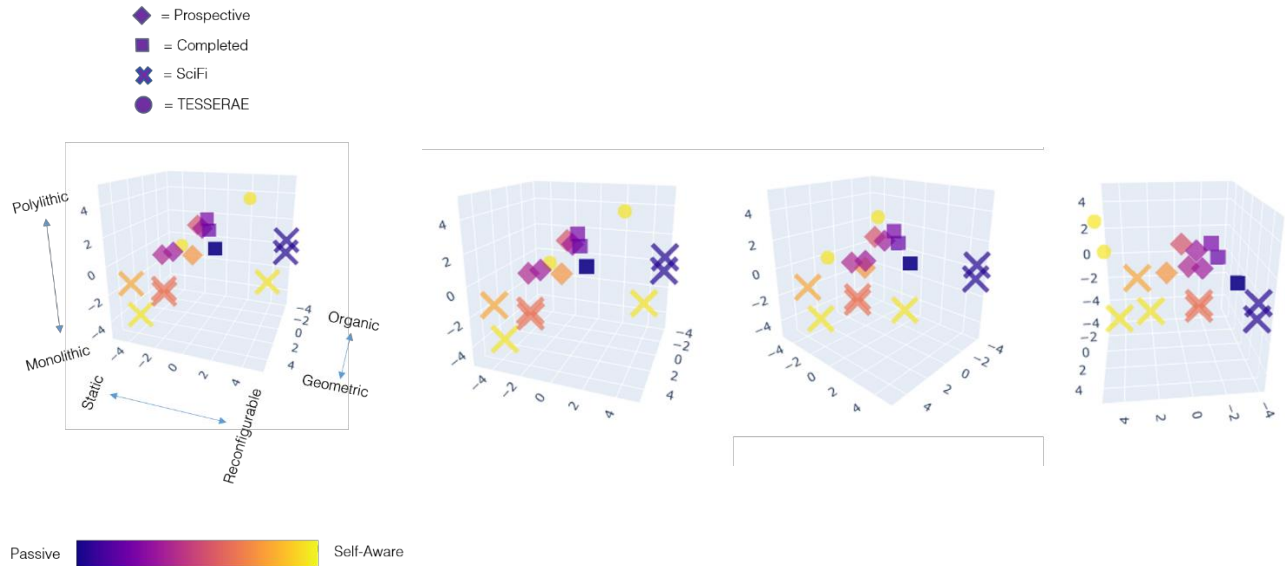


Figure 3-3. TESSERAE 3D Parameter Space design tool for space architecture, with key figure on the left and three alternative isometric views on the right.

Going forward, we intend to publish this tool for use by space architects and encourage a thorough industry-wide exploration of a biomimicry-inspired parameter space for space architecture. In the meantime, we have carved out our intended niche for TESSERAE—highly reconfigurable and decentralized (driven by the polyolithic structure) with an extensive palette of options for form depending on the Shell (buckyball) or Cell (volumetric module) approaches. This open opportunity for exploration of form constitutes one of the most exciting contributions of the TESSERAE platform—an opportunity to self-assemble into a range of shapes from a near-perfect sphere to a stunning, spiral display of parastichy through the docking of multiple nodes with a scaffold. Constructing such forms, laying out the variable mission ConOps that they enable and merging these concepts into the deployment realities of space architecture is discussed for both models (Shells and Cells) in Chapter 6. Proof of concept development and microgravity space testing was conducted, described in Chapter 4.

3.5 An Aside:

Aesthetics worthy of Life in Space, and a Life in Space Worthy of the Patterns of Nature

What are principles of architectural elegance, even architectural beauty, in space? In a Structuralist sense, how will these principles flow from the cultural and environmental dictates of space, or can we take a more platonic approach and define independently, aesthetically pleasing forms? To quote from Brent Sherwood in his 2005 treatise on Lunar Architecture and Urbanism,⁹⁹ in turn quoting Roman historian Vitruvius on the three core tenets that define good architecture, we must prioritize “firmness, commodity, and delight.”¹³⁶ In Chapter 4, we address the firmness—the hardware and tested prototypes of a future built environment that can be practically realized. In Chapter 6, we explore the commodity—how this paradigm of self-assembled architecture will lend itself to new functionality and uses for future space travelers. Here, though, we relish in an aside on

how to delight the occupant with themes and motifs from patterns in mathematics and the natural world that commune with the space environment.

There is much in space to delight the viewer—from new vantage points floating at the center of spires that may expand out in *all* directions, to ringworld horizons that wrap around you, to the infectious playfulness of microgravity.¹⁰ Some of this delight also comes from surprise—seeing forms realized that contradict our intuitions and create cognitive dissonance for our visual cortex that has evolved over several millennia of gravity-bound existence. But a certain sense of delight can also come from seeing old forms in new ways, from seeing the familiarity of the Fibonacci spiral or a radiolarian’s symmetry in an altogether unfamiliar environment.

3.5.1 Informing Form

The majesty of mathematical ratios

D’Arcy Thompson’s *On Growth and Form* explores many of nature’s most intriguing mathematical relationships. Of interest for us here is his work on spirals and particularly the ratios defining parastichy, a particular pattern of leaf arrangement or phyllotaxis. We are reminded that the Fibonacci series is to be found in the relative dimensions of the rhomboidal definition of the leaf (or for Figure 3-4 below, the scales of a fire-cone), as two competing spirals produce the intriguing visual affect shown in many plants (Figure 3-5).

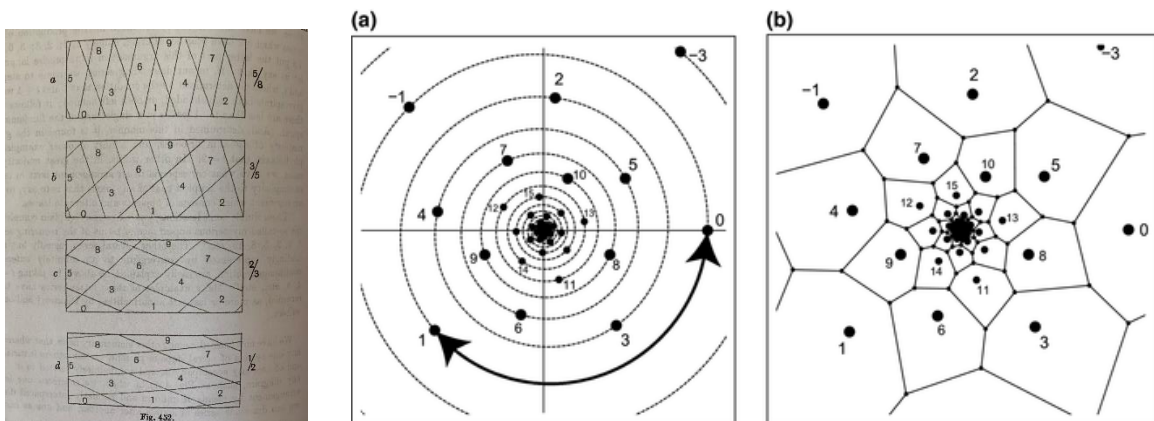


Figure 3-4. Left: Image from *On Growth and Form*,³ showing the divisions of parastichy and consequent dimensional relationships among the scales of the fire-cone. Right: Plots showing the Bernoulli spiral lattice (left) and voronoi spiral tiling (right), showing the potential for geometric, mathematically driven planning for incremental, indeterminate growth (image credit: Sushida, et al.¹³⁷).

¹⁰ From our experience across several parabolic flights, sharing the joys with dozens of research colleagues, microgravity is much like nitrous oxide at the dentist—despite some initial apprehension, you just can’t stop laughing and enjoying yourself.



Figure 3-5. Parastichy in plants, revealing plant growth that follows mathematically defined ratios for phyllotaxis. Image credit: Creative Commons.

Much as we see the Fibonacci sequence reflected throughout nature, other common reoccurring ratios like the “golden ratio” can be found everywhere from quantum behavior at the atomic scale in the magnetic resonance of certain cobalt crystals¹³⁸ to intentional inclusion in ancient¹¹ and modern¹² architecture. The elegance of returning, repeating, and fundamental sequences beckons us to include these considerations in future space architecture.

And while we might consider shapes like the dodecahedron and truncated octahedron (buckyball) to be particular to the modern moment, defined crisply by mathematical computer-aided design (CAD) software of the 21st century, these shapes have captivated designers for centuries for that same inclusion of variations on the golden ratio—notably Luca Pacioli and his illustrator, Leonardo da Vinci, for the *Divina Proportione* (Figure 3-6).¹³⁹ TESSERAE builds on two of these shapes in particular, the truncated octahedron (TESSERAE Cells) and the truncated icosahedron (TESSERAE Shells), the latter shown in Figure 3-6 on the middle left.

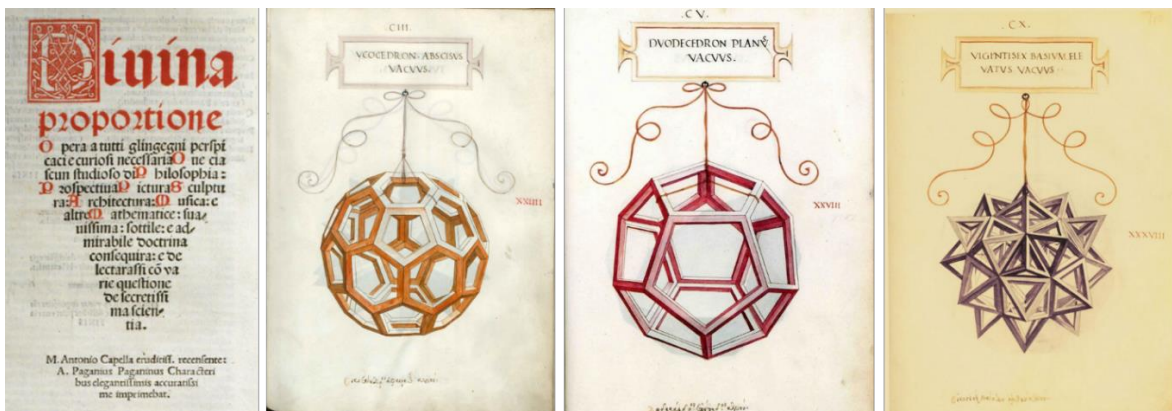


Figure 3-6. Pages from the *Divina Proportione*, speculated to have been composed around 1498 in Milan. Concept by Pacioli, drawings by Leonardo da Vinci.

¹¹ Many examples from ancient Greece, but also Islamic and Buddhist architecture.

¹² Famously incorporated by Le Corbusier in his architectural proportions scale.

Finally, while space presents many of its own challenges, the benefit of microgravity makes possible certain platonic structures that have been conceived but never realized. What better way to honor Newton, whose laws of motions still govern much of space travel (at non-relativistic speeds, that is) than to finally bring Boullée's Cenotaph to Newton to life at the intended scale (Figure 3-7).

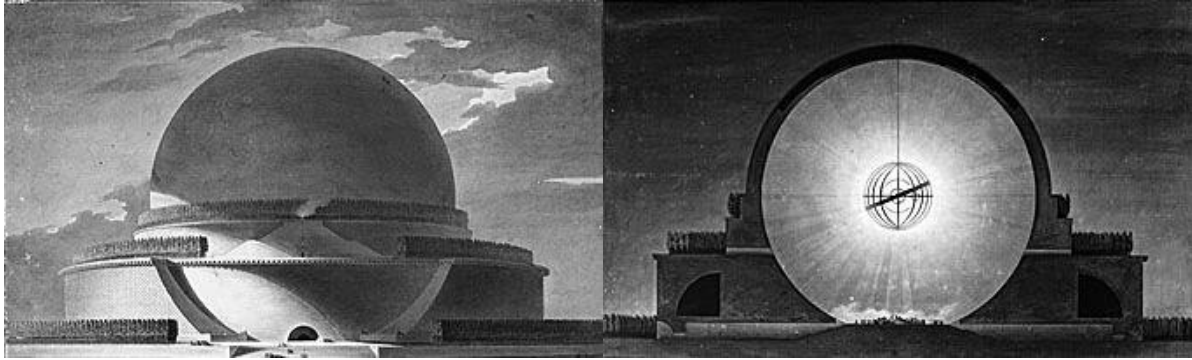


Figure 3-7. Image depicting Étienne-Louis Boullée's grand proposal for a memorial to Isaac Newton, to be constructed at a height of 150m.

Fractals

Both 2D and 3D fractals have heavily influenced the TESSERAE design, building on a notion of self-similarity in form and fractal packing density that leaves room for local niches, nooks, and crannies while defining a global structure that can provide the framework for iterative architectural additions. Benoit Mandelbrot characterized and popularized fractal patterns in nature,² creating a body of work and many collaborators (including mathematics professor, Michael Frame, at Yale University, to whom the thesis author owes an early debt of inspiration) that have carried this forward. In scoping prototype choices towards future work, the TESSERAE platforms considers both 2D fractal planes and volumetric fractals (like the stacked pyramid and Romanesco shown below, Figure 3-8) as design primitives for self-similar, incrementally expanding space architecture. Geoffrey West has further connected the scaling relationships across organisms and cities to certain concepts within the field of fractals,¹ informing our mission architecture design of an MVU of space architecture (Section 6.2.2) and the required resource distribution to sustain a space city growing with fractal density.



Figure 3-8. From left to right, Mandelbrot set (not an immediate candidate for space architecture, but of note for the connection to the creator of this field), the Romanesco vegetable and a fractally stacked pyramid.

Symmetry

When looking to candidate forms for space architecture, many of the most compelling precedents come from the ocean. The two domains, deep sea and deep space, share this curious quality of floating; over eons of evolution, the sea has produced creatures immediately visually indicative of this buoyant environment, often with intriguing symmetries. While by no means required, and with many equally compelling cases for asymmetry, symmetry in a microgravity environment may still generate that sense of delight from a rational form that we often seek on Earth. The application of symmetry need not be boring nor purely ornamental—we need only look at the patterns of appendages on the many incarnations of microalgae—diatoms and radiolaria in particular, with their delicate silica-based skeletons, to see engaging forms that also recall the bug like radiator and solar panel appendages of current space architecture. As shown in the right image in Figure 3-9, the base of these radiolaria could very well be the exoskeleton of a space module, with antennas, solar arrays, and telescoping thermal radiator poles extended for the usual suite of required functionality. Noting the striking similarity to Platonic polyhedral shapes, Hermann Weyl's mathematics staple, *Symmetry*,¹⁴⁰ even features this particular image from Haeckel's drawings.

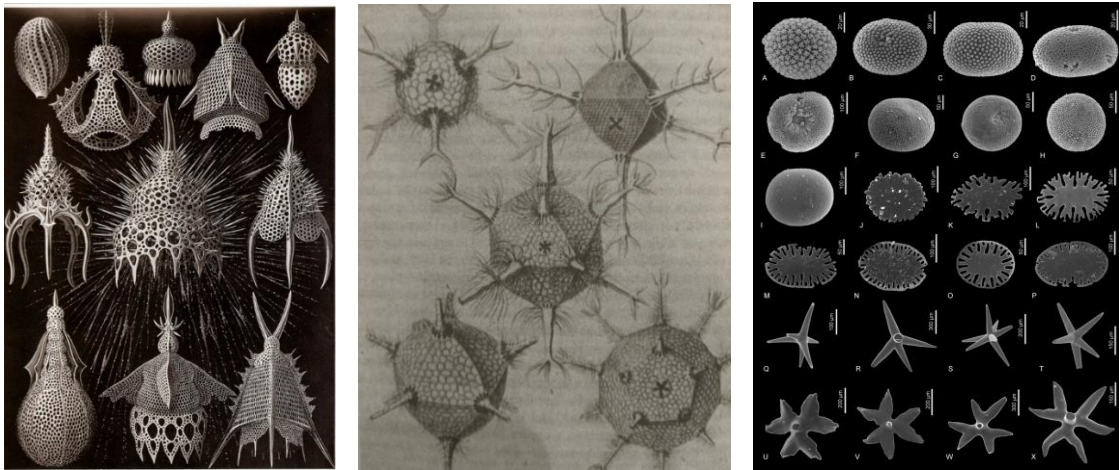


Figure 3-9. Left: Haeckel's 19th century drawings of radiolaria;¹⁴¹ Middle: a further Haeckel illustration, noteworthy for the uncanny resemblance to what real space structures of the future may need to look like, with solar panel and radiator appendages; Right: Sponge spicules showing gradations of different radial symmetry (image credit: Magdalena Lukowiak¹⁴²).

3.5.2 Shaping Surfaces: Tilings and Tessellations

Tilings and tessellations constitute a major part of this thesis—emphasized in the name of the TESSERAE platform (Tessellated Electromagnetic Space Structures for the Exploration of Reconfigurable, Adaptive Environments), so named for the tiny glass tiles used in ancient roman mosaics.¹³ In addition to Roman influences, we note inspiration from the extensive use of mosaic tiling patterns—both periodic and aperiodic—in Persian architecture (Figure 3-10). Examples of human-created parastichy can be found in the archways and alcoves of many Safavid buildings such as the creative inclusion of decorative muqarnas or small, nesting chambers. These structures provide a captivating premise for scaffolds that might someday support a parastichy of TESSERAE Cell nodes for space architecture that recalls its organic origins from Earth.

¹³ Inspiration for this name came directly from a Civil Engineering-sponsored archaeology trip to ancient roman mosaic sites taken during the course of the author's time at MIT, including visits to Priverno, Pompeii, and other sites throughout Italy.

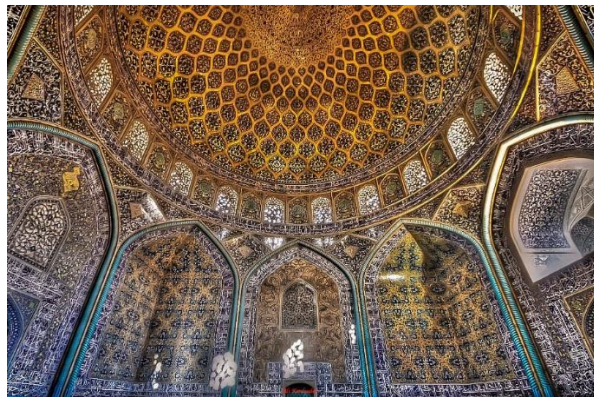
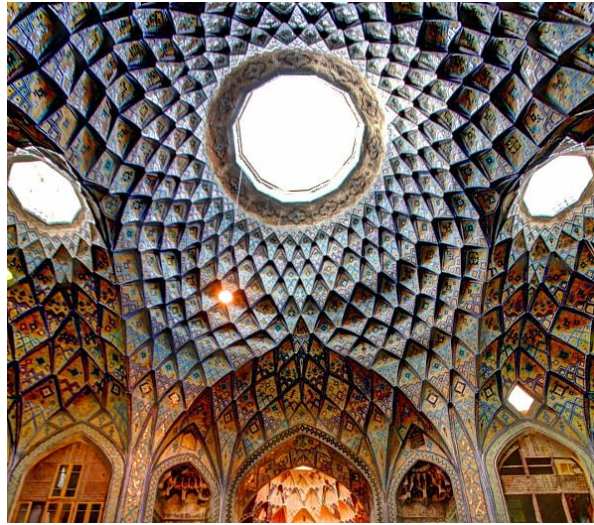


Figure 3-10. Top to Bottom: Bazaar of Kashan, Grand Mosque of Isfahan, Sheikh Lotfollah Mosque. Images courtesy of Arch2o¹⁴³.

Our constant companion in this thesis, inspiration from nature again points us to examples of surface tessellation, such as the radiolaria shown in Figure 3-9. In addition, we show another different radiolaria model, with a neighboring diatom from Thompson’s *On Growth and Form* (building on Haeckel’s many drawings from the HMS Challenger Expedition) in Figure 3-11.¹⁴⁴

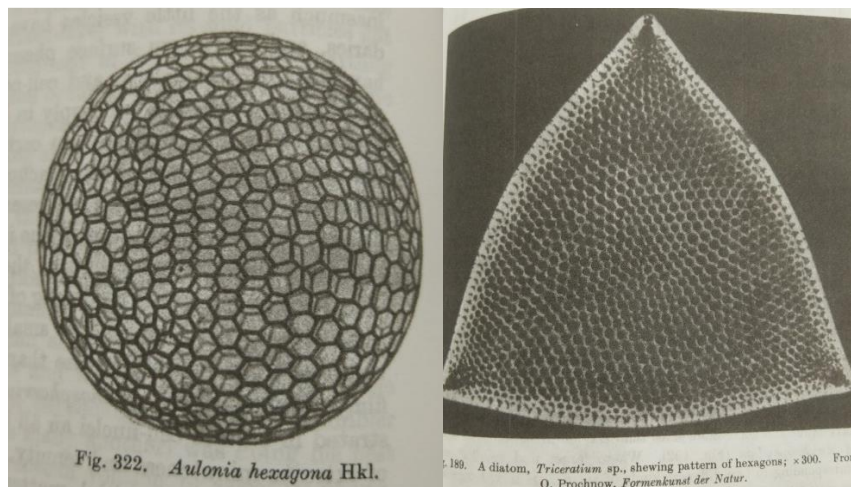


Figure 3-11. Drawing of a radiolarian (left) and diatom (right), showing evidence of tessellation even at quite small scales in nature (note: no full sphere can be tessellated by only hexagons as appears in this photo, but organic deformations and skews in each segment allow a wrapping here). Image Credit: *On Growth and Form*.

The TESSERAE Cell also relies on a notion of tessellating 3D Euclidean space into space-filling solids, or plesiohedrons. This class of volumetric units pack densely like crystalline structures, creating 3D tessellations.

The surface tessellations for the TESSERAE Shell are derived in a different way. Tilings that cannot be accommodated in the *xy*-plane can give rise to 3D shapes when bent to meet vertices. While a honeycomb tessellation can repeat indefinitely in 2D, if we add pentagons, the corners do not converge—that is until you bend a sheet of such tessellations out of 2D and into 3D space where a regular pentagon and hexagon tiling (of the correct number of units) can create a buckyball (Figure 3-12).

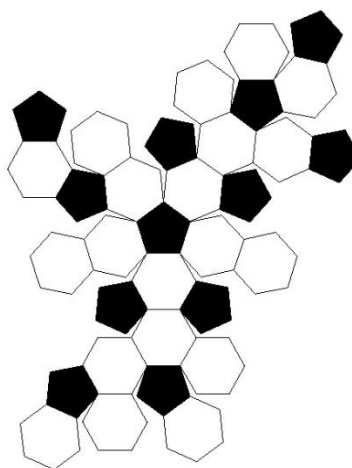


Figure 3-12. 3D tiling for a buckyball that does not fully tessellate in 2D. Image courtesy of Creative Commons.

Both shapes are shown in Figure 3-13. Until we can achieve surface continuity in space architecture—entirely smooth, unibody modules requiring either massive payload fairing or advanced in-orbit manufacturing from raw materials—we will likely rely on prefabricated shells and tilings from the ground. While the tile delineations are currently quite obvious in appearance, we envision developing the TESSERAE platform towards ever finer tessellations and meshes, to the point where a TESSERAE tile might become a “material pixel”⁶ in its own right. It might contribute to complex surface tessellations and stunning tilings that not only create livable volumes when self-assembled but also commune with the ancient designers of the Mediterranean and Middle East, offering humanity the promise of mosaic habitats in space.

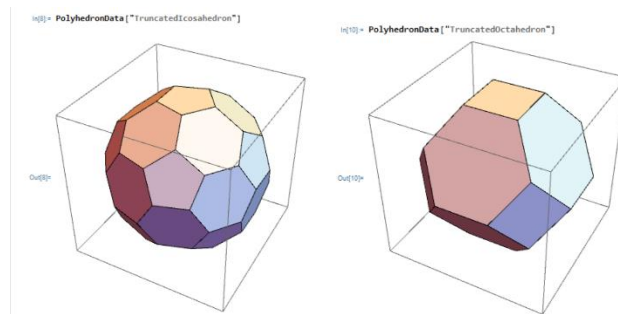


Figure 3-13. Mathematica renders of the truncated icosahedron or buckyball (Left), and truncated octahedron (Right). Both shapes are under consideration and testing for TESSERAE mission deployments.

3.5.3 Choosing Cladding

Feasibility constraints will likely dominate the choice of cladding and texture application for space architecture in the near term. Reflective sheets and blankets are often used to wrap satellites for thermal management, and iridescent solar panels will need to cover as much surface area on the TESSERAE modules as possible. Within those constraints, there is still ample room for design, as recently shown by the creative team of Bigert and Bogström behind the Solar Egg (Figure 3-14).



Figure 3-14. Solar Egg as an example of intentional aesthetic choice with futuristic solar power cladding. Image courtesy of ArchDaily.¹⁴⁵

The Solar Egg reminds us that there is still playfulness to be had in metallic finishings, even perhaps the ubiquitous chrome of 1960’s era space aesthetic. Overall, however, we hope to avoid the sense of sterility that often pervades modern buildings built entirely of reflective glass and steel and offer instead a vision of space

architecture that can be intriguing and welcoming, rather than othering. Long duration space travelers may miss Earth, needing explicit “grounding” or inspirational ethereal visuals depending on the moment, more welcome than a default industrial aesthetic in this very foreign environment. We hope to find ways for the occupants to sense the detail, thought, and richness of intent behind the creation of a space structure, in the way we sense the generations of craft-work and human ingenuity that went into cathedrals. Ironically, in this domain of such advanced technology, we may need the familiarity of certain historical aesthetics more than ever.

3.6 Summary

We have presented the contributions of the TESSERAE design theory, centered on a biomimetic framework and focused on realizing indeterminate growth in space structures. As with any natural system, the resulting structure should be a proper creature of its environment, leading us to consider the ways in which we can design in concert with the space environment, in contrast to the prevalence of the current design paradigm which frames space architecture and the biology of the human body in opposition to the (admittedly) severe challenges presented. We share a new design tool for exploring the “parameter space” of space architecture, with a grading system for biomimicry-inspired form, function, structure and status that we hope will aid future space architects in exploring a broader scope for structures in the near-term. Finally, our multifaceted design inspirations from nature and mathematics inform many of the downstream choices of this thesis—from aesthetic choices that might be applied to future demonstration missions in orbit, to the selection of geometric base units that inform our suite of prototypes, to planning architectural logistics for space cities. Rather than simply “accommodating” humans in orbit, we hope to both protect and delight them—with structures worthy of our natural origins from Earth, our literary science fiction past, and the technological advances of our space exploration future.

4. TESSERAE Hardware: Space Environment Experiments and Results

Chapter 4

“There is a great satisfaction in building good tools for other people to use.”

–Freeman Dyson

To make progress towards autonomous self-assembly of large-scale space structures in orbit, we developed and extensively tested hardware prototypes along a technology development roadmap. We rely on responsive sensing to augment the physical shell material of modular space structures, guiding tile navigation and neighbor-neighbor bonding. This facilitates decentralized, agentless space structure construction that is independent of astronaut EVAs and robotic agents, and also robust to single-part failure via a system of radiofrequency (RF)-enabled smart assembly nodes.

The TESSERAE hardware and software contributions of this thesis address a gradient from purely stochastic, passive self-assembly protocols to quasi-stochastic protocols with error correction, to more deterministic, controlled autonomous swarm dynamics. For each hardware platform, the work began with stochastic, passive assembly in a microgravity environment to test the base concept. This allowed us to explore each self-assembling unit’s geometry in detail, to test how finer points of mechanical design can influence the individual and collective behavior of objects (in the style of Tibbits¹⁶ and Bachelet¹⁴ where “physical logic” for self-assembly can be designed into each base unit), to test how varying patterns of magnet placement and polarity affects rotation and bonding behavior in microgravity, and to test a unit’s mass-to-magnetic field strength ratios for determining the efficacy and speed of magnet-mediated self-assembly across spatial scales.

Moving to quasi-stochastic self-assembly, we were able to learn from the error modes found in the passive regime, and then detect and correct these to assist the assembly towards completion of a target geometry. Error modes to be corrected include various scenarios where self-assembling units have bonded out of plane, bonded unstably, or joined together in a way that blocks other tiles from accreting properly (e.g., clumping, inverted bonds, or meta-stable bonds; Section 4.1.1). This quasi-stochastic approach relies heavily on responsive sensing and control software to detect the state of local individual tiles, neighbor relationships, and global assembly status. The sensing and decision architecture of the control software then determines how detected errors are handled. The hardware described below relies on controllable electro-permanent magnets¹⁴ (EPMs) to pulse tiles away if an error in bonding occurs. We found this approach to be best suited to a system already using

¹⁴ Electro-permanent magnets (EPMs) are combinations of a magnetic core and surrounding coil that are attractive in their passive state. Current is pulsed through the coil to neutralize or reverse the magnetic polarity of an EPM unit. This is the opposite of a traditional “electromagnet,” where the unit has no attractive capability until current is added.

magnets to induce self-assembly by drawing proximate tiles together; this allows us to marry the attractive and corrective functionality for the units into a single magnet part. Our quasi-stochastic control paradigm, however, remains agnostic to the type of functionality used to separate tiles and address errors, thus offering an extensible framework for mediating and correcting stochastic self-assembly. Other spring-based, reversible lock-and-key, or motor-driven clamp mechanisms could also be used to separate tiles.

The TESSERAE hardware also offers certain capabilities for deterministic self-assembly, where more aspects of the system are controlled to direct the units towards completion of a target geometry. The EPMs described above could be selectively turned on and off, not only for error correction, but for tunable magnet torquing to bring certain units in and out of bonding range, or to change unit rotation by repelling sides with particular polarities. Akin to the magnetic levitation bullet trains, but at much lower speeds, the hardware supports use of tunable electromagnet polarities to guide tiles through physical space. The control code can be adapted to allow for ordered, conditioned release of tiles such that new units are only added once the prior units have completed accretion into a “good bond” configuration, thus reducing the complexity of a stochastic, multipart system. Though we did not explore propulsion or extensive deterministic guidance, navigation and control (GNC) in the TESSERAE work to date, the hardware can be easily retrofitted to include propeller-like systems that would allow for path planning and directed traversals through microgravity spaces; when combined with node-to-node mesh architectures for data exchange between tiles, this would allow for controllable swarm dynamics. Selective use of these deterministic techniques in certain TESSERAE deployments is discussed in Section 4.1, with consideration of the broader adaptability to a fully deterministic system covered in Section 5.1 (simulation modeling) and in future work.

The quasi-stochastic protocols developed in this thesis offer an energy-efficient compromise with greater rates of successful assembly than the purely stochastic models and less resource consumption (i.e. propulsion fuel, computation cycles) than purely deterministic, controlled models. This electro-mechanical “sweet spot” most closely resembles the elegance and energy efficiency of nature in adaptive, self-correcting organic systems and thus forms the core of the thesis hardware contributions for “growing” space architecture. The hardware developed under the TESSERAE platform aims to supply a comparable balance of structural predictability and adaptive variability to what DNA in plant cells offers plants—the cell carries information on its contribution to the rough form of a tree, but in no cell is the future of every branch nor of every leaflet pre-determined. As the tree grows, it adapts to opportunities and challenges in its environment that might induce a branch to grow towards the sun, or away from an obstruction; if an “error” occurs in development, say a creature eats a new bud or shoot, the plant can regenerate another shoot and try again. Similarly, the mechanical design of the TESSERAE units lends certain proclivities to guide the stochasticity of the assembling structure—e.g. the tendency of TESSERAE tiles to form a buckminsterfullerene geometry due to the dihedral angles of the bonding faces—while using the error-correction of the EPM pulsing to allow the system to dynamically adapt and try again for bonding if needed. We developed the TESSERAE responsiveness from principles of biomimicry to build robustness into the foundation of the technical contributions. Robust, redundant systems are crucial for high risk, resource-constrained operating environments like deep space. We hope the technical choices taken in the quasi-stochastic TESSERAE hardware and software development will lend the platform the resilience and adaptability needed for complex operating environments, changing missions, and the need to be able to re-purpose and reinvent hardware over the long time scales inherent to space travel.

Within this spectrum of stochastic to controlled systems, the hardware explores the two geometric paradigms identified in the introduction: shells (hollow geometries) and cells (volumetric packing). The bulk of the sensing-mediated hardware development, taken through parabolic flight, suborbital, and orbital testing milestones, focused on the TESSERAE Shell buckyball tile geometry, discussed in section 4.1. Additional hardware design and preliminary testing was undertaken for the TESSERAE Cell truncated-octahedron nodes, for an exploration of self-assembling polyhedrons, discussed in Section 4.2. This chapter draws heavily on text from

several of our published academic papers^{119, 146, 147, 148, 149}. As we progressed through iterative design, prototyping and test efforts for TESSERAE, we followed a spiral theory of development that generates prototypes at each stage, all linked in a roadmap to a future technology demonstration mission in orbit. Videos documenting the flight tests and live TESSERAE behavior can be found at: arielekblaw.com/tesseract.

4.1 TESSERAE Shell Prototypes and Testing

The hardware developed for the TESSERAE “buckyball” shell includes pentagonal and hexagonal tiles, beveled to provide a bonding angle such that tiles can come together to form a closed spherical-approximation volume, or buckminsterfullerene. The name and nature of the structure hearken to the small, colored tiles used in Roman mosaics, where many standard pieces, or “tesserae,” interlock to create the image. We make this reference to ancient history while designing an artifact of our space exploration future to tie architectural elements together across scales and across millennia. We chose the buckyball structure as the target assembly shape for several reasons. The buckyball structure recalls the architectural geodesic dome, a shape that describes both an energy-favorable configuration state in nature and a visual form that has intrigued imaginations for decades, from biospheres¹⁵⁰ to entertainment and concert halls.¹⁵¹ Buckyballs, as spherical approximations, offer highly efficient space-filling options for a given surface shell area (a critical consideration for mass-constrained payloads and resource-constrained orbiting deployments). This shape can be assembled from 12 pentagonal and 20 hexagonal tiles, with several tile features that help to constrain the geometry and ensure a successful assembly. Each tile edge is beveled at the proper dihedral angle, shown in Figure 4-1, to establish the expected buckyball curvature, as tiles begin to bond together. This beveling also establishes a flush mating surface and exposes two recessed magnets on each mating edge that draw tiles together for bonding. The spatial configuration of North and South polarity for our bonding edge magnets defines two joint types (Figure 4-2 below), guiding the proper neighbor tiles towards each other, and ensuring that incorrect tile matches are easily perturbed and repelled by pulsing off the permanent electromagnets. We have intentionally designed the system with the minimum number of unique joints that will force a buckyball structure, thus improving the probability that any two neighbor tiles can bond correctly. Rather than every joint being unique, any two hexagons can bind together on certain faces and any hexagon can bind to a pentagon on the other faces.

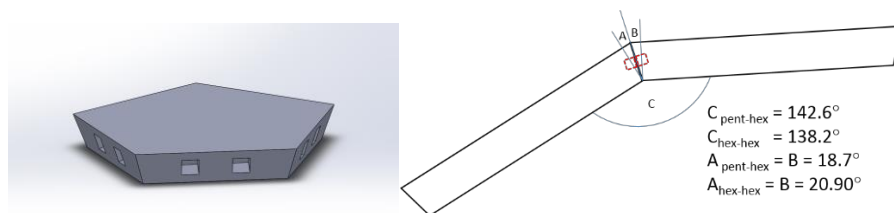


Figure 4-1. A sample pentagon tile with recessed holes for magnets on the bonding face (Left). Dihedral bonding angle C, with tile slope angles A & B shown in cross section for pentagon-pentagon and hexagon-hexagon tile bonding (Right). Hashed, red lines show the recessed magnet pair across tiles.

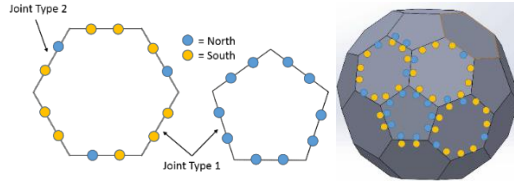


Figure 4-2. Polarity map for pentagon and hexagon tiles (Left). Application to 3D joints (Right).

As discussed in the introduction, the geometric tiles that form our TESSERAEE Shell self-assemble quasi-stochastically via EPM jointing to form a closed surface (building on prior work^{50, 51} demonstrating feasibility of magnetic docking approaches). Our process employs an energy-favorable “annealing ramp” approach where stirring energy and kinetic perturbances (e.g., adding in additional tiles, actuating the EPMs selectively to induce tile motion, using fans) can be tuned to induce accretion of many separate parts (inspired by the self-assembly of DNA coils and validated at macro levels^{12,14,17}).

EPMs on each bonding face serve two purposes. In their unpowered state, they exert a constant magnetic attraction. When embedded on the TESSERAEE bonding faces, this creates a polarity map that intentionally draws hexagons and pentagons into a particular configuration for “additive construction.” In their brief powered state, the magnetic attractions are neutralized to allow two previously bonded tiles to separate, or undergo “subtractive construction.” This second functionality allows us to manage error control, when tiles may have bonded into an incorrect configuration or meta-stable state. We can also use the EPMs to actively repel, selectively apply torques, buffer tiles away from each other, and correct meta-stable error states. The use of EPMs allows us to reduce the TESSERAEE power budget on-orbit (in contrast to using traditional electromagnets that must be constantly powered to provide attractive force). Separate clamps and sealing gaskets may ultimately be used to reinforce the EPMs during steady-state operation for a pressurized mission (magnets are only briefly power-actuated during quick bursts for assembly and disassembly). The EPM actuation is governed by control code and a decision tree that relies on the tiles’ supervisory sensing network (see Figure 4-3 for a diagram of the hardware integration with the sensing PCBs).

The supervisory sensor and communication network on each tile facilitates swarm-based path planning and error correction (e.g., EPMs are pulsed “off” if an incorrect tile-tile bond occurs and can be used for on-demand physical buffering between tiles based on proximity range sensor data). We use magnetometers to register a tile-tile event for analysis and to detect the “bonding signature” for comparison against good bond and bad bond thresholds. Proximity sensing then helps us further characterize the bond as “good” or “to-be-rejected,” as there are certain edge cases where the magnetometer alone is not sufficient. Captured inertial measurement unit (IMU) data can be used to assess the moment when tiles lock together and are joined in their motion vectors, while also supplying inertial measurements that feed into spatial tracking for the tiles. Tiles communicate status and data exchange to each other via RGB emitters/sensors and Bluetooth Low Energy (BLE). Together, these sensor and communication inputs contribute to a “bonding diagnosis” then feeds into our control algorithm (Figure 4-4). The control algorithm determines whether to preserve the bond or activate the EPMs and separate the tiles. The control logic, governed by a state machine, runs continuously throughout the tile’s deployment (while battery life lasts) constantly assessing tile status, neighbor status, and watchdog functions for hazards (e.g. forced limits on the rapidity with which EPMs can pulse). This approach to GNC allows us to mediate the self-assembly process, hence the “quasi-stochastic” self-aware self-assembly, speeding up the construction process and efficiently and effectively correcting error modes. BLE communication between the prototype sensor nodes enables during-assembly cross-tile communication and post-assembly emergent sensor network functionality when all tiles have properly assembled. In future on-orbit versions of TESSERAEE, these tile-embedded sensor nodes could be used to support secondary applications post-assembly,

such as radiation detection, life support system monitoring and on-demand, adaptive changes to the structure via coordinated control of the electromagnets.

The particular suite of sensors, communication modules, and evolving complexity of the control algorithm across the various prototype generations is documented (Sections 4.1.1–4.2.3).

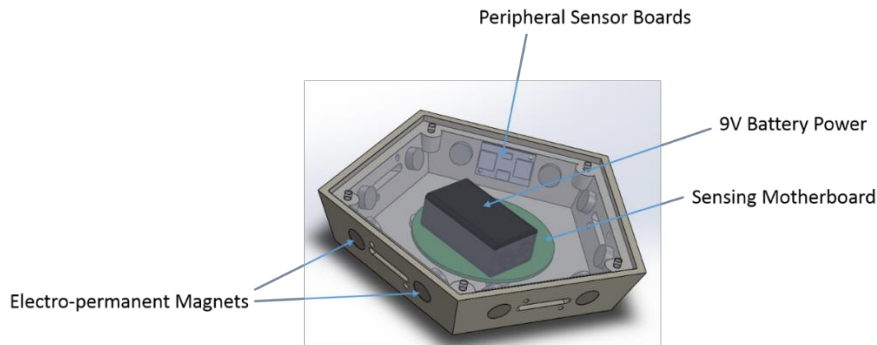


Figure 4-3. Sample TESSERAE tile housing, comprising a 3D printed plastic shell of either five sides (pentagon) or six sides (hexagon), with recessed holes for two electro-permanent magnets (EPMs) on each face. A central motherboard handles: the EPM driving circuitry; wireless communication to a remote computer “downlink”; Time of Flight (ToF) ranging and traditional proximity sensors for closing-distance calculation between tiles and bonding neighbor diagnosis; an inertial measurement unit (IMU) to track relative position, rotation, and translation of the tiles; and the interfacing with a peripheral sensing board on each tile edge. The peripheral sensing boards include a magnetometer (for detecting and diagnosing the electromagnetic bonding signature between mated tiles) and an RGB emitter/sensor pair to communicate between tiles bonding faces. Sensor data is gathered and analyzed through a multi-stage algorithm to actuate the EPMs as needed for control and correction. The EPMs dominate the power consumption (even though used only minimally to pulse “off” the magnetic attraction) and various hard-case lithium ion batteries have been used, usually chosen for capacity and flight heritage. This model depicts Generation 2 of the TESSERAE hardware, used for the Blue Origin suborbital flight test with a 9V battery, in this case.

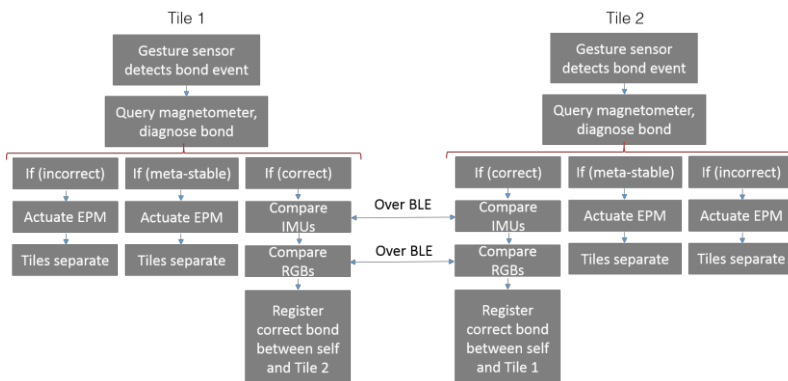


Figure 4-4. Summary logic for TESSERAE’s bonding control and correction algorithm, including redundant checks to ensure incorrect bonds are not misidentified as correct bonds.

All together, the integrated hardware and software platforms are used to, as they like to say in the particle physics world, “probe the parameter space” of microgravity self-assembly. Our experimental parameters for guided self-assembly include (several are interrelated, see Figure 4-5):

- Circulation: facilitating tile movement through the containment space to maximize bonding surface exposure to likely neighbors.
- Containment: optimizing the containment volume for efficient circulation (too large and tiles will settle away from one another into stable local minima configurations; too small and tiles may be blocked from freely rotating to fit in proper recesses and self-correct).
- Seeding: design and timely introduction of base units into a system to promote a particular shell geometry accretion (akin to crystal nucleation).
- Stirring Energy: perturbations required to dislodge local minima and aid in circulation.
- Redundancy: exploring the optimum distribution of pentagon and hexagon tiles (e.g., adding extra tiles up until the point where crowding and resource waste creative inefficiency; can assist in solving the “hole-filling” problem where the last few pieces of an assembly create the long tail of the time distribution for assembly).
- Reversibility: maintaining ease of joint reversibility for later disassembly and reconfiguration (rather than intricate lock-and-key twist joints, for example).

	Tests Circulation?	Tests Containment?	Tests Seeding?	Tests Kinetic Disturbance?	Tests Redundant Tiles?
Gen 1 (parabolic flight)	YES	YES	NO	NO	NO
Gen 2 (Suborbital flight)	YES	YES	YES	NO	NO
Gen 3 (ISS)	YES	YES	YES	YES	NO
Simulation Model	YES	YES	YES	YES	YES

Figure 4-5. Table showing progression of the TESESRAE hardware and simulation contributions across self-assembly experimental parameters.

We explored this shell model of hardware, testing and assessing the above self-assembly experiment parameters, across four prototype generations and four flight opportunity evaluations, with accompanying updates to control code, culminating in a 30-day ISS mission in March 2020. Our November 2017 parabolic flight successfully validated the stochastic magnet-based assembly, with subsets of tiles drawn together over centimeter distances in a matter of seconds. This flight established tile assembly behavior and error modes that we incorporated into our later quasi-stochastic control models. Our May 2019 suborbital launch and August 2019 parabolic flight tested a proof of concept three-unit tile set with full sensing, EPM actuation capability, and control code. The ISS mission tested our largest count of full-electronics-integrated, fabricated tiles to date, at a further miniaturized size (to fit inside the constrained volume); this mission also added conditioned release based on the progress of the assembly. The preliminary results from all deployment tests were used to calibrate our simulation modeling (Chapter 5) for on-orbit deployments. This progression is described in Sections 4.1.1 to 4.1.3 (summary Figure 4-6 below), including a discussion of preliminary work to extend the current hardware

centimeter scale sub-systems to a life-size tile at meter scale (4.1.4). In addition to technical development on the pentagon and hexagon tiles, we explored several latch, clamping, and holster deployment mechanisms for containing and releasing the tiles, optimized for various environments, as described throughout the sections. In Section 4.1.5, we consider the immediate next steps and future work for follow on technology demonstration missions, and ultimately, an in-orbit test at scale.

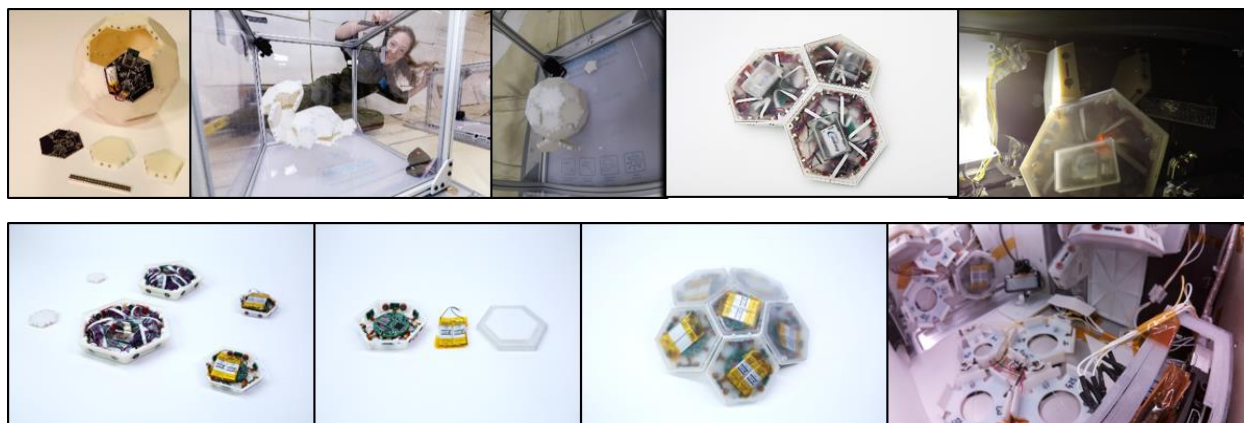


Figure 4-6. From L to R, Top Row: proof of concept hardware model with sensing prototype (Generation 1); tiles loose and self-assembling in microgravity on Nov 2017 parabolic flight test; tiles near-final assembly at end of parabolic flight 2017; tile hardware for suborbital test (powered, sensing, GNC); view inside Blue Origin suborbital chamber. Bottom Row: Tile hardware progression showing all three generations; close-up on ISS tile hardware; tile partial-dome with ISS hardware; view inside ISS NanoRacks BlackBox 30-day mission chamber.

4.1.1 Generation 1: Tested via Parabolic Flight

Hardware Development

The first prototype, deployed on a November 2017 parabolic flight, included tiles that form a buckminsterfullerene and explored purely stochastic self-assembly in zero gravity via magnetic joints. Two sets of thirty-two polygonal tiles were released to swirl around each other in a contained volume and passively snap together, without the need for propulsion, GNC, or advanced robotics. For Generation 1, the mechanism of self-assembly relied on passive, neodymium magnetic jointing between the tiles, each 3D printed on an Eden Objet light-curing photopolymer printer to strict tolerances with recessed holes for the 3mm cube magnets. Tiles measured 5-6cm across, depending on the hexagonal or pentagonal geometry. Each tile edge was beveled at the proper dihedral angle to establish the expected buckyball curvature, as tiles begin to bond together. This beveling also establishes a flush mating surface and exposes two recessed magnets on each mating edge that draw tiles together for bonding, as shown in Section 4.1, Figure 4-1. Magnets were affixed in their holes with epoxy, with special care taken to check the orientation and polarity of each magnet prior to insertion (for over 360 magnets per model, for two complete 32-tile models).

For these Gen 1 tiles, we also designed an independent sensor node to communicate with other tiles and a base station. The original list of desired sensing elements included IMUs, Hall sensors, LIDAR Time-of-Flight (ToF) sensors, and even a microphone (for capturing interior sounds post-assembly), with a subset of these sensors ultimately implemented on the prototype circuit boards discussed below. Hardware and software development

in this phase benefitted from iterative development in Neil Gershenfeld's How to Make Almost Anything course (Figure 4-7) and later refined in Kerri Cahoy's 16.343 Spacecraft Sensors class (Figure 4-8).

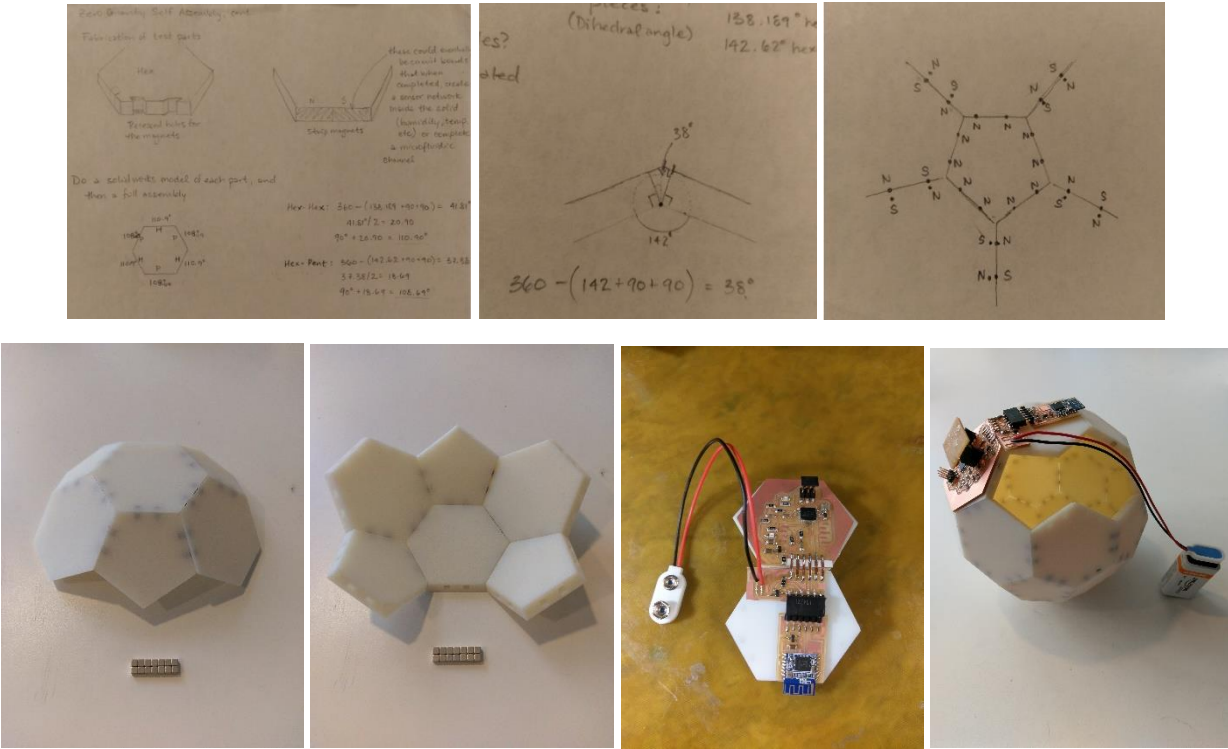


Figure 4-7. Top Row: Hand drawings from the earliest design of TESSERAE tile geometry and bonding joints. Bottom Row: Initial tile and in-house milled and stuffed PCBs, developed in Neil Gershenfeld's How to Make Almost Anything course at MIT (2016).

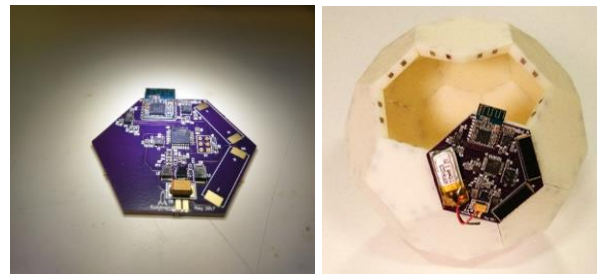


Figure 4-8. Version 2 of the Generation 1 hardware, refined in Kerri Cahoy's Spacecraft Sensors course at MIT (AeroAstro 16.343, 2017) with PCBs now professionally fabricated through OshPark (in-house assembly in the Responsive Environments group at the MIT Media Lab)

Following these identified sensing needs, a subset of components was carefully selected, taking into account several metrics that flow from our payload requirements and prototyping feasibility: functionality and contribution to the sensing application, power consumption, package size, and cost. With the latest revisions of our custom PCB, we hoped to keep costs low and fit all components into the fixed dimensions of the base hexagon tile. This allowed us to mount the PCBs onto the hexagon tiles as affixed sensor nodes that can track the lifecycle of the assembly—from initial tile release, to full structure configuration, to steady-state sensor reporting. Keeping costs low allowed us to develop a proof-of-concept plan for hundreds or thousands of these nodes, with an intention to create a swarm of tiles from which structures can stochastically arise. Keeping power consumption at a minimum was also critical for this stage of the project, as we envisioned deploying the sensor node tiles with small, onboard batteries and running data collection and reporting for multi-hour durations. Our approach employs an energy harvester solar power charging chip, paired with solar cells on the external tile surface, to test recharging via incident sunlight during lighted periods of a future orbit. See Figure 4-9 for a summary of component selection.

Key Components	Purpose	Notes on selection
AT Mega 328P	IC	Chosen for sufficient pin number, low power modes and familiarity/ease of prototyping
LSM303dlhc	6 DoF Accelerometer + Magnetometer	Includes a low-resolution temperature sensor, 16 bit
L3G4200DTR	Gyro	Low power, 3 axis angular rate sensor, 16 bit
HM-11 BLE	Bluetooth Low Energy module	Convenient prototyping model, good documentation of AT commands
BQ25570	Energy Harvester/Solar Charging chip	Chosen for notable low power consumption, to avoid constant drain on the battery (under 5nA)
3.7V Li-ion, 105mAh	Battery for onboard power	Chosen primarily for small footprint, 11.5mm x 31mm and matching mAh for desired duration of battery-powered operation.
KXOB22-01X8F	PV cells	Chosen primarily for small footprint, 22mmx7mm, and for matching open circuit voltage (4.7V) to that of the BQ25570

Figure 4-9. Table of major PCB components for TESSERAE Gen 1 boards.

The simplified schematic flow diagram shown in Figure 4-10 summarizes the main power rail, I2C connections for the sensors, SPI connections for the programming pins and UART Rx/Tx communication for the BLE module. The battery and photovoltaic (PV) cells feed into the BQ25570 energy harvester and are regulated down to supply a consistent 2.8V to the board (power and logic).

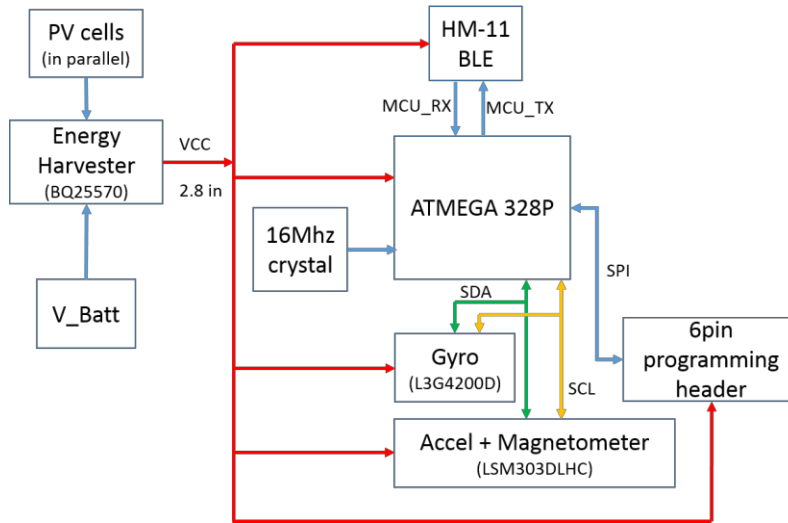


Figure 4-10. Simplified schematic for TESSERA E Gen 1 PCBs.

A key consideration for this board design was to keep the power consumption as low as possible, in order to achieve maximum operating duration with a relatively small Li-ion battery. In a significant redesign of our initial proof-of-concept board, this v2 design incorporates two monocrystalline PV cells (in parallel), selected to match the maximum open-circuit voltage of the MPPT bq25570 and provide supplementary re-charging for the battery. The PV cells are selected to provide more than the desired power output, to account for losses due to the imperfect efficiency (22% solar cell efficiency for the KXOB22-01X8F). The KXOB22-01X8F PV cell is also notable for its wide spectral sensitivity (300-1100nm), providing functionality in both indoor and outdoor settings.¹⁵² While initial deployment of this prototype was confined to indoor settings, we intended to explore this same PV cell (Figure 4-11) for use in time-limited, early external deployments.

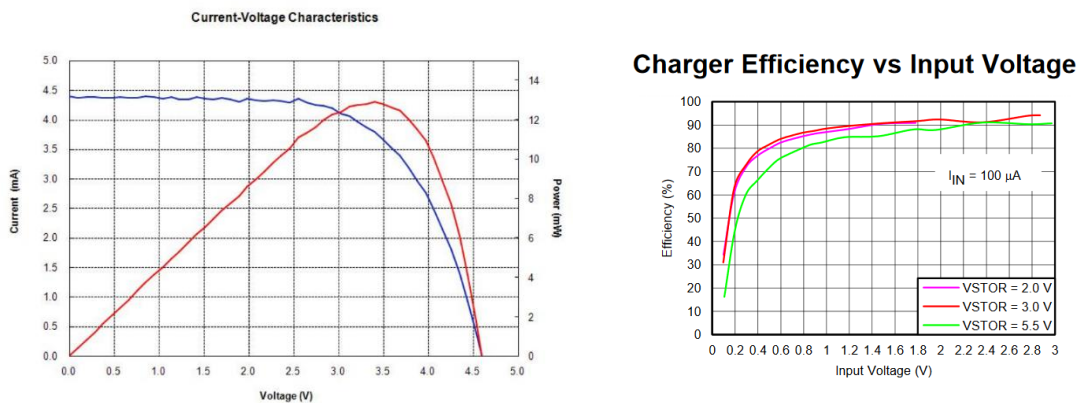


Figure 4-11. Performance curves for the KXOB22-01X8F PV cells.

The BQ25570 is notable for its impressively low “full operating quiescent current” state (488nA) and its approach for dynamically managing the load to meet the max power “sweet spot” on the PV cells' IV curve. As noted in the datasheet, the BQ25570 device is “specifically designed to efficiently extract microwatts (uW) to milliwatts (mW) of power generated from a variety of high output impedance DC sources like photovoltaic solar or thermal electric generators (TEG) without collapsing those sources.”¹⁵³ In addition, we have designed the circuit to achieve the maximum charging efficiency regime for a given value of VSTOR (Figure 4-11). Texas Instruments provides guidelines for choosing the resistors that populate the key VBAT_OV (max storage element voltage), VBAT_OK_HYST (threshold voltages for normal operation), and VOUT (the input VCC for the downstream circuit) lines, depending on the nominal battery voltage and desired output voltage. These values also affect the lifecycle of the battery (number of charging cycles, discharging rate, etc.) and our goal is to optimize for battery longevity (as the tiles will be remotely-deployed with no means to replace the power supply). We regulated the VCC down to 2.8V, to match the optimal operating regimes for the sensors and ATmega328P, per their datasheets.

Component	Full Power (mA)	Sleep State (uA)
ATmega328P	0.2	0.75
HM-11 BLE	15	600
BQ25570	Negl.	.445
LSM303dlhc	0.11	1
L3G4200DTR	6.1	5
TOTAL	21.4	607

Figure 4-12. Current draw by operating mode for major Gen 1 PCB components.

The low total current draw for this board lies well within our goal range (Figure 4-12), defining an achievable load for our chosen Li-ion battery. At peak current draw, we could run for just under five hours with the 105mAh capacity of the chosen batteries. The addition of the KXOB22-01X8F PV cells provides a modest amount of supplementary current: 3.8mA each, at peak performance. Together, the PV cells could supply a maximum of 36% of the current draw in the current configuration.

This power source and power consumption model gives more than ample operating time for the expected assembly period, and a subsequent period of low-power and sleep-mode operation. We note that the power in both modes (full and sleep) is dominated by the HM-11 BLE module. For subsequent revisions, we may seek out a lower power version, or power it directly off a pin from the micro-controller to be able to power it off completely when not in active use.

In addition to the IMU sensor packages, we were interested in range-finding between tiles as they dynamically assemble. We are also interested in measuring the distance between tiles once they are stationary, to confirm that the anticipated buckyball configuration, with proper steady-state separation between tiles, has been achieved. These requirements led us to consider various ToF sensors, which use a LIDAR approach. We anticipated placing a ToF sensor on the underside surface of each tile (the surface that faces the interior of the structure), and ultimately did do this for the Gen 2 Blue Origin hardware discussed in Section 4.1.2.

While we ultimately selected the VL6180x and VL53L0x (“sister” chips, varying primarily in their range of detection) for testing, we also considered other gesture, ambient light and IR ranging sensors (APDS-9960 RGB gesture sensor—used later in the TESSERAE technology roadmap) before settling on ToF sensors for their improved precision and applicability for our use case. The two sensors are both notable for their small size (a benefit to our spatially-constrained PCB design) and their ability to report ranging data independent of target reflectance. Both modules are also designed for low power operation.

A proof-of-concept, miniaturized PCB was fabricated to test the above sensor node design with a BLE network topology for sensor-sensor and sensor-to-central downlink node communication. After careful consideration of the various wireless radio modes often considered in similar project contexts (xBee, ZigBee, WiFi, etc.) we chose BLE 4.0 for its extremely low-power operating states, its adaptive frequency hopping (AFH) capability to avoid data transmit channel collisions, and its relative ubiquity in consumer devices.¹⁵⁴ Early deployments of our prototype were subsequently tested in environments where other BLE devices were present and this will continue to be the case (e.g., an onboard computer for sub-orbital testing, astronaut laptops) and we will greatly benefit from the ease of connecting with and interfacing with proximate devices for data transfer. In addition, the bandwidth limits, range and network size all fit our requirements. We do not require the thousand-node support that Zigbee offers, at this time. While we have initially designed the communication architecture in a standard BLE star topology (a central node communicating and dynamically pairing with multiple peripheral nodes), we look forward to exploring the mesh-supported topologies in BLE 5.0. See Figure 4-13 for a comparison of the available communication modes.

Name	Bluetooth Classic	Bluetooth 4.0 Low Energy (BLE)	ZigBee	WiFi
IEEE Standard	802.15.1	802.15.1	802.15.4	802.11 (a, b, g, n)
Frequency (GHz)	2.4	2.4	0.868, 0.915, 2.4	2.4 and 5
Maximum raw bit rate (Mbps)	1-3	1	0.250	11 (b), 54 (g), 600 (n)
Typical data throughput (Mbps)	0.7-2.1	0.27	0.2	7 (b), 25 (g), 150 (n)
Maximum (Outdoor) Range (Meters)	10 (class 2), 100 (class 1)	50	10-100	100-250
Relative Power Consumption	Medium	Very low	Very low	High
Example Battery Life	Days	Months to years	Months to years	Hours
Network Size	7	Undefined	64,000+	255

Figure 4-13. Communication protocol comparison chart¹⁵⁴

The custom PCB sensor nodes were manually bonded to the outer surface of the 3D printed tiles, when necessary for testing. See Figure 4-14 for the PCB layout and a close-up of a populated board. While never flight-tested in this exact configuration, this board and the low power optimization principles continued to evolve through our spiral process for prototype development through the three generations of TESSERAE hardware.

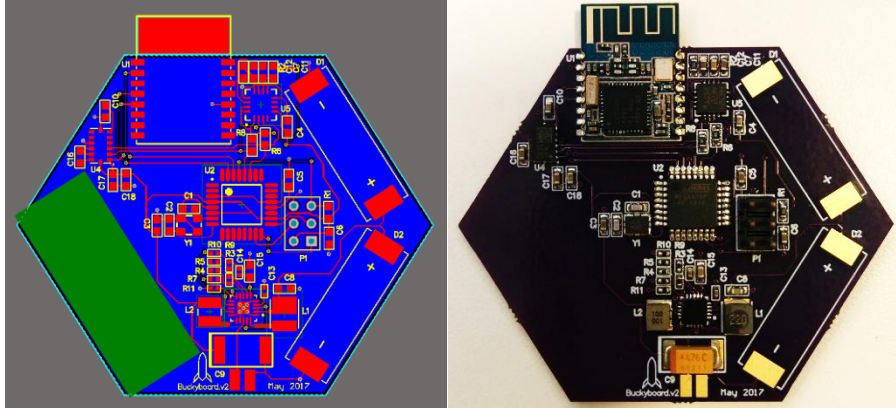


Figure 4-14. PCB layout in Altium (Left); Populated board with room for small battery and two miniature PV cells (Right).

Parabolic Flight Methods & Results:

For our November 2017 parabolic flight, we deployed two Generation 1 sets of 32 tiles each, at 1:53 scale when compared against the prospective habitat deployment size outlined in Chapter 6. Each set was identical and designed to assemble into a 13cm diameter C60 buckyball structure. The tile edge length was 2.86cm, with a total volume (internal void and shell) of 1293cm³. Passive, neodymium magnets served as the jointing mechanism, as testing at this stage was focused primarily on validating the mechanical concept and assembly time-scale. The first set was placed in an 18" x 18" x 18" container; the second set was placed in a 14" x 14" x 14" container. These volumes were selected based on the anticipated buckyball outer diameter, to explore whether additional free space facilitates quicker assembly via greater flexibility in tile rotation and circulation exposure, or whether it inhibits assembly by providing too much space for tiles to settle away from one another. The experiment ran over 20 parabolas (including two lunar and one Martian parabola at the beginning of the flight). The oscillation of the gravity environment in the plane provided an informal “kinetic perturbation” for the system, ensuring that tiles were jostled significantly into interaction with neighbor tiles. We did not deploy the PCB sensor nodes as part of this test—our results discussion centers on camera analysis instead. As our very first zero-gravity deployment, this parabolic flight was intended to investigate two questions:

Baseline Performance: do the tiles come together as anticipated and self-assemble via the magnetic joints?

Containment volume: holding all other variables the same, how does containment volume affect the dynamics of assembly?

Figure 4-15 shows our initial setup, with the tiles arranged on the floor of the two containment boxes. Tiles were arranged in a pre-set pattern in each box prior to the first parabola, and allowed to float free during the repeated periods of microgravity. Though the bottom surface areas of the two boxes are different (by design), an attempt was made to be as consistent as possible in the initial tile placement for the two boxes. During breaks, tiles were re-arranged in preparation for the subsequent string of parabolas. Three regimes were tested: (a) all tiles separate, (b) seeding method where tiles were pre-assembled into groups of three to five, and (c) hole-filling test where the majority of tiles were manually pre-assembled and we tested the ability of the remaining tiles to fill the holes.

With this parabolic flight test, we were able to validate the basic mechanism of self-assembly and confirm that the tiles are drawn together over a separation distance of several centimeters, over the course of a parabola's 10-15 seconds. We noted successful, independent assembly of subsets of the buckyball geometry, though not

of the full structure. We observed that the full set of parts gathered together (in various states of expected and unexpected geometries) over a shorter time-scale in the smaller-volume box than in the larger-volume box, due in part to the increased prevalence of tile-tile interaction. In addition to the hypothesized assembly behavior (constrained to matching magnet joints), we also observed extensive clumping, where weak magnetic forces on the top and bottom surfaces of tiles captured neighbor tiles. This was due to the neodymium magnets' extra bonding faces exerting attractive forces through the plastic shell, above and below the recessed holes (rather than solely acting through and bonding via the exposed faces). Fortunately, this presented a clear mitigation strategy: tile designs with greater thickness of plastic above and below the recessed magnet holes (i.e., overall thicker tiles) to more effectively block undesired surface interactions and detection of clumping via proximity sensors on all faces.



Figure 4-15. Experimental test apparatus for microgravity flight (Left/Center), assembly behavior during flight (Right).

We note four key takeaways from a shell architecture perspective:

1. Baseline Performance: Even without the assistance of electromagnetics, we were able to confirm the efficacy of our magnet joint polarity design and validate the fundamental assembly mechanism. Tiles were drawn together over a separation distance of several centimeters, over the 10-15 seconds of true microgravity on each parabola. Longer microgravity periods were needed to conclusively determine the optimum containment volume as a function of fully-assembled TESSERAЕ module volume—this later parameter is also extensively explored in the simulation modeling in Chapter 5.

2. Erroneous Behavior: While the system yielded partial-shell fragments of the intended assembly curvature, we also noted extensive clumping and metastable bonds. This was due to magnetic interactions outside the exposed bonding face, as the force of magnetism acted through the plastic layers. Fortunately, we can mitigate this straightforward issue by thickening the tiles and increasing the distance, r , between the embedded faces of magnet that should be non-interacting. Due to the scaling of magnetic force with $1/r^2 - 1/r^4$ depending on the magnet geometry, even a small distance increase yields a significant drop-off in attraction between tiles. The addition of electromagnets in future prototypes also helped to address this via the error correction mechanism (on-demand repelling actuation) and enabled us to avoid over-thickening the shell tiles.

3. Time to Assembly: Speaking to the time-scale of assembly predictions, we noted that both self-assembly tile systems (Box 1 and Box 2) reached an equilibrium state after two to three microgravity parabolas (~60 seconds of microgravity total); the tile bonding pairs and clumping groups established by this point did not materially change through subsequent parabolas until we intervened manually. This suggests two conclusions: first, that the magnet-mediated self-assembly bonding converges rapidly to an energy-favorable state when adequately contained; second, that active error control must be included to correct for local minima structures and keep the assembly progressing towards the desired topology.

4. Extensibility Beyond Microgravity: With favorable implications for future on-surface deployments, we were able to fly two lunar gravity ($\sim 1/6$ Earth gravity) parabolas and observed that proximate dyad pairs (a pentagon and hexagon) were able to snap together from resting position on the floor surface. While tiles could not further combat gravity to accrete upwards on the structure, this base-level attraction speaks to the ease with which magnet assembly can facilitate on-surface construction (provided the force of magnetic attraction is strong relative to the force of gravity acting on the tile).

Generation 1: Summary

At 13 cm in diameter, this prototype offered a meaningful, small-scale test of each general element of an adaptive, self-assembling system as identified in the Introduction: base unit, jointing method, assembly protocol, and holistic function. With fixed hexagon and pentagon tiles, tuned to the proper dihedral angle and embedded with magnets, we created a base unit that is simple, easily replicated and assembles with neighbors when brought into close proximity. The magnet joint polarity design need only define two unique joints, allowing us greater flexibility in the jointing method and improving the probabilities for predictable assembly in a stochastic system. The assembly protocol—passive, stochastic assembly in zero gravity—was validated on the November 2017 parabolic flight. This test validated the feasibility of stochastic, magnetically mediated, microgravity self-assembly in a contained volume. Our test results established a clear pattern of 3D self-assembly error modes and meta-stable states (Figure 5-1 in Chapter 5) that we then preemptively designed against in our later quasi-stochastic prototypes. Finally, the sensor nodes and communication architecture developed at this stage provided the foundation for critical assembly-process monitoring, data-gathering and information-exchange that we relied upon in subsequent prototypes and deployment tests. This Generation 1 proof-of-concept pointed towards a fully networked, sensor-augmented “self-aware” self-assembly system for the future of in-orbit habitation structures.

4.1.2 Generation 2: Tested via Suborbital Launch and Parabolic Flight

Hardware and Software Development

The Generation 2 tiles increased in complexity and feature suite. Hardware development for the Gen 2 tiles was extensively scoped by the requirements in the Blue Origin Payload Users Guide (PUG) and their Payload Data Package, and through the iterative hardware milestone reviews with their team. We undertook the Gen 2 development knowing we were aiming for deployment on a specific New Shepard mission (NS-11 ultimately flew on May 2nd, 2019) from the beginning. We also deployed the same hardware on a subsequent parabolic flight in August 2019. The main deltas between Gen 1 and Gen 2 hardware are:

- Larger tile shell, with two pieces (base and clear lid for LED troubleshooting) creating an accessible inner compartment
- Integrated electronics and sensing, with a motherboard and new, additional “peripheral” boards for each exposed bonding face
- Integrated communication between tiles and a shared Raspberry Pi (RPi) base station
- Actively controllable EPMS (consumer off-the-shelf parts, or COTS)

See Figure 4-16 for the hardware components integrated into the tile shell. This tile generation included a two-part tile shell, a motherboard and five or six ribbon-connected peripheral boards (depending on hex or pent geometry), and two commercial, off-the-shelf miniature EPMS (diameter 10mm) on each bonding face. We selected an advanced lithium hard-shell 9V battery to power the hardware, primarily based on flight heritage and launch regulation constraints.

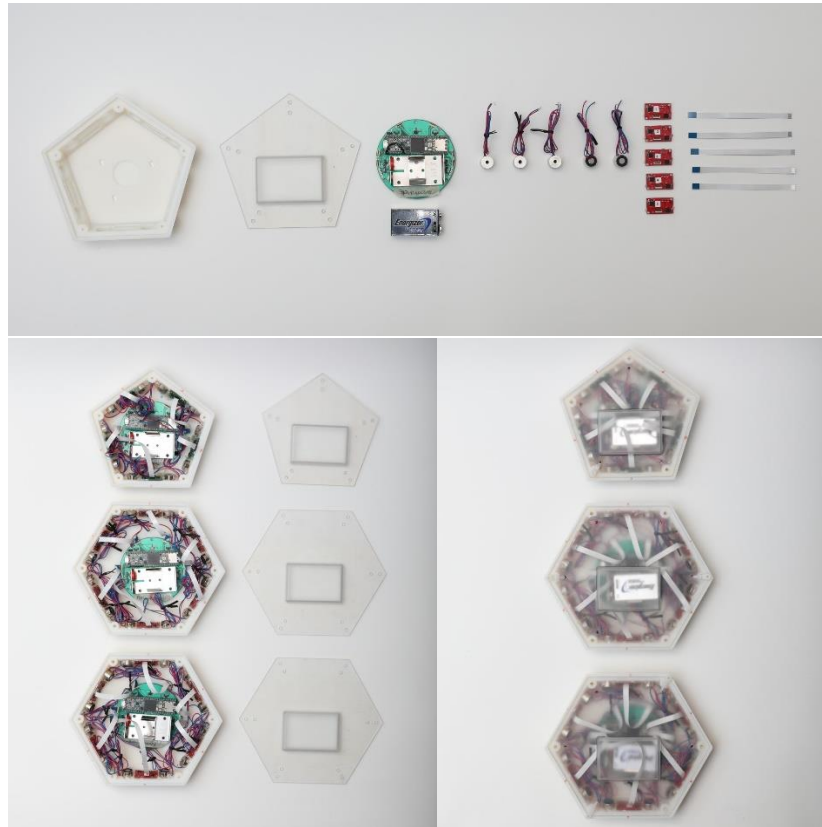


Figure 4-16. From top, constituent part breakout for Gen 2 tiles, tiles assembled with lids off, and fully assembled tiles from top-down view.

Now, for the first time, we also developed an extensive Arduino (C++ for the Teensy microcontroller now used in place of the single package ATmega from Gen 1) and python code base and control architecture. The sensing inputs drive autonomous diagnostic decisions that then drive EPM activity. We considered several, integrated sensing suite approaches, including at one point capacitive touch contacts for determining bond events. In the end, we settled on a stepped diagnostic algorithm that began with proximity gesture detection and concluded with RGB color exchange between the tiles. An intermediate magnetometer step proved critical in correctly differentiating between bond event types (good bond, metastable, bad bond), and we tested several units (there is significant variability even between magnetometer packages of the same part number) to establish proper thresholding based on the sensor package response. We used the magnetometer sensing data to make clear delineations between good bonds meeting the thresholding values, meta-stable bonds detected and clearly below the good bond threshold, and unbonded states. Also, for the first time, we integrated communication between the three tiles and a base station developed for flight, using a BLE architecture developed in collaboration with Aswin Venkatapathy at the TU Dortmund Fraunhofer Institute. This communication

architecture took telemetry inputs (during the Blue Origin flight, these were sent by the onboard rocket computer and corresponded to key flight engine cutoff stages) and sent signals to the tiles to enter a low-power wakeful standby state, enter the active state-machine run state, and/or store sensor data depending on the flight milestone. Figure 4-17 through Figure 4-23 show the key components of the Gen 2 PCB, the logic for the overall control algorithm, the magnetometer threshold fine-tuning, and the communication architecture logic.

Key Components	Purpose	Notes on selection
MLX90393	Magnetometer (peripheral boards)	Prior combo accelerometer + magnetometer from Gen 1 was discontinued; MLX Melexis offered improved performance.
APDS-9960	RGB sensor/emitter (peripheral boards)	Useful combo of digital proximity, ambient light, RGB and gesture sensor
Teensy 3.6	IC (motherboard)	Integrates with Arduino for ease of bootloading and programming; sufficient pins with separate I2C multiplexer
BNO080	IMU (motherboard)	Bosch, high-end VR-grade IMU
VL53L0x	ToF (motherboard)	Time-of-Flight ranging sensor, selected over cousin VL680x for more applicable range.
HM-11	BLE module (motherboard)	Communications chip, validated in prior hardware
TI - LM2623	Boost Converter (motherboard)	Take 9V battery power and convert up to 12V for EPM pulse

Figure 4-17. Table of key components on peripherals and motherboard for TESSERAE Gen 2 hardware.

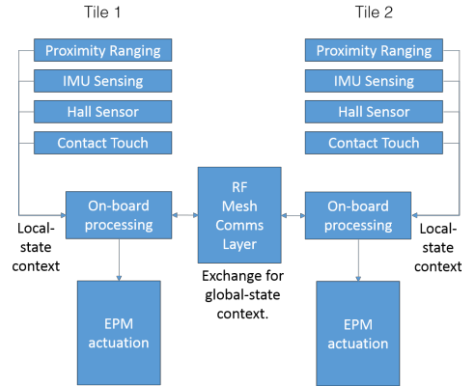


Figure 4-18. Early plan for TESSERAE Gen 2 control algorithm, showing alternative sensing flows that were considered.

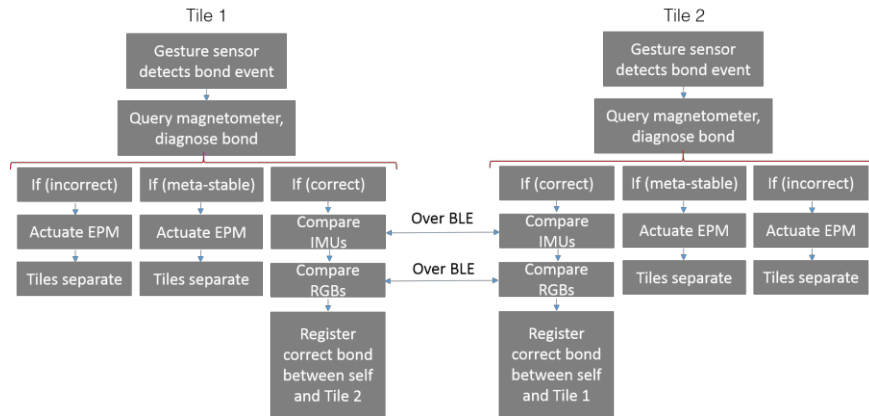


Figure 4-19. Final control logic plan for TESSERAE Gen 2, post-learnings from May 2019 Blue Origin flight; implemented in this configuration for the subsequent August 2019 Zero-G flight.

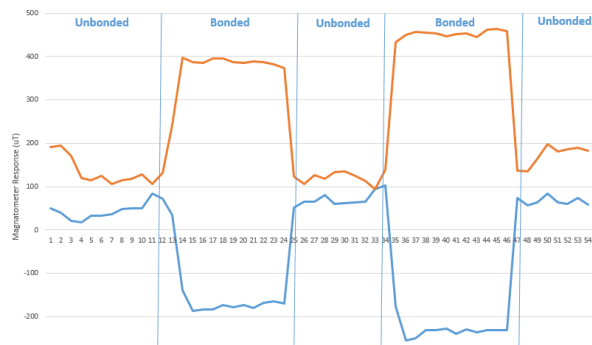


Figure 4-20. Magnetometer data (uT) for a pentagon tile (orange) and a hexagon tile (blue) drawing together in two distinct, separate bonding events over one minute. Plot shows activity on magnetometer z-axis.

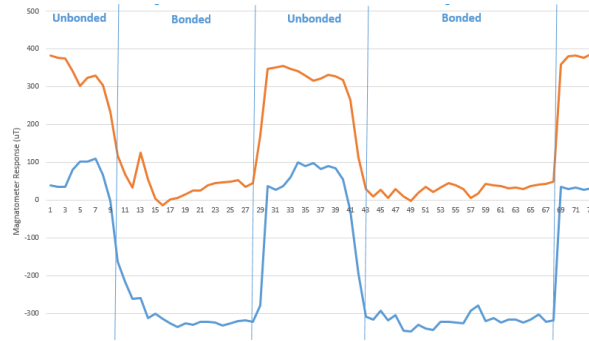


Figure 4-21. Magnetometer data (uT) for two hexagonal tiles (orange, blue) drawing together in two distinct, separate bonding events over one minute. Plot shows activity on magnetometer y-axis.

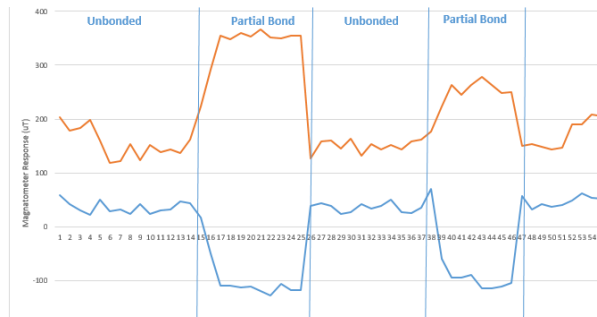


Figure 4-22. Magnetometer data (uT) for a pentagon tile (orange) and hexagon tile (blue) in a metastable bond. Partial bond is detected and correctly diagnosed as metastable due to magnetometer values lying below the threshold for a stable bond.

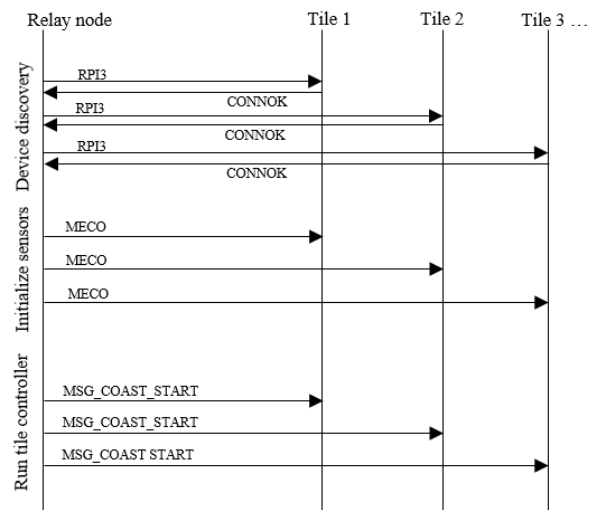


Figure 4-23. Communications architecture for suborbital launch test, with experiment-prep signal (MECO) and experiment-start signal (MSG_COAST_START). Image courtesy of collaboration with TU Dortmund Fraunhofer Institute.

As we prepared for flight, we also developed extensive documentation and analysis of the hardware, including a comprehensive bill of materials and center-of-mass analysis, shown in Figure 4-24.

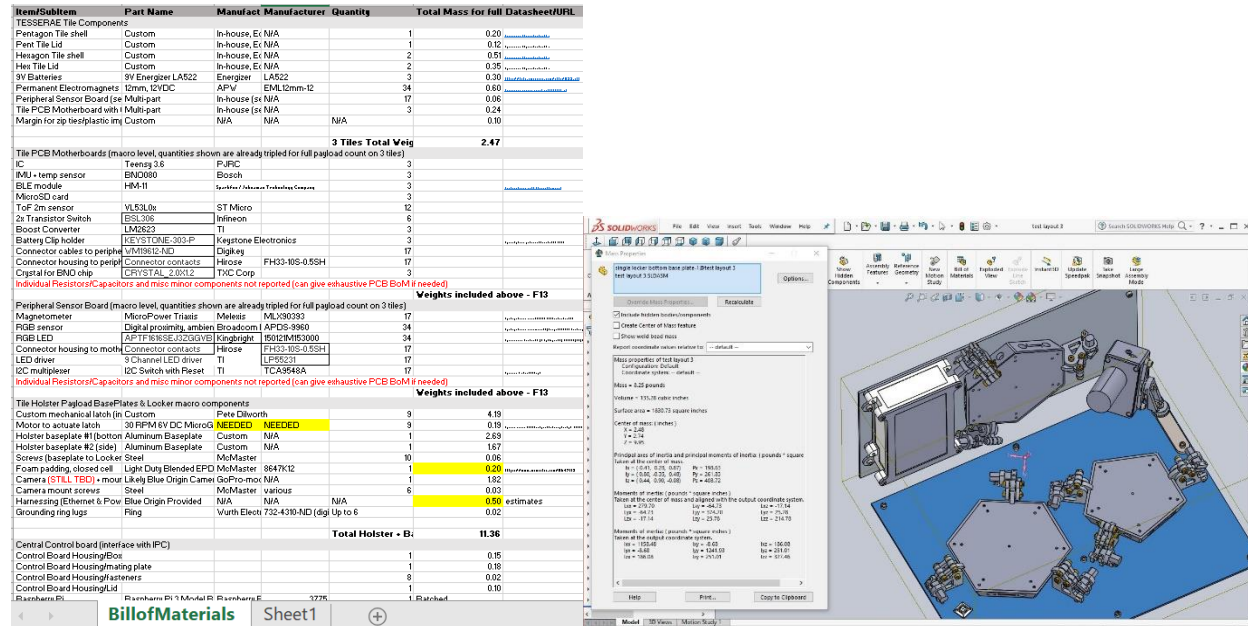


Figure 4-24. Screenshot of a selection of the TESSERAE Generation 2 bill of materials for the Blue Origin New Shepard flight opportunity. Screenshot of a center-of-mass analysis performed for the launch readiness acceptance packet, courtesy of Peter Dilworth via Solidworks.

Suborbital Launch Pre-flight Integration and Test, Methods and Results

For our 2019 suborbital test, we deployed three responsive TESSERAE tiles inside Blue Origin’s single payload locker. The tiles, latches, and full experiment apparatus were extensively tested at MIT Lincoln Laboratory across a three-axis random vibration test and sine sweep—the hardware passed the test with no modifications required and evidenced no vulnerabilities at the frequencies of vibration expected during launch. After many months of development, the hardware and software preparation culminated in an intensive four day on-site integration at Blue Origin’s West Texas Launch Facility. We thoroughly tested all functional aspects of the tiles, in addition to integration testing into the Blue Origin single payload locker hardware apparatus and software telemetry system (IPC). A detailed experiment check-out plan was put in place, to ensure proper pre-flight configuration (batteries loaded, SD cards loaded, latches shut, final flight config code loaded, lid bolted down, etc.) for a midnight handover prior to the early morning launch. Figure 4-25 shows the final check-out and hardware inspection with the Blue Origin team.



Figure 4-25. Final experiment integration and check-out at Blue Origin's West Texas Launch Facility.

Three tiles (two hexagons and one pentagon) were fixed rigidly against the sides of the payload locker during launch, released at the beginning of the coast period, and allowed to float free and circulate. The containment chamber kept the tiles in close enough proximity that the EPMS only needed to act over small distances (inches) to bring the tiles together (thus allowing for lower field strength, lower mass magnets). All parts included (tiles, base plates, latches, RPi experiment control board, harnessing, and all) weighed in at just under 15lbs (Figure 4-26).

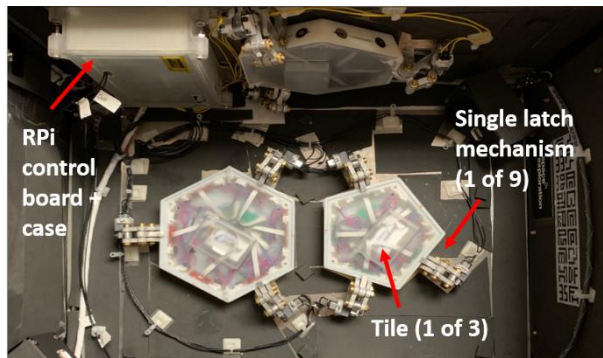


Figure 4-26. Initial arrangement of TESSERAE Tiles for 2019 suborbital launch test, situated inside Blue Origin Single Payload Locker experiment chamber.

For our 2019 suborbital flight, we designed custom latching mechanisms to secure the tiles during launch, while still ensuring robust confidence in timely and clean release in microgravity. In Figure 4-27, we show the latch mechanism used on three sides of a tile inside the Blue Origin single payload locker container. This latch design is predicated on a hybrid motorized “vise-grip” design, where counter pressure ensures a tighter static grip (e.g., for reinforcement during launch loads) but the tab mechanism can be elegantly and smoothly retracted with a small motor on demand (credit to Peter Dilworth for the vise-grip design and latch fabrication). During mission deployment, all nine latches successfully actuated on the first attempt, upon receiving the trigger signal from onboard flight control to release.



Figure 4-27. Left: Close-up of suborbital launch latch mechanism. Right: Three latches in action, securing pentagon TESSERAE tile for flight. Designed by Peter Dilworth.

Tiles were powered on prior to beginning flight (insertion of 9V batteries) but placed in an ultra-low power sleep mode for energy conservation prior to launch. Tiles were latched securely against side walls and an RPi experiment control board was primed to receive rocket launch stage telemetry data signals at the experiment-prep milestone (during final stages of ascent and engine cut-off) and at the experiment-start milestone during the beginning of the coast start (the most pure, undisturbed period of microgravity after the boosters have shut off). Upon receiving the experiment-prep signal, our RPi control board woke up all three tile PCBs via a BLE wireless signal and activated our sensors autonomously. Upon receiving the experiment-start signal, the latches were released, and tiles were allowed to circulate freely within the single payload locker cabin; the tile controller state machine was switched into active self-assembly mode. Sensor data was continuously logged during flight onto onboard microSD cards on each tile's PCB motherboard. Specialized cameras mounted in opposing corners of the enclosure captured video footage. The experiment proceeded for approximately three minutes of stable microgravity before the New Shepard craft returned to the ground and our experiment was returned in post-flight configuration.

Over three minutes of clean microgravity, we validated our latch design (all nine latches actuated on the first signal), observed the tiles being lightly ejected from their housings, confirmed the state machine entry into live-communication mode and sensing mode, and confirmed that the tiles draw together successfully over centimeter distances in a matter of seconds (see progression in Figure 4-28 and experiment operation timeline in Figure 4-29). We observed one bond event (the motion of two tiles becoming rigidly linked) and were able to gather data on the resultant local minima energy state. These two tiles settled into a rare metastable bond that was outside the range of our proximity sensors, and thus, the system did not have time over the short three-minute mission to successfully detect and pulse off nor perturb this into a proper in-plane bond. As discussed in the feature set of the new EPMs for the ISS mission (Section 4.1.3), this led to a redesign of the sensing approach and control state machine to instead rely on the magnetometer for bond event detection. This also motivated an interest in swivel bearings for the EPMs.

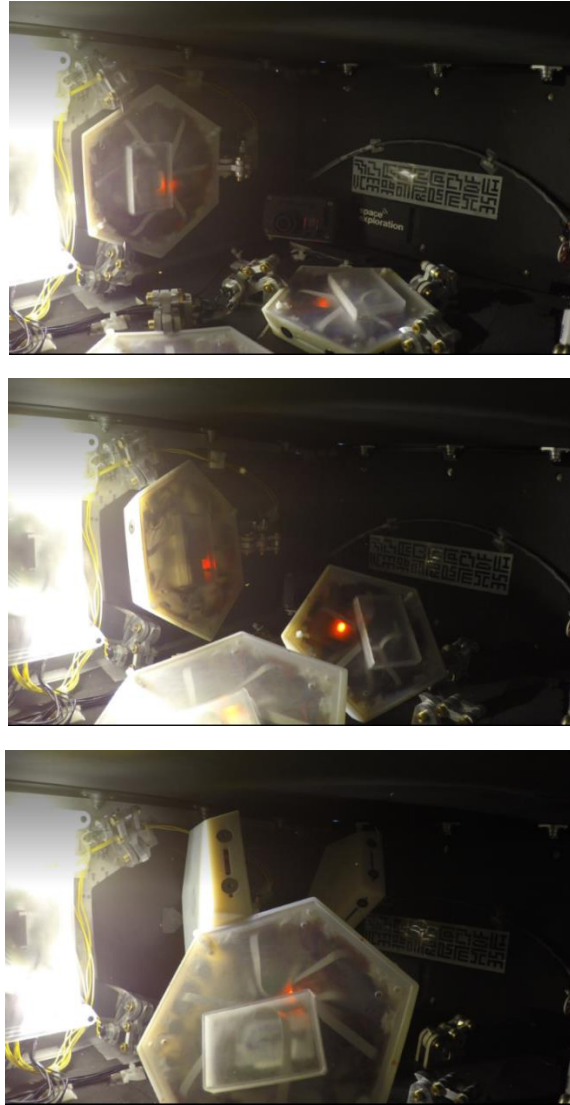


Figure 4-28. Top to Bottom: Tiles latched, released, and bonded on Blue Origin suborbital flight.

Action Trigger	Description of Payload or IPC Action	Anticipated TESSERAE Payload Power Draw from Blue
~5 minutes prior to T-0	IPC is powered on and running	0W
Flight Warning: Liftoff Imminent	Cameras turned on. RPi and Tile sensor board running in low power modes.	6.75W
Flight Event: Coast Start Detected	Cameras on. RPi and Tile sensor boards running in high activity mode. RPi actuates latches to release tiles, #1, #2, #3 in close succession. RPi high activity for BLE comms (2W).	14.5W
Flight Event: Apogee	Cameras on. RPi and Tile sensor boards running in high activity mode. Tile sensor board actuating electromagnet separation sequences as required/initiated by sensing action and onboard code. Tile sensor boards communicate motion data and bonding data to each other and to RPi over BLE. Backup data is logged via Ethernet from RPi to onboard controller.	7W
Flight Event: Coast End Detected	Cameras on. RPi and Tile sensor board return to low power modes.	6.75W
~5 minutes after CC Landing	IPC is powered off. Cameras turn off and RPi powers down safely.	0W

Figure 4-29. Experiment operation timetable, with power consumption from Blue Origin onboard system. Internal power consumption of the tiles (battery-powered) not included.



Figure 4-30. Liftoff for the NS-11 mission on the morning of May 2nd, 2019. Team celebration after the successful launch (including fellow MIT SEI payload teams and their separate experiments) and capsule return later that afternoon.

Parabolic Flight Methods & Results

For our 2019 parabolic flight, we deployed the same three TESSERAE responsive tiles inside an 18" x 18" x 18" enclosure. Tiles were powered on prior to beginning flight (insertion of 9V batteries) and left in a loose, patterned arrangement on tile floor (Figure 4-31). Upon receiving power, sensors were automatically activated for data logging and the autonomous control algorithm began processing through our state machine. Sensor data was continuously logged to onboard microSD cards on each Tile's PCB motherboard. GoPros mounted in opposing corners of the enclosure captured video footage.

We observed tile behavior (watching for self-assembly events, and maintenance of formation flight) and system stability (watching for light signals indicating active sensor recording and status updates, thermal checks in case of magnet overheating, etc.) over 20 parabolas, including a mix of lunar, martian, and zero-g.



Figure 4-31. Initial arrangement of TESSERAE Tiles for 2019 parabolic flight.

Over multiple parabolas, we were able to test and maintain formation flight (Figure 4-32), where all three TESSERAE Tiles stayed bonded in the correct topology configuration (after having been manually set into the proper state in an earlier parabola trial). Due to the extremely short periods of zero-g (only 15-20 seconds per parabola), the system generally does not have enough time to self-assemble at this tile mass (greater inertia), and thus this test centered primarily on maintaining a steady-state constellation of tiles after a proper three-way tile bond had been pre-set. Together, the tile assemblies weighed approximately 1.13kg and were able to repeatedly withstand falls back to the bottom of the box (upon return of gravity at the end of the parabola) from 15-25cm high. This shows that the TESSERAE assembly, at this relative ratio of EPM holding force to tile mass, can withstand gentle collisions even without reinforcement clamping. The parabolic flight TESSERAE software included an update using the magnetometer input *first*, for both bonding event detection and diagnosis.



Figure 4-32. TESSERAE tiles in formation flight, 2019 parabolic flight test.

Generation 2: Summary

Generation 2 TESSERAE shell tiles successfully demonstrated integration of sensing and control algorithm activity into a quasi-stochastic self-assembly system. We developed new, larger tiles and integrated off-the-shelf EPMs for prospective on-demand tile separation for bonding error states. This hardware was tested over three minutes of sustained microgravity on a May 2019 Blue Origin New Shepard suborbital flight (re-usable rocket) and again a few months later, with code modifications, on an August 2019 ZERO-G parabolic flight. The Blue Origin launch marked the first time TESSERAE hardware flew in space, as the experiment crossed the Kármán line at an altitude of more than 100km. This brings the TESSERAE project to two major hardware generations across three total microgravity or space environment deployments. Our experiment progress to date—successes and limitations—greatly influenced the design of the follow-on mission to the International Space Station.

4.1.3 Generation 3: Tested via ISS Mission

The third generation of TESSERAE shell hardware improved considerably upon prior models, leading to a successful 30-day mission onboard the International Space Station (ISS) in March and April 2020, integrated into the NanoRacks BlackBox platform. In assessing the prior parabolic flights and suborbital launch results, we identified several areas for improvement, discussed below. These features were addressed, and new hardware was rapidly generated from scratch through prototyping and lightning speed development over six months from August 2019 to the ISS integration and safety review period in January 2020.

Generation 3 hardware goals:

- Validate quasi-stochastic self-assembly over a longer duration in orbit via magnetic attraction
- Demonstrate on-demand, autonomous error detection and successful error correction via the TESSERAE sensing platform, control logic state machine, and EPM actuation

Summary learnings from Generations 1-2, adapted into the 2020 ISS Generation 3 design:

- **Optimized use of the magnetometer.** We now begin the bonding diagnosis with the magnetometer, rather than the proximity sensor. While initially useful for determining neighbor-ranging behavior, the proximity sensor suffers from edge cases where partial bonds do not trigger correction, if the tile slots remain primarily unblocked despite a magnet attraction event (e.g., a heavily skewed or out of plane metastable bond between tiles, like what occurred on the Blue Origin flight; Figure 4-33). Moving the magnetometer sensing to earlier in the logic test queue provides for two key benefits: (a) a reliable “event” threshold when tile magnets come close enough to each other to engage in bonding activity and trip our magnetometer threshold and (b) via pattern analysis undertaken in the ISS 2020 sensor code, we can identify and differentiate signatures of “good bonds” where two pairs of magnets are perfectly aligned, from partial or metastable bonds where magnets are in different spatial coordinates, to accurately inform the next step of the control algorithm. Perfectly inverted, incorrect tile bonding between N-N (pent) and S-S (hex) tiles produces the same magnetometer signature as the proper bond (Figure 4-34), so a mechanical feature is added to keep this inversion from mating securely; this ensures the magnets remain offset, producing a different magnetometer reading and inducing a proper “bad bond” diagnosis.



Figure 4-33. Two Gen 2 tiles inside the Blue Origin chamber bonded without completely obscuring the proximity slot; ISS hardware and control code was updated to correct for this and rely instead on the magnetometer for bonding event detection and first-pass diagnosis.

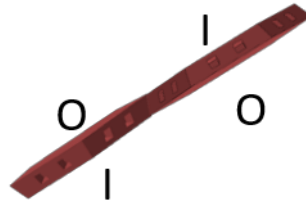


Figure 4-34. A diagram showing an inverted tile pair, where the outside surfaces (O) of the two tiles are not aligned; For NN-SS pairs, this produces the same magnetometer signature as the properly aligned case, so additional physical blocking must be undertaken to prevent this from forming a permanently stable bond.

- **Tile topological features.** To address the above edge case with the magnetometer, and in general to disadvantage inverted tile bonds, we designed a custom topological feature on the bonding sides of the tiles, in the style of Bachelet’s puzzle-piece blocks,¹⁴ but with a different purpose. The tile shell modification provides a protrusion on pentagons and matching recession on hexagons that only allows flush mates when tiles are in the properly aligned (not inverted) configuration, to avoid stable bonding of inverted tiles. See further discussion in the *Mechanical: Tile Housing* subsection below.

- **EPM redesign.** Limitations from prior COTS parts motivated a custom EPM design. We pursued the following features, ultimately realizing four out of the five (the last, swivel motion, proved infeasible with the miniature tile size for this particular ISS deployment):
 - Distinct North and South polarities on each cylinder cap end (the interacting face of the magnets), rather than a coaxial polarity, to fully realize the assembly benefits of the original design delineation (Section 4.1) between NN, SS, and SN faces for the tile edges
 - Ability to actively repel, beyond simply neutralizing the permanent magnetic field
 - Smaller physical housing to meet the miniaturization needs for constrained operating volume on the ISS
 - Swivel capability, via encasing the EPM in a ball bearing housing, such that tiles mated at one magnet pair point can pivot to fully align the bonding faces and self-correct from a metastable bond to a stable, full face good bond
- **Charging and power handling.** To achieve a longer interaction experiment period, we needed a way to keep the tiles alive for extended periods after initial activation, while supporting pulse requirements for the EPMs. This posed a challenge given the size and chemistry limitations of standard flight-allowable batteries. We settled on a charging approach that allowed the tiles to be flown with batteries that were depleted (a launch requirement for ISS) and topped off via inductive contacts once power was turned on for our larger experiment control apparatus. While not needed in this flight experiment, as tiles did not return to the charging holsters after deployment in the ISS chamber, the charging system and battery selection design allows for repeated recharging of the same tile, which we did use extensively during on-ground testing. In combination with the charging approach, we turned to supercapacitors (supercaps) to supplement the steady-state battery for adequate pulses of high power (up to ~15-20W for two seconds).
- **Safety checks for magnet overheating.** Issues with power hungry COTS EPMs straining our 9V batteries on the prior suborbital deployments led us to implement safety checks on EPM actuation to avoid overheating. Code logic prevents more than one side of a tile from actuating magnets at the same time (can later be removed when power system is less constrained), and a 60-second cool-down timeout is forced between subsequent re-actuations of the same magnet pair (also aids in providing time for the tiles to distance themselves after a bad bond correction, avoiding over-actuation of the EPMs for a single error-handling case). In addition, the supercap recharging implementation off the steady-state battery requires time, adding a natural buffer against runaway EPM firing.

Work began in earnest in August 2019 with a redesign of the tile PCB features to accommodate improved sensing strategies, a combination flex-rigid approach for the miniaturized motherboard and periphery boards, and a new EPM actuation profile, which levies requirements on the power delivery and regulation system on the boards. Custom EPM development proceeded through the fall, with integration coming together over the 2019-2020 holidays for PCB stuffing, EPM and power wiring, and physical incorporation into 3D printed tile housing. Functional and integration testing at various levels (tile subsystems; experiment apparatus subsystems; full experiment walkthrough) proceeded in January and February, including two trips to the NanoRacks ISS mission facility in Houston, TX for flight qualification and NASA safety review. We integrated our experiment apparatus into the NanoRacks BlackBox platform, which in turn integrates with the ISS interior experiment racks, and handed over on February 22nd for a March 2nd launch at Cape Canaveral, ultimately rescheduled due to rocket systems checks to a late-evening launch on March 6th. The experiment was installed and power activated off the ISS experiment racks on March 10th, running with intermittent result downlinking until deintegration in the first few days of April and Dragon Capsule return splash down in the Pacific Ocean on April 7th. The tiles were retrieved and full camera footage and sensor logs were subsequently analyzed. The new

technology contributions, functional testing, systems integration approach, flight plan, and flight results are described in the following subsections.

In implementing these extensive Generation 3 changes and preparing the overall, broader apparatus for the ISS mission, we were fortunate to have the support of a fantastic team of contributors from both outside (Aswin Venkatapathy – TU Dortmund; Levi DeLuke – MIT MechE) and inside (SEI staff engineers Jamie Milliken and Pete Dilworth; SEI research affiliate Ara Knaian) the Lab.

ISS Mission Hardware and Software Development

The Generation 3 tiles included four main subsystems: mechanical housing, electrical sensing and processing, EPM actuation, and supervisory state machine that provided control logic for the quasi-stochastic self-assembly. The following sub-sections detail the development considerations and technological contribution outcomes, in each area, for the thesis.

Mechanical: Tile housing

All prototype tiles to date have been 3D printed to sub-millimeter tolerances via an Eden Objet (now Stratasys) light-curing photopolymer printer. This fabrication method provides a rapid turn-around time for design changes and re-prints, while also supplying the tolerances necessary for avoiding gaps between tiles when neighboring exposed magnet-faces come in to bond. Across the 32-tile buckyball target geometry currently used for our prototypes, it is critical that we keep the slope angles between tiles accurate (aka the dihedral bonding angles for the buckminsterfullerene C60 chemical form) in the physical hardware to allow for a completed assembly, as tolerance errors accumulate and could result in a final hole to fill that is too small for the remaining final tile.

The mechanical modifications reflected in the Generation 3 tiles include fine-tuning features for improved sensing, ease of tile lid and bottom removal for prototype testing, integration with a charging docking holster, and assembly error handling. Due to limitations in the volume available for an experiment chamber on the ISS, we miniaturized the tiles, keeping most dimension relationships the same. We did widen the slots on the bonding sides to better accommodate new peripheral sensing boards that must “see” out the sides and we created a recessed area that matched the tallest component on the peripheral boards to allow these parts to lay flat and stable for affixing to each side.

For ease of access to the electronics and a board that is now two-sided (requiring SD card access on top and battery plug access on the bottom), we added a “trap door” removable bottom for the tile. The tile lid is raised slightly to accommodate the internal layering of battery, motherboard and supercaps, and seats into place via two tiny side clasps with a single screw-in point for reinforcement. Two holes to accommodate V+ and GND charging posts include delicate copper contact pads affixed to the outside. Chiral protrusions and matching recessed areas on the pentagons and hexagons, respectively, aid in ensuring that the tiles only mate flush when their outward faces are aligned (when one tile is flipped or inverted, the trapezoidal protrusion will not nest fully, thus forcing a metastable bond that can be detected and corrected). Inside the tile shell, we mount a motherboard and five or six peripheral side sensor boards (pentagon and hexagon side count respectively). These PCBs control the responsive sensing and downstream activation of EPMS, as required.

With all parts included, the pentagons created for flight weighed in at 73g (ten EPMS total, across five sides), and the hexagons (with only three of the six sides populated with magnets) weighed in at 71g. Due to the space

restriction on the ISS, and only being able to deploy one “petal” worth of tiles (one central pentagon and five hexagons, with one backup pentagon), we decided to maximize chances that the hexagons would bond to the pentagon and reduce the need for unnecessary battery consumption correcting bonds between hexagon sides. This led to only populating the pentagon-bonding sides of the hexagon tiles with EPMs. See Figure 4-35 for detailed views of the Generation 3 tile features and Figure 4-36 for a close-up on the tile charging holster.

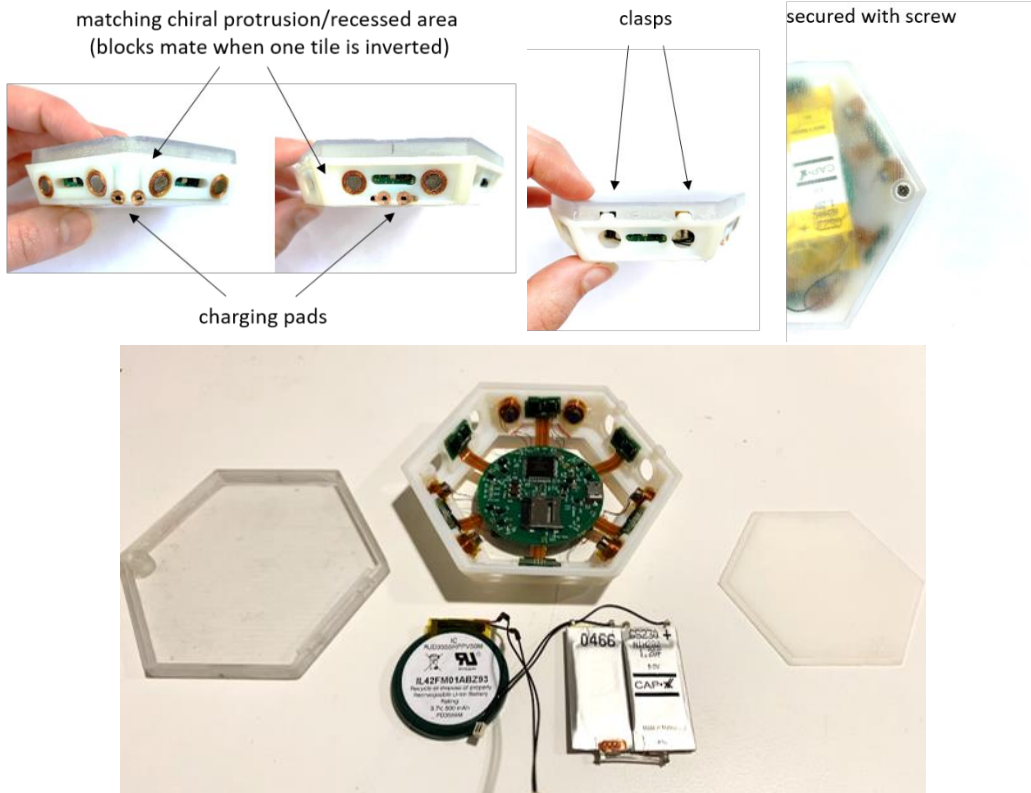


Figure 4-35. Top: diagrams showing tile mechanical features, for fine-tuning the hardware for ISS deployment. Bottom Image, Left to Right: tile top lid, tile housing integrating with PCB, battery and supercap pair, tile bottom flap.

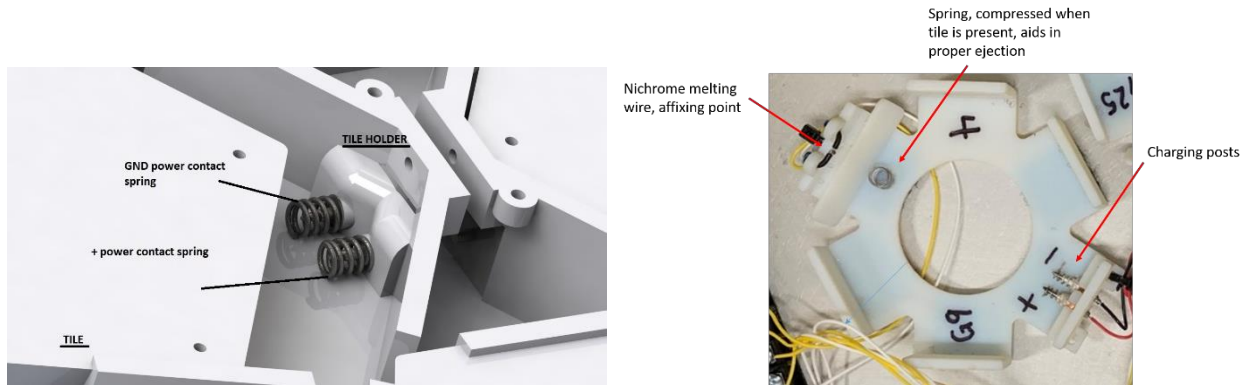


Figure 4-36. Left to Right: Close-up render depicting holster configuration with powered springs and encased rods that both make contact with the tile’s exterior copper pads for charging and reinforce the tile’s stability in the holster prior to release; 3D printed holster with labeled components. Credit to Peter Dilworth for tile holster fabrication.

In Figure 4-37, we show the newly designed mechanism for securing the TESSERAE tiles to the walls of the BlackBox chamber for launch, and later controlled release at the start of the ISS mission deployment. Due to the particularly constrained physical space, we designed a latching system that lays flat against the interior chamber walls, reinforces the tiles for launch, and can gently eject tiles on-demand upon controlled, low-level heating of nichrome wire that burns through and releases a nylon holding strap. To accommodate the tightening of the nylon across the tile for launch loads, we carefully sanded down the tile lid edge across which the nylon string lies, to avoid the risk of premature wear, abrasion and separation before intended release.

While we do not expect to release TESSERAE tiles from rigid side walls with mounted latches in the at-scale, orbital use case, the suborbital and orbital generations of latch hardware are invaluable for providing new flight heritage models for other research in our department, and as design primitives for the TESSERAE holster mechanism that will ultimately eject tiles from a stacked configuration in a payload fairing, out into a containment membrane for self-assembly.

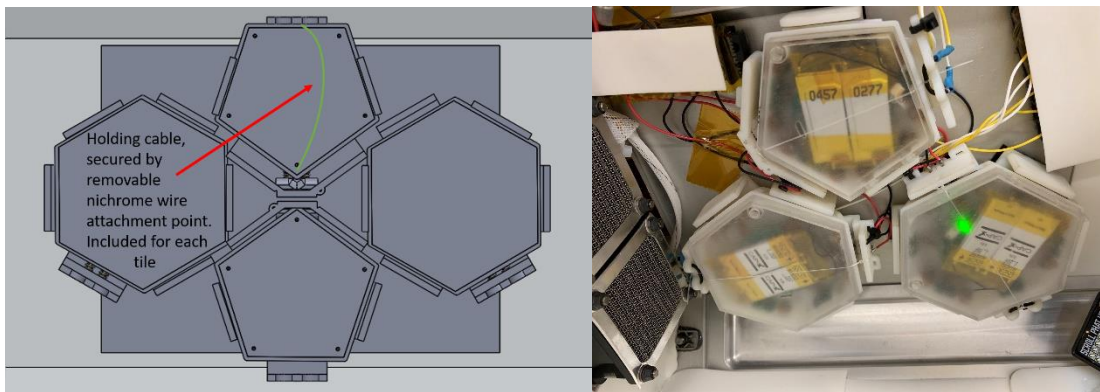


Figure 4-37. Left: diagram showing four-holster bank with indication for nylon strap attachment points; Right: several tiles in a three-holster bank, showing the nylon strap containing them against a vertical wall in pre-flight ground testing.

Electronics: Sensing, Communication, and Power Handling

Between the Blue Origin suborbital deployment and the ISS deployment, the primary driver for change in the PCB design was the need for miniaturization. The boards had to fit in a much smaller tile housing, while supplying the same functionality as before (see Figure 4-38 for a listing of the major sensor, communication and processing components), and accommodating new EPM firing circuitry. This led to a redesign with a six-layer PCB, with flex arms extending to peripheral extension boards that affix to each tile-bonding side slot for neighbor sensing. The flex arms provided the ability to keep electrical connectivity across different spatial planes (flat bottom, angled side slope) and provided some give for accommodating slight changes in the dimensions of the tile housing while we tweaked mechanical fit with the tile holsters.

<i>Component</i>	<i>Part Reference</i>
Bootloader IC	Teensy 3.6
MicroSD card for data storage	Generic, 16GB
VR-grade IMU	BNO080
Time-of-Flight ranging and proximity sensor	VL53L0X
Proximity, ambient light, RGB and gesture sensor	APDS-9960
Magnetometer	MLX90393
Assorted LEDs for status indication	Generic
Bluetooth Low Energy module	HM-11

Figure 4-38. Sensor and communications component table for Generation 3, ISS hardware.

Power Handling:

While the scales and environments in which we are currently conducting proof-of-concept testing are quite different than our ultimate goal of deploying in the vacuum in orbit (e.g., we will need to select entirely new radiation-hardened and non-outgassing components for many of the sensors and ICs listed above), we can still maintain one optimization across all models—minimization of power consumption. This is useful both in our interim testing, where we are physically space constrained and cannot afford to have large batteries taking up precious interior deployment volume within our chartered flight boxes, and also when we transition the architecture to an orbital deployment where we are limited by the surface area of solar panels that we can realistically add to the structure. See Figure 4-39 for an overview of the power handling components in the Generation 3 tiles.

<i>Component</i>	<i>Part Reference</i>
Li-ion over-charging and over-discharging protection	AP9211SA
Power distribution load switch	AP22815
Battery Charger IC	MAX8808X
DC-DC Boost converter (up from 3.3V to 8.3V for EPM actuation)	MCP1661
Hard case Li-ion 3.3V 500mAh battery	RJD3555
Cap-XX Supercapacitor 1.2F each	HA230F

Figure 4-39. Power Circuitry Component Table

For the latest Generation 3 design for ISS deployment, we designed the system to run on a 3.3V 500mAh coin cell battery, supplemented with two 1.2F supercaps to provide short-pulse, high current power to the EPMS during actuation windows. The battery is rechargeable, with carefully designed charging circuitry to avoid over-discharge, over-voltage, and over-current protection to meet NASA safety standards. Furthermore, the coin cell battery includes short circuit protections. The tiles survive seven to eight hours on baseline power in a sleep state off the RJD3355 battery; we placed a code limit on the number of allowable supercap actuations (e.g., 20 per tile, per mission) to ensure that even after many actuations, enough power is left for basic data gathering and BLE exchange with the RPi control base station. Through extensive testing and circuit optimizations assessing the voltage drop across all components and even the length of traces, we ultimately settled on an EPM power circuit architecture with two 1.2F supercaps in series and a V_{mag} of 8.3V post-boost, targeting 5.85V and 4.5A through the coils. This allowed us to achieve significant repulsive force between EPM units (only one coil actuated in each bonded pair, to reverse polarity and reduce energy consumption), see prediction plot and sample of our supercap discharge behavior analysis below in Figure 4-40, with further discussion of the EPM design and behavior in the following section. Figure 4-41 shows a system diagram overview of the TESSERA E Generation 3 tiles.

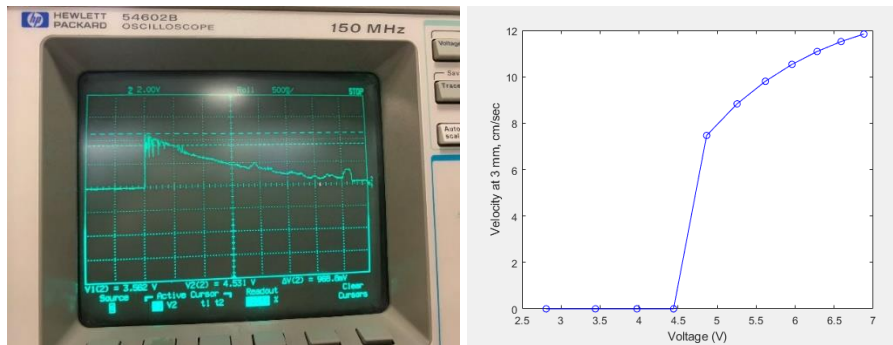


Figure 4-40. Left: Supercapacitor discharge testing analysis to determine peak voltage output while hooked up to our in-tile power circuitry. Right: prediction plot for velocity of tile repulsion given V_{mag} ; plot assumes $R=1.3$ ohms for EPM coil and tile mass 70g. Plot generated by FEA COMSOL EPM model, created with Ara Knaian.

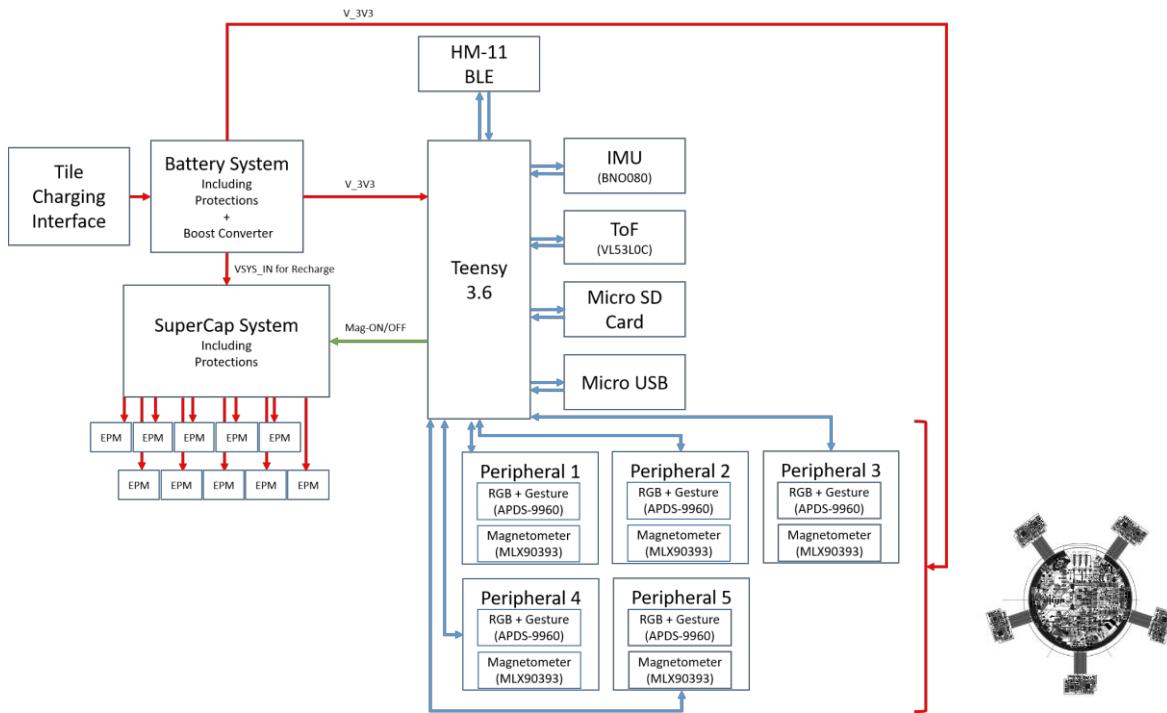


Figure 4-41. Overview system diagram for TESSERAE PCBs, showing pentagon configuration.

EPM Theory, Design and Fabrication

An electro-permanent magnet (EPM) is a device containing both a permanent magnet and a coil. Applying a pulse of electrical current through the coil can temporarily neutralize and/or reverse the magnetic field from the permanent magnet. In this work, we apply sufficiently low currents such that the magnetic field returns to its original value after the current is removed. As we progressed through prototype tests, we identified a pressing need for EPMs with a distinct set of functionality—a smaller cylindrical package, on the order of 5-10mm, than what can usually be found with COTS parts; active repulsion rather than strictly neutralizing the magnetic field; and a distinct North and South pole (so that a single unit can be used in all TESSERAE joints, while still achieving the required NN/SS and SN/NS polarity maps). Building off the “programmable matter” miniaturized EPM work^{23,28} and in direct consult with Ara Knaian, we designed a new EPM in COMSOL with our desired magnetic field strength and orientation, power profile and feature response to pulses of moderated current, and physical geometry constraints. This model provides an extensible platform that can also be used to design the macro-scale EPMs that will ultimately be used in orbit for a life-size TESSERAE. We then tested many model candidates by winding prototype EPMs with the matching parameters for in-lab testing and performance analysis.

The preliminary modeling results shown below are based on candidate EPM prototypes with 3mm diameter permanent magnet disks (we explored both neodymium and samarium-cobalt) and steel slug cores, wrapped in copper wire varying from 26-32 gauge. We solve Maxwell's equations with magnetoquasistatic¹⁵ boundary

¹⁵ The quasi-static approximation implies that the equation of continuity can be written as $\nabla \cdot \mathbf{J} = 0$ and that the time derivative of the electric displacement $\partial \mathbf{D} / \partial t$ can be disregarded in Maxwell-Ampère's law, per [COMSOL Reference Manual, Available: https://doc.comsol.com/5.5/doc/com.comsol.help.comsol/COMSOL_ReferenceManual.pdf].

conditions for the magnetic vector potential in the steady state (COMSOL mf application mode) and specify the constitutive relations (B/H curve) for the permanent magnet material and for the steel slugs. Ampere’s Law is applied on bounded geometries in the model to relate the integrated magnetic field around a closed loop to the electric current passing through. We then define expected solenoid coil parameters and a force relationship (based on the Maxwell stress tensor) to be able to measure the predicted Newtons of attraction and repulsion, at varying distances, between the two EPM faces. We cross-validated the initial conditions of our passive model, before running a current simulation, with our actual EPM prototypes and a gauss meter for: (a) magnetic field readings between two EPMS with 1mm or less separation (~1200-2000 Gauss depending on exact meter placement); and (b) magnetic field readings between 2 EPMS with 30mm separation (~400-700 Gauss depending on exact meter placement).

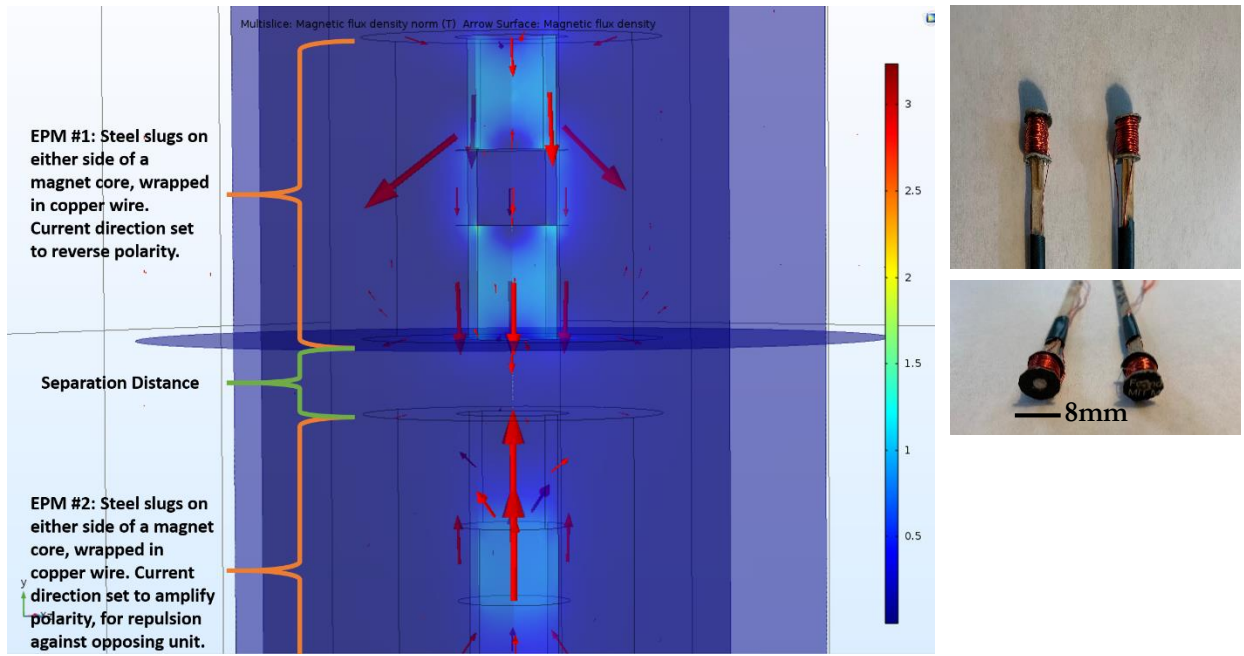


Figure 4-42. Left: COMSOL model of two EPMS, scale showing magnetic flux density in T. Right: EPM prototypes.

Below is the Maxwell Stress Tensor, in expanded form for air,¹⁶ where p is the air pressure, I is the 3x3 identity matrix, and the electric and magnetic fields (\mathbf{E} and \mathbf{B} , respectively) are 3 x 1 vectors:

$$T_2 = -pI - \left(\frac{\epsilon_0}{2} \mathbf{E} \cdot \mathbf{E} + \frac{1}{2\mu_0} \mathbf{B} \cdot \mathbf{B} \right) I + \epsilon_0 \mathbf{E} \mathbf{E}^T + \frac{1}{\mu_0} \mathbf{B} \mathbf{B}^T \quad \text{EQ(1)}$$

¹⁶ While the TESSERA modules will eventually be deployed in the vacuum, these EPM units were designed using the Maxwell force tensor in air, due to the expected deployment environment inside the pressurized part of the ISS.

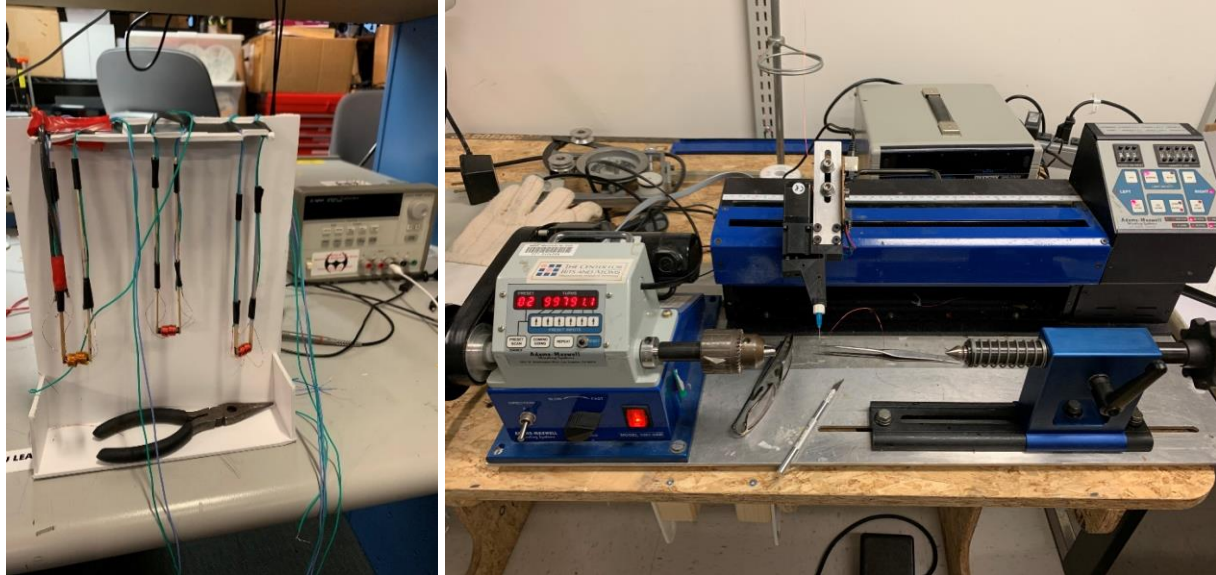


Figure 4-43. Showing in-lab test rig for EPMS with varying permanent magnet cores, various wire gauges and winding coil counts.

We were able to fine-tune precise aspects of the EPM design (diameter and depth; relative placement of the magnetic disk between the steel slugs; thickness of each sandwich component; number of coils and wire gauge, etc.) and run an extensive parameter suite across these factors to determine the best prototype candidates prior to mass manufacturing 150 units (75 North, 75 South given default current direction). We ultimately chose a pareto-optimal design along the 20W parameter contour (constrained by the maximum possible power delivery of our PCB design at the time), with asymmetrical placement of the permanent magnet disk between the steel slugs, Figure 4-42. We supplemented the model design specifications with in-person validation of the manufacturer's coil winding ratio, to determine the exact performance needed for the coil (dependent on the wire gauge and particular packing density for the finished coils) and settled on 126 turns with 32 gauge bondable wire with in-lab testing (Figure 4-43). We were able to validate the strong repulsive force predicted in the model (over three times stronger than the steady-state attractive force between the EPMS) experimentally with a live current test of the prototypes, and ultimately, with the successful and dramatic pulse-off events observed in microgravity onboard the ISS (see *ISS Mission Flight Plan and Results* subsection). We had predicted previously in Figure 4-40 a maximum theoretical velocity of 10cm/s due to EPM repulsion for tiles in the 70g mass range with our powering pulse profile. With the real hardware, we ultimately observed 2-3cm/s velocity due to EPM repulsion in the lab (with gravity moderated by a string test, but the tile's free motion was still partially stymied by the restoring force of the pendulum string), and around 5-7cm/s velocity of tile separation in the ISS experiment chamber with proper microgravity (see *ISS Mission Results* subsection). Figure 4-44 through Figure 4-47 show the design software views in COMSOL, our performance parameter sweep, manufacturing drawings, force calculation predictions and the final, professional manufactured units for our custom EPMS.

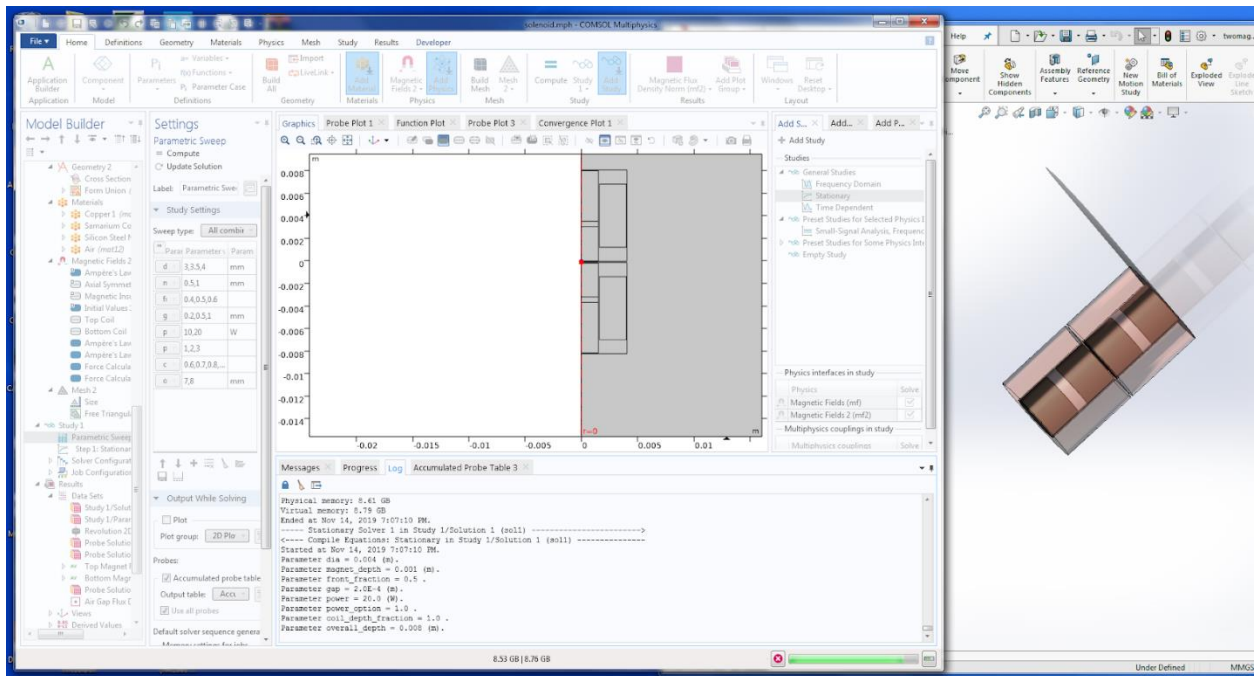


Figure 4-44. Screenshot from COMSOL EPM design model.

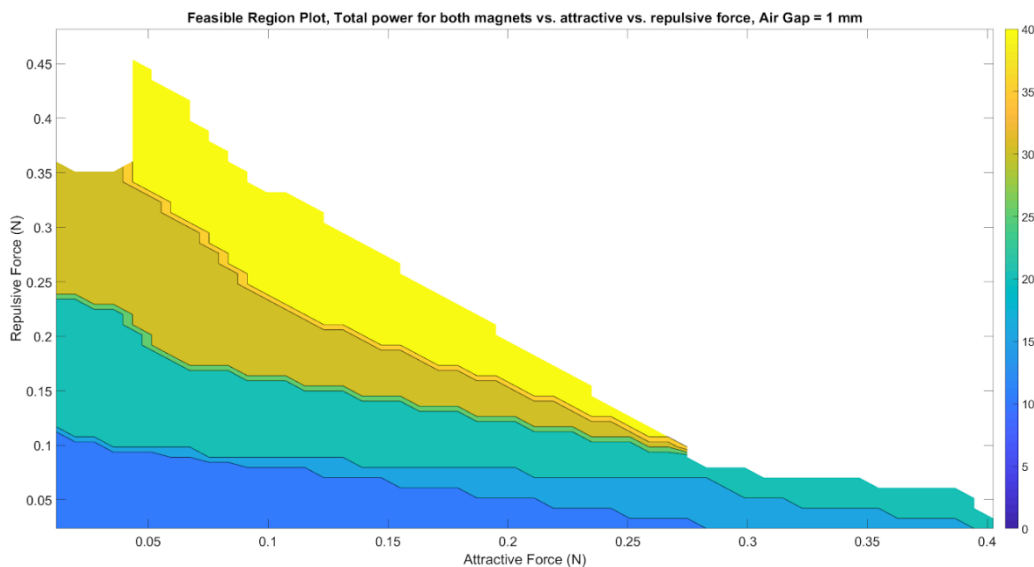


Figure 4-45. All EPM's shown here are 8 mm diameter and 8mm long. To access different places in the design space shown, we use different magnet diameters, thicknesses, positioning inside the unit, coil winding, and drive polarity combinations. This plot shows the 3D Pareto frontier of the design space. With our power supply we were able to operate anywhere up to (and including) the “20W” region. We carefully weighed the tradeoff between anticipated attractive force (which determines the efficacy of self-assembly in the first place, and suffers from a $1/r^2$ dropoff with distance) and the repulsive force (which determines the feasibility of forced tile separation for error correction). Image courtesy of Ara Knaian.

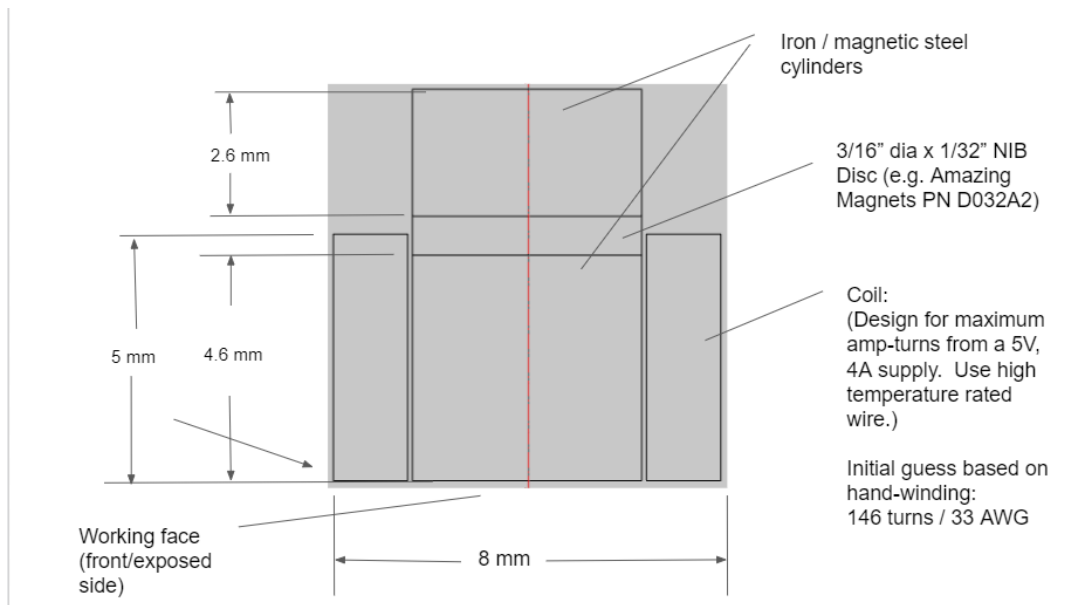


Figure 4-46. Drawing sent to manufacturer for final EPMs after extensive modeling and in-house prototype validation.

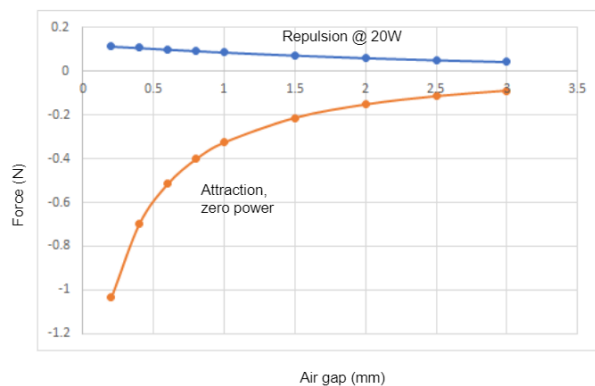


Figure 4-47. Left: Force vs Air Gap curve for the chosen design, showing attraction (orange) and repulsion (blue). Right: EPM units delivered in 75 N-S exposed pairs, for 150 total units.

This custom design work for a new EPM, tuned to precisely the needs of our experiment, proved invaluable. We were able to achieve a new level of functionality and successfully demonstrate effective error correction with an on-demand pulse of sufficient magnitude to separate two incorrectly bonded tiles. Beyond inclusion in the particular Generation 3 hardware, this EPM design approach lays the basis for custom EPM design for larger-scale units to be used in a future on-orbit technology demonstration mission, outside the confines of an ISS testing chamber.

A Control Algorithm for Self-Assembly: state machine code, error detection and correction

The TESSERAE tile platforms currently run on a modified “Bang-Bang” control paradigm, where tiles are switched between various discrete states based on a state machine with sensor data inputs driving the logic for the switch. This is also known as Hysteresis Control, due to the known dependence on the response gap timing between two states that cannot, in reality, be instantaneously switched.¹⁵⁵

$$\alpha^*(t) = \begin{cases} 1 & \text{if } 0 \leq t \leq t^* \\ 0 & \text{if } t^* < t \leq T \end{cases} \quad \text{EQ(2)}$$

Where $a(t)$ is the aspirational optimal control, with switching execution occurring at elapsed time t^* . After a $t=2-3$ second nominal EPM pulse and after the t^* switch completes, the EPM system remains in an Off configuration through buffering time in the state machine (to avoid rapid re-firing of the EPMs in the case of a persistent trigger that causes overheating and battery depletion) until a newly sensed event triggers the need for a subsequent pulse.

Figure 4-48 presents our state machine that controls the On/Off states for EPM actuation, as a form of self-assembly error control and mitigation when the tiles are forming incorrect or meta-stable bonds. As described in Section 4.1, we progress through a series of sensor checks to diagnose a bond event and either place that bond in a supervisory monitoring state (if assessed as a “good bond”) or actively separate the tiles via pulsing the EPMs (if assessed as a “bad bond”).

We made a key update between Generation 2 and Generation 3 hardware, switching to the magnetometer as the first-step bond event recognition and primary diagnostic tool. As a neighbor tile approaches, the magnetometer serves as the most effective early warning system, picking up the magnetic field from the incoming nearest magnet pair. This allows us to trigger a bond event and begin the diagnosis state machine. Once mated, even slight differences in the planes defined by the magnets in two opposing tiles yield distinguishable magnetometer signatures, allowing us to determine coplanar successful bonds or metastable, unsuccessful bonds, and progress through the state machine determination from there. Magnetometers do have limitations and are notoriously inconsistent from package to package. We found the best approach was setting a unique-to-tile set of thresholds for baseline (no neighbor nearby) and success conditions (good bond, with two pairs of magnets perfectly aligned), because the absolute values of the xyz-field coordinate readings from the MLX 90393 varied considerably across units.

After the magnetometer, the state machine progresses through checking proximity across the tile sensor slots, and then an RGB exchange of light pulses to ensure both tiles agree on their bonded status and progress in the state machine. If this multi-part RGB handshake proceeds successfully, the tiles have an optional setting to also complete a final check that their IMU sensors are reporting coordinated motion vectors, indicating a mate and synched tile motion (this final capability was not implemented in the ISS flight, due to time processing limitations in the state machine). If the sensor readings from either tile fail to meet a condition in this logic tree, the state machine redirects to an EPM pulse event, negotiating between tiles for which tile will do the actuation. It is important to avoid simultaneous EPM repulsion activation by both sides, as that means both sides switch their polarities with current actively pulsing through, which would create a stronger attractive force, rather than the intended flip of polarity on one side or the other. This aspect of the control algorithm provides an option for power saving, where only one tile need pulse off to correct a bad bond, thus collectively saving battery in a

two-tile neighbor interaction. This can be ignored, however, to let both tiles pulse off (but at different times) if redundancy is desired to ensure a backup chance at separation.

We place extensive requirements on the diagnosis of “good” bonds to avoid a false positive. We are more concerned with ensuring all bad bonds are corrected (as they inevitably block a full 32-tile assembly) than with preserving a borderline good bond, as a good bond can be attempted again, if needed. All code underlying this state machine is executed through .ino files on the Teensy 3.6 microcontroller. A shared code base has evolved across three flight opportunities, culminating in the current state for the Generation 3 hardware ISS mission with over 1500 lines of code. Phases 1-2 of the state machine are documented below, including a detailed RGB exchange, in Figure 4-48 through Figure 4-50. The state machine diagrams for TESSERAE tile controller code include wake-up sequence, bond diagnosis, and communication exchange. Drawings are courtesy of Jamie Milliken.

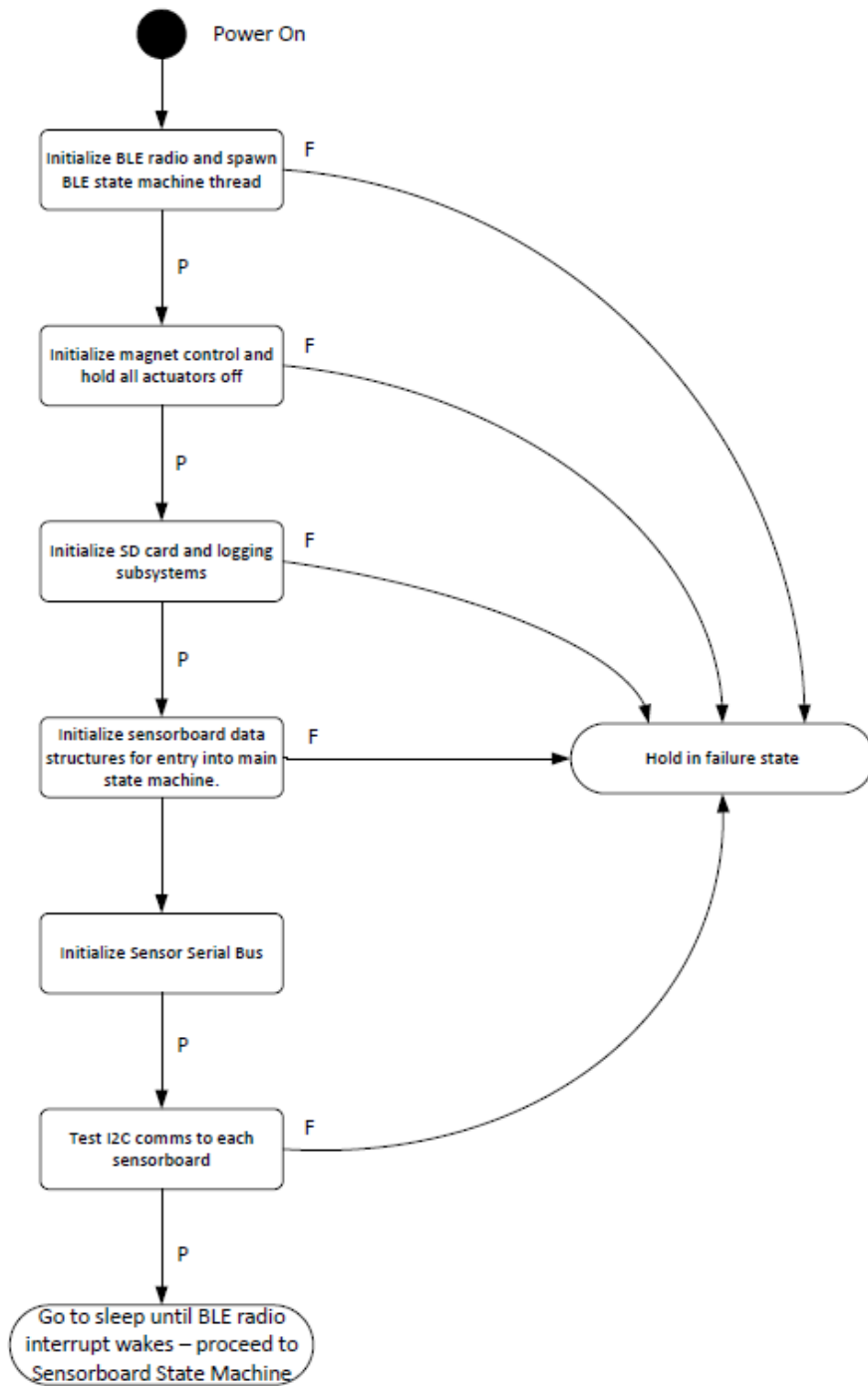


Figure 4-48. Phase 1. BLE communications and sensorboard initialization path; awaits BLE radio interrupt “wake” command from a base station to begin Phase 2.

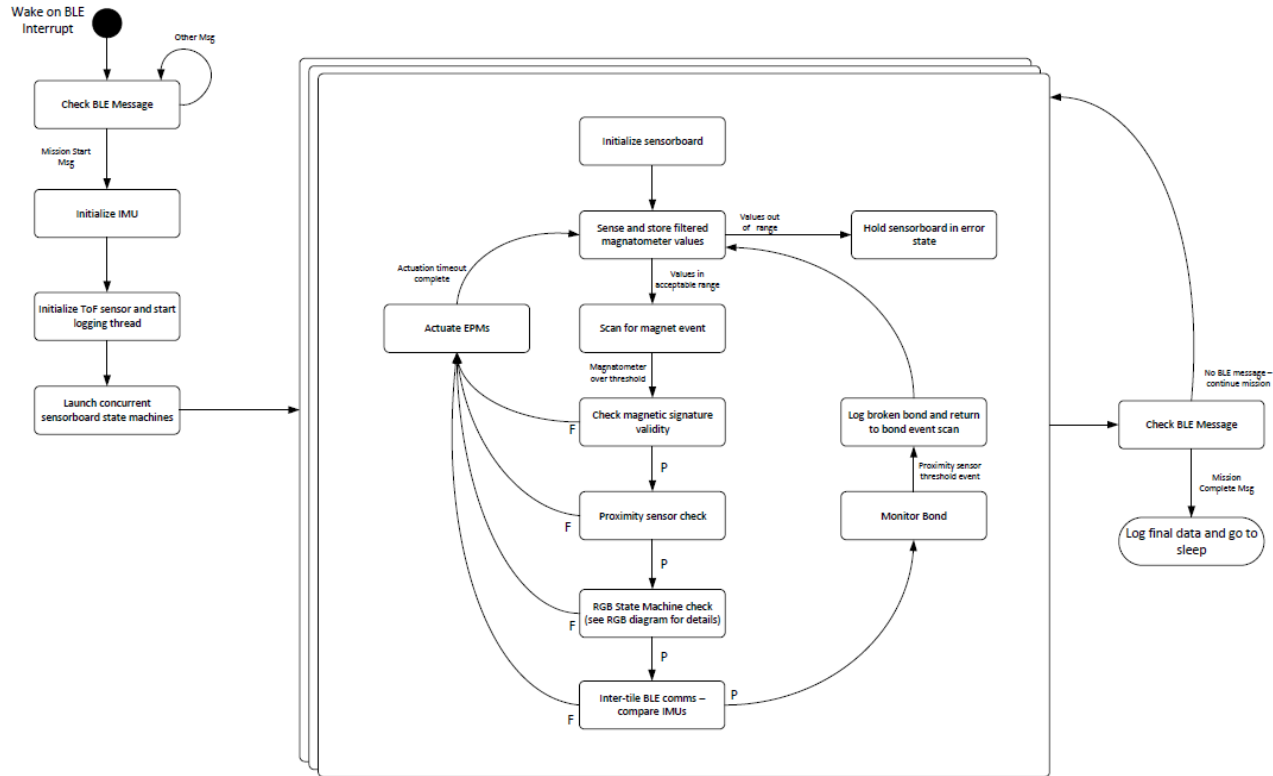


Figure 4-49. Phase 2. Primary state machine loop, progressing through iterative sensor bonding diagnosis checks; kicks system to actuate EPMS for any failure condition (e.g., detection of a bad bond) and commences error correction via negotiated tile separation; a perfect pass record for a bond event leads the tiles to a mutual monitor bond state, where a watchdog loop catches any off-nominal breaking of a good bond, and returns to the state machine diagnostic path if needed. Tiles communicate and agree on good bond status via the RGB exchange (shown below) and register their identity and bond status over BLE with the RPi base station.

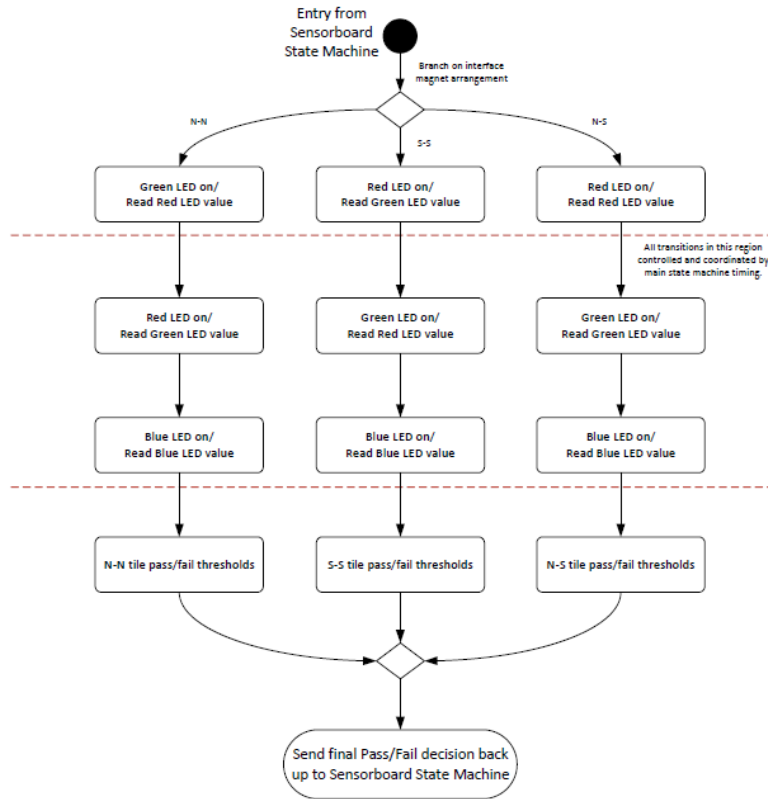


Figure 4-50. Inset detail on RGB state machine check in Phase 2. Light exchange handshake between tiles, depending on the side type (Pentagon N/N; Hexagon S/S; Hexagon N/S), allows the tiles to synchronize their bonding status and communicate whether they agree on good bond status. The robust capabilities of the APDS-9960 RGB emitter/sensor allows us to simultaneously broadcast and receive or interpret LED signals across two tile slots, though some timing and color optimization is required to avoid saturation in the tile slot.

Longer term, we are interested in developing a continuous control approach like Proportional-Integrative-Derivative (PID) control, which would allow us to have real-time looping feedback as tiles grow incrementally closer to one another and as the magnetometer, proximity chip and other sensors gradually log stronger bond signals. This would allow us to also use actuation of the EPMS to affect torques on the motion of tiles and actively guide path planning even when tiles are not in a near-to-finish-bond event configuration. Furthermore, as we scale to swarms of many tiles to meet a vision of redundant, always-available modular parts for generalizable self-assembly, we will consider adaptation of swarm and localization protocols, as detailed in the Nagpal lab Kilobots work.²⁶

ISS Mission Functional and Integration Testing: in Lab and at NanoRacks

After completing technology development for the main tile subsystems (tile housing, PCBs, EPMs, control code), we integrated (Figure 4-51) seven “flight” units and numerous sacrificial units for functional testing. Core categories of tile testing included:

- **Fit checks.** Ensuring individual parts fit within the housing, given part variability; tiles mating together with optimized tolerances for the chiral protrusions/recessions and flush, aligned mating for the EPMs; etc.
- **State machine performance tests.** Extensive bond testing, placing tiles into good and bad alignments, and iteratively improving the control code to detect edge cases and progress properly through the diagnostic logic; improvements to the state machine timing and speed of processing loops; etc.
- **Repulsion performance tests, via suspended tiles.** Tiles suspended with strings, placed into good and bad bonds, to determine integrated efficacy of state machine and the force of repulsion observed when EPMs are actuated and tiles try to separate; early insights from this testing category led to the crucial power optimization off the boost regulator, changing the V_{mag} line to 8.3V rather than the lower 5V range, as discussed in subsystem design, above.
- **Communication performance tests.** Tiles must communicate reliably over BLE to both kickstart the experiment and to exchange status information and data with the RPi base station for the experiment control, requiring careful documentation of BLE module addresses per tile and proper assignment in the code; extensive testing was undertaken to characterize the power profile during active communication, to ensure all seven tiles can reliably negotiate near-simultaneous communication on a shared BLE comms topology, to validate the communication handling manager.py code, and to ensure all edge cases are handled to avoid placing the tiles in limbo.
- **Fault and safety tests.** Ensuring that the code is bug-tested and does not cause nor allow magnet overheating, ensuring all wiring polarity is correct to avoid reverse biasing the circuits or puffing the supercaps in flight, etc.

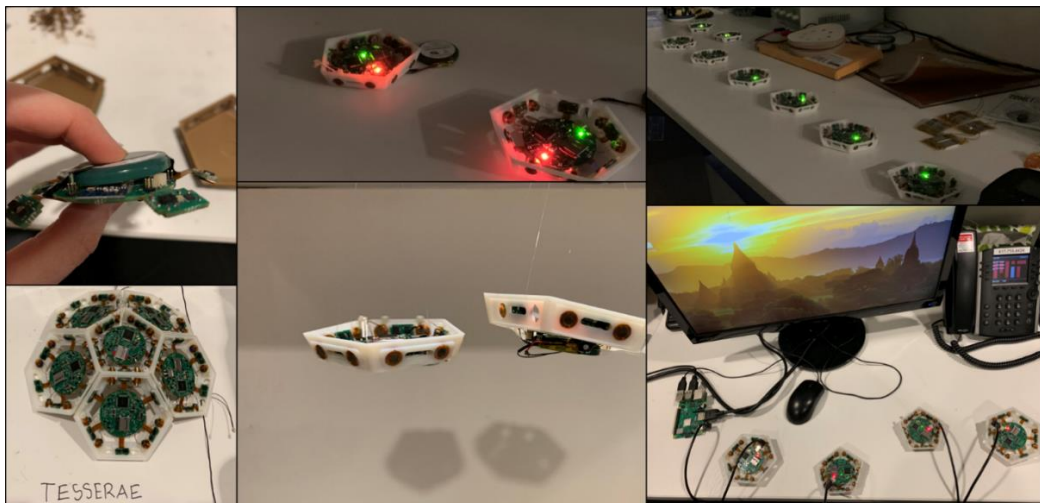


Figure 4-51. Clockwise from top left: Intra-tile fit check with battery and PCB; state machine performance test via LED indicator lights; passive power depletion test with all units in sleep mode (green light array); communications test with fellow tiles and RPi BLE connection; suspended string test; inter-tile fit check for dome or “petal” shape.

Beyond the development, integration and testing of the tile subsystems, the ISS experiment required many layers of functional and integration testing, from the tile scale to the fully embodied ready-to-fly experiment apparatus that must pass NASA environment and safety testing. In parallel with tile hardware and software engineering for seven units (two pentagons, five hexagons), we designed, integrated and tested:

- **An integrated tile holster system** that provides for tile charging, nichrome-wire burning of nylon containment strap for controlled release, carefully calibrated spring force mechanism to encourage tile deployment away from holster—all to withstand launch loads. Spatial layout of each tile holster was carefully considered to make the most use of the constrained interior volume, to give the maximum room for release, and to maximize the likelihood of finding proper neighbors post-release.
- **An RPi control board system** that directs multiple power lines (12V, 5V, USB) from our ISS interface through the NanoRacks BlackBox platform to various downstream experiment loads, controls lighting, kickstarts the experiment, and mediates new tile release based on prior tile bonding performance via a manger.py watchdog, and records data.
- **A specialty Teflon-coated wiring harness** with integrated fuses, to prevent the nichrome units from pulling excess current or from staying on too long due to unforeseen faults in the code that would risk a smoking event; extensive iterations were taken to minimize length of wire (and thereby lower resistance) to maximize the current able to reach downstream experiment loads, after the introduction of time-blow fuses added considerable resistance to the lines.
- **An experiment-level fault plan for key safety issues**, such as padding to mitigate tile damage during return and splash down, proper electrical insulation, default grounding, ensuring code has safety checks (such as a watchdog script making sure GPIOs are not left high) in the event of missed bugs, graceful shutdown in the face of unexpected power loss, and effective mitigation of electrical hazards via intentional power shutoff if required.

Figure 4-52 shows the crucial last five weeks of the in-lab integration schedule, prior to the first of two onsite integration tests in TX at the NanoRacks facility (photos documented in Figure 4-53). We completed the first integration of our payload into the BlackBox platform the week of January 27th, 2020, preparing the payload for NASA environment and safety testing (e.g., EMI/EMC, acoustic, power quality). The hardware was subsequently de-integrated and returned to us for final flight preparations. We returned to the NanoRacks facilities for re-integration into the BlackBox enclosure and final handover over February 19th- 22nd, 2020.

Week of-->	Dec 23rd	Dec 30th	Jan 6th	Jan 13th	Jan 20th	Jan 27th
In-house EPiMs	Need minimum of four asymm-style for testing. Will be getting trained to use CBA coil-winder (Dec 23rd in person session) + delivery of our own winder.	Back-up coil winding as needed for testing. Integrate test EPiMs with proto-hex and proto-pent.	Back-up coil winding as needed for testing.	Back-up coil winding as needed for testing.	Back-up coil winding as needed for testing.	NR testing in TX
Classic Coil EPiMs	Week of Arbor + glue fixture making. Ensure sufficient sourcing for them to complete 150 units.	Either in-person or remote-supervised test of two Co-produced units, before full run completed. Telecon on 12/30 to ensure clear guidelines on winding and fab.	Pick up full run of 150 units (due Jan 6th)			NR testing in TX
Final PCBs	Board Fab finished by Epec this week. Ariel to call on 12/27 and ensure delivery timeline on track.	Hand-delivered by Ariel from Epec to IMS on 30th, for 3 day turn on populating on 1/3 EoD. Pick up final, populated boards from IMS.	Run checklists for PCBs (basic bring-up, sensor routines) / then load full experiment code and begin testing.	Integration Testing	Integration Testing	NR testing in TX
Tile Code	Ariel and Jamie confirm feature list.	Asvin working remotely on comms code, as needed.	Push code to tiles as soon as boards are received/checked-out.	Functional testing and iterate code as tile behavior is observed.	Functional testing and iterate code as tile behavior is observed.	NR testing in TX
Holster—electromechanical	On hold, ensure BoM is complete and sourcing 100% confirmed.	On hold in current state, ensure BoM is complete and sourcing 100% confirmed. Jamie to complete RPI build (need to create two—one for backup in case NR fires one during Jan 27th period testing).	Test proto-holster with integrated RPI board (charging, dispensing circuitry mainly).	Submit new design to TOM for final printing NO LATER THAN FRIDAY 1/17	Integrate with tiles, final RPI board, prepare for shipping.	NR testing in TX
RPI/Central control board + Code	Fab On hold in current state. Ariel to determine operation scenarios to guide code dev.	Jamie, Asvin and Ariel to work on RPI experiment control code and operational scenarios.	Test proto-holster with integrated RPI board (charging, dispensing circuitry mainly) with preliminary control code (Ariel/Asvin-remote).	Integration testing, continued. Focus on getting code and BLE integration working ASAP.	Integration testing, continued as needed.	NR testing in TX
Integration testing	Proto-pent and proto-hex board arrive from Dortmund, basic prep towards testing hooked up to EPiMs, battery, supercap.	Continued: Proto-pent and proto-hex tested while hooked up to EPiMs, battery, supercap, with latest code test.	Sold tiles, now that PCBs and EPiMs have arrived. Powered string tests of suspended tiles to test both sensor code and epm functionality.	Continued powered string tests with tiles. Integrate all parts into physical box mock-up for fit, wiring plan, and mock-deploy.	Integration testing, as needed.	NR testing in TX

Figure 4-52. Timeline by week and subsystem, in modified Gantt duration style, charting final tasks for integration work over the 2019-2020 holidays.

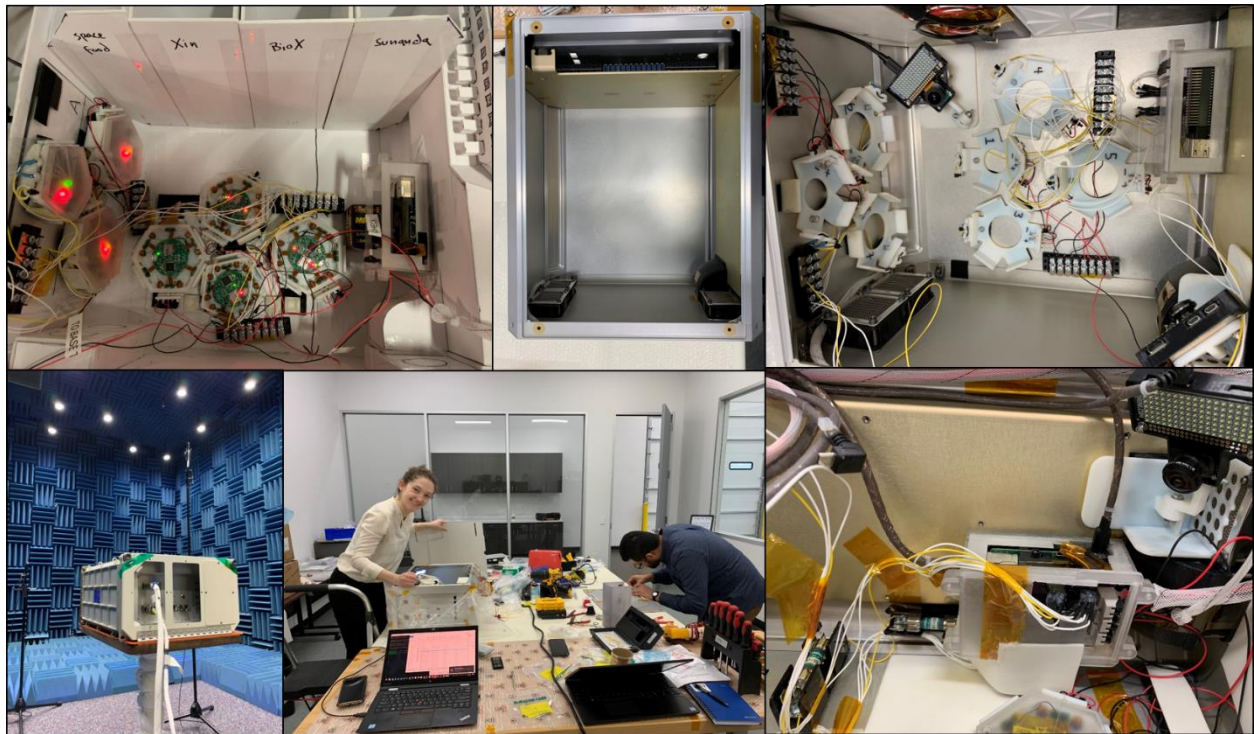


Figure 4-53. Clockwise from top left: experiment apparatus subsystem fit check inside a to-scale foam core model of BlackBox (model courtesy of Pete Dilworth); empty BlackBox at NanoRacks facilities in Texas prior to integration; layout of TESSERAЕ experiment sub-systems inside BlackBox; close-up on RPi control box, power lines to the fuses, and camera; integration team on-site, completing final tasks prior to NASA environmental testing; anechoic chamber for acoustic testing of the integrated payload, NASA Johnson Space Center.

ISS Mission Flight plan and Results

Flight Plan

Our overarching goal for this mission was to validate the two goals laid out at the beginning of Section 4.1.3, namely: validate quasi-stochastic self-assembly over a longer time duration in orbit via magnetic attraction; and demonstrate on-demand, autonomous error detection and successful error correction via the TESSERAE sensing platform, control logic state machine and EPM actuation.

Our flight plan dictated a conditioned, performance-based release of new tiles, predicated on a successful prior “good bond” event between the previously released tiles (communicated over BLE to the RPi control station making the next-release decision), to avoid a chaotic mess of many tiles floating at once. In the event where a good bond was not registered within an hour, we implemented a forced timeout to release the next tile, both to add kinetic perturbation into the system in case it has settled, and to force progression of the experiment while the previously released tiles had battery (we had seven to eight hours total within which to operate, before the first tile would fully deplete once away from the charging station). This was a new approach, motivated by learnings from the prior parabolic and suborbital flights, when all tiles were released simultaneously. While the nominal mission would last 30 days, we intended to deploy most of the tiles within the first day of continuous operation, to ensure they had time to interact with each other during overlapping battery life.

Figure 4-54 describes the step-by-step flight plan. Several underlying configuration values support the activity in this table.

- For each tile release, the nichrome heaters were turned on for 15 seconds to melt the nylon restraining strap; this is a duration of three times the experimentally-tested required time, to reduce likelihood of a failed release.
- For each tile, a limit was set of 20 mag pulses across all sides, to further reduce the risk of overheating and circuit fault (given the serious safety precautions worthy of the ISS). We expected this cap to be well above the intended EPM actuation count per tile, to give ample room for proper system operation, which proved to be correct (no tile pulsed more than two to three times due to volume and time operating constraints of this particular deployment).
- For each tile, the wake-up BLE signal was sent five seconds after tile release. This was carefully calibrated to overlap with the 2-3 seconds taken for the nichrome to burn fully after the release signal, such that the tile was “awake” immediately after escaping the holster, and not before. This was necessary to avoid the sensor baseline code picking up on the environmental conditions in the holsters (proximity and magnetometer values would be skewed by close proximity of other holster walls and nearby tiles with stationary magnets, respectively). We wanted the tiles to baseline only after floating free of the holsters. This proved a complicated timing window to perfect, as the attractive self-assembly magnets performed so well that tiles were immediately drawn together once freed, sometimes even before the sensor baselining had completed. This created a few scenarios where tiles bonded to one another during initialization, then recorded that as the steady-state starting status, and therefore did not report a bond event. This behavior identified an area of improvement for future code revisions—speeding up the initialization loop and pre-baselining the sensor values in the lab prior to flight—and hardware revisions, such as potentially using less powerful magnets as we fine tune the scaling relationships between mass of tile and magnetic field strength of the EPMS.
- Tiles store limited telemetry on their local SD cards (e.g., logs of commands received from the RPi base-station, snippets of sensor data around key diagnosing moments) and communicate bonding status over BLE back to the RPi.

Experiment step	Elapsed mission time, on experiment RPi	Rationale
Power on. Time counter runs for 24 “experiment” hours	<i>From T=0 to T+24hrs, where T=0 marks the power on moment, post-install.</i>	Avoid experiment start (after which tiles immediately begin battery depletion), until we are certain to have been fully deployed and stably integrated into the ISS experiment racks. This avoids false-starts and premature tile release in the case of any unplanned power-ons during pre-launch countdown at the Cape.
First tile release	<i>T+24hrs</i>	Pentagon, to maximize available bonding edges for next tile
Second tile release	<i>T+24 hrs, 3 minutes</i>	Wait just long enough for the pentagon to likely have settled, to enable a robust analysis of the speed at which the new tile independently finds its pentagon mate.
Subsequent tile releases	Variable: T = <ul style="list-style-type: none"> • <i>T(previous release) + t(for good bond to register)</i> OR <ul style="list-style-type: none"> • <i>T(previous release) + 1hr</i> 	Subsequent tiles are either released immediately after a good bond event is registered, which triggers the next nichrome release to burn, or in the event of no bonding progress, the next tile is released after a timeout of 1 hr.
Last tile (backup) release	T+20 days	Set far in the future for the experiment, to avoid accidental release if unneeded, but available to be remote-commanded to release early if required.

Figure 4-54. ISS step by step flight plan.

Launch and On-Orbit Install

Our experiment launched March 6th, 2020 on CRS-20 (SpaceX Falcon 9, with the experiment inside the Dragon capsule) out of Cape Canaveral, arriving at the ISS on March 9th, 2020 at 10:25 UTC. Our NanoRacks-provided experiment chamber “BlackBox” was removed from Dragon and installed inside the ISS experiment racks, or “International Standard Payload Rack,” in the U.S. Destiny module for the duration of its 30-day mission in orbit.

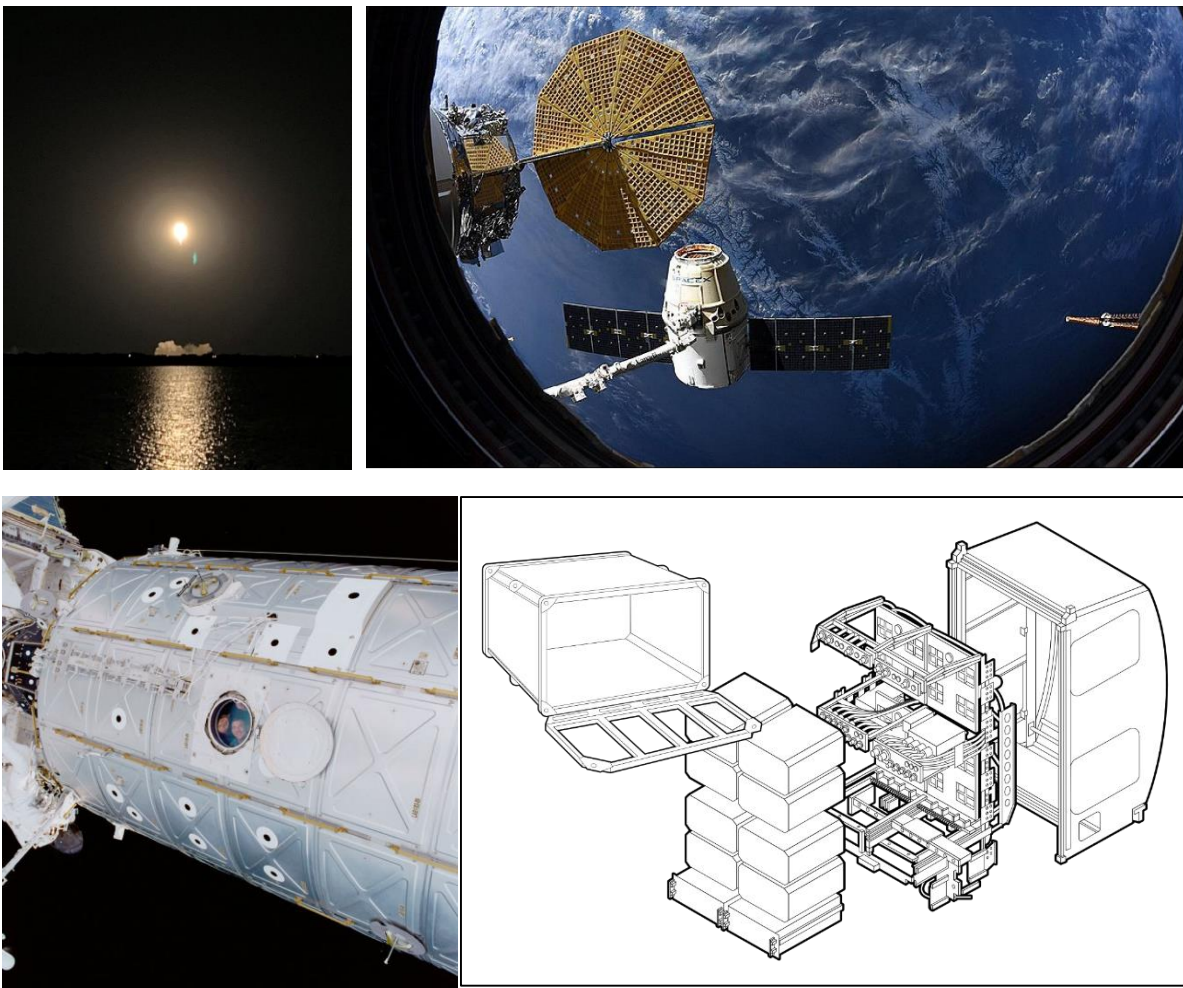


Figure 4-55. Clockwise from Top Left: Image taken of the launch onsite at Cape Canaveral from the MIT team viewing location; Dragon capsule attached to the ISS via Canadarm2 robotic arm; ISPR system showing integration of scientific experiments into ISS racks¹⁵⁶; external view of the USA Destiny module, where the experiment remained for the duration of its 30-day mission in orbit.

The first image downlinked to the ground confirmed that our interior hardware had survived launch with no known issues. See Figure 4-56 for an annotated photo of the TESSERAE experiment apparatus in orbit prior to experiment activation.

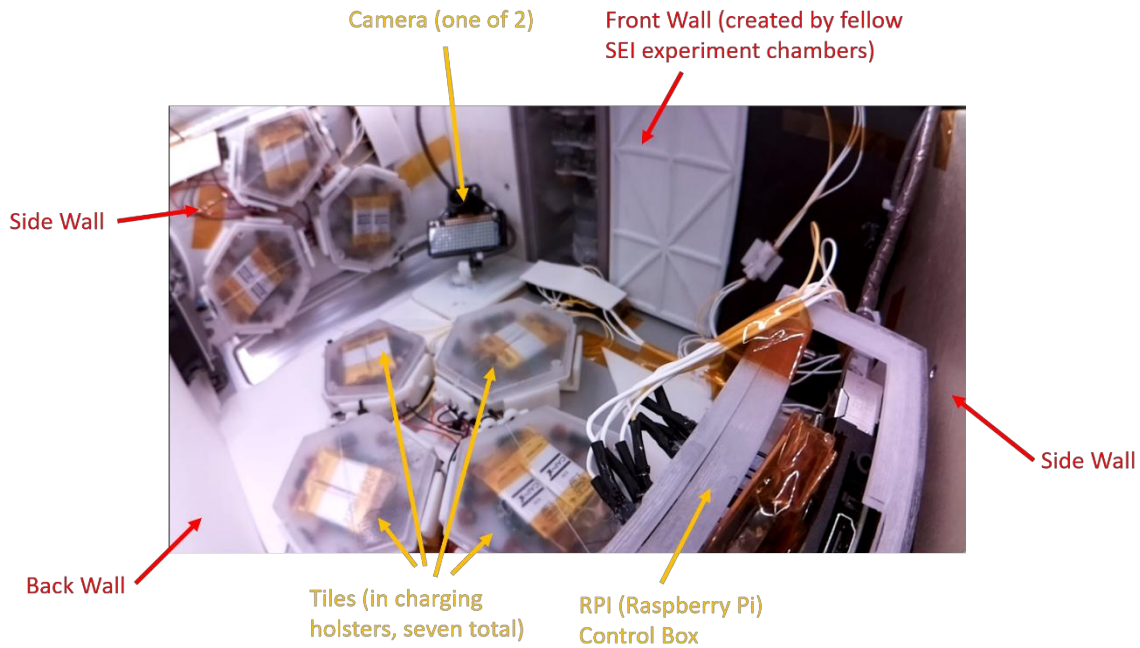


Figure 4-56. TESSERAE experiment apparatus prior to experiment start. Red arrows indicate chamber bearings and labels used subsequently to describe 3D motion through the space. Yellow arrows indicate hardware subsystems.

From here out, Prussian military commander Helmut von Moltke’s 19th century observation “no plan survives first contact with the enemy,”¹⁷ held true—fortunately, in ways that proved the robustness of the Generation 3 hardware for unforeseen circumstances and ultimately converged in a successful demonstration of *both* experiment goals from Section 4.1.3. We were able to observe several groupings of tiles self-assemble quasi-stochastically in a matter of seconds across the experiment chamber, and also observed several correctly-initiated EPM pulse-off events, validating the extensive custom hardware design undertaken to enable autonomous error detection and correction.

¹⁷ Note, the sentence used above is the modern phrasing of the original translation: “No plan of operations reaches with any certainty beyond the first encounter with the enemy's main force” [Oxford Online Reference].

Experiment Phase I: On-orbit experiment prep, kickoff, tile bonding activity

Due to infrastructure hardware issues (not ours) and a desire to validate the charging activity before releasing the first tile (we had had to fly the units with depleted batteries per launch regulations, making successful recharging a critical component of success), we waited several days after power-on to begin the experiment. The full experiment tile set was therefore taken through several more power cycling events (full charge and discharge) than initially planned and handled this gracefully, without any power failures nor downstream detriment to performance (Figure 4-57).

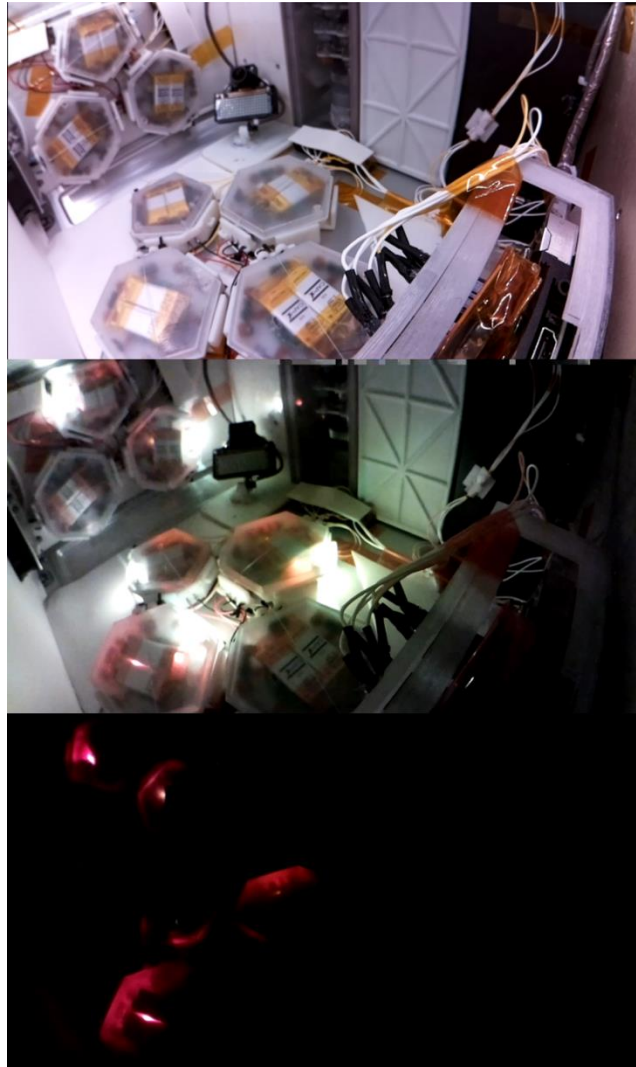


Figure 4-57. Comparison of three on-orbit images taken to validate tile wake-up and charging behavior. Top: view of experiment chamber with 12V overhead LED lighting washing out the tile on-board LEDs; Middle: overhead lights switched off shortly after 5V line power-on for the tiles, shows red charging lights and bright LED initialization lights; Bottom: steady-state with overhead lights off, tiles have completed initialization and are in active charge state (red lights). Red lights turn off when tile is charged to capacity.

The experiment formally began at 9:38pm UTC (station time) on March 13th, 2020 with a successful release of the first pentagon tile (identifying address: C2BA), followed three minutes thereafter by the first hexagon tile (2117). Logs from the NanoRacks power source confirm short power load increases during the 15 second periods of nichrome release for both tiles, as expected. From pentagon release to settling at the back wall, 17 seconds elapsed. From hexagon release to settling in a stable bond with the pentagon (lower right photo of Figure 4-58), nine seconds elapsed. Both tiles successfully completed an initialization sequence and recorded sensor data during these events.

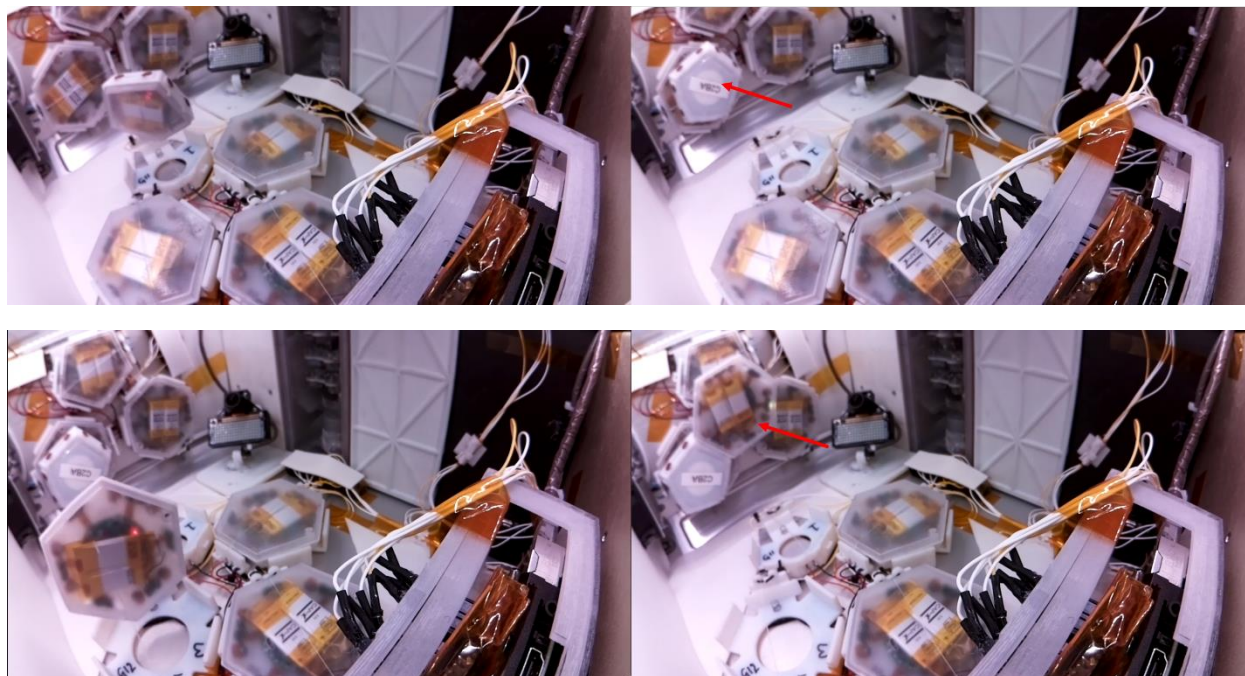


Figure 4-58. Top row, from left to right: Pent C2BA just moments after release, Pent settled against side wall. Bottom row, from left to right: Hex 2117 just moments after release, Hex settled against side wall.

The third tile release, Hexagon 70C6, was stymied due to a copper burr on the charging pad that resisted the spring force ejection and held the tile in place after the nichrome was burned. After the initial run through releasing all tiles, we returned attention to this tile and remote-commanded an additional duration of nichrome burn to ensure the nylon containment strap was completely free. The tile remained in place, but was later (near the conclusion of the mission) successfully dislodged in-orbit, thanks to the kind effort of the Expedition 62 crew who briefly de-integrated our experiment box to shake and add a perturbation event for the experiment, and then replaced the experiment.

The fourth tile release, Hexagon 865F, proceeded as planned, with 31 seconds elapsed between release and settling into a bonding event on previously released Pentagon C2BA. Together, they formed a metastable bond, providing a key opportunity to test the error detection sensing and responsive correction control algorithm. Pentagon C2BA was the first to detect the bond event and successfully completed diagnosis, through to pulsing of the EPMs on that face, leading to successful tile separation. Due to the volume constraints of the ISS chamber, the ejected Hexagon 865F tile bounced off a nearby face and returned for another metastable bond with the same Pentagon, which was in turn corrected again with a subsequent EPM pulse and tile separation.

This double-EPM event (Figure 4-59) provided a fantastic view into the operation of our safety code, which correctly and as intended, handled these back-to-back events with a forced 60 second separation to ensure the supercap had properly recharged and would not contribute to rapid-refire magnet coil overheating. Our RPi state machine flight logs corroborate that the two pulse-off events seen between Hex 865F and Pent C2BA were initiated by the Pentagon.

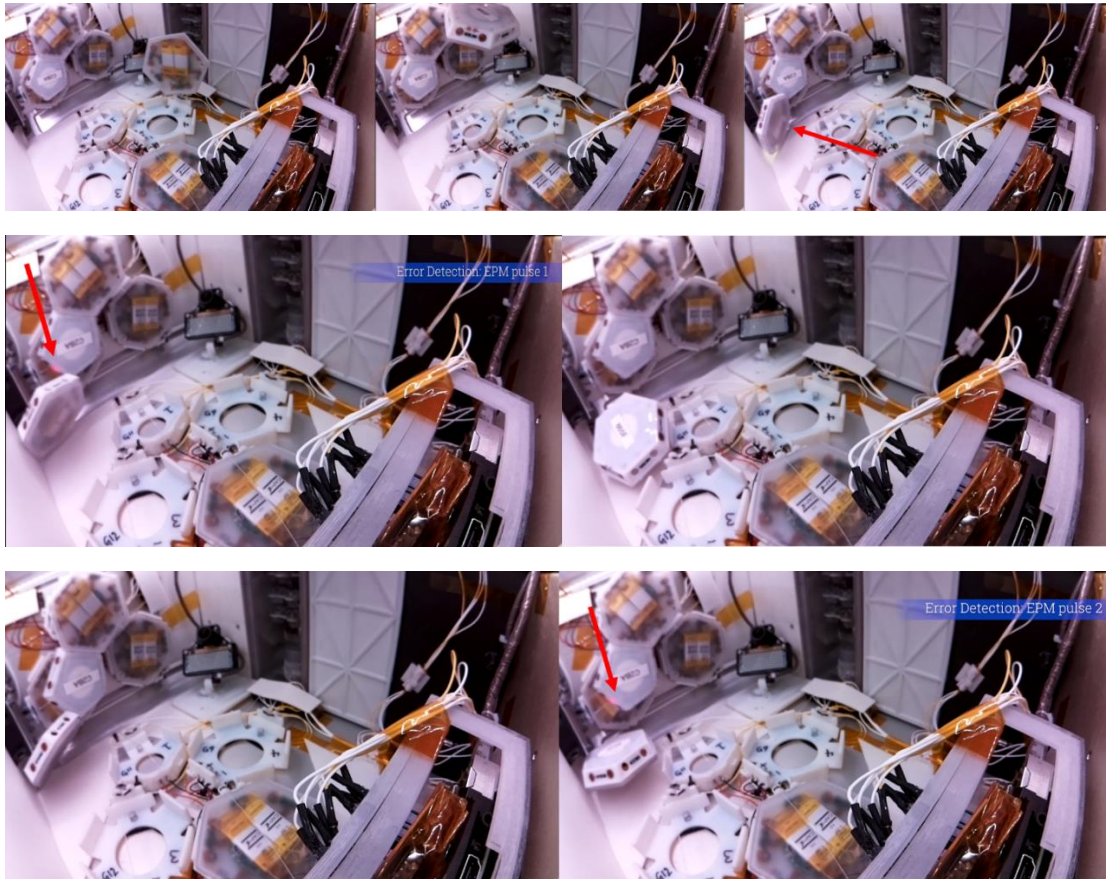


Figure 4-59. Top row, left to right, shows Hex 865F release, floating at the top of the frame, and settling at the bottom left of the frame in a metastable bond (captured a green LED sensor loop initialization light flash). Middle row, left to right, shows the initial EPM firing (red light edge indicator) and nearly instantaneous tile ejection, with separation shown in the next image (somewhat stymied by the small experiment chamber and crowded operating landscape). Bottom row, left to right, shows a return of these same two tiles into a slightly different metastable bond, which is again corrected with the EPM firing from the Pent C2BA (red light edge indicator again).

For subsequent tile release, the system now had to contend with a large mass of tiles having accreted against the wall of next-to-be-released neighbors. Tile 5, Hex 212E, was blocked for release despite a successful nichrome burning (ultimately freed by the successful astronaut crew box shake later on), while tile 6, Hex 1E35, appears to have suffered from an unexpected fusing of the nylon to the tile lid surface, trapping it in the holster for the duration of flight. On the first pass through, from Tiles 1–6, the experiment proceeded fully autonomously with no input from the ground. This allowed us to assess the autonomous operation of the RPi experiment controller, basing subsequent tile release on communicated data received from the active, previously-released tiles (e.g. indicating good bonds → release a subsequent tile or wait for the timeout). The RPi experiment supervisory code worked as intended, successfully mediating the BLE communication

exchange between tiles and the base station, recording global system logs, and progressing through a self-governing set of rules for experiment next steps.

Experiment Phase 2: remote-commanded interventions

In addition to autonomous progression, we wished to assess the feasibility of remote-commanding aspects of the experiment, to prove that our overall sensor reporting and live camera feed provided sufficient information and a comprehensive description of experiment status to be used to make in-situ decisions, update the experiment plan, and address any off-nominal behavior as needed. We thank the NanoRacks ISS console team for their extensive support of the data-downlinking and active command access to the BlackBox avionics interface, as we transmitted RPi commands to them for execution in-orbit. As described in the flight plan table above, we had reserved deployment of the “backup” tile 7 (Pent CE64) for testing this capacity. We chose to deploy the backup tile to attempt to dislodge the tile mass that had accreted at the side wall, and this worked quite effectively, successfully pivoting the three-tile mass and adding the seventh tile to this, for a total grouping of four, through a new bond event (Figure 4-60). The new tile mass made its way over to the front wall, completing this entire maneuver (from backup tile release to settling) in 45 seconds. Interestingly, about 20 minutes later, we observed the tile mass beginning to pivot back to the original side wall, likely due to the slow attraction between this multi-tile accretion and the two tiles still in their holsters on that side wall (tile 5 and tile 6) having to overcome a pinch point at the bottom (the farthest tile in the tile accretion was stuck between the tile 6 holster and the bottom view camera).

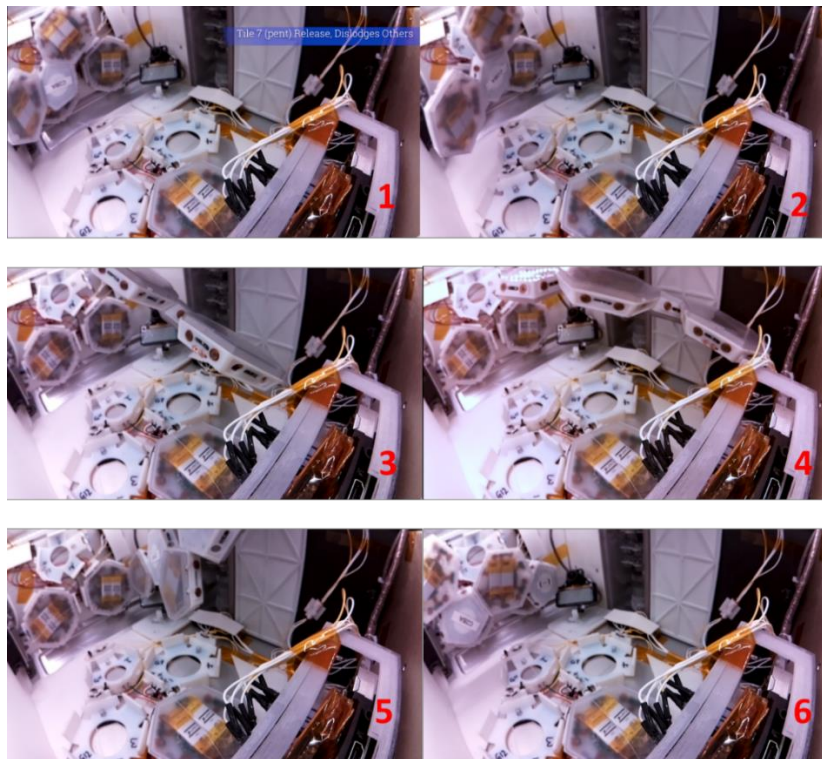


Figure 4-60. Proceeding left to right from top left, the Pentagon CE64 is remote-commanded for release (1), successfully begins dislodging the tile mass (2), tile mass pivots as Pentagon CE64 joins the tiles mass out of frame (3), Pentagon CE64 now bonded, seen at upper left boundary of frame (4), tile mass settles against front wall with pent trapped between tile 6 and bottom view camera (5), tile pivots back to side wall (6). Steps 1-5 proceeded quickly, within an elapsed time of 45 seconds. Step 6, the pivot back, occurred after ~20 minutes of resting against the front wall.

At this stage, we pursued additional remote-commanding steps, including selectively pulsing the air circulation fans controlled by the BlackBox platform (operating at a very low baseline level, required for heat transfer and cooling of the electronics). We were able to show that the fans, at this low level, had no discernable effect upon the motion of the tiles, which helps to increase our confidence that the observed dynamics are driven primarily by the magnet interactions. The fans had been covered by a fine mesh prior to flight, to further aid in achieving a diffuse flow and avoid any directed forces on tiles due to laminar flow. We believe this modification to have achieved its aim, and the baseline low level of air flow made it unlikely that any turbulent air was strong enough to displace the tiles (snapshots taken across three checkpoints before, during and after fan action led to this conclusion; Figure 4-61).

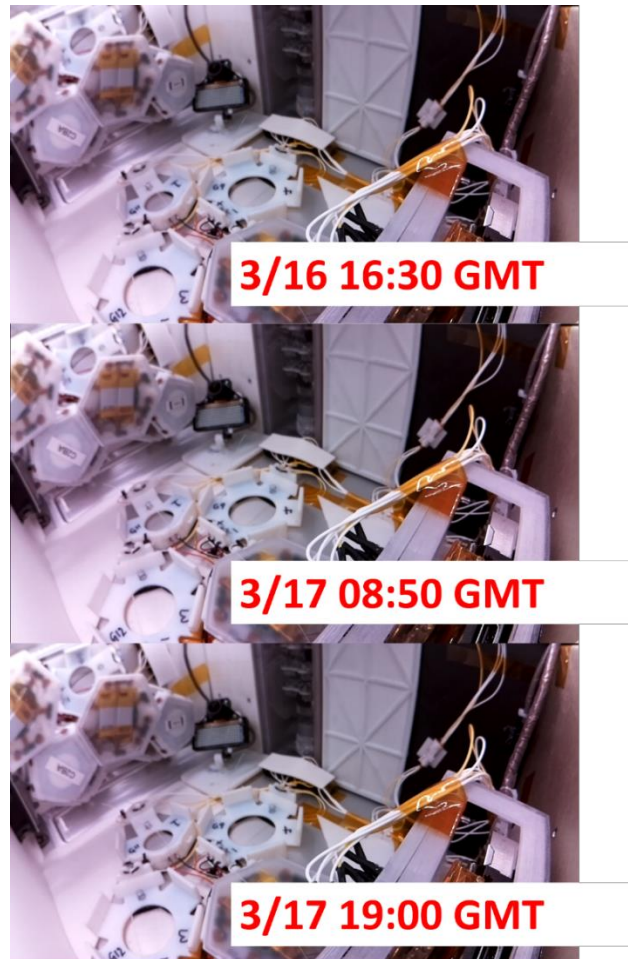


Figure 4-61. Top image from the day before fan action. Middle image is from a “morning” station-time fan test, tile mass accretion shows no displacement from the starting position. Bottom image is at the conclusion of the day’s fan testing, again showing no evidence of tile displacement.

Finally, near the conclusion of the 30-day mission, after the tiles had settled and no further action could be taken, we were fortunate enough to have Astronaut Drew Morgan of ISS Expedition Crew 62 agree to unplug the BlackBox from the ISS experiment racks, shake the apparatus, and return the BlackBox to its previously installed and powered state. Before the shake, we had validated via logs and visually with the overhead lights off that of the three tiles still stuck in their holsters (#3, #5, #6), both tile 3 and tile 6 were still alive and charging. We had an interest in trying to dislodge these remaining tiles that had experienced holster or

deployment issues to determine if we could generate further bond events with tiles that still had active batteries. Because the de-install required unplugging the box from power to be able to shake it, we could not capture camera or bonding event log data *during* the shake, but we were able to compare the beginning and end result to capture data on the effect of a large kinetic perturbation to a settled system (Figure 4-62). Tiles 3 (Hex 70C6-live) and 5 (Hex 212E-dead) were successfully dislodged and proceeded to bond and clump with other tiles; tile 6 (Hex 1E35) never did release, and a post-mortem of the experiment once back on the ground revealed the nylon strap had melted and bonded to the tile in such a way that the tile could not escape its holster.

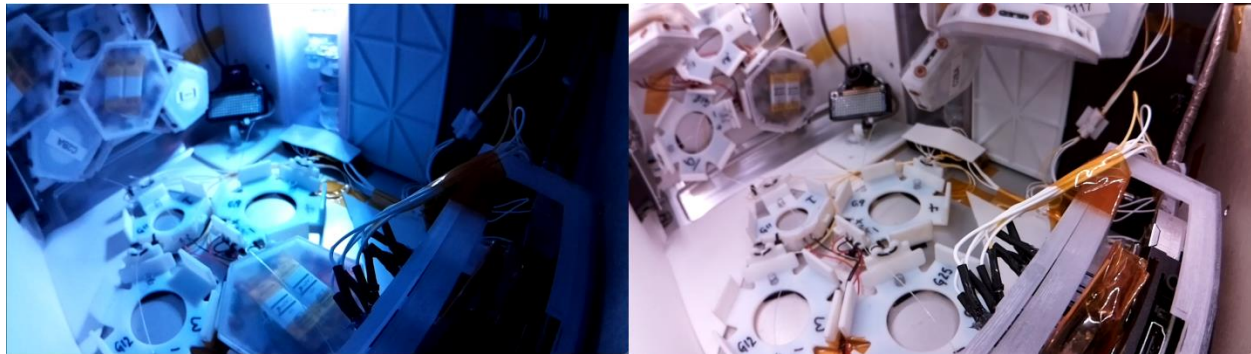


Figure 4-62. Left image (blue light due to a separate experiment running in the background), showing tiles just moments before the system power-off and de-integration for shake. Observe that the tiles along the back wall (the four released units) are in the same position as they were during the fan test and have not moved. Right image, showing new clump of tiles in the top foreground and a separate clump of tiles in the upper left corner, with two tile holsters newly vacated, demonstrating the potential for re-arrangement with even light shaking perturbances.

Tile (release number – type – last four BLE address)	Time to aggregate, post-release (seconds)
1 – Pent – C2BA	N/A (17 seconds to settle)
2 – Hex – 2117	9
4 – Hex – 865F	31
7 – Pent – CE64	5

Figure 4-63. ISS mission experiment summary performance table.

ISS Mission Summary

The Generation 3 hardware deployment on the 30-day ISS mission served as the capstone research deployment for the thesis. Through the phase 1 and phase 2 periods of the on-orbit experiment, we:

- Validated the ratio of tile mass to magnetic field strength: the tiles routinely zoomed right over to a neighbor, crossing centimeters of distance in a matter of seconds (Figure 4-63).
- Validated the energy-favorability of quasi-stochastic tile accretion (tiles want to come together and self-assemble; not a single tile remained unpartnered after experiment release)
- Validated the design of sensing hardware, a control algorithm for self-assembly and custom EPMS that together successfully executed autonomous error detection and error correction, with tiles effectively pulsed away from one another.
- Validated several aspects of a future mission ConOps, including autonomous conditioned tile release, remote commanding, and response to system perturbations.

4.1.4 Generation 4: Autodesk Architectural Scale

From Generation 3 to Generation 4, we jump two orders of magnitude in size, from 10^{-2} m range to 10^0 m. Via a residency with the Autodesk BUILD Space in Boston, MA (Figure 4-64), we are preparing life-size TESSERAE tiles for further testing and eventually an at-scale technology demonstration mission in orbit. In addition to the electro-mechanical considerations, this round of hardware development includes new aesthetic considerations for both the future interior use and external paneling—from interior furniture tie-ins to ferrofluid plates that we hope will convey the quasi-stochastic nature of magnetic-mediated assembly to future architecture biennale audiences. These life-size models are also under active design for re-use in analog resource constrained environments on Earth (e.g., natural disaster recovery areas and refugee camps) for use as robust, modular, low-cost, and easily assembled architecture.



Figure 4-64. Interior view of the next TESSERAE deployment and fabrication environment, at the Autodesk BUILD Space in Boston, MA. Public image online, courtesy of Autodesk.

The larger fabrication enables us to explore a more extreme EPM regime and power handling, power generation (integration of solar panels), and energetic system response (colliding tiles and observing when the kinetic energy leads to destructive collisions)—all more closely approximating what we might see in orbit. While the local and global challenges of Covid-19¹⁵⁷ stymied physical progress on this front by leading to the temporary closure of the Autodesk BUILD Space from March 2020 through the time of this PhD defense, we have still completed advanced mechanical design work on various subsystems. This section focuses on the TESSERAE tile 3D definition and clamp design for reinforcing bonding edges and ultimately pursuing a sufficient seal to be able to pressurize the structure; this is the most complete of the various subsystem designs at this time.

Through collaborations with Peter Williams (MIT UROP) and Peter Dilworth (MIT SEI), we explored the merits of various clamp paradigms (Figure 4-65, Figure 4-66). With Peter Williams, this thesis advised his UROP research into the applicability, benefits and limitations of rotating magnets, rack and pinions, and interleaved braces for clamping in microgravity.

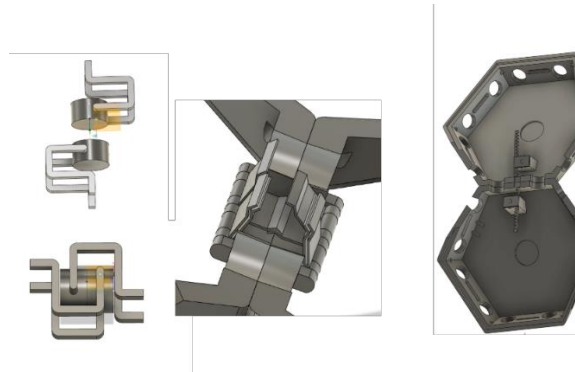


Figure 4-65. From Left to Right: Rotating magnet clamps; interleaved braces; rack and pinion model shown in context of the tile housing.

With Peter Dilworth, this thesis explored ruggedized clamps for deployment-scaled, reinforced tiles to counteract the expected expansion force due to interior pressurization pushing on tile joints. We ultimately settled on a comparison between two main models—a passive hook or “train car coupling” design where two arms extend and link the tiles together, and a rack and pinion design (informed by the early work with Peter Williams) that provides for cinching action across postulated, deformable gasketing to aid in a pressurizable seal. Figure 4-67 and Figure 4-68 distill this comparison and the principles we’ve settled on for the clamp functionality.

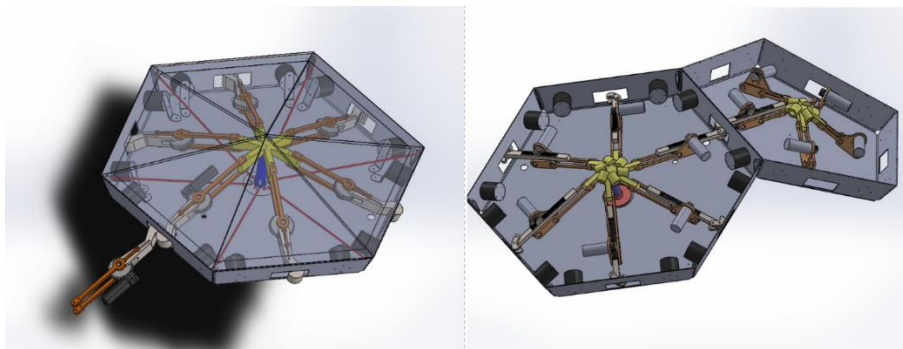


Figure 4-66. Left: coupling hook clamp model, exposed on each edge, with reinforcing bars; Right: rack and pinion model (motors are the round cylindrical units), with center mounting point.

	Pros	Cons
Coupling Hook	<ul style="list-style-type: none"> • Smaller motor (responsible only for horizontal in-plane motion to couple, not for pulling tiles in together) • Uses worm gears to avoid back-driving, therefore doesn't rely on constant motor driving or gear head to prevent slippage 	<ul style="list-style-type: none"> • Insufficient travel in the joint to effect cinching. Would only reinforce magnet bonding, likely not compress gasketing
Rack and Pinion	<ul style="list-style-type: none"> • Ability to cinch and tighten the joint, across deformable gasket material • Based on preliminary force analysis, less hardware required to stabilize • Keeps latches aligned against forces applied in all axes 	<ul style="list-style-type: none"> • Requires a beefy motor and gear head to withstand forces, and hold cinch in place

Figure 4-67. Comparison of two tile latch ideas.

Ultimately, we settled on the following principles for a target clamp design for the large-scale tiles:

Principle	Justification
Symmetric clamp or consistent chirality for manufacturing the same part on every side, for both pentagons and hexagons	For cost savings and simplicity of clamping in-situ
No static protrusions past the plane of the tile edge (temporary extensions allowed)	Avoid getting in the way of flush magnet-magnet action
No special timing requirements	One clamp arm should not have to come out before the other, in order to avoid fault cases due to lack of perfect inter-tile communications synchronization. Provides for better redundancy.
Latching style should not require active power to be held. Should hold in off-power state.	Optimized for constrained aerospace power budget
Should support cinching	To provide for a tighter seal, with deformable gasket material, that can support later pressurization
Should be able to be scaled up to in-orbit Space-Use-Scenario and hold at the force regimes specified	Practicality of spiral-theory of design, to be able to have intermediate prototypes used in Autodesk BUILD Space demos, while still applicable to in-orbit planning
Minimize mass while maximizing strength	Need to optimize for lower mass to orbit, for launch

Figure 4-68. Summary of TESSERAE large-scale clamp principles.

For next steps, once the BUILD center reopens post-Covid-19, we are exploring the electronics design and power system requirements for large, industrial scale EPMs and also recalibrating our sensing and communication approach for a newly scaled tile. After an initial prototyping round to build one to two large scale tiles, we will commence with suspended bonding tests via the large KUKA Robot arms. After learning from this initial prototyping round is complete, we intend to progress to a further phase with space-grade materials (e.g., non-outgassing parts, rad-hard electronics, etc.). On the outside of each tile top face, we are also designing a sandwiched ferrofluid plate that will show a dynamic view of the magnetic field interactions between tiles.

4.1.5 TESSERAE Shell Hardware Contributions Summary and Next Steps

The development of robust self-assembly in microgravity depends on extensive, iterative testing across proof-of-concept models, advancing through TRL levels. Through our in-house pre-flight testing and troubleshooting, 2017 parabolic flight, 2019 suborbital launch test and 2019 parabolic flight, and 30-day March 2020 ISS mission, we were able to:

- Validate that tiles can be brought together over centimeter distances in the span of several seconds, confirming the baseline approach for magnet-mediated self-assembly;
- Validate a geometric base-unit and magnet polarity map, specially designed to yield a target macro structure;
- Validate EPM functionality as a robust mechanism for both keeping TESSERAE Tiles together (at a certain holding force to mass-of-tile ratio) *and* separating tiles on-demand, when combined with integrated sensing for autonomous error detection and correction;
- Validate functionality of an integrated sensing and communications platform (proximity, ToF, RGB sensor, IMU, magnetometer, BLE, etc.) in an evolving TESSERAE PCB over several generations;
- Validate magnetometer sensing thresholds that can reliably delineate between good and bad bonds to kickstart the bonding diagnosis state machine;
- Validate a control algorithm that parses sensor input and executes bang-bang control effectively to provide correction for quasi-stochastic self-assembly; and
- Validate several aspects of a future mission ConOps, including autonomous staged tile release, remote commanding and response to system perturbations.

Ultimately, three different generations of prototypes were tested across four different flight opportunities (Figure 4-69), with a fourth generation planned for human-scale tiles. The results from these prototype deployment opportunities give us strong confidence in the viability of the core concept and the promise of responsive, self-aware space structures. Future work will explore the transition to larger-scale, space-grade subsystems for deployment in-orbit, which we hope to pursue with NASA and industry partners. In particular, the simulation (Chapter 5) helps us extend the latest learnings from our ISS mission to modeling of the TESSERAE Shell system at scale, in orbit.

Features	Gen 1	Gen 2	Gen 3
Size (hexagon widest diameter, to nearest cm)	6cm	17cm	10cm
Count fabricated	64	3	7 final, from 15+ test units
Magnet Type	Passive – Neodymium	EPM – COTS	EPM - custom
Joint Type	Hex/Pent: SS/NN Hex/Hex: SN/SN	Hex/Pent: SS/NN Hex/Hex: SN/SN	Hex/Pent: SS/NN Hex/Hex: SN/SN
Sensing	Preliminary: <u>Single Board</u> <ul style="list-style-type: none"> Gyro Accelerometer + Magnetometer Temperature 	Full: <u>Mother Board</u> <ul style="list-style-type: none"> Combined IMU 3x ToF <u>Peripheral Boards</u> <ul style="list-style-type: none"> Magnetometer RGB + Proximity + Gesture 	Refined Code and major modifications to state machine control loop: <u>Mother Board</u> <ul style="list-style-type: none"> Combined IMU 3x ToF <u>Peripheral Boards</u> <ul style="list-style-type: none"> Magnetometer RGB + Proximity + Gesture
Communication	BLE	BLE	BLE
Data Storage	Limited on chip	MicroSD	MicroSD
Programming Interface	USB AVR Programmer + 6 Pin ISP	USB Arduino Bootloader	USB Arduino Bootloader
Active Control	None	Joint Neutralization	Joint Repulsion and Separation
Power System	Li-ion pouch + miniature PV Cells + TI Energy Harvester	9V Advanced Lithium + Boost Converter	Coin Cell Li-ion + Recharging Apparatus + Supercapacitor discharge for EPMs + extensive protection circuitry
Tested via	Parabolic flight 2017 (no electronics)	Suborbital launch 2019 (complete system) and Parabolic flight 2019	ISS 30-day mission 2020 (complete system)

Figure 4-69. Summary of TESSERAE Generation 1 through Generation 3 hardware features.

Immediate next steps for the hardware development include: continued revisions for optimizing the control algorithm and sensing platform that controls error correction and detection; adding swivel functionality for the EPMs to facilitate self-righting motion in metastable bonds (Figure 4-70); exploring PolyMagnet¹⁵⁸ pixel-level polarities for fine tuning certain joint behavior; the addition of solar panels or power beaming receive-coils to the exterior surface for lengthening system life; and the addition of a deformable material gradient or gasketing at the tile edges to absorb collision impacts and aid in sealing during a future clamping process. As we explore material selection for the tiles, our goal is to find ways to natively embed a suite of sensors into the manufacturing of the tiles themselves—rather than adding the sensor nodes as separate PCB boards that must be assembled outside or inside a tile shell. By integrating sensing with the material, we can improve the modular properties of the structure and build a useful level of redundancy and robustness into our designs.

While the ISS mission provided an invaluable testing platform for longer duration microgravity, our next priority for deployment testing is to secure a larger, unobstructed interior volume in which to operate (as the tight quarters within BlackBox constrained some of the tile-tile bonding activity and circulation). New options for this are coming online, from large airlocks proposed for the ISS¹⁵⁹ to entirely new space stations conceived for LEO⁹⁷. An alternative would be to deploy a free-standing test, outside of existing spacecraft, that uses our concept for balloon inflation in orbit (Chapter 6) to provide a containment chamber.



Figure 4-70. Model of two tiles in a metastable bond, requiring a swivel bearing mechanism or low-friction surface (e.g., Teflon) to re-align.

Regarding further testing priorities, we will first prioritize a repeat test with a subset of TESSERAE tiles augmented with the latest hardware tweaks and learnings from the ISS mission. From there, we can progress to a full 32-tile set in orbit (likely still in miniature until funding becomes available for a life-size set) to compare real results against our simulation model for time duration of a full buckyball quasi-stochastic assembly. In parallel or shortly thereafter, we intend to test 3-4 life-size tiles in orbit for feasibility and selection of components matching the deployment constraints of the vacuum, building on our work out of the Autodesk BUILD Space. After assessing results from those three milestones, and obtaining funding (likely via integrating with NASA mission priorities for the Artemis program or private sector commercial habitat activity), we can begin planning for an on-orbit, life-size test with a full 32-tile set. In the future, we may also explore a hybrid propulsion and magnets model, where in the absence of a containment volume, coarse propulsion is used to achieve a certain general "quadrant" location and electromagnets are subsequently turned on to aid in closer-proximity docking and quasi-stochastic assembly in close quarters. Alternatively, the opposite hybrid model could also be employed effectively, where the bulk of the assembly still proceeds quasi-stochastically, but modest, electron-spray propulsion units like Accion's TILE¹⁶⁰ could be activated on the final few tiles in an assembly to speed up the "hole-filling" challenge where the last two to three tiles take the bulk of the assembly time.

4.2 TESSERAE Cell Prototypes

Throughout the TESSERAE Shell development process, we observed the challenges of assembling a hollow shell topology. Many out-of-plane bonding error states exist for the flat tiles, requiring extensive activity by the EPMS for error detection and correction. This, and the principles of the design theory in Chapter 3, led us to consider a more organic Cell unit that relies on the space-filling geometry of plesiohedrons to bond reliably to neighbors without requiring error correction. The Shell model still retains the benefit of creating large, unobstructed hollow interiors within a particular, target macro shape—best for the future gathering places and monumental application of space architecture, while the Cell model provides a practical alternative for module-based accretion and organic evolution of a structure (see comparison in Figure 4-71). Our initial explorations focused on the truncated octahedron, a shape with eight hexagonal faces and six square faces; this Cell approach is extensible to all other plesiohedrons or space-filling solids.

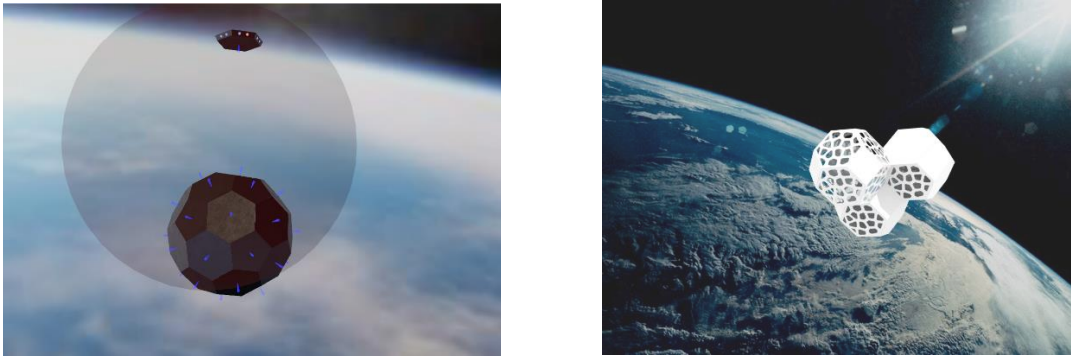


Figure 4-71. Left: outside view of a large, open chamber sphere volume created by self-assembly of “Shell” or flat tile units (from Cyberbotics Simulation). Right: exterior model view of smaller, modular “Cell” units self-assembled into a larger aggregate (artists render image credit: Sana Sharma). See Chapter 6 for further discussion of the aerospace mission pros and cons of each approach.

As described in the introduction, self-aware self-assembly lends itself to systems that can grow incrementally with modest resources. The Cell model facilitates this by providing regular bonding sites, much like molecular compounds or chain molecules, where additional units of the same joint-type can accrete and join an evolving structure. To realize this functionality in hardware, we designed a face with self-aligning magnets. Powerful neodymium disk magnets are affixed in recessed holes on the surface of the Cell units or “nodes” in a polarity pattern that causes the entire unit to twist and automatically align edges properly upon drawing into close proximity with a neighbor. The degree of rotational freedom in the polarity map is tuned to match the symmetry of the face geometry (e.g., should rotate freely through 90° on a square face, or increments of 60° on a hexagon face, when considering the truncated octahedron). This polarity map exerts significant torque on the tile faces, due to the bulk of the surface area being covered in exposed magnets. Other approaches are also feasible, where smaller magnets are placed at strategic pivot points, to avoid use of very large magnets at scale (if this becomes an issue when transferring this design to larger habitat modules). The discovery of a powerful self-aligning joint for these nodes allows us to return to a purely stochastic model for assembly, potentially vastly reducing the energy associated with station construction on-orbit. Future work will be undertaken to explore approaches for buffering the strong restoring forces to ensure that the whiplash of the self-aligning joints does not cause damage to a future habitat module.

Section 4.2.1 discusses the first generation prototype development and our exploration of an extensive range of disk magnet shapes, polarity maps, and bonding face selection across a family of 3D printed units. Two Cell types from this development suite, with 9 units each, were deployed on a 2019 parabolic flight. Section 4.2.2 discusses extension to shapes other than the truncated octahedron and next steps for scaling hardware development of this model.

4.2.1 Generation 1: Tested via Parabolic Flight

Hardware development

The hardware development for these Cell units focused on magnet shape selection and a design for a magnet polarity map that could achieve self-correction for aligning joint faces between neighbors *without* requiring electronics or active control. We worked the following principles into the design:

- Sufficiently constrain the self-aligning bond to achieve correction to certain set rotational points (e.g., a single circle magnet is insufficient, as this allows a part to bond at any rotation, without self-aligning the vertices to the matching neighbor)
- Avoid over-constraining the self-aligning bond (e.g., we ultimately settled on 120° rotational symmetry for the hexagon faces, rather than forcing this down to the level of 60° rotational symmetry)
- Optimize magnet selection for lowest number of distinct parts (e.g., can the same magnet be used on every face, for example, in different arrangements as needed?)
- Optimize polarity map for the highest likelihood to achieve perfect bonds, while avoiding metastable bonds
- Optimize joint definition to minimize the number of distinct joint types, in order to maintain the probability that any two matching faces that meet can bond

We progressed through many prototype designs (Figure 4-72) and ultimately settled on a configuration with three disk magnets in a tight triangle (we only needed three-way or 120° rotation to match up with other faces, not six-way rotation). On each face, the exposed magnets share the same polarity arrangement. There are four “N” exposed hexagonal faces and four “S” exposed hexagonal faces on each tile. Because these shapes are space-filling solids, providing for attachment points on all hexagons by definition draws a solid multi-unit packing together, without requiring additional magnets on the square faces. This allows us to both reduce parts and achieve cost-savings, and also extrapolate to a future use in orbit where some faces are dedicated bonding faces between tiles and other faces can be opened up for use as docking ports or airlocks.

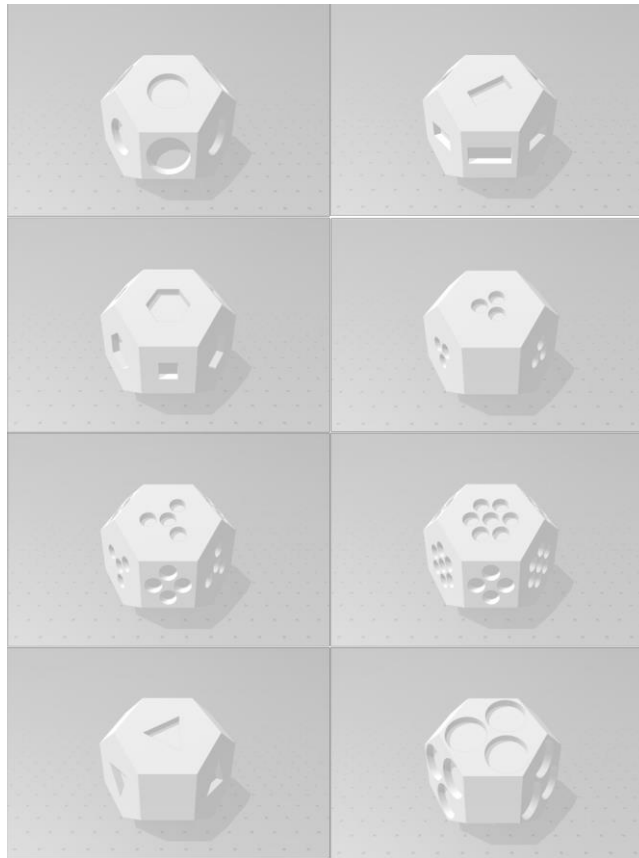


Figure 4-72. Shows our 3D object models used in 3D printing a suite of many nodes to test various magnet configurations on the bonding surfaces. We ultimately settled on the unit in the bottom right corner.

After settling on the model described above, we began to experiment with on-ground shake tests and manual assembly to determine the range of possible shapes. Figure 4-73 below shows several examples of possible multi-unit configurations. Several types of holes can be formed by encircling, showing we can use these models to grow structures with a dynamic mix of concavity and convexity, as demanded by future aerospace mission scenarios. “Branchiness,” or the tendency to form long arms, may later serve a purpose in habitat design for separating high-risk task types from central living quarters. Condensed, block-like structures may prove useful for high-use areas where a long hallway would not make sense, but a nexus of many ports and doors into adjoining spaces would better serve the mission ConOps. The exploration of these structures extensively influenced the generative design algorithm discussed in Chapter 5, where we apply fitness constraints and “grow” multi-module units addressing many of these considerations.

We ultimately printed and assembled two populations—one set (in black) where all hexagon bonding ports are filled with magnets, and another set (in clear purple) where one hexagon bonding face is blank and does not include magnets. We were interested to test how the distribution of bonding faces affects the aggregate structure. Again, in an aerospace context, there may be an interest in making more faces available for ports or open-interior doors, rather than structural joints, and the clear purple set addresses one such scenario.

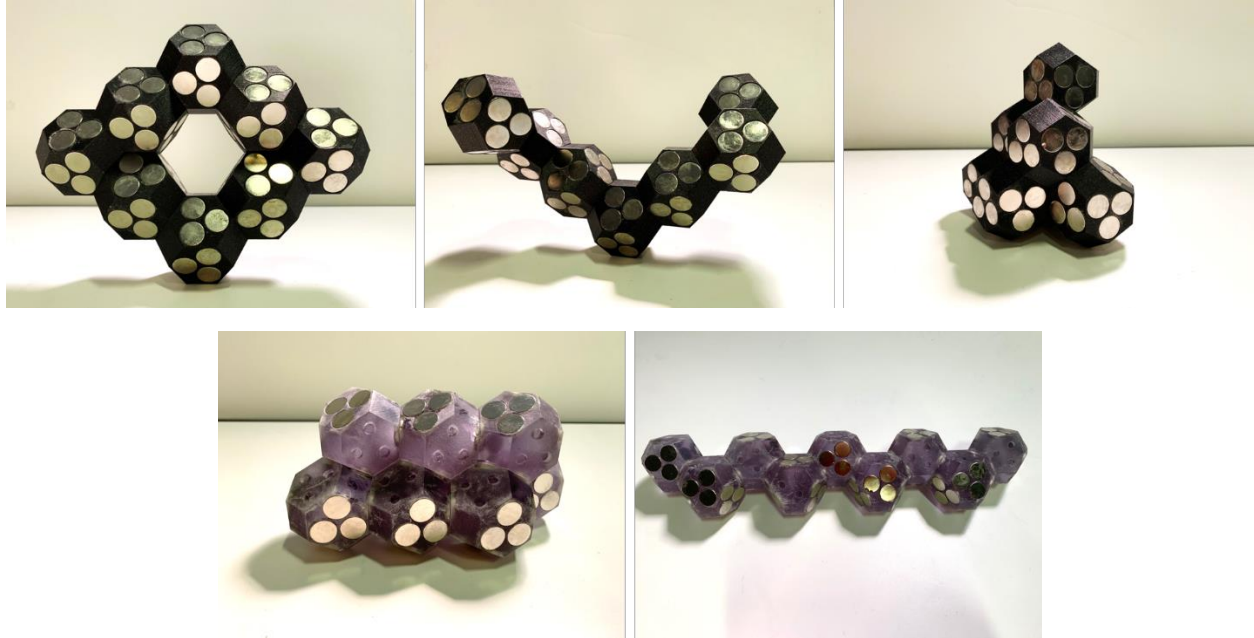


Figure 4-73. Top row: Black units with all hexagon bonding ports filled. Bottom row: Clear purple units with one hex face unpopulated. Altogether, many molecular-like shapes can be formed by these Cell units.

Parabolic Flight Methods & Results

Our experiment plan for the Zero-G 2019 flight tested both the black and clear purple units, and two different deployment methods: passive, arrayed units on the floor (Figure 4-74); controlled release by selectively introducing units from the top door of the containment box.

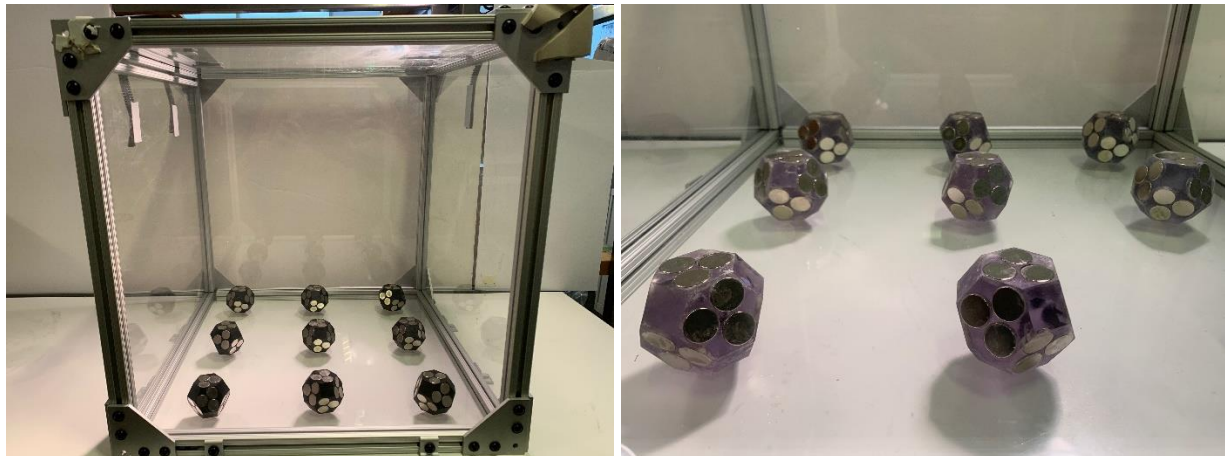


Figure 4-74. Shows pre-flight test configuration in lab of pre-arrayed units for passive, stochastic self-assembly.

We prepared the following in-flight plan (Figure 4-78), with the steps printed out and taped to the outside of the containment boxes, as once recommended to us as “best practice” by Astronaut Leland Melvin for the MIT Space Exploration Initiative student payloads. Figure 4-76, Figure 4-77, and Figure 4-78 show screenshots from our recorded flight videos, across both unit populations and both experiment conditions: passive pre-arrayed start and controlled release.

Flight Stage	Description
Prep:	<ul style="list-style-type: none"> • Box and Baseplate loaded and affixed to plane. Duct taped and padded corners. Foam on bottom. • Plexi cleaned • 2x Go Pros mounted, off. Check SD cards are present. Clean lenses • On plane tool + supply box of nodes stored
InFlight prep:	<ul style="list-style-type: none"> • Turn on GoPros • Load Black nodes into grid arrg. on box floor • Test pre-arrayed, passive release
1 st short break:	<ul style="list-style-type: none"> • Separate nodes for new assembly opportunity • Test controlled release
10 minute break:	<ul style="list-style-type: none"> • Swap from Black to Clear nodes • Check GoPros are still recording • Test pre-arrayed, passive release
2 nd short break:	<ul style="list-style-type: none"> • Separate nodes for new assembly opportunity • Test controlled release

Figure 4-75. NODES Experiment plan

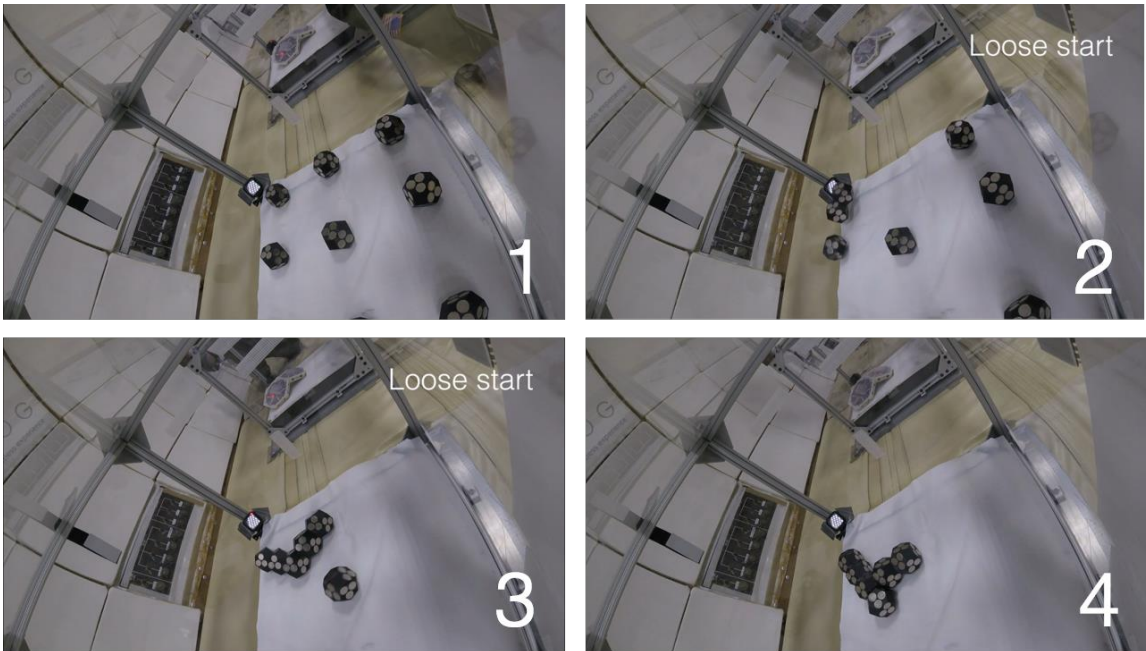


Figure 4-76. Showing evolution of the pre-arrayed, passive release from scene 1 to scene 4 over the course of a parabola.

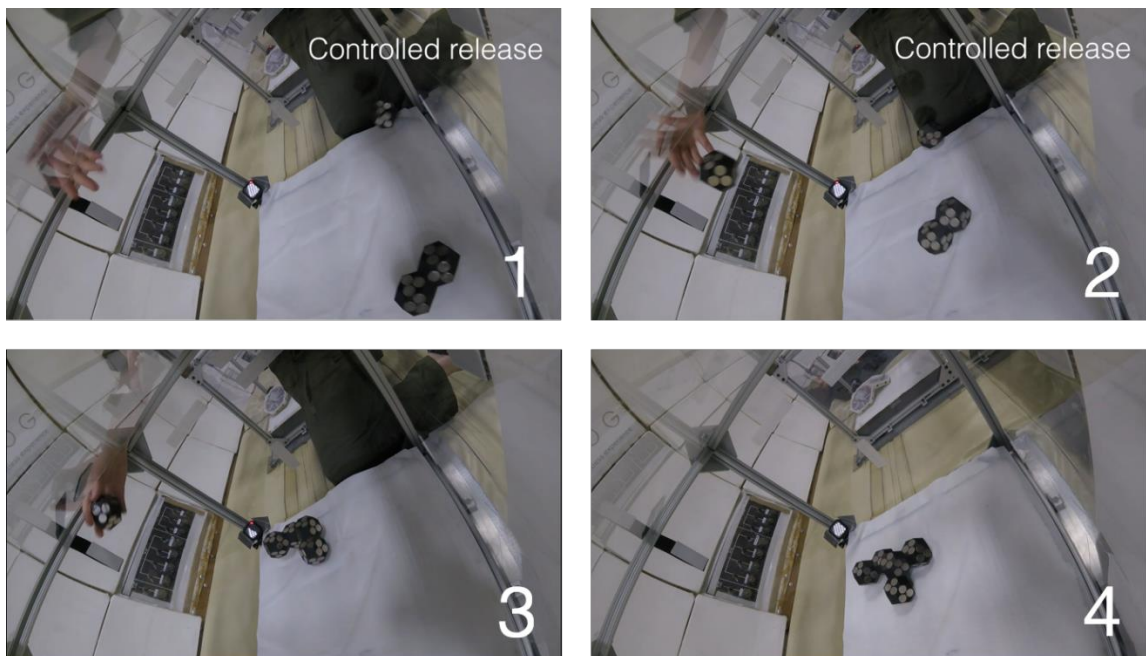


Figure 4-77. Showing evolution of the controlled release start from scene 1 to scene 4, over the course of a parabola.

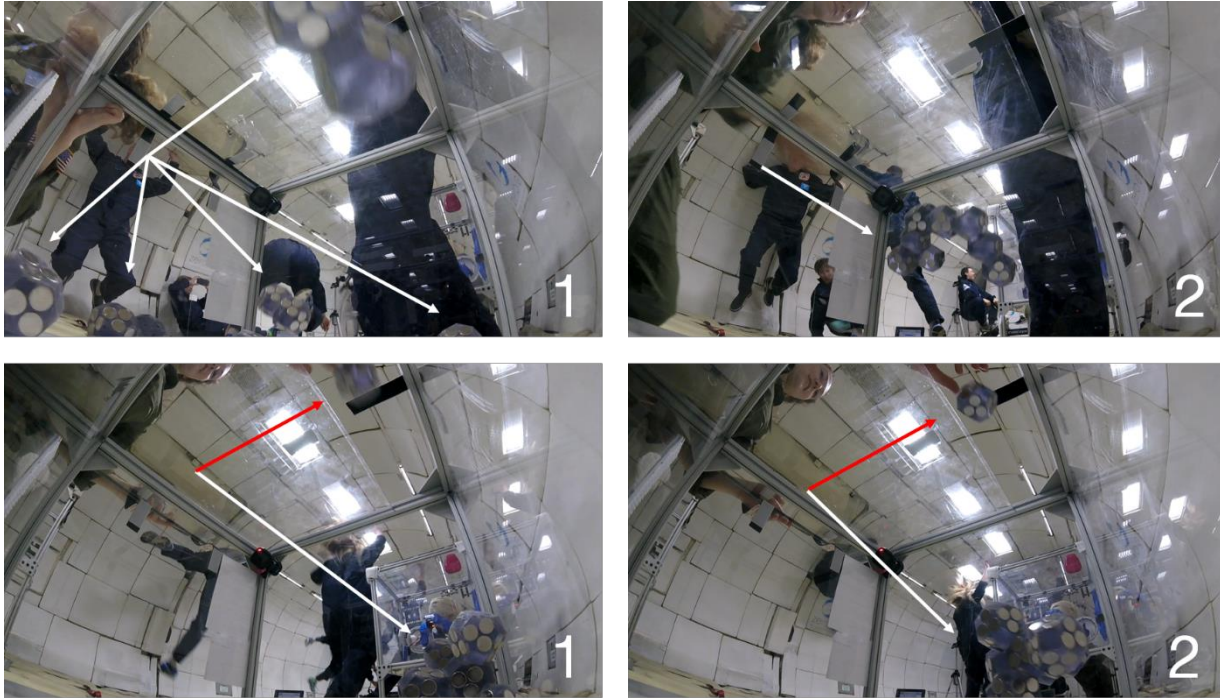


Figure 4-78. Top row shows assembly starting from bottom array, at rest; white arrows indicate separate clumps forming on their own. Bottom row shows controlled release (by hand) from top of the experiment chamber; white arrows point to accreting clump, red arrow indicates release point.

Summary

The parabolic flight validated the self-aligning joints design for the plesiohedrons Cell units, with a perfect record and no metastable bonds observed. This suggests a promising way forward to reduce the error detection and error correction steps in the future, when structures can dynamically self-assemble without errors. This hardware exploration further validated a principle of the design theory from Chapter 3, that the self-assembling artifacts be designed with “embedded logic” for the nature of the final target assembly. This model works well when the sub-units of a self-assembly structure can be subdivided into smaller, volumetric modules with a large proportion of the outer surface area dedicated to magnet joints. We also explored other models that reduce the consumption of surface area, and we will continue to refine the optimum magnet placement at pivot points.

4.2.2 Generation 2: Hardware Maturity Next Steps and “Cell” Extensibility to Other Shapes

Future TESSERAE Cell units will rely on controllable electromagnets (EMs), or electro-permanent magnets (EPMs), to achieve reconfigurability for the structure, much as we pursued for the TESSERAE Shell units. While the structures do not require extensive diagnostic sensing and control for error correction, as the more complex TESSERAE Shells do, the ability to pulse joints on and off will still prove useful in responding to changing mission ConOps where various modules may need to detach and re-assemble in other ways. Immediate next steps for the nodes include transitioning the structures to a hollow interior, with the augmented circuitry for face control with the EPMs and adding solar panels on the outside for prospective power harvesting. We are also interested in scaling the size dramatically and considering the introduction of deployable interior subsystems (e.g., environmental control and life support systems, thermal control via radiators, interior furniture or scientific racks), discussed further in Chapter 6. Immediate next steps for testing include a follow-on parabolic flight to test the controllable modules, then progressing to a longer duration test in microgravity (likely aboard the ISS for another 30-day mission, à la TESSERAE Shells), and ultimately a technology demonstration mission in orbit.

In addition to the truncated octahedron—chosen primarily for its regular, predictable shape that lends itself to dense space-filling and repeatable, predictable manufacturing (a crucial consideration for the practicality of aerospace deployments)—we are also interested in the segmentation of fractal, curvilinear and organic-inspired shapes.

Certain volumetric fractal shapes (Figure 4-79) offer the possibility of defining a common, simple base unit—much like the truncated octahedron in purpose, but with different individual part geometry—that could be repeatedly added to a structure. Thanks to the inherent logic in fractal geometry, these individual parts could accrete nearly indefinitely while following the originally intended pattern. This provides for the freedom to grow at will, incrementally (leveraging only modest resources at one time, rather than a massive and sustained political budget commitment), while still maintaining the practicality of knowing what shape the macro-space station will grow into. This combination of iterative, achievable growth and predictable expansion patterning could help us achieve the goal stated in Chapter 3—to support space architecture that evolves continuously, adapting to the needs of its inhabitants over the long time scales inherent to space travel.

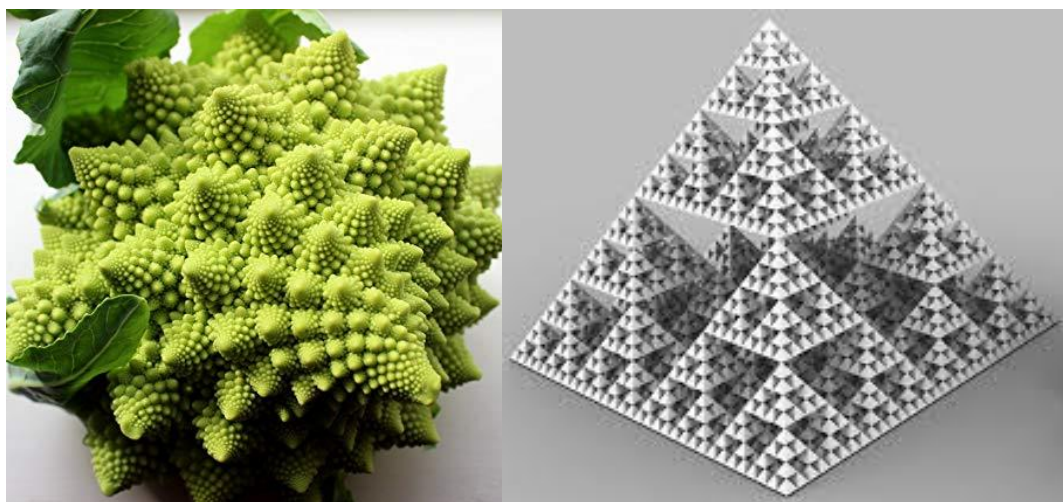


Figure 4-79. Left: fractal patterns (particularly nested parastichy) found in nature, like in this common vegetable, the Romanesco. Right: A type of volumetric fractal showing nested pyramids. Image credit: Creative Commons.

Other compelling “Cell” unit self-assembly candidates lie in the realm of triply period gyroids, and particularly Schwarz P structures (Figure 4-80), where 3D segments can be assembled to form lattice-like structures with curved, twisting, and Möbius trajectories. These shapes offer the potential for hierarchical design of space stations with different functional zones and priorities—where recessed, empty space is preserved to facilitate transit inside and between components (imagine a large space port or logistics center) and the space-filling walls of a given surface segment could be thickened with hollow interiors to allow for storage or habitation. Repeating “Cell” units would be fabricated by defining the limit of the repeating element (for the Schwarz structure, such a delineation is quite clear and ends by defining a certain radius for the six cylindrical arms) and would use magnet joints between mating faces to draw multiple units together for a macro-repeating structure.

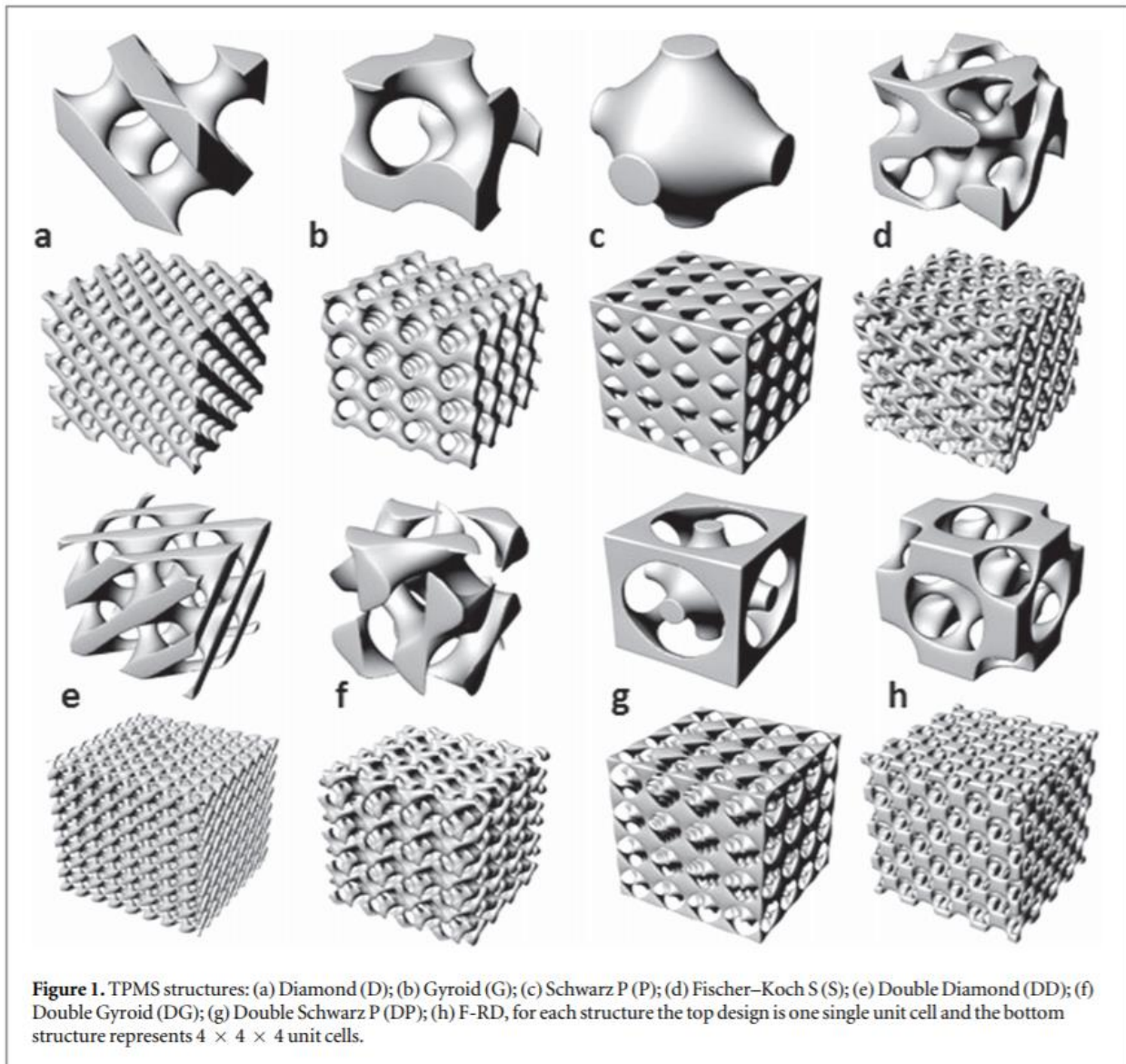


Figure 4-80. An array of triply periodic gyroids, showing a single unit and a repeating lattice of multiple units. Figure appears in Grijpma, et al.¹⁶¹

Moving beyond curvilinear shapes defined by repeating equations and sinusoids, we also take inspiration from rounded, bulbous forms that can come together to yield an altogether different texture—one that undulates and invokes softness or deformability. The BlobWall from Greg Lynn’s studio (Figure 4-81) demonstrates the potential for repeatable stacking and large-scale construction out of a single, nesting, curved shape. When coupled with our self-assembly approach, we can imagine an entirely new paradigm for decentralized, multi-module spaceships in orbit that offers gently rolling forms for habitation. Each individual unit could be scaled to a functional module size, thus creating different rooms and natural subdivisions within the space structure.

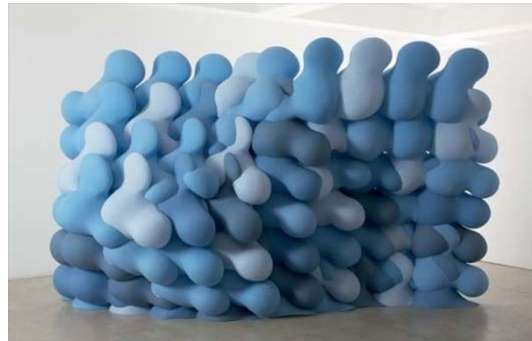


Figure 4-81. Greg Lynn modular “Blob Wall”¹⁶²

Finally, after exploring repeating, regular (even if curved) shapes, our ultimate goal remains: apply our paradigm for self-assembly to irregular, organic forms such that we can “grow” biomimetic space architecture natively in orbit. Many organic forms offer a natural pattern of chambers that lends itself to subdivision at predictable points. Of particular note are sea shells (Figure 4-82), often featuring spiral, repeating, hollow chambers that clamor for inhabitants and do already protect vulnerable Mollusca Gastropoda in their natural environment. While these shapes may not expand indefinitely from a single part or module type as the fractal and self-repeating gyroids do, they do still offer a predictable pathway towards accretion from segmented base units that are gradually scaled in size for each incremental addition.



Figure 4-82. Juxtaposition of a nautilus shell, a section of a spiral univalve, *Triton corrugatus* (images from *On Growth and Form*) and a speculative space station design (Julia Koerner’s Space Collective¹⁶³).

Together, this suite of potential shapes for tessellation, nesting and repeating accretion into larger structures represents a chaconne, or a variation on a theme. We hope the future self-assembling hardware infrastructure of space habitation can offer intriguing variability to the inhabitant and creativity to the architect, bringing choice and design flexibility to space architecture.

5. TESSERAE Modeling and Simulation

Chapter 5

“Without error-correction, all information processing, and hence all knowledge-creation, is necessarily bounded. Error-correction is the beginning of infinity.”

–David Deutsch

To inform how we expect the TESSERAE platform to behave at scale, in orbit, we have undertaken extensive simulation modeling for the TESSERAE Shell set (Section 5.1). We have built a robotics simulation model in WeBots,¹⁶⁴ predicated on both the underlying physics that governs the tile accretion behavior and on simulated control code for error detection and correction. This helps us bridge from the proof of concept hardware to predicting behavior dynamics, time to assembly, and power usage when the tiles are deployed. For the TESSERAE Cell nodes we take a different simulation approach, focusing instead on the future programmatic needs for a space station and how a quasi-stochastic system might evolve into certain architectural constraints via a generative design algorithm (Section 5.2). Videos documenting the simulation results can be found at: arieleklaw.com/tesseract.

5.1 TESSERAE Shell Robotics Simulation

To inform and refine the TESSERAE electromechanical interactivity, supervisory sensing design, and control algorithm, we scoped our modeling approach with the goal of: understanding and characterizing the tiles’ assembly dynamics over a range of orbiting environments, for various target structure sizes and mass distributions, for certain magnet strengths, for differing “stirring energy” requirements, and for various containment membrane volumes. These initial variables ultimately became just a few of the many parametric features included in the TESSERAE WeBots simulation (over 20 different controllable inputs). The outputs from the simulation efforts help us predict the timescale for complete assembly given varying input parameters, the nature of the collisions and kinetic energy profile of the system, and even characterizations that tie directly back into hardware planning—such as the power consumption of the EPMS over the lifecycle of an assembling tile.

We began by assessing various tools for modeling a 3D, 32-tile system of self-assembling solid pentagons (12 units) and hexagons (20 units), floating in microgravity and brought together via EPMS on their bonding faces to form a buckminsterfullerene shell. The simulation environment needed to include a rigorous physics

simulation engine (rigid body collisions, friction, magnetic field modeling and torques, accurate boundary conditions, fully embodied geometric tile descriptions and not just single-point approximations, etc.) and be able to accommodate the inclusion of our robotics control code. We prioritized a realistic, visualized render of tile activity through the full simulation (with the ability to speed up the graphics for ease of viewing. This enabled intuitive learnings while watching the simulation, facilitated comparison with the video-based results from the ISS mission and other flight deployments, and effectively communicated results to broader audiences.

Our control algorithm logic, and thus also the modeling, relied on early error categorizations from the stochastic assembly prototype deployed during the 2017 parabolic flight (passive, permanent neodymium magnets on each bonding face). As discussed in Section 4.1.1, we observed that adjacent, proximate tiles reliably snap together over centimeter distances in a matter of seconds. However, without correction, tiles frequently clumped or bonded out of plane. We used the results of this parabolic flight to identify likely error modes during self-assembly and have used these results to calibrate initial modeling efforts. The table below (Figure 5-1) summarizes our analysis of the correct bonding regimes and error behavior from our flight footage (over two deployed tile sets). We were able to identify a predictable pattern of tile-tile bonding modes and have confirmed comparable behavior (both in period of time over which tiles assemble and physical configurations of the tiles) in our simulations.

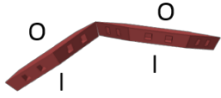
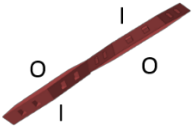






	Correct Bond	Error Mode: inverted full bond	Error Mode: meta-stable	Error Mode: clumping
Description	Correctly paired dyad, establishing consistent inner (I) and outer (O) surface, with dihedral bonding angle.	One tile is inverted. This is a stable error mode (based on current polarity map) that would require active intervention.	A single magnet pair attracts, leaving an uncompleted dyad pairing--one magnet from each side bonds, leaving tile bonding faces coplanar but not coincident. This meta-stable error mode is easily perturbed and self-corrected, but best to address with active intervention for efficiency of assembly.	Magnetic interactions outside the magnet-magnet bonding axis draw tiles together loosely. This unstable error mode is easily perturbed and self-corrected, but best to address with active intervention for efficiency of assembly.
Modeling				
Experiment				

Figure 5-1. Table showing both correct bonding and error modes observed during parabolic flight test, Nov 2017.

5.1.1 Preliminary Models: Unity and Simulink

As we progressed towards a rigorous full-system simulation for TESSERAE's assembly behavior in orbit, we began geometry and force modeling in both Unity¹⁶⁵ and Simulink¹⁶⁶ to compare the platforms.

Preliminary results from a Unity-based stochastic assembly model (see Figure 5-2 and Figure 5-3, with passive, permanent neodymium magnets on each bonding face) were consistent with the “toy model” deployed over the November 2017 microgravity parabolas, examining the core concept of magnet-mediated self-assembly in microgravity. This was a first step for the modeling, as we progressed towards a rigorous full-system simulation for TESSERAE's assembly behavior in orbit, before adding the overlaid control code (e.g., active control of the electro-permanent magnets).

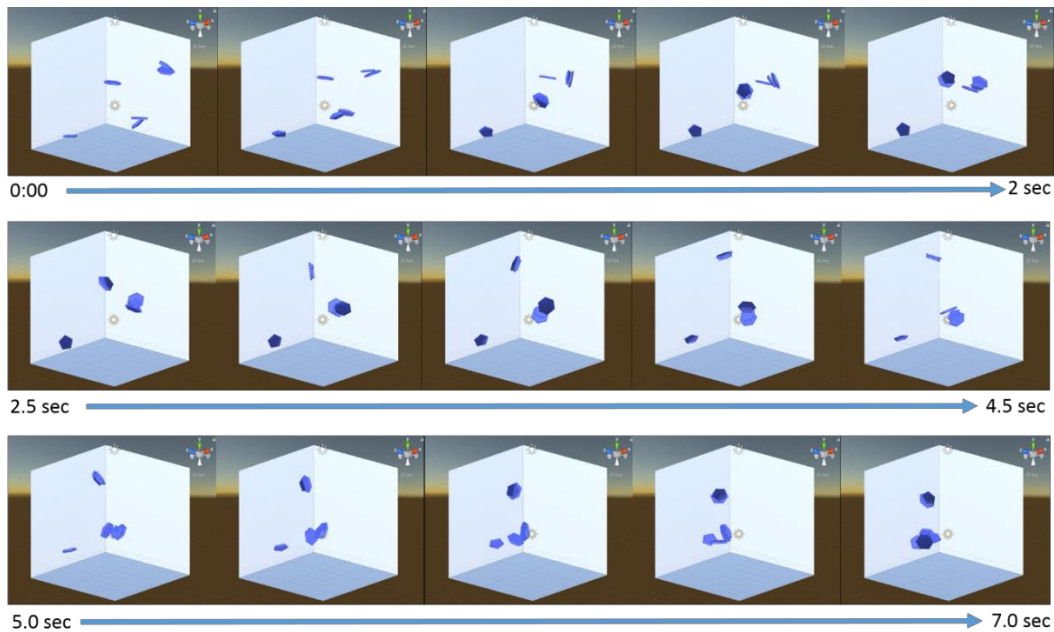


Figure 5-2. Output from Unity model (screenshots from sequential timestamps) showing self-assembly behavior in simulated microgravity environment; six freely circulating tiles (initial condition for 1st frame) condense into two batches.

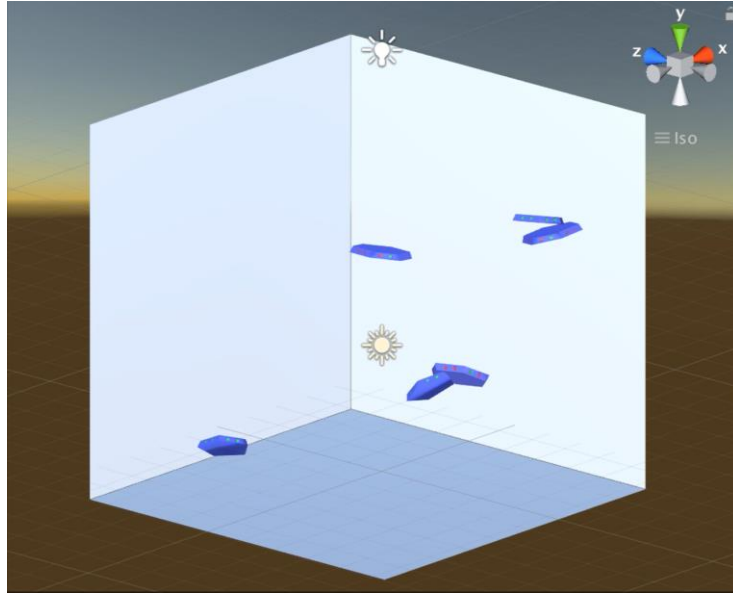


Figure 5-3. Close-up of Unity modeling environment, showing red and green dot (i.e., north and south) magnet pairs embedded on the face of each tile.

The Unity simulation faithfully produced tile-tile interactions expected from our microgravity flight experiment, including correctly bonded dyads, meta-stable states, and clumping. To provide the required precision for the rigid body collisions, we applied a mesh collider (albeit computationally expensive) rather than Unity’s standard box collider. Friction terms were also added to more realistically simulate tile motion and collision behavior, relying on the Nvidia PhysX engine in Unity. While this model yielded a useful first-order approximation of tile behavior, we ultimately determined that additional functionality was required and pursued alternative modeling options including Simulink (see below) and robotic simulation for the quasi-stochastic, active-EPM control use case.

We next explored a modeling approach for the magnetic interaction between the EPMS on the Blue Origin, Generation 2, CAD tile design (see Section 4.1.2) using Simulink. Magnetic relationships are established between tile bonding faces, with the tile properties (center of mass, inertia, geometric definitions) imported from Solidworks and augmented by Simulink plug-ins. Due to Simulink’s integration with MATLAB and extensive physics libraries, this modeling environment supported several, though not all, of the TESSERAE simulation needs. It addressed flexibility for programmatic simulation parameters and stricter coherence with the laws of physics governing the tile assembly behavior. Figure 5-4 shows two TESSERAE tiles modeled and interacting in Simulink. These 2nd phase modeling results progressed beyond the Unity capability with the ease of integration between SolidWorks, Simulink and MatLab, but ultimately, Simulink did not offer the extent of robotics-simulation tools needed for full behavior assembly with our control code. We turned to the Cyberbotics “WeBots” open-source software for its superior handling of world-based scenarios and intensively developed physics engine.

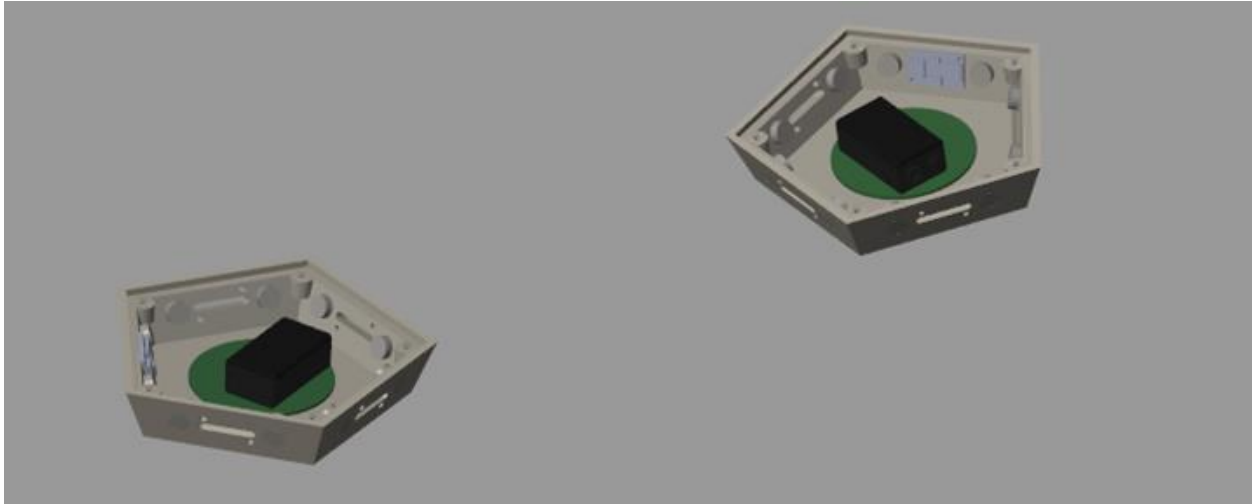


Figure 5-4. Snapshot showing preliminary modeling environment in Simulink.

5.1.2 Full Behavioral Model and Characterization Results

The TESSERA Shell simulation, built on the open-source WeBots platform, provides a parametric model environment for testing many self-assembling scenarios that use the buckyball tile geometry (see Figure 5-5). We rely on the ODE (Open Dynamics Engine) physics plugin for the underlying rigid body dynamics and on custom python code that translates our experimental control algorithm and state machine handling into the logic for controlling the robotics simulation. This is predicated on the Cyberbotics definition of “Worlds” as the overarching operating environment and “Controllers” as the actuation and logic mechanisms. The ODE plugin is considered an industry-best physics solver, though as with all systems, there are notable limitations.¹⁶⁷ We found the ODE integration with Cyberbotics performed amply well, routinely detecting collisions via mesh intersections well before any visual render showed a sign of overlapping geometries (where such visual incongruities are common in even best-in-class visual renderings and video games). Data exportation from the robotics simulation allows us great flexibility in plotting scenario activity, based on accessing the x , y , and z coordinates of the tiles’ center of mass and their linear and angular velocity vectors, their collision boundaries, the bonding status between tiles, and the time to any conditioned scenario (i.e., time to good first bond per tile face, or time to all 32 tiles bonded together in a complete assembly). The simulation scenario and guiding scientific and engineering choices for the model were made directly by the author, with extensive support for the python code development and a large custom codebase undertaken by the Cyberbotics software support engineers. We heartily thank the Cyberbotics team (notably David Mansolino) for their collaboration on this model.

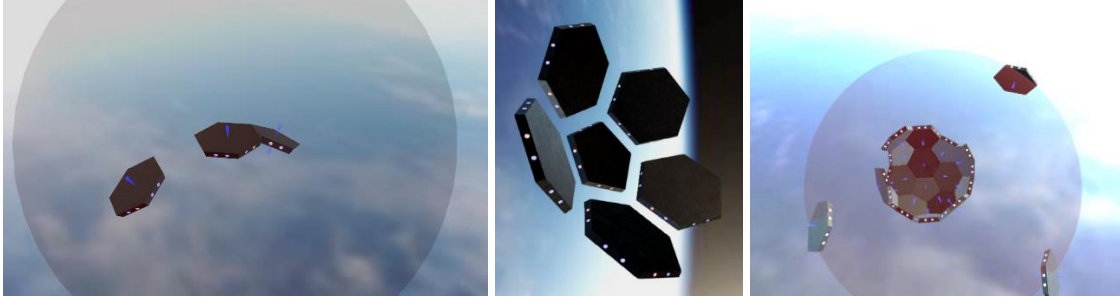


Figure 5-5. Panel showing simple tile attachment (left), pre-positioned petal assembly (middle), and quasi-stochastic self-assembly of one-by-one inserted tiles towards a full 32 tile assembly (right). Many such scenarios can be instantiated and tested with the parametric WeBots TESSERAE simulation.

5.1.2.1 Initial Conditions and Fixed Assumptions

By definition, no “model” is perfect. While our WeBots TESSERAE model ultimately yielded insightful results, the ultimate generalizability of these results depends on the constraints defined by certain initial scoping decisions and assumptions. Below, we present the core description of the underlying simulation and the assumptions and simplifications made in this first full version.

1. Governing Equation for Attractive Force Between the Tiles

The inverse square law formula for magnetic force between two poles is used to approximate the magnitude of the attractive or repulsive vector between the modeled magnets:

$$F = \frac{\mu q_1 q_2}{4\pi r^2} \quad \text{EQ (1)}$$

Where q_1 and q_2 are magnitudes of the magnetic poles, μ is the permeability of free space constant, r is the separation between the tile magnet faces and F is the magnitude of the resultant force vector. In the code implementation, we group the constants together into a single value and can toggle this parameter to model relatively stronger or relatively weaker magnets. Note that we are also able to update this formula to reflect the $1/r^4$ factor driving attraction between magnets of varying cylinder geometries, as reflected in Eq. 2.

Where:

R = radius of the cylindrical magnet

L = length of the cylindrical magnet

M = magnetization of the magnets

x = separation distance between the two axially aligned magnets

μ_0 = permeability of free space

$$F(x) \simeq \frac{\pi\mu_0}{4} M^2 R^4 \left[\frac{1}{x^2} + \frac{1}{(x+2L)^2} - \frac{2}{(x+L)^2} \right] \quad \text{EQ (2)}$$

When $x \gg L$, simplifies to the far field equation:

$$\frac{3\mu_0}{2\pi} m_1 m_2 \frac{1}{x^4} \quad \text{EQ (3)}$$

For the purposes of our simulation, we have generated two branches of code—one that uses the classical magnetic force equation between points (EQ1, as the default Cyberbotics implementation for magnet faces assumes monopole points, consistent with that equation) and a separate branch that tests a custom dipole implementation with the dimension relationships from our ISS magnets and relies on the more geometry-specific equations for magnetic force (EQ 2 and 3). The second branch is still under development, as the dipole implementation was not stable with the current Cyberbotics infrastructure. Results in this chapter are generated from the first branch, off the classical model and completion of the second branch will be pursued in future work. Figure 5-6 shows the relationships between the Length (L) and Radius (R) of cylindrical magnets and how the ratio of those two values governs the force between two identical magnets of those dimensions, when considering the dipole model and specific geometries.

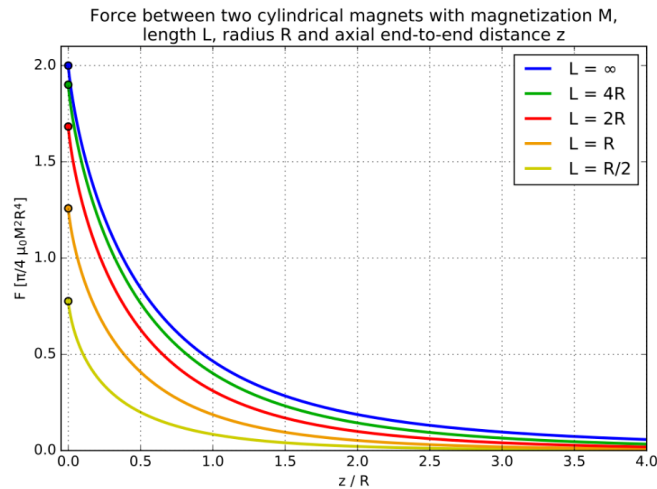


Figure 5-6. Showing the rapid drop-off in force between two cylindrical magnets, comparing varying constant curves relating the length L of the cylinder to Radius R of the cylinder. Our magnets in the TESSERAE ISS Hardware (Generation 3) roughly follow the orange L=R curve, as the cylindrical EPMs are as wide as they are long. Image Credit: Creative Commons CC BY-SA 4.0 (creator: Geek3).

Our approach to the force due to the magnetic fields generated by the EPMS approximates the units as magnetic poles, leaving the finer description of rings of coils to our implementation of the EPM in COMSOL for precise design generation and testing (see Section 4.1.3).

2. Definition and Treatment of a Good Bond

To detect a good bond between two tiles, we test for three aspects of alignment—the expected polarity matching between the interacting tiles (NN/SS for pentagon-hexagon or NS/SN for hexagon-hexagon sides), the separation distance in meters between two corresponding points on the planar bonding faces, and the rotation in radians between the two faces (where perfect alignment of all four sides of the trapezoidal face is defined as 0 rad). For the bulk of our testing and all results shown below, we employed a very strict good bond condition: the tiles must come within .05m and .05 rad, at which point a good bond is detected, the tile is allowed to complete its approach (as opposed to being pulsed away as a bad bond) and bond flush with the neighbor tile. These conditions for the separation distance and radians of angular displacement are controllable, toggle-able parameters in the simulation environment, allowing us to examine the effect of looser or stricter bond conditions on assembly completion time. After good bonds are made, we execute a mock “locking sequence,” to rigidly bond the neighbor tiles as if the clamp sequence has actuated in the tile hardware. This helps us avoid good bonds being knocked away by colliding tiles and is consistent with our intended deployment ConOps.

3. Handling Bad Bonds

The simulation code detects and identifies three classes of bad bonds—clumped, inverted, and metastable. The latter two are easily determined by the radian test, as the angular displacement does not match our good bond requirements. When one of these off-nominal bonds is detected, the magnets on only the interacting bonding faces are reversed and “pulsed” for separation. For the clumping tiles, which often interact outside the bonding faces on which we have the radian test, we have developed a test for detecting tile collision with a monitored timeout: if two tiles collide outside their bonding faces, and their coordinates stay coupled for over X seconds (a controllable parameter of the simulation), we flip all magnets (not knowing exactly which sides are interacting most strongly) and separate the tiles. We can also detect clumped tile pairs by comparing the distance between their centers—when two tiles are correctly bonded, their centers should be separated by the radius length of each tile (accounting for the dihedral angle offset). When two tiles have clumped back to back on their top or bottom faces, the tile centers will be too close together.

We are able to set the magnitude of steady state attractive and repulsive force (for the passively interacting North and South poles) separately from the active repulsion force generated by a simulated EPM pulse-off event (consistent with our ISS hardware implementation). Tuning this ratio of passive attraction/repulsion to active attraction/repulsion allows us to explore different energy profiles for the system. A stronger active repulsion induces greater motion into the system for an increase in stirring energy after a bad bond correction, but also consumes more energy for the power that must be dedicated to that EPM to induce the greater separation force. For the purposes of the results shown below, we kept the ratio of passive:active force to a conservative 1:2. This is lower than what was achieved during the ISS hardware testing—the active repulsion through the coil was much stronger than the base permanent magnet (better than 1:3)—but remains reasonable for the orbital environment where we will want to achieve assembly with the lowest feasible power allocation, which mean less difference between the active and passive regimes.

4. Containment Chamber

To contain the tiles and keep them proximate for assembly (required for efficiency of the simulation given the inverse drop-off in force due to separation, and our desire to avoid propulsion that would otherwise keep them from floating far away from each other), we model the system inside an elastic, spherical membrane. We can vary the diameter of the membrane as one of the core, toggle parameters of the system, allowing us to test for the optimum containment volume. Too much space leads to less proximate circulation, slower assembly, and lost tiles; too little space overly constricts circulation for neighbor-finding, with a “crowdedness” that also hampers assembly. The degree of restoring force that the membrane imparts to tiles that collide with it is a further, tunable parameter of the system, based on a variable where we set the elasticity of the membrane.

For our initial modeling, the chamber is artificially fixed in place. While tiles can bump and disturb the membrane, receiving a dampening effect, the chamber itself does not yet respond with the translational and rotational motion that would be expected from Newton’s 3rd Law as clumps of tiles collide with the membrane. In future work, we will update the simulation to free the containment chamber from its fixed position and analyze the degree of stirring energy that this gives back to the system. From here, we can determine whether the chamber should be fixed in reality (a difficult, non-trivial control and stabilization problem) or whether we embrace the reactive motion of the chamber as a beneficial contribution that perturbs the assembling tile system out of local minima states.

5. Earth’s Magnetic Field

We approximate the effect on the tiles due to Earth’s magnetic field, using a vector applied to the motion of the tiles. The magnitude and direction of the Earth’s magnetic field at our particular “location in orbit” is modeled off the International Geomagnetic Reference Field¹⁶⁸ and the stated values at the ISS orbital altitude (reported to be 0.35 Gauss).¹⁶⁹ Our implementation of this effect is currently an approximation based on these two references, and further work could be undertaken to both apply finer application of the harmonic series expansion to our particular orbit and to track the subtle changes in these values over time (perhaps even incorporating other, albeit mediated by our atmosphere, sources like solar wind). We have made the inclusion of Earth’s magnetic field an optional parameter for the model and the selection of results shown below does not include it to preserve generalizability to deep space orbits of greater interest (for missions beyond the particularities of Low Earth Orbit). Upon preliminary, initial testing with Earth’s magnetic field turned “on,” we did note an observable effect on the dynamics of the tiles, but this did not significantly affect the annealing process towards convergent assembly. Further testing and additional trials would be necessary to fully document the effect on the simulation.

6. WeBots Synchronization

The WeBots simulation infrastructure offers two options—

- a perfectly “synchronized” mode, where no global simulation steps are taken until all controller steps (i.e., loops) for the various state machines for the modelled robots (in our case, the tiles) have completed;
- and an alternative, asynchronous mode where global simulation steps are allowed to progress even if a previously called state machine loop is still running, and that controller logic is updated later in the simulation when it ultimately completes.

This choice is a feature of the WeBots implementation structure,¹⁷⁰ offered to speed up performance for the simulation by avoiding a wait delay from slower-processing controllers. While major logic controls are still observed the same way in both systems and the same input variable parameter set will run quite similarly (if not exactly the same), the asynchronous mode essentially generates “noise” for the simulation. We have chosen to operate primarily in this asynchronous regime, as the simulation progresses much closer to real time (a key benefit when running hundreds of trials) and we benefit from introduction of noise in modeling a stochastic system that will inevitably encounter variability in the real-world deployment. At the simulation output level, this choice means that repeated trials with the same exact input parameters will yield slightly different results. We compare intra-trial variability with inter-trial variability (changing input variables) in the subsequent results section. Again, the choice for synchronized vs. asynchronous is a simple toggle and future TESSERAE simulation runs could be just as easily run in the other mode, provided that the computing infrastructure and time allows.

5.1.2.2 Input Parameter Set

The WeBots TESSERAE simulation allows parametric control on many key input variables, from the initial velocity with which tiles are introduced into the containment chamber, to the relative strengths of the magnets, and even the presence or absence of Earth’s magnetic field. See Figure 5-7 for a comprehensive list of the current parameters.

ID Number	Parameter	Description	Notes
1.	Magnet attractive factor	Baseline constant for passive, permanent magnet attraction.	Kept the same as the magnet repulsive factor to keep consistency with physics laws governing magnet behavior. Used in the magnetic force equation calculation.
2.	Magnet repulsive factor	Baseline constant for passive, permanent magnet repulsion.	Kept the same as the magnet attractive factor to keep consistency with physics laws governing magnet behavior. Used in the magnetic force equation calculation.
3.	Magnet active attractive factor	Powered-on constant for EPM-mediated magnet attraction	Kept the same as the magnet active repulsive factor to keep consistency with physics laws governing magnet behavior. Used in the magnetic force equation calculation.
4.	Magnet active repulsive factor	Powered-on constant for EPM-mediated magnet repulsion	Kept the same as the magnet active attractive factor to keep

			consistency with physics laws governing magnet behavior. Used in the magnetic force equation calculation.
5.	Tile friction	Constant used to define the roughness of the tile surface	Used in tile-tile collisions
6.	Tile density	Constant based on material choice for the tile (i.e., ISS stuffed whipple shield or other), in kg/m ³	Implemented as a density, rather than a fixed mass, to facilitate parametric control of the dimensions of the tiles
7.	Tile thickness	Thickness of the tile from bottom plane to top plane, in meters	Must be the same for both pentagons and hexagons, thus defined only once, to produce a consistent inner and outer shell surface
8.	Pentagon tile radius	Defines the width of the pentagon tile, in meters	
9.	Hexagon tile radius	Defines the width of the hexagon tile, in meters	Subsequent calculations made off of this value, accounting for the fact that the hexagon tiles have two edge types with different side slopes (for binding to hexagon, and for binding to pentagons)
10.	Initial linear velocity	Introduction velocity for the pentagon and hexagon tiles, in meters/second	
11.	Initial angular velocity	Introduction velocity for the pentagon and hexagon tiles, in radians/second	
12.	Hard bound distance tolerance	Separation distance allowed between two corresponding points on the planar bonding faces of two tiles assessing a good-bond as neighbors, in meters	Used to assess and handle good bond recording
13.	Hard bound angle tolerance	Angular displacement allowed between the two planar bonding faces assessing a good-bond as neighbors, in radians	Used to assess and handle good bond recording
14.	Tile introduction timeout	The time, in seconds, the simulation waits after introduction of a loose tile	Allows the system to settle and for the introduced tile to

		before introducing a further tile (up to a cap of allowable loose tiles, governed by the related “max unbounded tiles” parameter).	(hopefully) bond to the main accretion group
15.	Max unbounded tiles	The maximum number of tiles, post-insertion into the simulation, that are allowed to float free. If the max is reached, no further tiles are inserted until at least one loose tiles bonds successfully to the structure	Assists in avoiding a scenario where tiles are continuously released and spend unnecessary energy interacting with each other rather than the main accretion group. Note: sub-group good bonds (i.e., two tiles bonding separately to just each other) are not allowed, due to the risk of non-complementary sub-groups forming that would not match with the available holes in the main accretion group. This element is a key optimizing parameter, as the “crowdedness” of the simulation directly impacts time to assembly.
16.	Stuck timeout	The time, in seconds, the simulation waits after detecting a tile collision with another object that did not result in a good bond (often a settling into the containment membrane, or attracted to the far side of the nearly-closed ball when the remaining hole bonding site is in fact across the way) before pulsing the tile magnets to encourage a return to activity	Assists in perturbing the system when a tile has settled somewhere outside the main accretion group and without a good bond; distinct from the handling of the bad-bond clumping detection and correction
17.	Max tiles	The total number of tiles introduced by the simulation controller over the course of the trial	Assists in solving the hole filling problem, by adding in extra tiles (above 32 count)
18.	Containment volume radius	Defines the size of the spherical containment membrane	

19.	Containment volume elastic factor	Constant defining the malleability of the containment membrane	Used in calculating the restoring force imparted to the tiles upon collision with the membrane
20.	Earth magnetic field	On/Off toggle for applying an approximation vector force on the tiles due to the earth's magnetic field interacting with the bonding face magnets	Calculated based on the IGRF and stated values of Earth's magnetic field at the ISS orbital altitude.
21.	Synchronization mode	On/Off toggle for choosing simulation operating mode	See discussion above—affects whether repeated runs of trials with the same initial parameter set produce identical, or slightly varying, results.

Figure 5-7. List of WeBots TESSERA parameters by name used in the codebase, with notes

5.1.2.3 Key feature decisions

1. Ease of parametric control and automatic simulation sweeps

To facilitate a parameter sweep across many different groupings of input variable values, we implemented a JSON config file that the WeBots software reads to pre-populate the simulation initial conditions and governing constants. This file can be generated with definitions for many trials, executed continuously one after the other, thus enabling automation of a simulation parameter sweep.

2. Avoiding sub-groups

Through the course of the simulation refinement, we discovered an improvement that reduces time to assembly and increases the likelihood that a trial will complete to 100%. We stipulate in the code that no two tiles can finalize a good bond if one of the tiles is not already part of the main accretion group (with the exception of tile 0 and tile 1). This ensures that tiles accrete to the main structure and do not form sub-groups that may or may not fit into resulting holes on the main ball.

3. Correcting tile settling

In some cases, tiles settle against the containment volume even when available bonding sites are open on the accreting ball. In some cases, this is due to the preponderance of exposed magnet faces exposing South (hexagon sides), when the free tiles that need to assemble next are also hexagons (south pole dominated). This means there is a narrow range of approach where a polarity map on the tile is feasibly rotated to feel an attractive force that can bring it in to bond.

Another form of tile settling occurs with a nearly finished ball, where one or two remaining tiles stick to the outside of the far side, feeling the pull from the open bonding site across the structure, but blocked by the ball itself from reaching this point.

In both cases, we have determined that a targeted pulse of the EPMS on the settling tile (after the “Stuck Tile” timeout has been met) adds stirring energy back into the system and can aid in perturbing the system into a new state where the remaining tiles can bond properly into the main structure.

5.1.2.4 Simulation Results

The data exportation functions from the simulation enable many different views and analyses. We present below a subset of the available characterizations to elucidate the potential for both intra-trial characterizations and across-trial comparisons when different initial parameters are set.

1. Intra-Trial Characterizations

Within a single trial, we can analyze the collision behavior of the tiles, the center of mass of the system and how this changes over time, patterns in good bonds and energy expenditure, and network nodes showing how insertion order and other parameters affect the way the buckyball shell anneals. The table below calls out notable initial conditions for the trial in question. A screenshot from the end of the simulation documents the final configuration (Figure 5-8). The following Figure 5-9 through Figure 5-16 show the data representations of the system for a successfully completed shell.

Parameter	Value for this trial
Passive to Active magnetic field strength ratio	1:2
Tile density	1240 kg/m ³ (drawn from a partial stuffed-whipple shield configuration, with additional compartment for storage)
Tile thickness	0.52m (assuming extra thick due to compartments for deployable interior, and for robustness to collision)
Pentagon tile radius	1.9m
Hexagon tile radius	2.26m
Initial linear velocity	1 m/s
Initial angular velocity	0.1 rad/s
Hard bound distance tolerance	0.05m
Hard bound angle tolerance	0.05 rad
Tile introduction timeout	600 seconds
Max unbounded tiles	5 tiles
Stuck timeout	60 seconds
Max tiles	34 tiles introduced
Containment volume radius	14m
Containment volume elastic factor	Moderate
Earth magnetic field	Off
Synchronization mode	Off

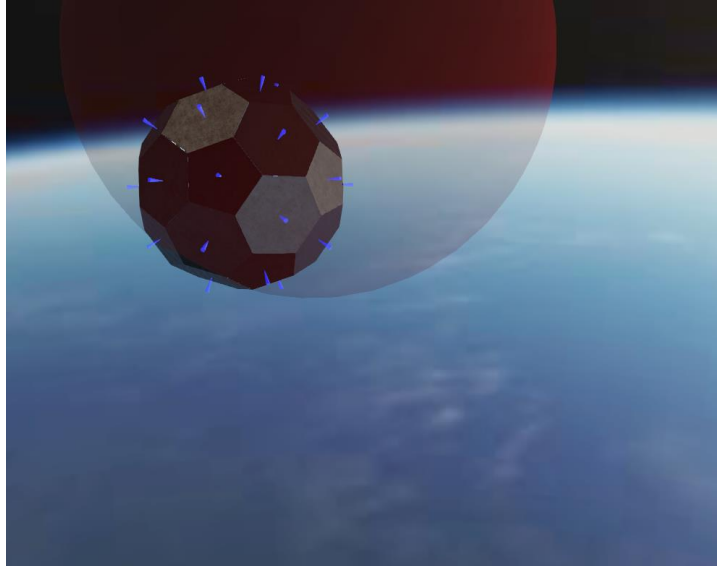


Figure 5-8. Table of trial parameters (above) and snapshot of completed assembly inside containment membrane at the end of the simulation.

Collisions Investigations

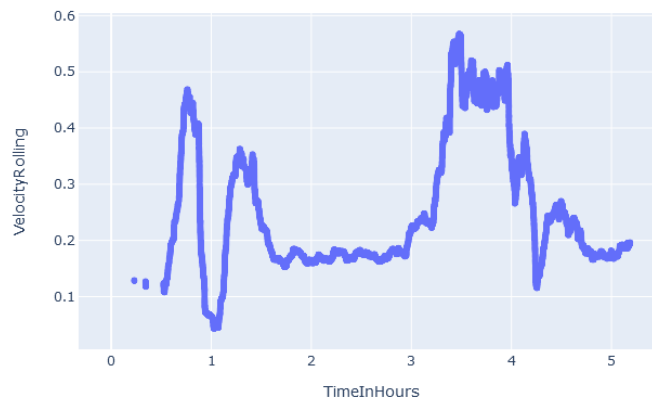


Figure 5-9. A rolling average over collisions of velocity in m/s, showing a relative quiescent period from hour 2 to hour 3, followed by increased activity from additional tile insertion and eventual annealing around hour 5. This suggests that a certain amount of “bonding activation energy” is needed (à la Whitesides¹³ and Bachelet¹⁴), and then the system anneals, coming together all of a sudden in fits and starts rather than in a strictly linear progression.

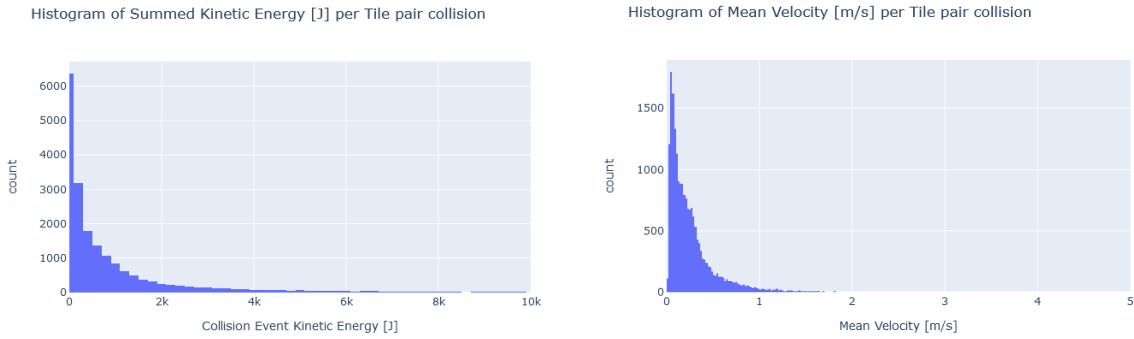


Figure 5-10. Histogram showing the prevalence of varying values of kinetic energy (summed across two tiles in a collision, using the average velocity of the two tiles) on the left and mean velocity, directly, of these collisions on the right. This is consistent with expectations as we see the bulk of events are under 1m/s (which is the initial velocity of insertion for this trial). These graphs will inform our planning for the on-demand buffering that may be needed to reduce the impact of tile collisions and the material choice for robustness to collisions. The vast majority of tile-tile collision events see kinetic energy under 2kJ; for comparison, a collision with a car at highway speeds (assuming 1500kg average mass, 55mph) involves ~450kJ. While the energy of our collisions, even the worst cases recorded (long tail between 8kJ and 10kJ), is still significantly lower, even minor damage to tiles from collisions will need to be avoided.

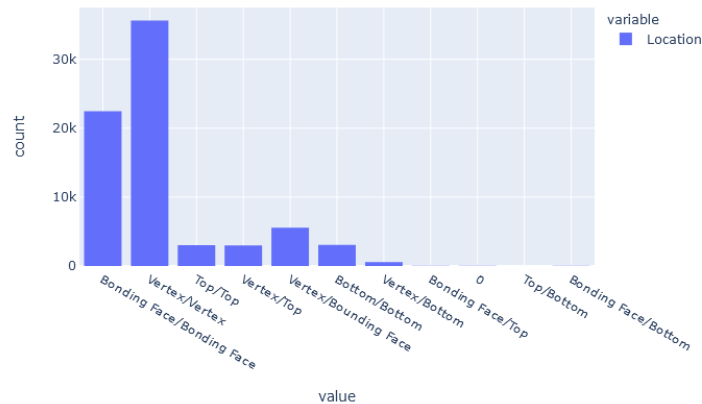


Figure 5-11. Categorical histogram showing location (on tile surface) of tile-tile paired collision events. Future work for the hardware development will respond to this graph, noting the likely need for deformable, collision-absorbing materials due to the prevalence of vertex-vertex collisions (if this holds true across many subsequent trial runs).

Center of Mass Investigation

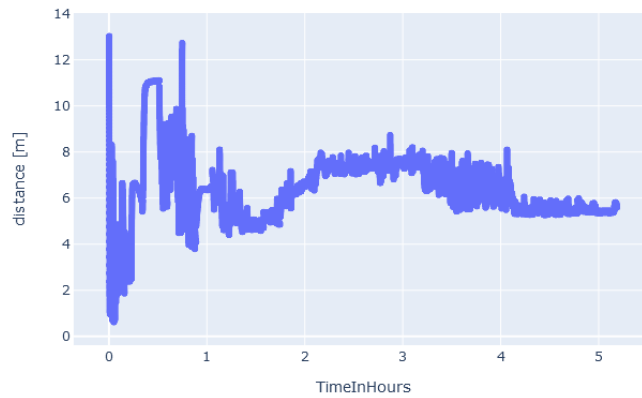


Figure 5-12. Center of Mass of the entire system. Calculates average distance from center of mass of all individual tiles to center of mass of the global system. Shows expected resolution to a stable value as tiles come in for accretion to the single buckyball shell.

Bonding Behavior Investigations

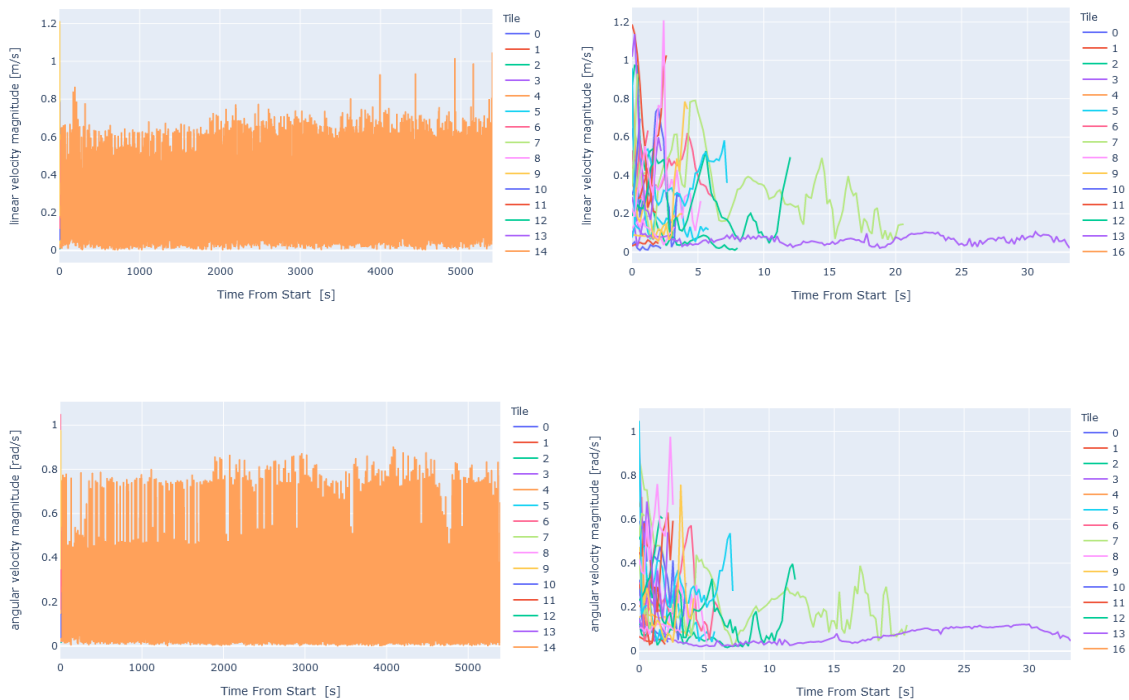


Figure 5-13. Dampening activity at the moment of good bond detection, shown for the first half of the introduced tile set.

Top row shows linear velocity, bottom row shows angular velocity. Left shows a graph dominated by the oscillatory behavior of Tile 14, which attempted to re-bond many times to the same neighbor port (trapped in an inverted bond in a hole that could not be easily self-corrected). When filtered out, we can see the behavior of the other tiles at their moments of good-bond attempt and the characteristic curves showing the dampening of the linear and angular motion as time progressed. The two extra tiles (out of the 34 total) that never bonded are excluded from these graphs, hence the absence of tile #15 in this view of the first half set.

Histogram of Time to Good Bond by Tile Edge

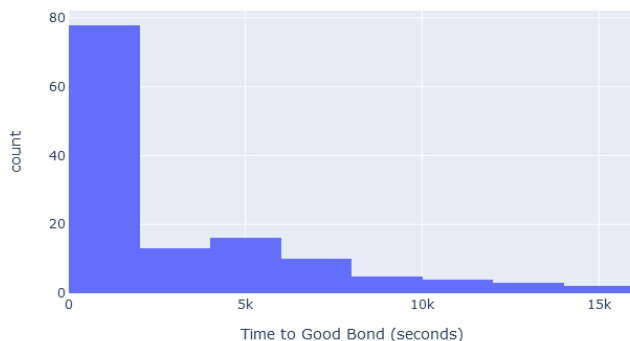


Figure 5-14. Histogram showing the distribution of time to good bond, by tile edge (not by whole tile). The longer tail represents tiles that either joined the ball early with an exposed edge left un-partnered for much of the assembly duration, or did not accrete at all until after a prolonged period of circulation. The time in seconds for this chart starts from the tile's relative t=0 at introduction (not the time from simulation overall start). The majority of good bonds form in under 2000 seconds (~33 minutes) of exposure.

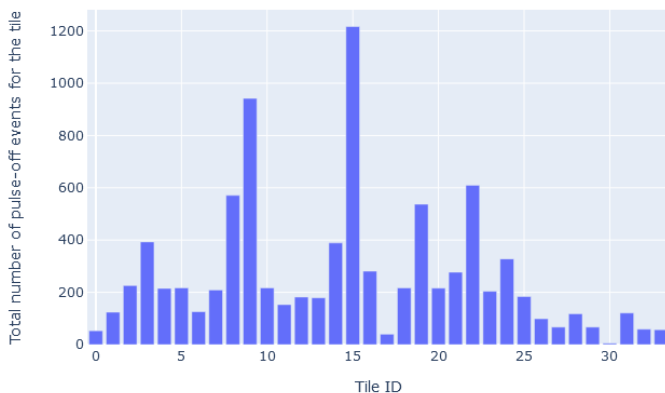


Figure 5-15. Bar chart showing count of pulse-off events (aka EPM firings) per tile. Tiles 9 and 15 did not bond until nearly the end of the simulation, despite their earlier introduction, hence the long lifetime and greater count of events. In future work for the macroscale tiles, when we know how much energy each EMP pulse takes, we can tie this to the feasibility of the power budget and make determinations for when to cut off pulsing activity or when to make a tradeoff for using electromagnets instead of EPMS (see discussion in conclusion for this section).

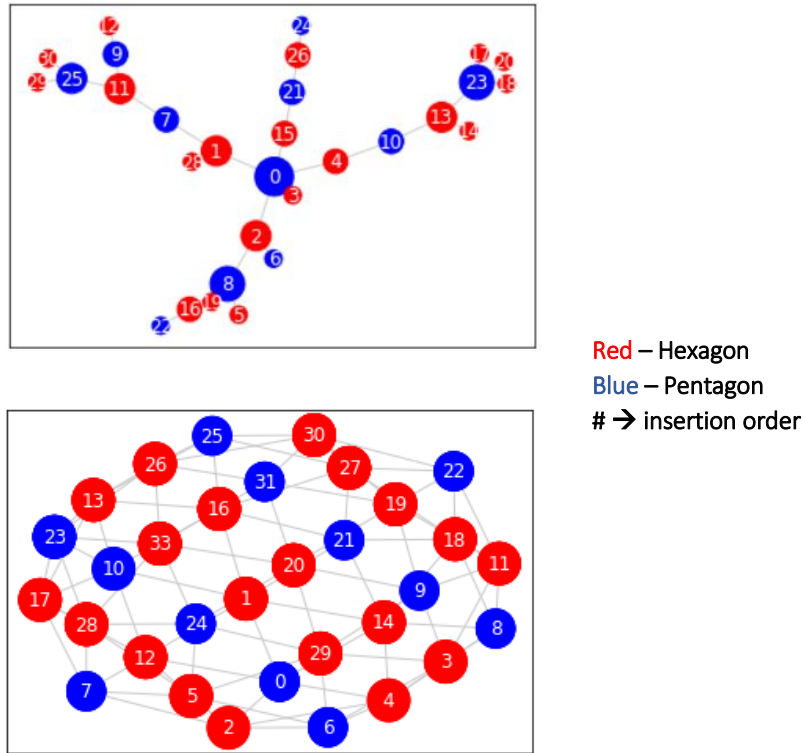


Figure 5-16. Network node graphs showing an incomplete ball from a different parameter set trial run (top) compared against a completed buckyball shell with the trial run parameters in question (bottom). Circle nodes represent tiles (red-hexagon, blue-pentagon), with the lines representing tile-tile bonds. Top: the ball did not complete (much larger containment volume), and instead, had a tendency to form branches (the simplest bond is a one-edge bond, rather than having to negotiate an $n=two$ or greater simultaneous bond, and this can lead to branching behavior). Bottom: the ball *did* complete, and the matrix of connections shows interesting patterns including a) as expected, pentagons only bind to hexagons, hence the single-depth color bands of blue and b) insertion order may not be as critical as we had previously conceived, as tile 1 ended up bonded to tiles 16, 24 and 20 (rather than strictly 0 and 2-6).

2. Comparisons across trials with varying parameters

Moving now into comparing the inter-trial behavior when different parameter sets are used, we present below an analysis that assesses “crowding” (Figure 5-17 and Figure 5-18), or the combination effect that the containment volume size and number of loose tiles has on the time to self-assembly completion for a full buckyball shell. For these trials, all other initial parameter values were held constant other than the “containment volume radius” and the “max unbounded tiles” parameter. This is just one example of the many parameter-effect comparisons that are possible, shown to elucidate how the simulation can serve as an effective tool. With these and other results, we are able to explore the parameter space for optimizing TESSERAE deployment in orbit.

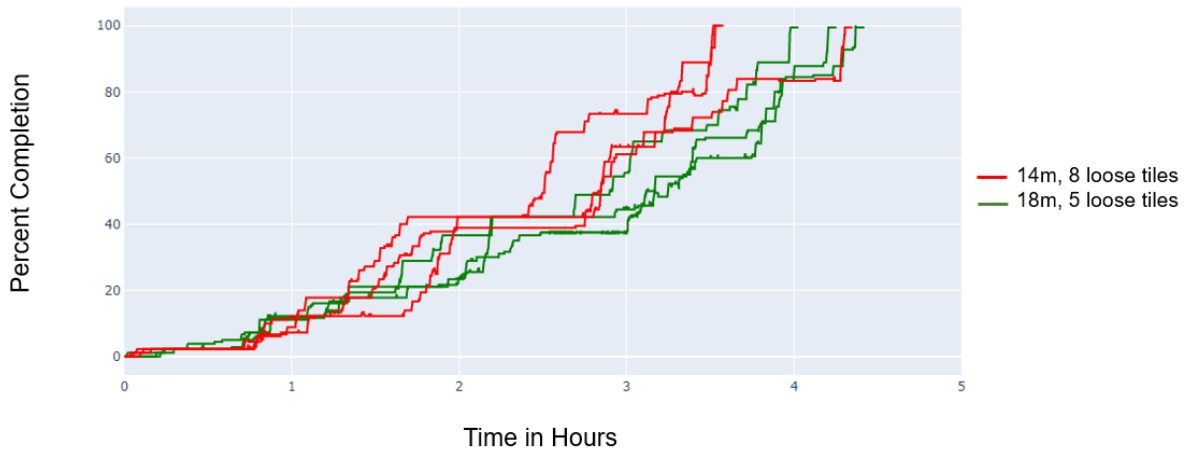


Figure 5-17. Out of six trials that completed (100% bonding completion, all 32 tiles filled in a perfect buckyball shell), we can observe the difference in time to assembly between a more “crowded” system with smaller containment volume and more loose tiles (red lines), and a sparse system with larger containment volume and fewer loose tiles (green). In this case, the more crowded system tends to present better opportunities for annealing the structure and assembles more quickly. While there is some cross-over in the behavior between the two (the simulation is still sensitive to noise and produces outliers), we do see two distinct behavioral tracks.

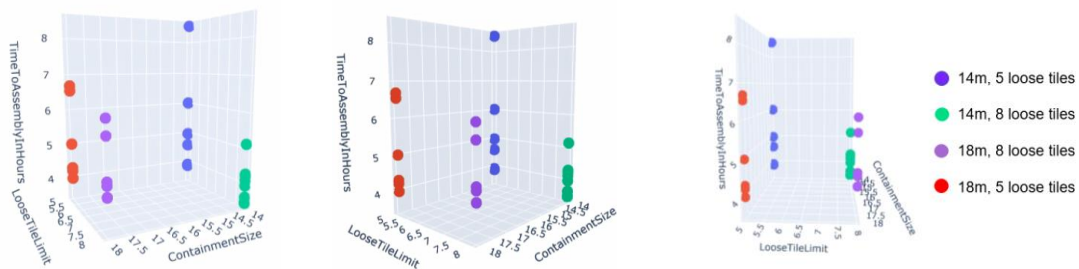


Figure 5-18. Snapshots from 3D plot showing comparisons across four trial types (colored markers), looking at the effect of both containment volume size and number of loose tiles on time to assembly. In addition to the vertical axis reporting on time to assembly, note the vertical spread within the same-trial-type—some parameter sets evidence greater variability than others. Overall, the 14m radius containment chamber with 8 loose tiles (green) proves to be the sweet spot out of this particular set—not only does it assemble to completion most quickly but also produces the most consistent time to assembly range (the shortest vertical spread) out of the trial batch.

5.1.3 Physics Simulation Conclusions and Next Steps

The primary contribution of this area of the thesis yields a parametric, extensible physics simulation for the TESSERAE Shell prototype. We modeled a 3D, 32-tile system at scale to predict tile dynamics and enable estimates of the time to completed assembly in real, orbital deployment scenarios.

Overall, the most striking takeaway from this current version of the WeBots TESSERAE model was the repeated, successful self-assembly of the 32-tile system in under 5 hours. While future work will examine a large ($n=1000$ or greater) trial set for statistical analysis of completion (e.g., what percent of trials self-assemble to completion with X parameter values, in under Y time), we have already identified several promising parameter descriptions that could be used to inform our next technology demonstration mission test. The salient feature subset includes: 34 tiles introduced, 14-18m containment volume radius, 5-8 loose tiles, and a 1:2 passive to active magnetic field strength ratio. Our results suggest that we can find a path to convergent assembly even with a quasi-stochastic self-assembling system. Other learnings from the simulation will be directly integrated into the next phase hardware as well, including a mechanism for bonding-group ID exchange over BLE that would allow us to ensure sub-groups do not form. In addition, we have identified effective ranges for certain timeouts in the logic of the system's state machine (e.g., the tile introduction timeout coupled with the "max unbounded tile" limit, and the stuck tile timeout) that can be directly implemented in our next hardware experiment codebase update.

Immediate next steps for the simulation will focus on updating the containment chamber to be responsive to the tile activity inside (rather than fixed in space), and then commencing an optimization matrix sweep where we run repeated trials at many feasible combinations of the 20+ initial input parameters, and across their respective value ranges. This represents a massive parameter space, for which we may turn to Bayesian optimization to help us map the space without having to directly run all trials. The output from this matrix sweep analysis may identify non-intuitive local optima—unusual combinations of parameters that we may not have found initially but could offer improved time to self-assembly with other benefits (like reduced power consumption, or less risk of tile-tile collision damage).

With optimized, predictive control in the future (we use only bang-bang control for the EPMS, currently), we anticipate being able to further optimize this system by reducing the prevalence of EPM pulse off events, and thus in turn, reducing the power consumption. We will also consider the trade-off space between using EPMS as we do currently, strictly electromagnets (that require power for docking), or a hybrid approach. While traditional electromagnets would not bring tiles together on their own over longer distances without active power, as the EPMS do, we may be able to rely on initial introduction vectors and circulation dynamics to bring tiles into close proximity and then, with predictive control, apply a targeted pulse of the electromagnets to achieve final docking. Use of electromagnets could help us in the future by avoiding the always-on magnetic field of the EPMS, which in some cases directs tiles away from each other when the repulsion vectors align and also causes clumping. Electromagnets would enable us to avoid these scenarios when tiles are already in close proximity with each other and may help us reduce the speed buildup that we see in the physical tile hardware tests with EPMS (which could pose a danger with large, high mass tiles that would collide destructively at those speeds). Finally, we can envision using electromagnets for deterministically guided assembly in concert with a particular tile insertion order, where only the magnets at the next intended bonding site are activated—essentially guiding the next tile in.

5.2 TESSERAE Cell Genetic Algorithm and Generative Design Model

To inform our approach for the TESSERAE Cell model “tissue generation,” where many TESSERAE module nodes might accrete together into an organic-styled, multi-module space station, we have created a generative design simulation that explores self-assembling growth patterns for the nodes. Our definition of practical use zones, or programmatic areas in architecture parlance, follows from notions of tissue differentiation in morphogenesis (as described further in Sections 3.1 and 3.2 of the Design Theory and Section 6.2 in Mission Architecture). We define an architectural base unit (a “cell”), with a high number of bonding sites and multiplicity of bonding arrangements, and then run a simulation with certain “fitness” constraints for growing an amalgam space station. Our genetic algorithm outputs an arrangement of the base units that solves for these constraints, essentially creating a functional “tissue” for space architecture. We can run the algorithm over repeated trials with varying weighted rewards for the fitness constraint values to create a suite of rendered space stations that meet certain design criteria. In this approach, we build on industry standards for generative design,^{171, 172, 173} but while most software packages take a subtractive approach (often yielding cellular solid frames for optimized weight-bearing parts), we take an additive approach over each generation as new TESSERAE Cells accrete to a growing structure. This simulation endeavor is an active and ongoing collaboration between the thesis author (concept development, scoping, and definition of aerospace fitness constraints), Che-Wei Wang (implementation of the genetic algorithm code in Processing and generation of the user interface), and Sana Sharma (renders of the generated shape outputs and user-centric architectural design).

For our initial base shape, we take the truncated octahedron—though as noted elsewhere in this thesis, we see a wide range of opportunities to explore generative design of space stations with other more fluid base shapes as well. As shown in Chapter 4, we first explored the range of possible shapes with our self-aligning magnet-jointed prototypes that flew in microgravity in August 2019 (Figure 5-19), and have since expanded this work to consider programmatic design considerations.



Figure 5-19. A selection of several compound shapes created by stacking the truncated octahedron and making use of its plesiohedrons properties.

5.2.1 Modeling Approach and Assumptions

This simulation does not treat the physics of self-assembly between the nodes. Instead, this model takes as its base assumption that the TESSERAE Cell nodes can already come together and snap in place reliably and now turns to look at the parameter space of potential outcomes when TESSERAE nodes can accrete into many different final configurations, guided by design parameters.

We rely on a genetic algorithm approach, mapped to the generative design codebase as follows:

Logic Type	Handling Description
Cell	“Cells” constitute the base level class structure with certain defined properties (truncated octahedron shape, number of bonding sites, presence or absence of neighbors, exposed vs covered faces, etc.)
Cluster	A group of Cells defines a cluster, which for us, defines the growing multi-module space station
DNA	The “DNA” defines a data list of which cells are turned on or turned off in a bounding box rendering of the cluster
Population	The “Population” comprises all known clusters and defines the members of a generation that are bred together (after selective mutations to the DNA data list) for iterative cycles. The Population is responsive to pre-defined fitness constraints.
Fitness Constraints	Fitness constraints layer our design choices (e.g., optimizing for more or less surface area, favoring or pruning branches, etc.) onto the weighted favorability of breeding between parents in the population. The selection process takes a mating pool, or group of clusters, and grades these clusters by multiplying a constant value depending on their fitness score. The reproduction process takes that mating pool, adds some variation (mutation), and splices in DNA from another mating pool to create the next generation (which is graded in turn, and continues on in the cycle until the generation progress is complete).
Completion Condition	Completion for the generation process can either be set programmatically—a fixed number of generation cycles, or aesthetically—whenever the repeated cycles have converged on a structure of interest.

Figure 5-20. Core elements of the TESSERAE generative algorithm codebase implementation.

Within this framework, we define the following fitness constraints and parametric toggles for the simulation:

- **Fitness Constraint:** Ability to maximize outer-facing surface area (e.g., for use with solar panels) or connected volume (e.g. for most efficient use of interior space if partition walls are opened via airlocks or removed)
- **Fitness Constraint:** Reward vs avoid long spindles or branches, defined for now as three or more nodes bonding in a line with only two neighbors
- **Fitness Constraint:** maximize filling all 14 bonding ports on each node vs filling $\frac{1}{2}$ of all bonding ports indiscriminately vs filling only hex bonding ports vs filling only square bonding ports, etc.
- **Fitness Correction:** removal of islands (nodes that generate within a bounding box with no directly adjacent neighbors)
- **Toggle Connection Strength:** determines the weighting for the degree to which the algorithm adheres to the bonding port connection stipulations (e.g., how much “freedom” in accretion)
- **Toggle Cluster Size:** Cluster size, or the max number of cells allowed to accrete (e.g., useful when dealing with manufacturing and building constraints, in the near future when we will be pulling from a limited total population of fabricated nodes)
- **Toggle Mutation rate:** Metric representing the extent of random changes made to the selected structures prior to the reproduction cycle

5.2.2. User Interface Features

We intend for this simulation to grow into a useful tool for space architects. To that end, we have created a preliminary GUI with toggle parameters (Figure 5-21 - Figure 5-23) and the ability to save both entire grid outputs and individual structures of interest as STL files. The Generate button, shown below, automatically runs the breeding and mutations cycles until stopped manually or until the output converges to a single, consistent shape that is essentially no longer updating. Alternatively, one can incrementally click through and observe each generational change by using the “grow” button. For the expanded use case where space stations may need to downsize in the future, we have also included a “shrink” button.

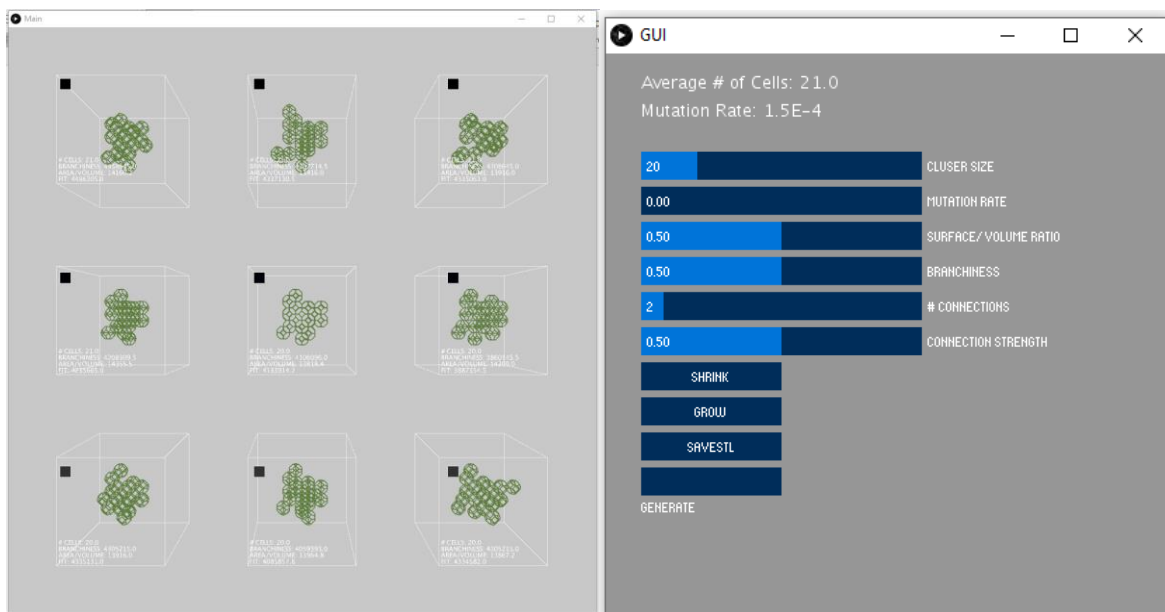


Figure 5-21. Screen shot of the output (left) from initial parameters (right), allowed to generate up to 20-21 nodes. The rendered matrix shows a selection of the population at each generation.



Figure 5-22. An example of a manually clicked-through run, with a mix of shrinking and growing steps that produces a wider variation in the final population morphology.

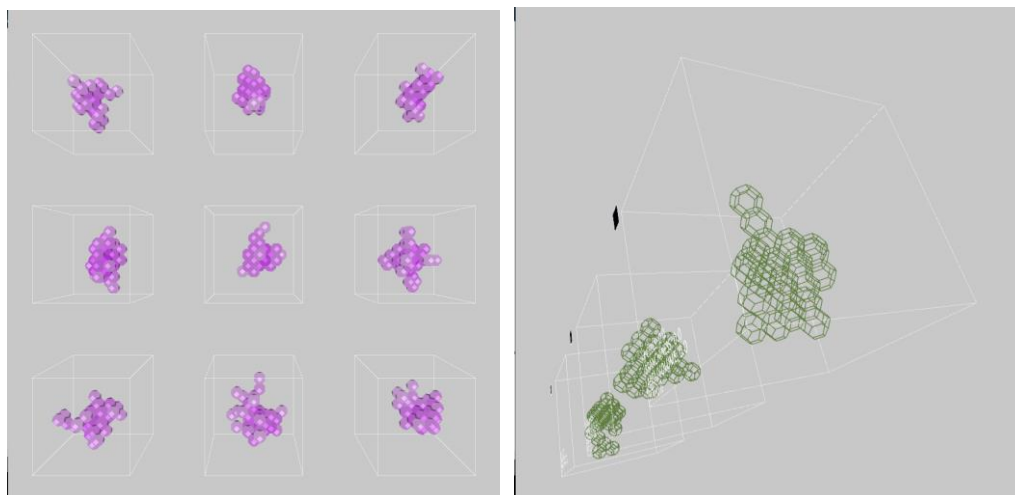


Figure 5-23. Alternative views, courtesy of Che-Wei Wang's GUI development, showing options for rendering nodes in-situ with context for the degree of exposure (interior nodes with more neighbors are a darker magenta, exterior nodes are lighter) or zooming in and panning to assess structures from different vantage points.

5.2.3 Output

Below in Figure 5-24 and Figure 5-25, we present two matrices showing a range of possible structural outputs from this simulation. Many more views are possible and these two are illustrative of the baseline functionality encoded in the model. The first shows a set of structures confined to grow mostly in 2D, with the second showing a panoply of options with greater freedom to expand in three dimensions. This style of presentation was inspired by the chaconne and our desire to demonstrate the variations on a TESSERAEE theme.

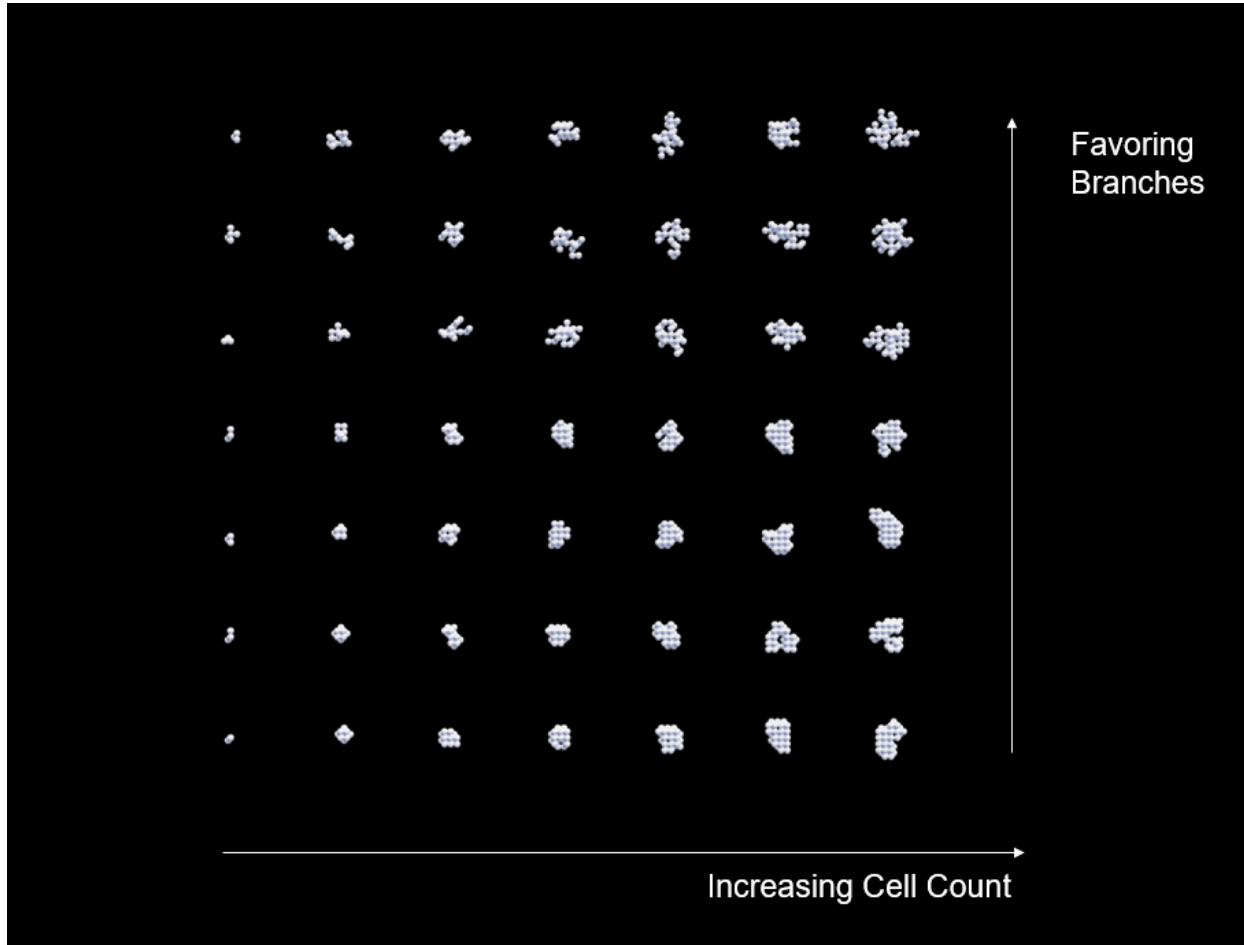


Figure 5-24. Matrix output from the generative growth approach, with 2D constraints. The parameters for this matrix are: x axis - cluster size [2 – 32] and y axis - branchiness [0.1-1.0].

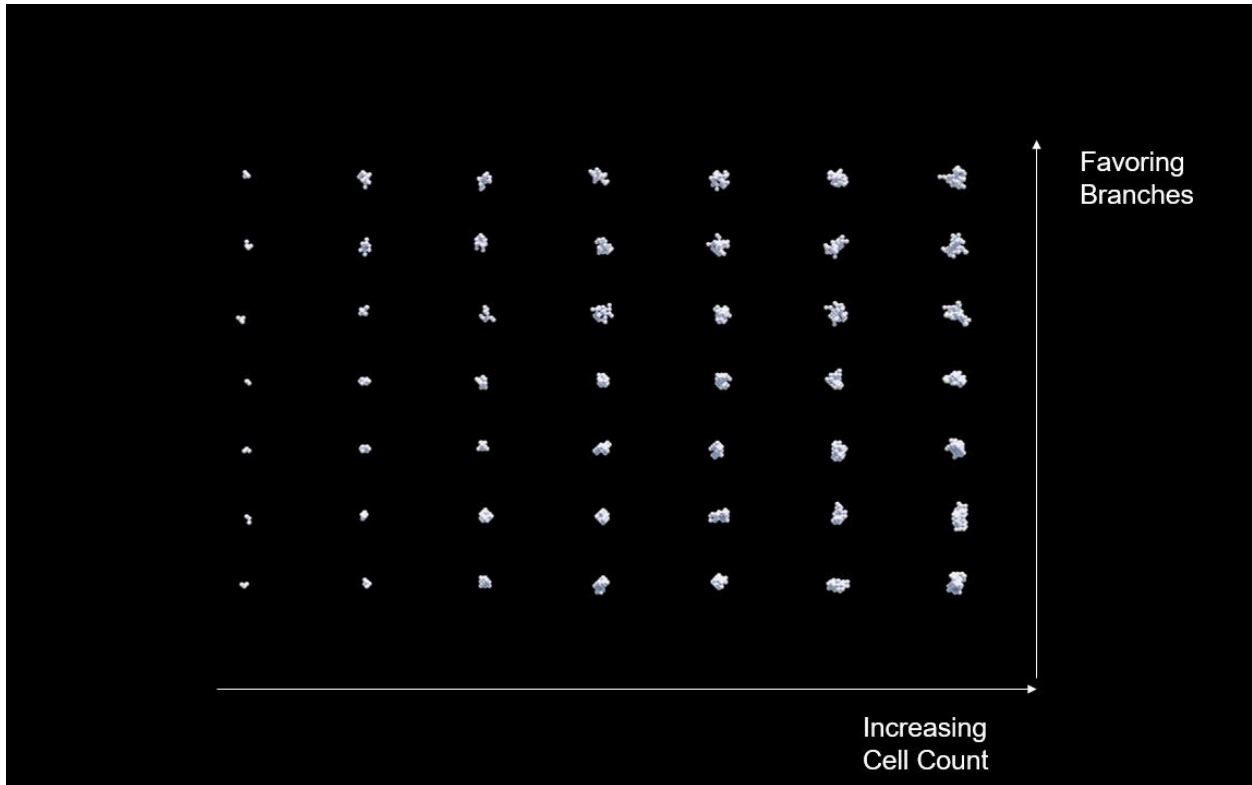


Figure 5-25. Matrix output from the generative growth approach, allowed to expand further into 3D. The parameters for this matrix are: x axis - cluster size [2 – 50] and y axis - branchiness [0.1-0.7].

5.2.4 Generative Simulation Conclusion and Next Steps

This contribution area of the thesis offers a TESSERAE Cell generative algorithm simulation tool and portfolio of simulated, fitness-constrained growth patterns and prospective multi-unit space stations. The outputs from this simulation are used in the Mission Architecture Chapter (Section 6.2.2) to support speculative, programmatically driven growth—where branches might be desired (rewarded by the fitness constraint weighting) to separate noisy areas from quiet areas, or alternatively, clusters might be encouraged to clump in multi-lobe fashion to define personal, communal and cross-over functional zones. The immediate next step for this simulation focuses on adding bounding box constraints where the growth can be induced to follow a particular geometric pattern, such as a 3D helix spiral or fractal pattern. Building on the feedback received from astronauts in separate work undertaken by the MIT Space Exploration Initiative (see Appendix), we are exploring ways to layer further programmatic constraints onto the generative design outputs as fitness constraints, such as separating dirty and clean areas or optimizing for spontaneity of interaction. With this approach, we build towards the vision of self-aware space structures that are also responsive to the needs of their inhabitants.

We intend for this simulation to serve as a tool for space architects going forward, exploring the application of indeterminate growth principles to space architecture. To make the tool more accessible, our next phase efforts will focus on porting the Processing implementation to p5.js and hosting this simulation online.

6. TESSERAE Aerospace Mission Architectures

Chapter 6

“There are 360 degrees, so why stick to one?”—Zaha Hadid

“You take gravity out of the equation and everything goes kablooy.”—Constance Adams

The space industry faces an inflection point—we note the combination of dropping launch costs,¹⁷⁴ increasingly accessible launch opportunities and growth of the space market,¹⁷⁵ NASA’s keen interest in transitioning the ISS,^{121,176} and a renewed commitment to return to the moon by 2024 leveraging Commercial Lunar Payload Services (CLPS) and other industry partnerships.¹⁷⁷ These developments suggest we are nearing a commercial “grand opening” of space exploration. The TESSERAE research program aims to supply transformational space structures technology for agile, reconfigurable modules among the many rising use cases—expansion of habitats for space tourism in LEO; modular, autonomously managed habitats that can support an influx in crew size for the Lunar Orbital Platform Gateway (LOP-G, now simply “Gateway”); orbiting bases to support martian on-surface missions, and more. To be able to simultaneously design, test, and serve these varying environments, we observed a need for generalizable self-assembly in orbit. Rather than designing custom-use, single-purpose space stations that are still constrained by the dimensions of a rocket payload fairing, the industry needs space architecture that can be packed flat in a rocket, deployed, and constructed on demand. From here, it can be reconfigured to meet evolving mission needs. The structure should be able to grow and expand beyond the designer’s original blueprints. The structures should also then be easily disassembled and shipped to the next operations site. This builds on the concept of “minimum inventory, maximum diversity,”¹²⁷ consistent with our biomimetic design framework for sustainable, indeterminate growth from Chapter 3.

Modularity and re-configurability in a structure offer a promise of cost savings (by re-using standard designs and interchanging a standard set of parts) and mission flexibility (by rebuilding the structure at whim to meet updated operation requirements). We see this philosophy emerging across the aerospace industry, from reusable rockets¹⁷⁸ to modular space structure design.⁸⁰ Self-assembling structures offer one such model for the next generation of zero-gravity habitats and science labs, parabolic mirrors, and satellites, with modularity and re-configurability inherently baked in. The current archetype of space architecture modules relies on curved shells for two primary reasons, among others: first, the surface area-to-volume ratio benefits of avoiding corners, as space deployments need to optimize enclosed volume for a given surface area (less building material dramatically reduces launch costs) and second, the unique affordances of zero gravity (less need for traditional weight-bearing walls where the focus lies instead on withstanding pressurization and surviving puncture). To

bring autonomous self-assembly into this shell-dominated architectural context, this thesis explores tessellation and multi-part structure aggregation strategies.

In particular, the mechanism of self-assembly for “energy favorable” structural configurations offers a compelling new construction paradigm. We note a growing potential for architecture based on efficiently stackable units for launch that then assemble stochastically or robotically, without manual intervention by astronauts. Structures need not be purpose-built, single use modules and should instead feature extensible units that support reconfigurable architectures by dynamically detaching and reattaching in on-demand geometries. Self-assembling architectures will be based on fundamental assembly units, or tiles, that provide enough degrees of freedom for multiple structural arrangements while retaining the required specificity to generate a predictable suite of desired shapes. Into these tiles, we can natively embed sensor networks that bring extra-planetary architecture into the realm of truly “responsive environments.” Space architecture of the future should enjoy a rich melding of engaging and enlightening architectural design, flexible and reconfigurable construction modalities, and the intelligent feedback systems supported by thoughtfully integrated sensor networks.

To address the changing concept of operations (ConOps) for space architecture, in anticipation of LEO space tourism and NASA’s strategy for crewed exploration missions to the Moon and beyond,^{121, 179} we propose the TESSERAE (Tessellated Electromagnetic Space Structures for the Exploration of Reconfigurable, Adaptive Environments) architectural modules (Figure 6-1). This approach to space architecture relies on multi-part, modular construction from a standard suite of base units (structural sides, airlocks, docking ports, etc.), that can be reconfigured on-demand with LEGO-like interchangeability. TESSERAE structures are intended to provide agile modules that can be packed flat during launch, assembled in orbit, reconfigured as needed (e.g., add a new docking port on demand, if a second craft arrives), disassembled, and transported to a new orbit or surface landing site for re-assembly and re-use. Entire TESSERAE modules can also be docked together for larger total volume space station configurations, in densely packed crystalline-like arrangements.

To achieve this level of modularity, the outer structural shell of the module must be tessellated and segmented into separate units. TESSERAE modules are designed to self-assemble in orbit from a “tile set” of regular polyhedral base units. The particular tile geometry (number of sides, tile thickness, dihedral side-slope angle, etc.) and number of units define a target macrostructure when fully assembled (e.g., 12 pentagons and 20 hexagons form a buckminsterfullerene as described in Section 6.1; or eight hexagons and six squares form a truncated icosahedron, that can be self-assembled from tiles or prefabricated as a volumetric unit and then packed as a space-filling solid, as explored in Section 6.2; shown in Figure 6-1).

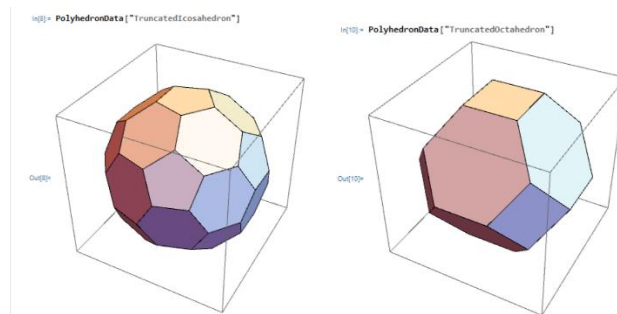


Figure 6-1. Mathematica renders of the truncated icosahedron, or buckyball, (L) and truncated octahedron (R). Both shapes are under consideration and testing for TESSERAE mission deployments. Figure repeated from design theory Chapter 3 for ease of reference.

In addition to the promise of modularity, the mechanism of sensor-mediated assembly for “self-aware” TESSERAE space stations inclines the structure to fully autonomous operation in the future. This avoids

extensive astronaut EVAs, which are dangerous for human crews to perform, and robotic agents. For the future of missions like Gateway, where autonomous operations are already prefigured as a necessity, a docked TESSERAE module would not only integrate seamlessly into the expected operations paradigm but also demonstrate the potential of autonomous construction and dynamic reconfigurability on-orbit. Among the sections below, we present our preliminary work in integrating the quasi-stochastic structure creation with autonomous robot swarms for constant in-situ servicing and maintenance post-assembly, thus creating a holistic, autonomous lifecycle from “cradle to grave” (with “grave” being perhaps an intentional disassembly for re-deployment in a new orbit or mission context). The sensor suite natively embedded in each TESSERAE tile or node provides a basis for data-informed autonomous construction, steady-state operations telemetry and data gathering, and remote intelligence and even remote-commanding from the “ground” (e.g., Houston, lunar or martian command centers).

To make progress towards this level of modularity and autonomy in space structures construction, we developed and tested a suite of proof-of-concept models for self-assembly in microgravity from 2017 to 2020, as described in Chapter 4. This chapter explores the mission architecture and ConOps planning that will be necessary to translate the prototype hardware development into future fully fledged aerospace missions. Section 6.1 explores the TESSERAE Shell model ConOps, with flat tiles that self-assemble to form a buckyball shell. Extensive consideration has gone into this first model for deployment in orbit, mission planning, integration into a holistic platform for autonomous habitat operations, feasibility review, and comparison to alternative existing and prospective habitat modules (all discussed in Sections 6.1.1-6.1.6). Section 6.2 introduces the different advantages, tradeoffs, and mission ConOps for the TESSERAE Cell model, where prefabricated volumetric modules self-assemble to form a space station aggregate (rather than a single-chamber shell). This section considers the promise of plesiohedrons (i.e., space-filling solids) for space architecture, how we might define the minimum viable unit (MVU) for module habitability, and extensibility to other modular space station geometries (all discussed in Sections 6.2.1-6.2.5). In Section 6.3, we present the applicability to current NASA mission priorities and discuss wider benefits of the technology development, including other aerospace applications and Earth-based spinoffs. Section 6.4 addresses the broader applicability of our tessellation and autonomous self-assembly approach to structures beyond habitats, including storage depots and space logistics centers (Section 6.4.1), parabolic mirrors and telescopes (Section 6.4.2), and modular satellites (Section 6.4.3). Section 6.5 explores speculative extensions of in-space, self-assembly manufacturing to continuous, rather than discrete, parts, notably extrusion (Section 6.5.2), thus completing a full suite of options for self-assembly across scales and spatial dimensions (1D, 2D, and 3D base-units that all form enclosed, habitable spaces). This chapter concludes with a discussion of immediate next steps and future work in Section 6.6. Throughout this chapter, we draw on material from our published papers.^{119, 147, 149}

6.1 TESSERAE Shell ConOps:

To re-summarize the TESSERAE Shell approach from the thesis thus far: in the aerospace structures deployment context, the geometric tiles that form our TESSERAE buckyball shape self-assemble quasi-stochastically through EPM jointing to form a structural whole. The tiles are designed to be released into a temporary, inflatable container and allowed to float freely in orbit. Tunable magnet polarity (controlled via current coursing through an EPM) on the tile bonding faces mediates which tiles bond to which neighbors and corrects errors when two tiles bond together incorrectly. By precisely controlling the beveling angle between tiles, or the “dihedral angle” from the buckminsterfullerene chemistry context, we can drive the assembly towards an energy-favorable, stable final geometry. The constituent parts passively, stochastically self-assemble into a holistic structure, without requiring propulsion or GNC. Embedded, custom sensor networks on each

tile provide feedback on the status of self-assembly and inform an autonomous state-machine loop that drives error detection and control for a convergent assembly.

Across the four generations of proof-of-concept models, the ConOps assumes tiles are:

- Free to circulate in near proximity (contained by a temporary, removable, and inflatable enclosing volume);
- Drawn together for neighbor-neighbor bonding over short distances through magnetic field attraction;
- Engaged in pairwise and system-global exchange of sensor data for diagnosis of bonds, error detection, and correction via EPM actuation (e.g., pulse magnets off and allow tiles to separate if incorrect bonding geometry is detected); and
- Recording sensor data for steady-state operation post-assembly.

For Sections 6.1.1 – 6.1.5, we rely on the dimensions in Figure 6-2 for sample calculations and feasibility review.

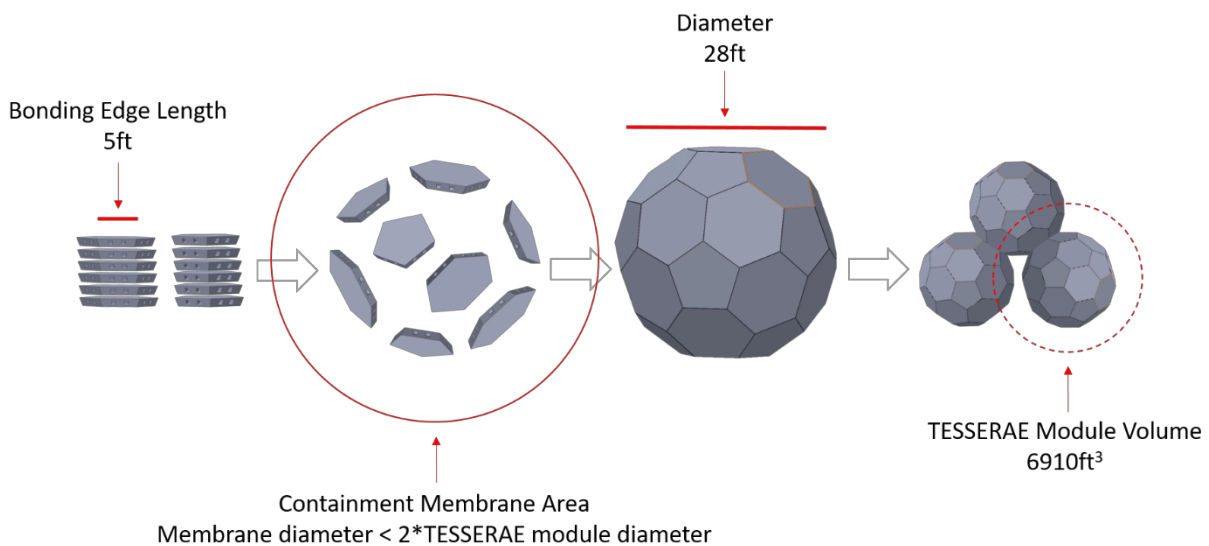


Figure 6-2. Evolution from TESSERAE flat-pack for launch to a multi-chamber station.

Underlying Technology Assumptions to Support Mission Reconfigurability

Magnetic Jointing

We can use the EPMs to selectively apply torques, buffer tiles away from each other, and correct meta-stable error states. The use of EPMs allows us to reduce the TESSERAE power budget on orbit (in contrast to using traditional electromagnets that must be constantly powered to provide attractive force). Separate clamps and sealing gaskets are used to reinforce the EPMs during steady-state operation (magnets are only briefly power-actuated during quick bursts for assembly and disassembly). The EPM actuation is instigated by a supervisory sensing network, described in detail in Chapter 4.

In addition to aiding in habitat-use flexibility, the integration of the EPMs facilitates error correction. In the event that two tiles have incorrectly bonded (e.g., due to a single point N-S bonding that does not match the buckyball shell surface topology) or a tile has been trapped inside a partial shell enclosure, we can reverse the polarity of the magnets in question and induce a repelling force to separate the tiles. When coupled with sensing to detect incorrect bonding, this error correction procedure can proceed autonomously. Akin to the magnetic

levitation bullet trains but at much lower speeds, we will be able to use tunable electromagnet polarities to guide tiles through physical space.

While we intend to keep the relative velocities of the self-assembling tiles quite low (in a contained, stochastic system), the electromagnets provide a useful buffering feature. Should two or more tiles approach each other with sufficient kinetic energy to cause destructive damage upon collision, LIDAR proximity sensing and accelerometer diagnosis data signals can automatically engage the electromagnets in question and actuate a multi-point repelling response (across all exposed, pairwise magnet faces in play) to buffer the impending collision.

Finally, the electromagnets can also aid in perturbing the system, should the stochastically assembling tiles settle into a local minima energy state without completing assembly. By cycling the polarity of various bonding-face electromagnets (or by perhaps also including boundary enclosure electromagnets on the inflatable container surface), we can induce motion back into tiles that were at rest, and improve the continuing circulation of the swirling tile system.

Sealing Joints for Pressurization

While the addition of so many additional “seams” or edges may at first seem an over-complication compared with the simpler cylindrical shell models currently deployed in orbit, we explicitly accept the challenges that these seams present in an effort to preserve the re-configurability and modularity of the structure. We intend to be able to pop tiles on and off as needed—to replace damaged wall segments, trade out tile-specific subsystems, re-position operational mission elements like airlocks and berthing ports to meet a new mission need or an incoming re-supply trajectory, and more.

While the EPMs do provide for steady-state, fixed joint mating after initial assembly (from their always-on permanent magnet state), we anticipate a need to correct fine tolerance gaps and reinforce the seams against the internal force due to air pressure. To do so, we rely on clamps and deformable edges on each tile (either a material stiffness gradient that becomes more flexible as we tune the Young’s modulus near each bonding edge, or the addition of surface-bonded gasketing material). Certain industrial strength clamps can be powered down and still exert their holding force, thus avoiding a constraint drain on our power budget. The feasibility analysis for clamping across these seams is discussed further in Section 6.1.2.

Beyond the primary focus on clamp-reinforced edges, we considered a second approach relying on tensegrity-tensioned cabling. Rather than affixing each tile to proximate neighbor tiles, we could tension opposite tiles along centerlines of the buckyball by attaching paired cabling. This cabling would inherently balance the forces, as opposite tiles are pulling away from each other along a shared centerline due to the internal pressurization. Fortunately, the geometry of the buckyball ensures that each tile has a perfectly paired tile at a shared centerline across the sphere. This approach complicates the self-assembly process however, adding an extensive set of steps where cables must be deployed internally after the initial geometry is set, and prior to pressurization. While numerous approaches could be envisioned (e.g., autonomous deployment of cables in a controlled harpoon or grappling hook fashion, automatically extending telescoping rods), this approach raises a number of engineering challenges, including attachment point robustness concerns and order of operations for cable deployment to avoid tangling. A network of crisscrossing cables also places constraints on how the interior volume can be used, and may inhibit efficient use of the space. Thus, for the bulk of the mission architecture analysis discussed below and prospective life-size tile development (as discussed in Chapter 4, Section 4.1.4), we focus on the bonding edge clamp-reinforcement approach.

6.1.1 TESSERAE Mission Concept

In support of NASA’s strategic vision for a “human return to the Moon, followed by missions to Mars and beyond,”¹⁸⁰ we have designed TESSERAE to support a hybrid mission ConOps. The sample TESSERAE mission concept centers on supporting activity in lunar orbit and perhaps also on the surface of the Moon: a TESSERAE module “shell set” is packed flat, launched from Earth, deployed inside a flexible containment membrane (which is later removed) and self-assembles in lunar orbit to support the Gateway.¹⁸¹ The TESSERAE unit can support an influx in crew numbers (as is expected with the varying, seasonal activity of the Gateway) by docking through standard attachment ports, or provide additional storage volume for supplies or science payloads. When ready for a surface deployment, the TESSERAE module can be de-pressurized and packed flat again, this time in a transit vehicle for entry, descent, and landing on the lunar surface. The tiles can then be moved from site to site by rover and re-assembled as modular architecture on the surface wherever needed; the EPMS will aid in easy snap-assembly of at least a half-dome (with the aid of a deployable ladder and simple pulley, when in a gravity environment). Because the tiles will have already been built to passively shield in-space radiation for the in-orbit habitation context, TESSERAE tiles could be used creatively as shielding in combination with other inflatable or 3D printed, on-surface habitat concepts. The ConOps design efforts necessary to realize this mission can be repurposed and adapted for a comparable mission to Mars (MOSAIC, or Mars Orbiting Self-Assembling Interlocking Chambers) in subsequent years (Figure 6-3 and Gateway-like station shown in Figure 6-4).

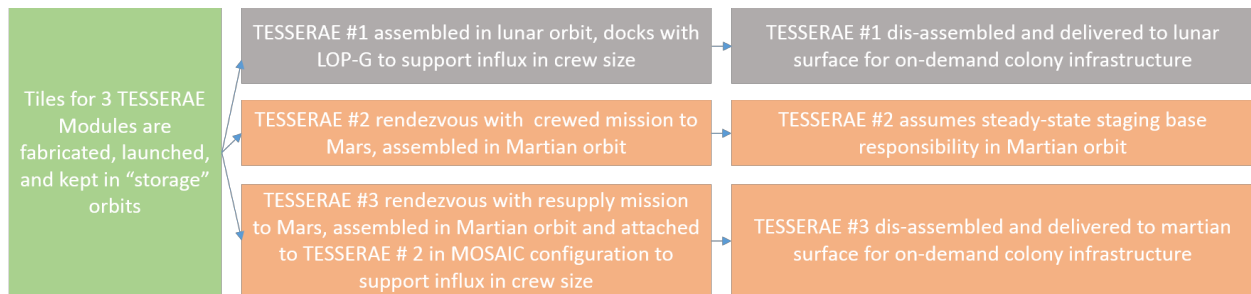


Figure 6-3. We propose a sample TESSERAE mission for lunar activity (gray bars), with a Mars continuation mission (orange bars) in mind for a prospective follow-on. This maps TESSERAE to NASA’s Moon to Mars strategy.

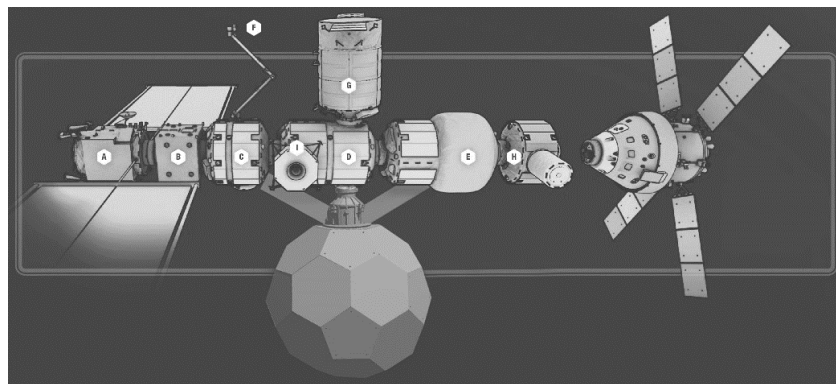


Figure 6-4. Until development allows space stations made entirely of TESSERAE modules, TESSERAE chambers may need to dock to existing structures. This artist’s render, courtesy of MIT SEI Visiting Student Anastasia Prošina, shows how TESSERAE might dock to a concept akin to the Lunar Gateway. Radiator wings are assumed for thermal transfer, with solar panels planned for the flat hexagon and pentagon outer faces.

Mission Stages Overview and Highlights

The sections below present a comprehensive overview flow of all stages of TESSERAE Shell mission deployment, from launch to steady-state operation, including highlights on launch packing, two paradigms for interior-use considerations, and integration into a holistic, autonomous space station system, among other considerations like the suite of aerospace-grade material properties required for the mission (Figure 6-5).

Overview: Ground to Orbit Process

The TESSERAE tile units will begin the mission in a stacked, flat-pack configuration within a rocket payload fairing (see Figure 6-6 for this and all downstream steps). The tiles are designed to be packed flat in a rocket for efficient use of limited payload volume. We anticipate fitting all 32 tiles in a single launch (see launch vehicle discussion in Section 6.1.2). Like inflatable habitat concepts, this allows us to transport structures whose final, fully-assembled dimensions are larger than the fairing's volume boundaries (in contrast to the ISS fixed-shell modules).

A temporary, flexible membrane will encapsulate payload elements and undergo autonomous inflation upon completing orbit insertion and ejection from the payload fairing. While benefitting from the ease of inflation in a low- or no-pressure environment, the elasticity of the membrane must of course balance the force due to pressurization from the inside. This containment ensures that the component tiles are kept in close proximity when released into the microgravity environment, to improve the likelihood of finding neighbors (ensuring that magnets need only act over short ranges, per the $1/r^2 - 1/r^4$ drop-off in magnetic force). Our proposal for this inflation concept builds on a previously explored concept¹⁸² and leverages the ease of inflation with even minimal air pressure in the vacuum.⁵⁷ Current TESSERAE mission design envisions a holster-actuated process, where tiles are released one at a time into this inflated chamber from a dispensing structure to allow for incremental assembly in “accretion” style, much like a crystal nucleation process.

Released tiles then circulate quasi-stochastically throughout the confined membrane volume and self-assembly begins. As tile bonding edges pass near one another, tiles are brought together and snap into place via the EPMS on each bonding face. As explained above, this process proceeds passively without active control until an incorrect bond is detected. The supervisory sensing network and bonding diagnosis algorithm detects incorrect bonds (which should already be minimized due to optimized design of the tiles' EPM polarity map), and selectively pulses the EPMS off to free tiles for circulation back into the assembling pool. As discussed in Chapter 4, this approach builds on magnetic docking of space assets^{183, 184} and active control for electromagnetic formation flight and space structure deployment.^{185, 186} Actuation of the EPMS can also be used to:

- selectively apply torques to certain tiles (e.g., for forcing bonding faces into planar alignment);
- dynamically buffer tile-tile interactions (e.g., two tiles approaching each other at incorrect bonding angles, or coming in with excessive velocity vectors); and
- aid in the application of stirring energy (e.g., to perturb two tiles that may have settled away from the accreting structure or into a local minima configuration).

After the full structure has assembled and any remaining extra tiles have been gathered separately, a series of autonomous structure-finalization tasks begin. Each tile-tile bonding face executes a clamping sequence, where tiles are latched together firmly (pressed against sealing gaskets). These latching-style clamps (providing a hold force without ongoing power draw) are used as a complement to the EPMS that are providing their own continuous, unpowered holding force. By cinching in the TESSERAE seams and compressing the deformable gasket material, the clamps would aim to provide a sealable, pressurizable volume. To provide a second layer of sealing for mission robustness if needed, an internal bladder can be inflated within the TESSERAE Shell, which would ultimately contain the pressurized air and living space accommodations. Various options exist for

actuating this internal bladder deployment; one proposal involves the bladder unfurling from within a given tile's compartment and inflating from stored air tanks (comparable to the Bigelow Expandable Activity Module air inflation process¹⁸⁷). Given that this internal bladder would separate payload items (like frames and racks) from the external shell where they would be traditionally anchored, we intend to augment the bladder with rigid tie-in points and ribbing. An alternative solution uses magnetically attractive payload elements that could be reversibly bonded to the inner walls of the TESSERAE Shell, acting through the bladder membrane material depending on final material composition. If the bladder can be avoided, much further flexibility exists for furniture and interior elements to be deployed from within tile compartments into the main hollow space of the structure.

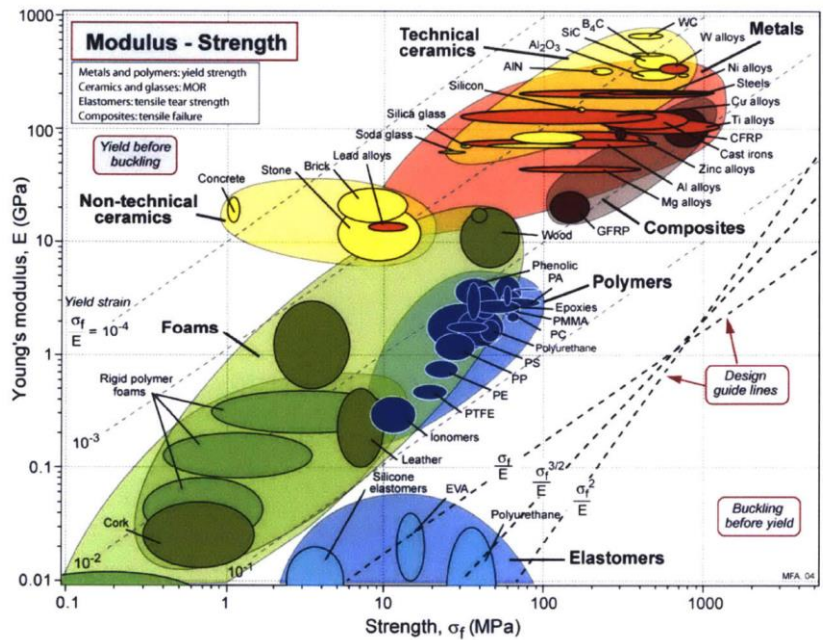


Figure 6-5. The full TESSERAE mission architecture will make use of many material classes, from metals and composites in the exoskeleton, to non-outgassing polymers to protect electronics (e.g., certain epoxies) to deformable materials for the bonding boundaries of tiles to absorb impact, to elastic materials for the containment chamber for keeping tiles proximate during self-assembly. Image credit: Michael F. Ashby, as originally conceived in 1989.¹⁸⁸



Figure 6-6. Flow chart tracking step-by-step deployment for TESSERAE self-assembling habitat system, including pre-launch to assembly (green, 1-7), post-assembly finalization tasks (blue, 8-17), and end-use cases in orbit or on a planetary/moon surface. See arielekblaw.com/tesseract for an illustrative video depicting this deployment and hybrid use.

Highlights 1-7 below cover specific aspects of this flow from Figure 6-6 in greater detail.

1. Packing for Launch

While the fully expanded TESSERAE, at the particular dimensions from Figure 6-2 above, would constitute a large spherical volume for interior use, the individual, separate tiles can pack tightly into a condensed volume for launch. This vastly improves the prospects of deploying architecture with dimensions greater than that of the rocket fairing. This is one example of escaping the “gantry-limitation” model, where architecture can only be as expansive as the largest constraint on the building—typically a gantry or crane, or in a space context, the size of its “ride” to orbit (Figure 6-7).

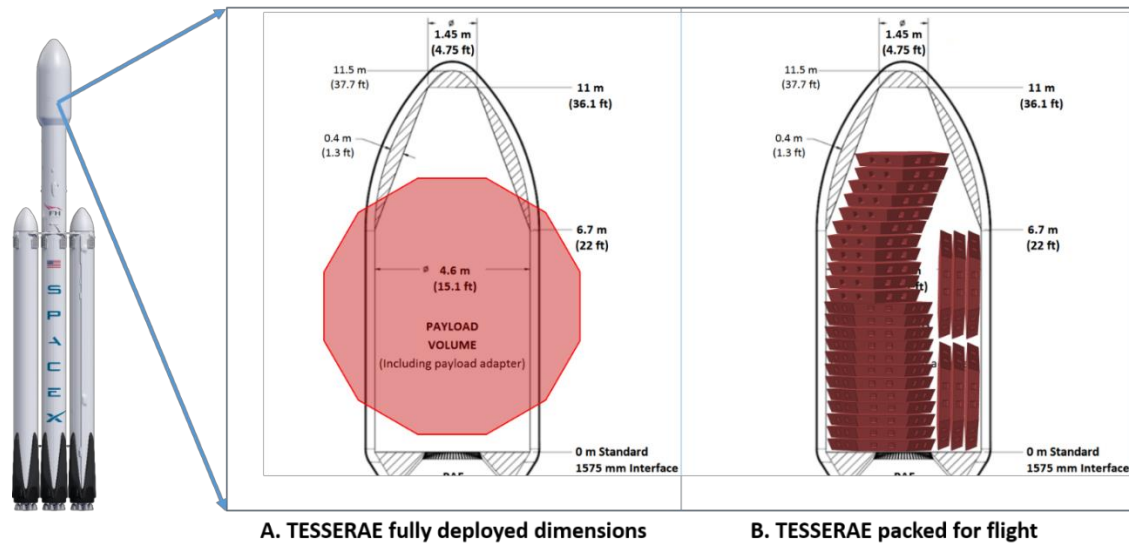


Figure 6-7. Scale comparison of fully deployed vs. stacked TESSERAE, in SpaceX’s Falcon 9 Heavy payload fairing. In reality, the payload will likely need to be centered for mass properties, but the side tiles are shown currently to indicate the volume of the flat-pack in its entirety.

Though we have initially focused on the buckyball geometry, we note many shell geometries of interest for space habitats. Rotating tori, for example, are often proposed for induced-gravity environments and the TESSERAE project will soon expand to consider tessellation approaches for these and other shapes (Section 6.1.5). Such models still rely on flat tiles for the tessellation and could be similarly condensed and loaded in a flat-pack for launch. In Section 6.1.4, we discuss a modification to the TESSERAE deployment scheme that relies on a particular pattern of hinged joints to create an origami-inspired unfolding. This arrangement also packs flat and lends itself to this same payload fairing plan.

While Figure 6-7 shows the SpaceX Falcon 9 Heavy¹⁸⁹, we also anticipate launching TESSERAE tiles to orbit in the prospective SpaceX Starship,¹⁹⁰ Blue Origin New Glenn,¹⁹¹ and NASA’s SLS,¹⁹² all of which offer greater volume that may accommodate multiple TESSERAE Shell sets and thus the opportunity to simultaneously deploy several full TESSERAE chambers out of one launch.

2. Deployment paradigm

The basic insertion plan put forth for TESSERAE missions relies on a holster model, with controlled, staged tile release (one-at-a-time) that waits for prior tiles to bond before adding additional units. This reduces the complexity of the assembly and the likelihood of erroneous bonding events. Through our at-scale simulation results in Chapter 5, however, we have also identified promising modifications to this approach:

- Staying within the controlled holster paradigm, we can release up to eight loose tiles at a time for circulation and still see improved results for time to assembly. As proven out in the simulation, we impose a logic condition that loose tiles are only allowed to keep good bonds that accrete to the primary structure. This prevents loose tiles from forming competing sub-groups that may or may not fit into the main structure's available bonding sites. There are many ways to implement such a logic condition. One example: Every tile, prior to bonding with neighbors, has a distinct bond ID. When the first two tiles bond, they negotiate a BLE communications exchange and establish a shared ID that can be communicated to other tiles in the global system. Now, when subsequent loose tiles achieve a good bond, they check if their new partner(s) shares the target (e.g., main accretion ball) ID; if yes, they keep and register the bond and assume the global, shared ID; if not, they pulse off (even a good bond), knowing that that bond was a small sub group and not an accretion onto the main structure. These additional loose, circulating tiles add a critical perturbation to the system and help in avoiding local minima states where progress on the assembly stalls.
- While this logic condition means we could also then attempt a simultaneous release of all 32 tiles, knowing that they would *not* form competing, non-complementary subgroups, we then have an energy trade-off problem. Loose tiles forming sub-group good bonds and then having to pulse them off is a waste of battery and solar-power generated energy, which must be conserved for the system. We have found that introducing 5-8 loose tiles constitutes a sweet spot. This gives us sufficient perturbation for optimum circulation without inducing too many false-accretion pulse off events during the progression of assembly.

The insertion order for the deployment mechanism is also of interest. Again, from CAD and simulation, we have identified several patterns of release that correspond to incremental wall-building additions that avoid extra holes (other than that of the final tile) forming as the structure accretes. One such insertion order (see Figure 6-8) builds up the structure from a base petal, adding alternating rings of hexagon and pentagon tiles until the jagged, exposed edge can only accept tiles of the "other" type. An alternative insertion order forms a spiral bonding path from a base pentagon up and around to the cap pentagon of the structure, much like peeling an orange in a single, curving slice. This latter spiral path is discussed in detail in Section 6.1.4, associated with an origami approach to unfolding an entirely hinged structure (rather than floating separately and quasi-stochastically accreting). Though tiles are inserted in one of these orders, there is no guarantee that they will bond in exactly this order; still, we rely on insertion order to increase the likelihood of a favorable assembly path from tile 1 to tile 32. These insertion paths could also inform further hybrid TESSERAE approaches that add propulsion, if desired, for deterministic, path-planned assembly. See speculative render of the TESSERAE holster deployment stack in spiral path order in Figure 6-9.

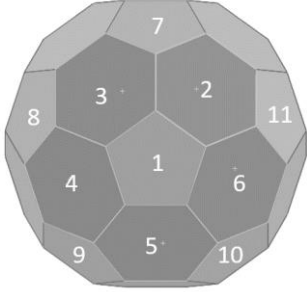
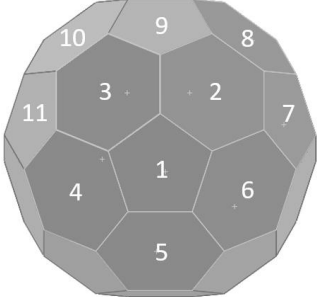
Path Definition	Tile Insertion Order
	<p>Ring Building:</p> <ul style="list-style-type: none"> 1 pentagon 5 hexagons 5 pentagons 10 hexagons 5 pentagons 5 hexagons 1 pentagon
	<p>Spiral Arm Building:</p> <ul style="list-style-type: none"> 1 pentagon 5 hexagons 5x [1 pentagon, then 1 hexagon] 5x [1 hexagon, then 1 pentagon] 5 hexagons 1 pentagon

Figure 6-8. Insertion path approaches that show how varying tile insertion orders wrap the buckyball geometry. Left column: representation depicts ring building and spiral arm building through the first 11 tiles. Right column: insertion ordering for a full 32-tile set.



Figure 6-9. Speculative view of TESSERAE tiles packed flat in deployment holster in Spiral Arm insertion order, ready for payload fairing separation in orbit around Mars. Image Credit: TU Dortmund Fraunhofer Institute, for TESSERAE.

3. Re-configurability

One of TESSERAE’s unique advantages lies in the inherent re-configurability of a modular structure. All “structure finalization” tasks as described in Figure 6-6 (flow chart) are reversible. The structure can be depressurized, unclamped, and de-bonded (by pulsing current through the EPMs to neutralize magnetic attraction) back to individual tiles. This separation could be executed around a single tile or small group of tiles for targeted replacement, repair, or re-design (e.g., where a window tile was yesterday, now an airlock or additional docking port is needed and can be swapped in). In addition, the entire structure could be disassembled for habitat relocation to other orbit or surface missions of interest.

4. Role of multifunctional tile suites

Our work on TESSERAE focuses primarily on the creation of the shell as an extensible platform for multifunctional use in orbit, with reusability for surface operations as well. We do not intend to proscribe a particular habitat function—rather, we aim to make TESSERAE applicable and adaptable for LEO space tourism, lunar orbit in conjunction with the Gateway, Mars-Phobos orbit to support on-surface missions, etc. To do so, the plan for TESSERAE space-grade tiles involves embedded, modular functionality in each tile such that TESSERAE units can be retrofitted for various environmental control and life support systems (ECLSS), astronaut activity interfaces (airlocks, docking ports), tie-ins for remote-sensing payloads, and varying attitude control and GNC orbital maneuver technologies. For extensive propulsion beyond simple station-keeping, we would anticipate docking the TESSERAE Shell with a dedicated, propulsive unit. Tiles will be initially designed with radiation and debris shielding comparable to systems currently used in ISS modules (e.g., Whipple Bumper and stuffed shield^{193, 194}), with tests on alternative, advanced, and lighter materials conducted as feasible.

We envision multiple, interlocking TESSERAE structures joining together to form larger space stations on-demand. This figures prominently in our design for agile mission operations. One particular instantiation of this concept, the MOSAIC constellation, would allow for dynamic creation of new habitable volume to meet waxing and waning crew needs in orbit. A single TESSERAE sphere could accommodate the first orbital crew, then dock with additional self-assembled modules as additional crew arrives, then detach and condense back to a single module in orbit as other units are disassembled, packed flat, and shipped to the surface for re-use as a land-based habitat. This agility in habitat design and module re-use requires the TESSERAE tiles to support a multifunctional hardware architecture.

We envision “banks” of stored TESSERAE tiles of various functionality at certain stable orbits, possibly Lagrange points, to supply backup tiles and change-out orders for stations in need of retrofitting or new tile functionality. In the future, rather than having to custom design each module and plan ahead for only a subset of potential use scenarios with that particular hardware, a standard suite of interchangeable TESSERAE tiles could be used to allow one space station core to service many adapting, evolving scenarios. For example, while a completed TESSERAE Shell module may have been serving its purpose most recently as a galley, with perhaps a single airlock tile back to the main structure, that module could be depressurized, retrofitted to include multiple berthing port tiles and welcome several docking spacecraft as a make-shift arrival node for a convening in space.

5. Habitat Interior Use

In our effort to extend our “self-aware” self-assembly concepts to pragmatic habitat designs, we have identified two models for interior use. The first addresses near-term scenarios where, due to limited resources and constrained operating support, space habitat structures must still be filled by optimizing space allocation for mixed needs within a single volume.

Near-term, limited space

For this model, we utilized the largest possible configuration of tiles allowable by near-term rocket payload fairings to facilitate comfortably hosting up to an eight person crew (note: these dimensions assume a 20% increase in the original TESSERAE at-scale dimensions shown in Figure 6-2 in Section 6.1.1; see updated Figure 6-10 below). As shown in Figure 6-11 and Figure 6-12, our interior design includes several functional spaces, assuming we must meet the usual suite of required astronaut support areas (sleeping quarters, galley, research racks for scientific exploration, entertainment, a window and mental health meditation corridor, etc.).

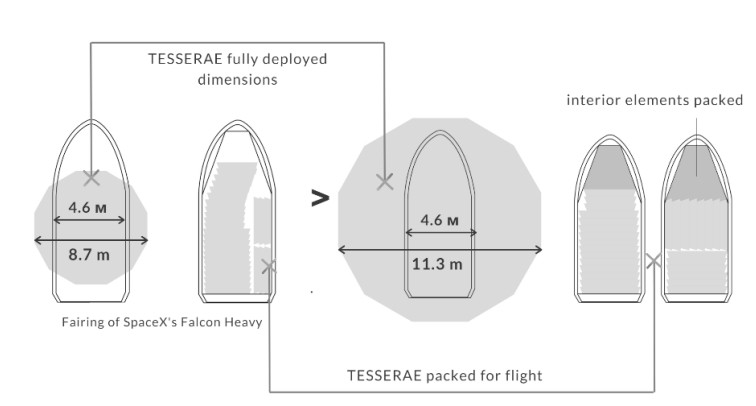


Figure 6-10. Original conception of TESSERAE module size (left) compared to prospective TESSERAE module size to accommodate all core functions in a single mixed-use chamber (right). Would require two Falcon Heavy launches. Figure courtesy of MIT Visiting Student Anastasia Prosina.

Our aesthetic choices draw from Japanese architectural display, in particular, the integrity and modularity of Metabolism—a post-war Japanese architectural movement that combined ideas from architectural megastructures with organic biological growth (presented in Chapter 2).¹⁹⁵ Our design also borrows from the idea of shoji, a room divider consisting of translucent paper, for mixed-use space utilization. Having proposed the buckminsterfullerene shape, a relatively new geometry to space architects (in comparison to the many designs proposed for cylindrical habitats), we have had to develop new design primitives for the interior life subdivisions. The diagrams and functional spaces discussed below are a preliminary attempt and part of ongoing work to marry our adaptive, self-assembling shell concepts with the practical needs of a crew of eight. Care was taken to ensure that interior features added post-assembly would fit through a conservative airlock diameter of 3 ft.

Racks—

For scientific racks, we based our design on the “Random Access Frame” reconfigurable racks of the NASA Jet Propulsion Lab’s (JPL) space architect Scott Howe.¹⁹⁶ The design provides a multipurpose and flexible system of racks for use by life support systems, research equipment, and storage. We further optimized the frame shape to better fit into the fullerene geometry without any gaps. Ideally suited for the fullerene station, the rack system is easily repairable, reconfigurable, and lightweight, which makes it a practical choice for space design. Utilizing existing rack systems, with some optimization, saves time and allows for cheaper production costs.

Galley—

Every cubic inch proves vital in this near-term model of a space habitat. For efficient construction of a galley, we employed a cabinetry tessellation to ensure fully optimized use of physical space. We investigated various types of tessellations and ultimately chose the tetragon tessellation as it mates well with both TESSERAE tile shapes—pentagons and hexagons. To maintain storage packing efficiency, any angle of a package should not be less than 60 degrees. The hexagonal tile best allows this, and thus, the hexagonal tile properly serves as a galley cabin that can be fully stowed for launch and then deployed inside the closed habitat after assembly has completed.

Habitation Core—

Located in the middle of the module, the Habitation Core ensures convenient access to any location within the capsule while providing the privacy needed for sleeping and personal tasks (Figure 6-11). The private quarters are equally divided by partitions, with storage for personal belongings located in the center division (shown in teal). Each inhabitant can enjoy a virtual viewing experience projected on the curved containment wall by their berth for recreation, per feedback from our astronaut user research sessions that open-space projection is preferred to virtual reality (VR) headsets. The habitation core is centered in the volume of the TESSERAE module and therefore more protected, should the crew experience a micro-meteoroid impact or other external danger.

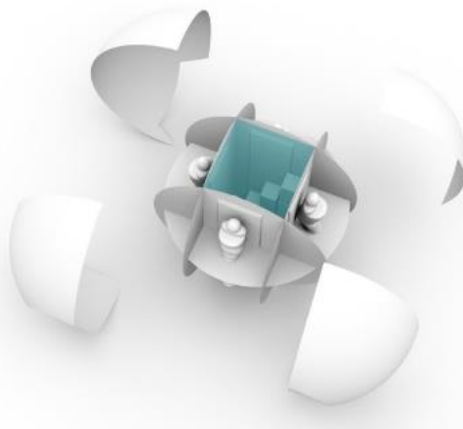


Figure 6-11. Habitation core showing personal space divisions, with prospective mummy-like sleeping bags to provide the sense of embrace for comfortable sleeping. Image and functional space definitions credit from above: Anastasia Prošina.

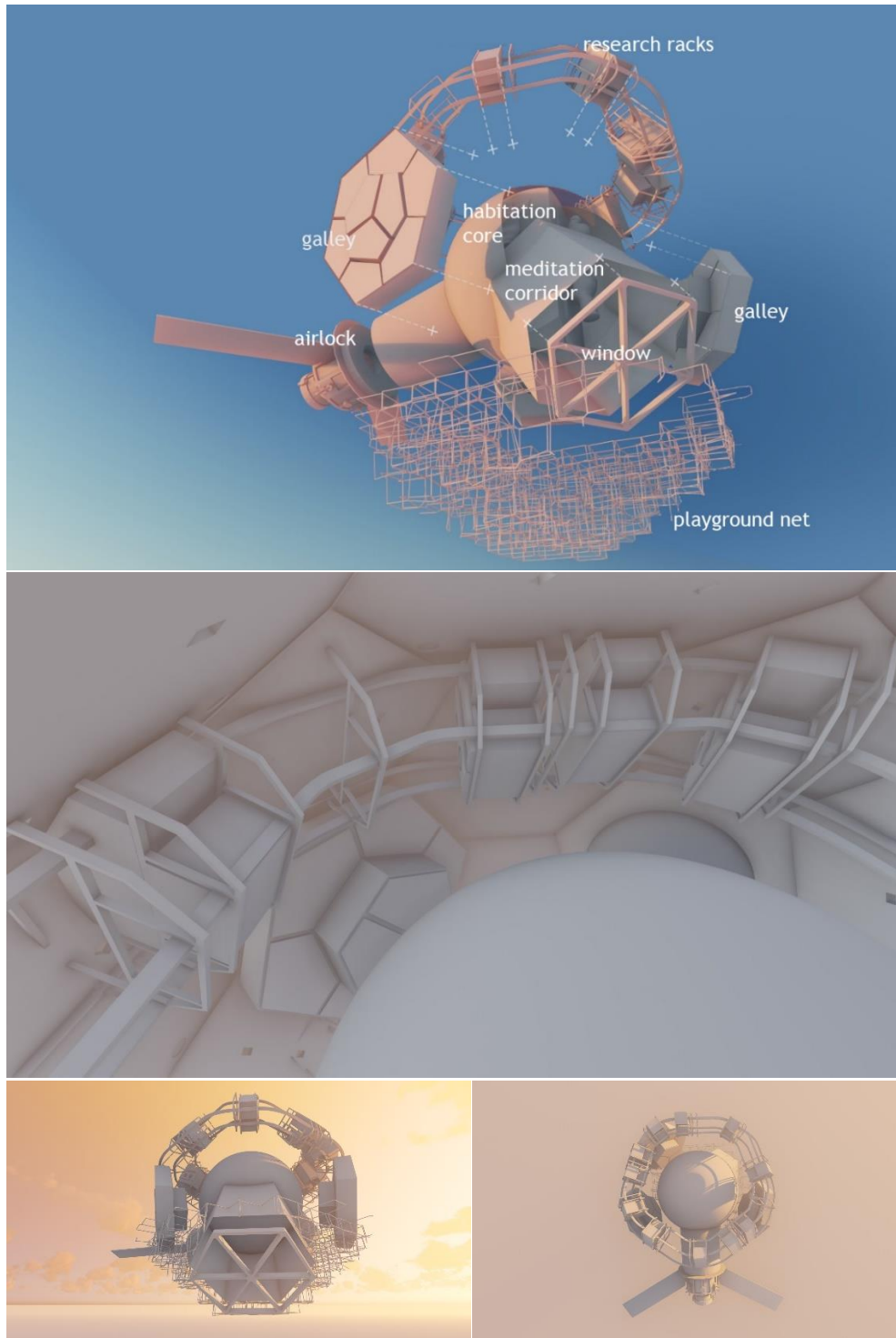


Figure 6-12. Top: exploded view of TESSERAE multi-functional interior design, fit within buckminsterfullerene modular geometry. Functional zones include airlock integration, galley tessellations, sleeping quarters, research, and entertainment spaces. Center: Close-up of scientific rack tie-ins to TESSERAE hexagon and pentagon side wall segments. Bottom row: alternate views showing the packing of the multiple activity and functionality zones into a condensed space, with focus on cupola window (left) and airlock, radiator wings for thermal management, and a ring of scientific racks (right). Artist's render and design work courtesy of MIT SEI Visiting Student Anastasia Prošina. The outer shell is removed in these images to show interiors.

Medium-term, intermediate space constraints

A secondary, medium-term approach to space habitats will allow for longer sightlines and open spaces, where a single TESSERAE module may be devoted to a single purpose—say the command and operations bridge of a spacecraft, or a large and expansive entertainment area. We spend less time proposing this model in this thesis, as this use case is likely more than a decade away, but present below an artist’s conception of the TESSERAE modular architecture shell with this use case (Figure 6-13). This figure also depicts many projects underway at the MIT Space Exploration Initiative (SEI), discussed in further detail in the Appendix.

Larger TESSERAE modules with rotational symmetry could prospectively be spun to generate artificial gravity—the holy grail of habitation in orbit—to provide areas where astronauts can exercise and counteract the physiological changes of long-duration life in microgravity. A large enough spherical approximation habitat like the proposed buckyball could be spun about its axis such that a sensation of gravity (from centripetal force) is induced at the widest point, or equator, while maintaining microgravity at the poles. Combination wheel and spoke models, with TESSERAE modules at the extremities of the spokes, could also be spun to induce artificial gravity. Clamps will need to be designed (see preliminary work in Section 4.1.4) to maintain structural integrity while spinning.

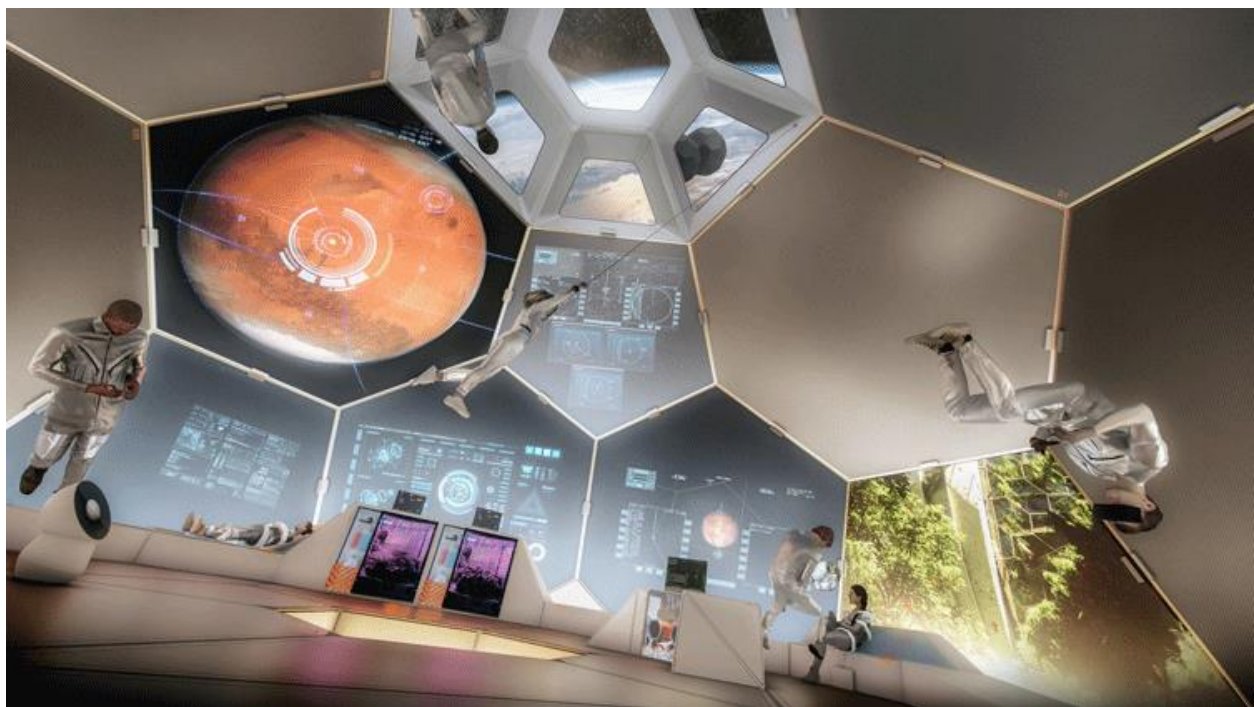


Figure 6-13. Speculative TESSERAE interior in medium-term conception of physical space allocation (envisioning an era that is beyond our current survivalist period, pre-Stanford Torus “abundance in space” period). Figure also depicts over ten different MIT Space Exploration Initiative ongoing research projects (see Appendix). Render courtesy of Igor Neminov.

6. End-to-End Trusted Autonomy, via Integration with Swarm Robotics

Long predicted by science fiction and often prioritized in NASA JPL’s vision for robotic exploration,¹⁹⁷ robot agents will be employed in synergy with human astronauts in this next wave of space exploration. Future in-space operations—across LEO, lunar missions, and out to Mars—will heavily leverage robotics and autonomy to increase systems performance, reduce risk to human crews, and contribute to mission success. As the NASA Platform for Autonomous Systems (NPAS) team at NASA Stennis notes, “Autonomous operations are critical for the success, safety and crew survival of NASA deep space missions beyond low Earth orbit, including Gateway.”¹⁹⁸ In particular, we anticipate extensive operations support from swarms of autonomous robots, likely of varying size, locomotion and end-effector status, such as what is described in the near-future envisioning in Neal Stephenson’s *Seveneves* and being explored currently by NASA Ames and MIT collaborators.¹⁹⁹ TESSERAE steady-state operations will require both interior and exterior servicing and maintenance—tasks that could be accomplished by coordinated teams of miniature robot populations, feeding off sensor data from the tiles and their own micro-sensing platforms, while keeping in constant contact with the habitat base station and even a remote ground control via wireless communication. In-space servicing has been identified by Newman, et al. as a crucial upgrade needed for the next generation of space assets.²⁰⁰

To explore this symbiosis of “Trusted Autonomy,” a key focus of the Science and Technology Partnership Forum guiding autonomous systems development for lunar missions,²⁰¹ we are positioning TESSERAE tiles to interface with MIT collaborators’ miniature “rovable” robots (Figure 6-14) for quality control and inspection sensing, and eventually repair and maintenance tasks on steady-state structures. Several of the robotic approaches will have cross-over applicability for structures assembled and in need of maintenance on the lunar surface, though we focus our initial work on controllable microgravity mobility. The current “rovable” models will be augmented with BLE communication modules to be able to interface with the BLE-enabled TESSERAE tiles. In a suite of parabolic test flights planned for 2021, we will integrate the robot population and the TESSERAE tiles (for surface analysis). The agentless, self-aware assembly platform that TESSERAE offers for in-space construction couples with the use of swarm robotics for in-situ servicing to offer a holistic, autonomous space station system. Further work in other areas of the space industry must be undertaken to upgrade current designs for habitat sub-systems (e.g., ECLSS); together, we can chart a path to robust, autonomous space architecture in orbit.

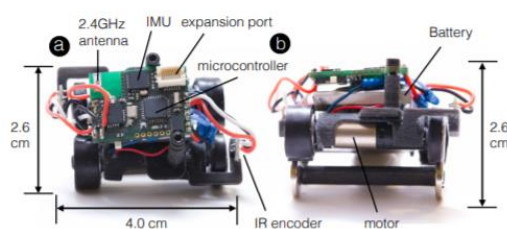


Figure 6-14. Annotated model of the Rovables, miniature robotic platform with wheel mobility created by Artem Dementyev, for prospective modification with the TESSERAE self-assembling system.²⁰²

7. Dual Use On-Surface

In addition to providing orbital habitat volume, TESSERAE tiles could be used for planetary surface shielding and habitats (Figure 6-15). While the self-assembling nature of TESSERAE construction works best when least-constrained in microgravity, the ease of snapping TESSERAE tiles in place can facilitate quick, modular construction in normal and reduced gravity environments as well. Our 2017 parabolic flight test demonstrated that tiles snap together readily with minimal human intervention in both lunar and Martian gravities, due to the reduced g-load in concert with an attractive magnet force that remains the same. TESSERAE tiles could be disassembled from their orbital configuration (e.g., a staging base), packed flat in an entry, descent and landing (EDL) transfer vehicle, and re-assembled with human or robotic assistance on the surface of the Moon or Mars. The EPM polarity map allows tiles to be intentionally assembled like a puzzle set without the need for quasi-stochastic assembly, when an agent is present to take over the assembly process. Depending on the scale of TESSERAE tiles employed, to achieve assembly of a half-dome structure on a planetary or moon surface, a ladder and simple pulley system may be required. Again, due to TESSERAE's re-configurability, the shell tiles could be assembled as a habitat for initial use at a landing site and then disassembled, moved by rover, and reassembled elsewhere to meet evolving on-surface mission needs.

The introduction of fine, sharp lunar dust poses a challenge to all prospective lunar-surface hardware; because the TESSERAE clamping system plan does not rely on precise tolerances for the bonding edges, but rather on deformable gasketing material, it is anticipated that the clamps may be able to execute even with limited dust inside the joints. Over time, however, sharp lunar dust particles (due to the lack of erosion forces on the lunar surface) will wear down and limit the useable life of the TESSERAE tiles. A comparable issue exists in other surface contexts as well, though to a slightly lesser degree on Mars where erosion has smoothed the dust and fine particulate matter over time.

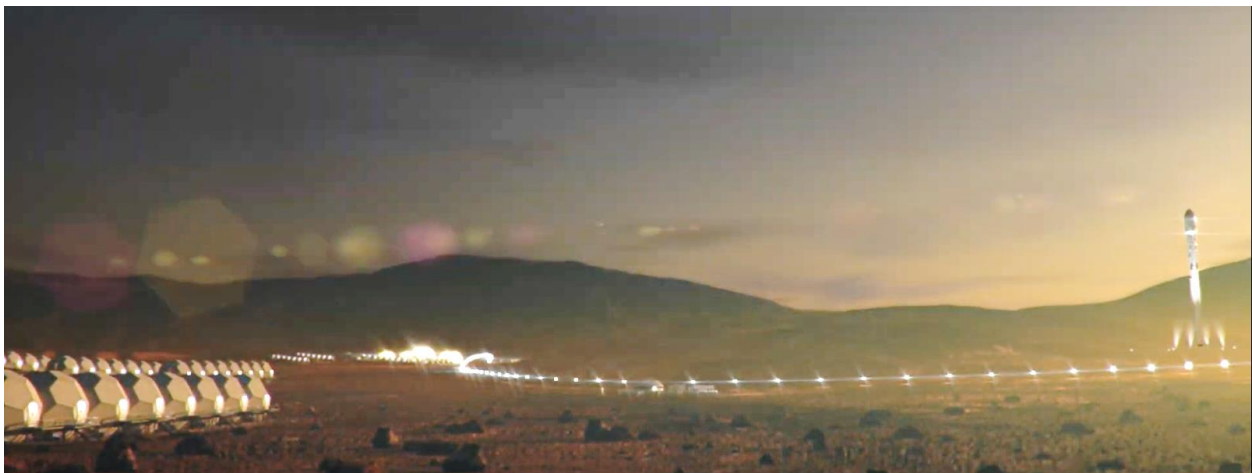


Figure 6-15. Speculative landscape showing TESSERAE Shells repurposed on the surface for a Martian settlement. Render courtesy of collaboration with TU Dortmund Fraunhofer Institute.

6.1.2 Deployment Feasibility Analysis – At Habitat Scale

While TESSERAE could be deployed at varying volume scales by tuning the size of the standard hexagon and pentagon tiles, we propose the below scale for initial technology demonstration mission design and feasibility review. Note: what is described below is consistent with the TESSERAE dimensions first presented in Section 6.1 (not the mixed-use habitation-ready station described in Highlight 5 of Section 6.1.1).

To explore the feasibility of this system in a deployment context, we model an example TESSERAE system corresponding to the introductory figure in Section 6.1: tiles of bonding-side length equaling 1.52m (5ft), thus yielding a total truncated icosahedron volume (shell and enclosed area) of 196m³ (6910 ft³) with an interior open diameter span of 8.7m (28.4ft) (following the formulas for volume of a truncated icosahedron). To compare this with the ISS and its component modules currently in orbit, TESSERAE’s proposed interior pressurized volume would be approximately 20% of the full pressurized volume available on the ISS (916m³, 32,333 ft³). Due to varying requirements on use of space onboard ISS, the actual “habitable” volume is only 388m³ (13,696 ft³), split across multiple modules.¹⁹⁴ A single TESSERAE module at this sample scale would therefore offer around half of the total livable space of the ISS.

Using this baseline size, we have completed preliminary scalability and feasibility calculations for an on-orbit deployment (see items 1–6 below). While a fixed TESSERAE mass has not been determined at this scale (as the final value will depend on material choice and shell thickness, which will vary for different applications in orbit), we can extrapolate from the published Columbus Module specifications and NASA standards (Figure 6-16) to approximate the mass due to several layers of stuffed bumper, thermal and aluminum shielding. Taking the 14.7g/cm² area density of the 7.9cm (3.11in) thick Columbus Module,²⁰³ we would expect an upper cap of ~23,000kg (~50,000lbs) for the TESSERAE Shell mass. Keeping consistent with Columbus Module thickness, the interior usable TESSERAE volume would then be approximately 175m³ (6,180 ft³). This predicts a *worst-case mass*, and we expect to be able to reduce this mass considerably with advances in lightweight, space-grade materials since the Columbus module was built in 2008.

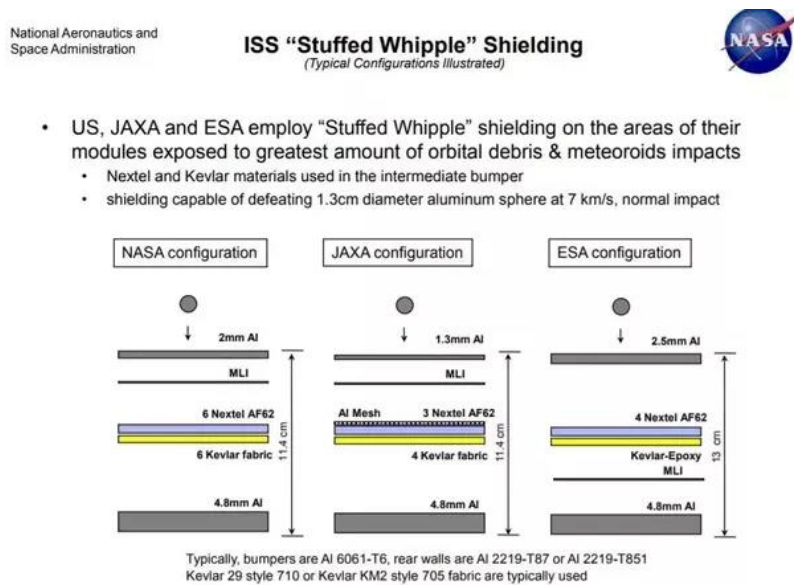
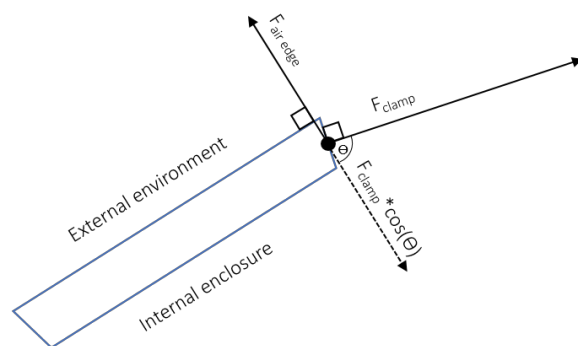


Figure 6-16. TESSERAE initial shell material based on the “Stuffed Whipple” shield used (with certain variations) in the modules of the International Space Station. Image credit: NASA.

1. Ride to Orbit—At a maximum capacity of 23,000kg for the TESSERAE structural units, we can confirm that the SpaceX Falcon 9 Heavy could deliver this mass (and stacked volume) to LEO, per the specifications describing an allowable payload weight of 63,800kg to this orbiting altitude range.¹⁸⁹ Other prospective vehicle delivery options, including SpaceX’s BFR rebranded Starship,²⁰⁴ Blue Origin’s New Glenn,¹⁹¹ and NASA’s SLS,¹⁹² all offer stated capability that would allow us to fly multiple sets of TESSERAE tiles to further orbits, to facilitate self-assembly of more than one shell module in parallel.

2. Pressurization in Orbit—We have modeled the force due to air pressurization on the TESSERAE tile joints and have confirmed that industrial clamps already exist at the required hold force regimes. Our clamping system is intended to provide full redundancy in the case of EPM adhesion failure, and thus we have designed TESSERAE to withstand the full 14 psi (for consistency with ISS conditions), or up to $9.7 \times 10^4 \text{N}$ of air-expansion force along a tile’s bonding edge. The tile bonding surfaces will be augmented with deformable gaskets to allow for press-sealing upon actuation of the clamp. Clamps will latch closed without requiring constant power to maintain fixed position. This approach is comparable to the 16 connecting bolts used to secure the latching mechanism for the Common Berthing Mechanism (CBM) on the ISS.²⁰⁵

At this scale, with tile surface area dimensions of 4m^2 (43ft^2) for pentagons and 6m^2 (65ft^2) for hexagons, and an interior pressurization of $\sim 100 \text{kPa}$ (14psi) for consistency with ISS conditions, we expect an air-expansion force ranging from $7.7 \times 10^4 \text{N}$ to $9.7 \times 10^4 \text{N}$ acting along each tile’s bonding edge. Planning for the highest of these anticipated forces (along the hexagon-hexagon joints), and taking into account the component angles along which an example clamping device would act, we anticipate a required total clamping force per tile bonding edge of $3.0 \times 10^5 \text{N}$. Comparable clamping forces are already seen in industrial use,²⁰⁶ and such hardware could be modified for use with TESSERAE. Chapter 4, Section 4.1.4 also discusses our in-house development of suitable clamp designs. The clamping channel between the mating face of tiles will be augmented with a gasket to aid in sealing strategies. Additional sealing strategies (reversible chemical binders, or internally inflated air-tight chambers) are under consideration as well. See Figure 6-17 below for a diagram of the simplified clamping and air expansion forces at the tile boundaries.



Sample calculations for hexagon tile:

$$F_{\text{air total}} = 96.5 \text{kPa} \times 6 \text{m}^2 = 5.8 \times 10^5 \text{N}$$

$$F_{\text{air @ edge}} = F_{\text{air total}} \div 6 = 9.7 \times 10^4 \text{N}$$

$$\text{For force balancing, } F_{\text{air @ edge}} = F_{\text{clamp}} \times \cos(\theta)$$

Therefore, a clamp system acting normal to the bonding face, where $\theta = 71.3^\circ$, must exert:

$$F_{\text{clamp}} = 3.0 \times 10^5 \text{N (repeated at each edge)}$$

Figure 6-17. Showing simplified force model at tile edge, cross-sectional view. Outward force due to pressurization can be modeled as distributed evenly along the five or six edges of a pentagon or hexagon, respectively. Note: this is a narrow analysis focused on pull-force—further analysis is required for the bending and shear forces on the clamp.

Inside the enclosed volume, we envision inflating a fabric-like, air-tight chamber to provide redundancy via double containment. As noted in Section 6.1.1, while the clamping of many additional “seams” may at first seem an over-complication compared with the unibody cylindrical modules currently deployed in orbit, we embrace this challenge to preserve the reversibility of joints that enables re-configurability ConOps and the repair and replacement modularity of the structure.

3. Power Budget—We anticipate covering the outer surface area of each TESSERAE tile with solar panels, where feasible, to supply power for EPM actuation, sensing, and clamping during assembly. The panels will likely require a protective cover that can be retracted or jettisoned after assembly, to avoid damage while tiles self-assemble (i.e., to mitigate risk from collisions). The outer surface of TESSERAE yields 169m² of available area. We will assume only 80-90% of this area can be fully templated with solar cells; assuming comparable energy yield to the ISS²⁰⁷ in W/m² (84-120kW out of 2500m² of array gives ~33.6-48.0 W/m²), we would conservatively anticipate 120-173W for the pentagonal tiles and 182-260W for the hexagonal tiles.¹⁸ While tiles will harvest varying levels of energy individually due to varying incident sunlight angles, an approach for maintaining electrical connection through the magnet bonding pairs could allow us to transfer power between tiles and redistribute as needed to batteries. At this level of power generation, with modest onboard power storage for each tile, we can supply the necessary power draw for intermittent actuation of the EPMS and always-on low power sensing during self-assembly. Future analysis will be undertaken to inform the expected timescale of assembly (per the simulation results in chapter 5) based on power availability for the expected count of EPM actuations, and whether we would be waiting on power generation to catch up to the speed of the assembly process. To supply the power needed for the clamp actuation after structural assembly is complete, all tile batteries will need to recharge over 1-2 orbits (in LEO) before executing the latching tasks, depending on final battery selection. Additional solar arrays wings can be deployed subsequently, out away from the structure in the model of the ISS power arrays, to power steady-state habitat operations if required for life support systems and other functions. We are exploring various designs for thermal management and directing radiative heat, including deployable radiators (e.g. the ISS approach) and use of innovative MIT research in photovoltaics and wideband thermal diodes to convert waste heat back into electricity.²⁰⁸

4. Electromagnet Mass and Strength Considerations—When analyzing the feasibility and practicality of embedding electro-permanent magnets (EPMS) on each bonding face of each tile, we must consider both mass and holding force (minimizing the former while maximizing the latter). As prior ESA analysis on inter-satellite coulomb forces⁵⁵ has shown, micro-Newtons are sufficient to effect satellite swarm configurations and gradually move objects in a microgravity environment over tens of meters. This is comparable to the max distance expected between TESSERAE tiles while assembling, with the containment membrane keeping the tiles within this bound. We have identified several widely available, industrial EPMS with holding forces in the hundreds of Newtons and mass under 1kg.^{209, 210}

EPMS can also be custom designed by tuning the magnetic material, cross sectional area and other parameters to achieve high capacity adhesion and attractive forces.²¹¹ At this mass order of magnitude, all 12 EPMS on a hexagonal tile would contribute less than 1% of the tile's total mass (based on the mass estimate using Columbus module shell density). The sample EPMS in question draw power in the 30-70W range and would be pulsed “on” (thereby neutralizing or repulsing the unit and breaking away from any currently bonded element) only briefly during error state management and disassembly. Commercially available magnet product lines, prior examples of magnetic docking,^{183, 184} and electromagnetic formation flight^{185, 186} suggest we can design a custom EPM for TESSERAE that will be low in mass and power draw while still having ample strength for actuation and assembly purposes. We would also build on the custom EPM development described in Section 4.1.3 from our successful ISS mission, to scale the behavior of these EPMS to the operating regime needed for self-assembly at scale. This constitutes a key area for further study and development in the TESSERAE future work continuation plan.

¹⁸ The quoted energy yield is a conservative estimate, given advancements in photovoltaics since deployment of the ISS solar panel cells.

5. Guidance, Navigation, and Control

While TESSERAE, by design, does not require active propulsion navigation nor extensive attitude control *during* assembly, certain control systems are still needed to shepherd the tiles towards desired configurations (hence the “quasi-stochastic” label). Rather than conventional GNC actuators (CMGs, reaction wheels, jets, etc.) we employ a supervisory sensing algorithm and swarm-based adaptive control of the tile interactions via on-demand actuation of the EPMS. As described in Section 6.1, we can use the EPMS to selectively apply torques, buffer tiles away from each other, and correct metastable error states. For example, we propose to address entrapment (tiles trapped inside a nearly-closed module) by exchanging both local and global state information between tiles, detecting and diagnosing the entrapped state via proximity sensors and tile-tile bonding logs, detaching tiles to make an escape path and actuating torques to induce motion of the trapped tiles back through the opened hole. Ideally, entrapment can be avoided from the beginning via the holster deployment method that facilitates accretion piece by piece into the desired topology. While less deterministic than using propulsion and active control to guide tiles, the TESSERAE adaptive swarm architecture approach entirely avoids the payload weight and consumable-resource-constraints associated with traditional GNC systems. *After* assembly, we anticipate needing station-level attitude control to keep the habitat from spinning and tumbling—this could be achieved by adding the relevant subsystems into a few tiles distributed across the surface or by docking onto large, existing stations with their own station-keeping, depending on the ConOps for that mission.

As a brief aside on the GNC issue of tiles colliding destructively—we are designing the tile release mechanism and elasticity of the containment membrane to keep tiles at standard docking speeds²¹² (e.g., around 0.0325 m/s for the Shuttle to ISS, and generally under 1 m/s max) relative to each other. Our simulation results from Chapter 5 show that the vast majority of tile-tile collisions are consistent with this goal (and we can further tune the input parameters to achieve greater compliance). Further design studies will be undertaken to determine whether single-material or multi-material elasticity gradients can be used in the construction of tiles to provide buffering upon first collision while maintaining an overall rigid body. Results from the assembly simulation model in Chapter 5 discuss the kinetic energy of tile collisions and the overall formation over time, and help us identify and avoid threshold scenarios where the energy of the colliding system passes from effective to destructive (as tile mass increases in larger deployment contexts).

6. Timescale of Assembly—To serve as a practical space structures deployment protocol, the TESSERAE system must be able to self-assemble efficiently. We are currently targeting assembly completion in under eight hours and have repeatedly achieved five hours or less, at scale, with our simulation model (see Chapter 5). Small scale tests in short microgravity periods show that proximate TESSERAE tiles within a few centimeters distance from one another snap together in a matter of seconds. A paper on 2D stochastic assembly out of the Bachelet Lab¹⁴ shows that a system of 18 custom-joint blocks self-assembles in 1-2.5 hours with 50% reproducibility, even while fighting gravity. In this system, exact neighbors must find each other; we take a more bonding-favorable approach, working with the minimum number of unique tile joints (currently only two types) to ensure each tile has a high probability of finding a neighbor tile with which it can pair.

It is a well-known behavior of stochastic systems that the last 10-20% of the assembly can take 80-90% of the assembly time (essentially the “hole-filling” problem). We note several mechanisms by which to address this: (a) as the final step, hole-filling can be achieved by reserving one tile in the dispensing holster, released and directed toward the remaining area to be filled, (b) through selective use of the EPMS, we could torque and direct both the remaining tile and the partially-assembled module towards each other, (c) design the self-assembly “annealing ramp” conditions (à la the favorability energetics for DNA) to produce two halves or four quarters that can come together easily without producing a hole to fill, or (d) introduce extra, redundant tiles into the assembling system, so that a final hole is not waiting for a single tile to circulate nearby. Our simulation

model employed the latter technique to great success, showing that only two extra tiles (34 total, rather than 32) are required to increase the likelihood of assembly completion in a reasonable amount of time.

For items 1-7 above, the various estimates for deployment size and associated applicable forces are reported as illustrative examples. Early TESSERAE models deployed in orbit for mission testing will likely be 1:10 or 1:20 reduced scale models, to allow the entire deployment to take place inside an ISS airlock (such as the one currently under development by NanoRacks¹⁵⁹) or smaller inflation chambers free of the ISS and in separate test orbits.

6.1.3 Comparison with Alternative Habitation Module Concepts

The charts below show mass, volume, and feature comparisons between the proposed TESSERAE concept, traditional ISS modules, and the BEAM inflatable habitat.

	Mass (no payload)	Interior/Usable Volume	Mass to Volume ratio
TESSERA E	23,000 kg (max cap, could be much lower)	175 m³	131 kg/m³
ISS: Columbus Module	10,275 kg	75 m ³	137 kg/m ³
ISS: Destiny Module	14,500 kg	104 m ³	139 kg/m ³
ISS: BEAM	1,413 kg	16 m ³	88 kg/m ³

Figure 6-18. This table shows that TESSERAE would offer a more efficient mass to usable volume ratio than comparable ISS modules (as we would expect from the optimized geometry). While BEAM's mass to usable volume ratio is the most efficient, we project that TESSERAE's advanced functionality (re-configurability at the shell level), condensed packing for launch, and rigid, protective shell offer sufficient benefits beyond the inflatable model. At these sample dimensions, TESSERAE also offers significantly more internal, livable volume than other alternatives.

	Modular at Space Station Level	Packs Flat for Launch	Autonomous Assembly	Re-configurable at the Shell Level
ISS	✓			
BEAM	✓	✓	✓	
TESSERAE	✓	✓	✓	✓

Figure 6-19. TESSERAE enables unique functionality and facilitates entirely new mission ConOps. The BEAM inflatable habitat approaches TESSERAE's feature suite, but does not fully autonomously assembly (astronauts completed the air inflation process) and the fabric layers cannot be removed, replaced and exchanged in the way that TESSERAE tiles can be reconfigured.



Figure 6-20. Comparison photos of the cylinder-dominated Destiny (left), Columbus module (center), and the ellipsoid inflatable BEAM (right). ISS module specifications are drawn from Columbus,²¹³ Destiny,²¹⁴ BEAM.²¹⁵

For this comparison, we have intentionally over-estimated the mass (extra margin built in) to show that TESSERAE is *still* competitive even with our overly-conservative performance estimates. In addition to the shell mass-to-volume ratio benefits that TESSERAE offers, the system architecture enables unique functionality and facilitates entirely new mission ConOps. Per the comparison chart, TESSERAE is not only modular at the space station scale (e.g., adding additional entire TESSERAE modules to form the MOSAIC, comparable to adding Destiny or Columbus on to the ISS) but also reconfigurable at the shell layer. Accounting for the primary habitation modules, the ISS required seven major launches (and over 20 other launches total) to complete assembly. To achieve a comparable volume of livable space in orbit (approximately two TESSERAE modules as defined in Section 6.1.1), we would conservatively require only three launches due to the advantage of flat-packing and optimized volume for a given surface area (minimum two launches for the tiles themselves, and likely a third for accoutrements). TESSERAE's self-aware self-assembly construction also reduces the propulsion budget on-orbit and lowers crew-time resource consumption thanks to autonomous docking activity. Rather than engaging astronauts in high-stakes, high-stress robotic arm and manually-shepherded docking maneuvers, the TESSERAE tiles can assemble quasi-stochastically while the crew's attention is devoted elsewhere.

Below, we have adapted two figures shown previously in the design theory Chapter 3 to compare TESSERAE against all completed or realistically prospective space stations in orbit (Figure 6-21). The TESSERAE buckyball shell model offers significantly greater responsiveness and self-aware, autonomous activity than even the most recently proposed stations (Axiom and Gateway) and benefits from an inherently more decentralized structure. The TESSERAE Cell model will be discussed later in Section 6.2.

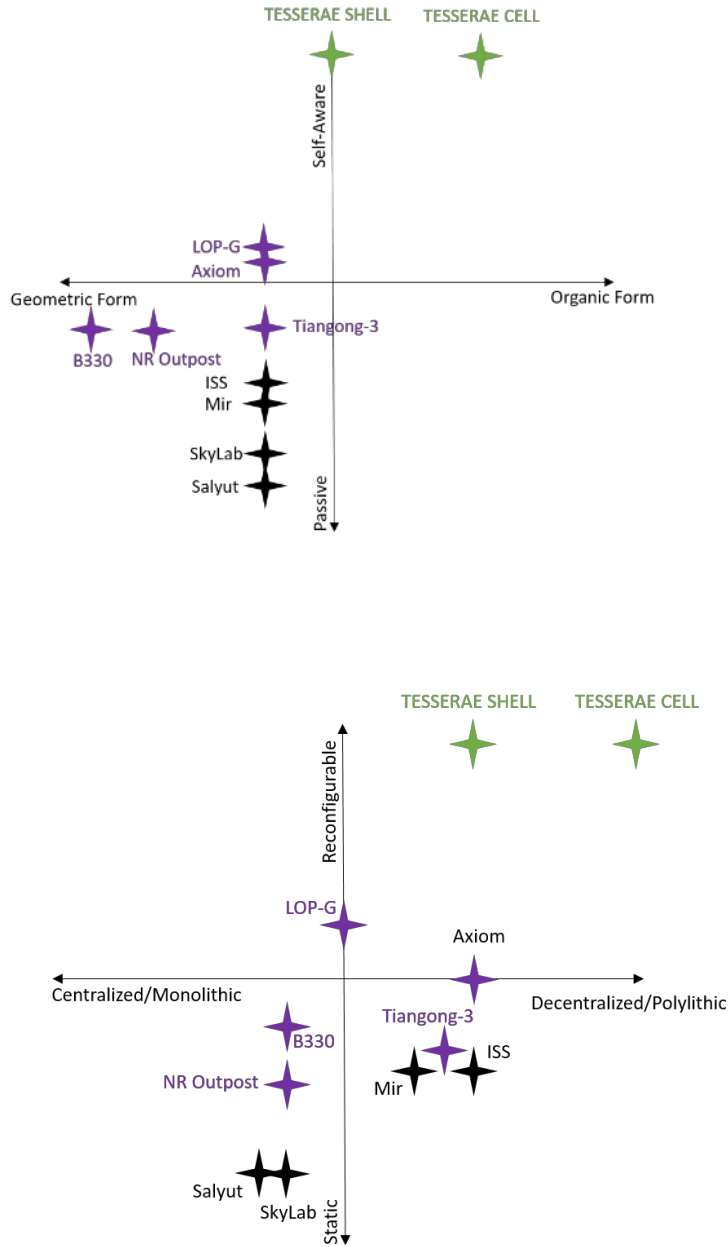


Figure 6-21. Quadrant charts map the parameter space of form (Geometric/Organic; Monolithic/Polyolithic) and function (Passive/Self-Aware; Static/Reconfigurable), placing all known space stations and near-term, realistic prospective stations in this framework. Black stars represent completed stations, purple stars represent prospective stations, and the TESSERAE models are shown in green.

Weak Points, Limitations and Accompanying Mitigations

- As noted above, the TESSERAE model presents many different seams that must be sealed if the structure is to be used for habitation. Section 6.1.2 presents our clamp design to reinforce edges, while also introducing a back-up inflatable bladder that could be used inside the clamped interior to provide a second level of containment. If, despite these precautions, a seam was to fail (or even if a micro-meteoroid punctured the flat surface), the chamber would eventually depressurize depending on the size of the gap and rate of air leak—for this reason, we intend to employ the same best practice used in other space structures where airlocks separate major sections and can be used to retreat into a separate, still pressurized chamber (if part of a larger station).
- A further alternative to relying on clamping seams would be to design a structure where the interior air pressure reinforces the seal, rather than stresses it. This approach is taken on airplanes, where the interior higher pressure at altitude (compared to the lower pressure air outside) pushes on the exit doors and reinforces them in their frames. We are also exploring a buckyball skeleton frame (bars at all edge segments, empty between) where tiles can self-assemble into the negative-space slots and plug into respective hexagon and pentagon holes. Requiring such a large, habitat-scale frame would at first pass appear to violate the principle of condensed packing inside a modest payload fairing for a ride to orbit. A fixed, rigid frame the size of the envisioned TESSERAE habitat would not fit in any known rocket fairing. However, future work with TESSERAE may explore adaptation of the Hoberman Sphere collapsible frame (Figure 6-21) for condensing such a frame during launch and then deploying it in orbit.

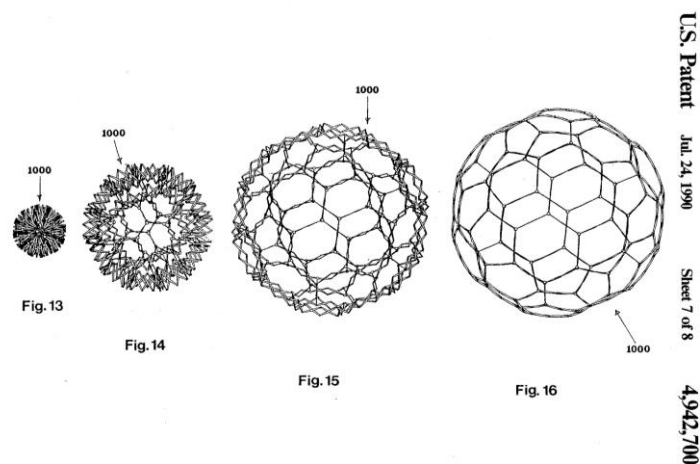


Figure 6-22. Drawing of collapsible truncated icosahedron frame, Hoberman Sphere patent. ²¹⁶

- The elegance of the self-aware self-assembly relies on an extensive sensor suite and integrated control algorithm, as discussed in Chapter 4. If these systems were to fail on a single tile, or multiple tiles, during assembly, or if the communication system between tiles were to fail, assembly could still be saved by capturing tiles with a robotic arm and drawing them in for mediated snap-assembly (much like the model proposed for on-surface deployment). Alternatively, if no robotic arm is available, we have also considered augmenting the tiles with limited-use, emergency thrusters that could be used in such a scenario. These would likely rely on modest impulse electro-spray-propulsion, perhaps units comparable to what Accion¹⁶⁰ currently manufactures.

- The nature of TESSERAE’s modularity, while essential for reconfigurability, creates a certain difficulty in comprehensively outfitting an entire module prior to launch with all systems pre-loaded and furniture pre-configured. While mounted systems and interior furniture could deploy from compartments on the interior surface of the tiles, the maximum tile size constrains the largest dimension of any such subsystem. This is not an unheard-of constraint, as airlock size often also constricts introduction of new elements, but still, we acknowledge that the TESSERAE interior may not lend itself to large, custom, or single-piece luxurious interior item that would need to be integrated on Earth. If there was a desire to include a large interior object after assembly, the shell could prospectively accommodate this by hinging open a few tiles in a co-located area to create a loading opening. We further address this limitation in the TESSERAE Cell model—a volumetric unit that is indeed prefabricated on Earth and self-assembles at the module level, rather than at the base shell level (discussed in Section 6.2).

6.1.4 Alternative Shell ConOps: Origami Assembly

While exploring the insertion order optimization for the deployment of loose tiles in the quasi-stochastic assembling system, we discovered that the TESSERAE tiles can also be flat-packed in a narrow profile hinged stack for origami-style unfolding and unfurling. By applying hinges at selective sides that define a spiral pattern (see Figure 6-23), the tiles can be folded back and forth into a condensed stack and then released in orbit where the magnet joints operate directly to lock in a much more deterministic assembly approach. This process follows the reverse of peeling an orange in a single band—the linked TESSERAE tiles create a 2D spiral arm that self-assembles, bonding row over row, into a closed topology buckyball. As has already been shown, the size of this TESSERAE stack can fit within standard rocket payload fairings. Though the EPM joint functionality would not be needed for assembly in this case (as the hinging and spiral arm geometry ensures proper mating behavior), the mission ConOps still benefit from EPMs for the potential of pulsing apart the spiral for reversibility and re-packing the tile set for use in a new orbit. We estimate the unfolding time-scale in minutes, rather than hours for the quasi-stochastic TESSERAE assembly.

While the origami model offers a compelling alternative to the release and wait time for free-floating tiles, a trade-off remains: this approach gives up the full reconfigurability of the TESSERAE Shell where any tile can be dynamically pulsed off, replaced, or augmented. In this case, the hinges between tiles would prevent a crisp ejection. An approach could be taken where the hinges are retractable, or able to be disabled for selective ejection, but this would require adding significant mechanical complexity to each tile—thus creating great risk for part failure and mission interruption.

We see the origami approach as a high-potential supplement to the TESSERAE free-floating model, where certain immediate mission needs could be quickly serviced by this format of deployable architecture. Stacks of origami modules could be kept in reserve for quick-deploy, less customizable additions to a larger, fully flexible TESSERAE station. With coming advances in scaling transformable meta-materials²¹⁷ and programmable matter by folding³⁰ to larger dimensions, we see this area of research expanding into broader applications of origami in orbit.

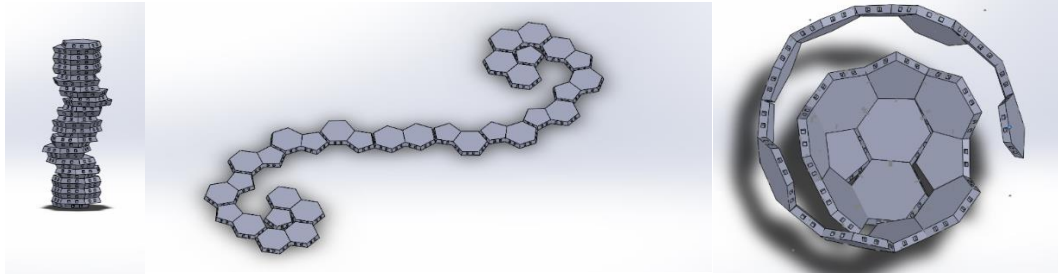


Figure 6-23. Alternative arrangement of TESSERAE tiles for launch with hinged-action for an origami inspired assembly approach. Left: Tiles prepared for launch in a condensed flat-pack configuration; Center: example unfolding of all joints to a single plane (not required for assembly, but illustrative of the underlying spiral arm jointing path); Right: CAD simulation of the buckyball self-assembling from the spiral arm created from the selectively hinged joints.

6.1.5 Extensibility to other Geometries

While our initial investigations into self-assembling space architecture focused on the truncated icosahedron, or buckyball, we expanded our modeling and design portfolio to also consider alternative surface shell tessellations and module-scale packing arrangements for other geometries of interest for space architecture and space exploration missions.

Surface Shell Tessellations

The TESSERAE Shell ConOps, from launch to orbit to surface deployment, benefits greatly from the predictable regularity of the tile base units. While organic, cell-like tessellations of surfaces can produce similar modularity and segmentation of a surface (e.g., Voronoi tiling), the TESSERAE tiles must adhere to a regular geometry for consistency of manufacturing and interfaces, packing for launch, and predictability of assembly once in orbit. Though spheres, and spherical approximations like buckyballs, are an efficient shape for in-space habitation (maximizing usable volume, while minimizing the costly shell surface area), future space stations may be interested in other curvilinear solids, such as the traditional cylinder or a rotating torus for generating artificial gravity. We can apply the same shell modularity approach to these shapes, after properly segmenting and approximating the curved surfaces. Figure 6-24, below, shows an approach for tessellating the torus with regular hexagons and diamond tessellations of the beguiling helix zome. While the sizes of the polygons do vary (requiring more than one standard size hexagon, for example), this size variation can be constrained and accounted for, yielding a repeatable “tile shell set.”

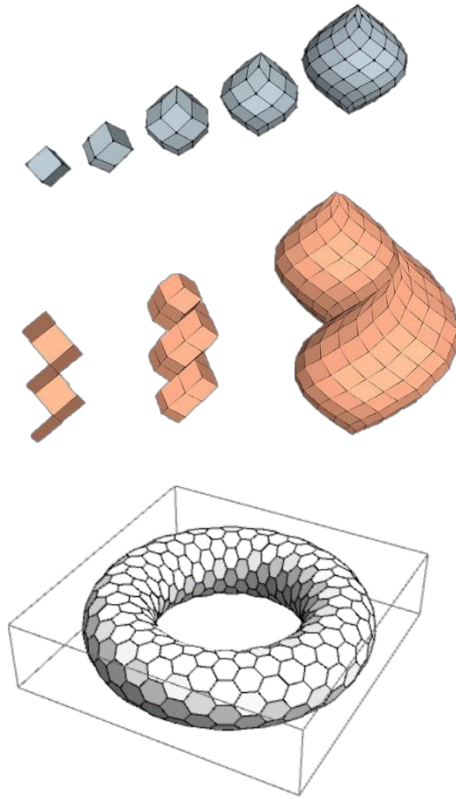


Figure 6-24. Top: diamond or rhombus tiling of a helix zome, image credit: Rob Bell. Bottom: hexagonal tiling of a torus, generated in Mathematica, referencing code and approach from online tutorials. ^{218, 219}

Adjustable Base Units

When we consider truly generalizable tessellations, or base units that could self-assemble into any number of shapes without a fixed target in mind, we are likely to rely on triangles (building on the tradition of mesh generation that underlies most CAD software). Even still, when triangles meet at angles outside the xy-plane, a dihedral bonding angle must be established and cut into the thickness of the tile to establish the curvature between shell units. A generalizable set of triangular tiles would not have the custom dihedral bonding angles needed for particular surface curvatures, but could be augmented with filler-material, inflatable bladders or expandable jointing to address the internal-surface gaps. One such concept is shown in Figure 6-25.

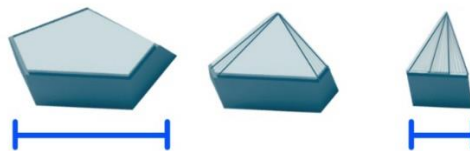


Figure 6-25. Expandable and variable slope-angle TESSERAE base units. Image credit: MIT Visiting Student Anastasia Prosina.

The TESSERAE self-assembly approach generalizes to other surface shell tessellations and module-scale docking arrangements, offering a wealth of creative, modular shape primitives to the future space architect.

6.1.6 Summary: TESSERAE Shell ConOps

To accompany the hardware development on TESSERAE proof-of-concept prototypes, we have described a hybrid mission plan (primarily in orbit, with cross-over use on the surface) and considered many facets of a Concept of Operations for an at-scale buckyball shell habitat. From packing for launch, to steady-state operations and a suite of reconfiguration options, we present the breadth of the TESSERAE deployment and space architecture concept, with accompanying accoutrements for a holistic, autonomous habitation platform in microgravity. Several renders of interior spaces and exterior arrangements of habitat subsystems offer a vision for future astronaut or space tourist life within TESSERAE, while feasibility calculations for power budget, pressurization forces, timescale of assembly, and more keep us grounded on a practical path to realizing a self-assembling habitat system in LEO and beyond. We draw comparisons between the prospective TESSERAE habitat models and current modules flying (or soon to fly) in orbit. We conclude that TESSERAE offers an unprecedented level of reconfigurability and mission flexibility, while also leveraging the added benefit of space-efficient, condensed launches and freeing up the crew and robotic agents to focus elsewhere while their next habitation module self-assembles. In discussing the role of origami unfolding, other surface shell tessellations, and adjustable base units, we demonstrate the extensibility of the concept and potential for application to a wide variety of shapes and target structures in orbit.

Next steps for the mission architecture work in the TESSERAE Shell portfolio will explore detailed integration of habitat-critical subsystems and protections, including ECLSS, thermal management, and radiation threat mitigations, among others. We will also begin to plan more extensively for interior definition of user-defined zones and user-centric designs for the TESSERAE interior chamber volume. Our work with the Autodesk BUILD Space (discussed in Chapter 4) will continue to focus on large-scale tile maturation, including clamp design, macro-EPM power system design, material gradients to buffer tile collisions, and more. To advance development of the support infrastructure for a TESSERAE deployment (mounting, stabilization and release mechanisms in a payload fairing; the containment membrane and inflation tanks; holster insertion mechanism; etc.) we will begin prototype work for multiple prospective technology demonstration missions (either in parallel with or after completion of the base tile hardware development roadmap and technology maturity steps outlined in Chapter 4, as funding allows).

6.2 TESSERAE Cell ConOps

Though we have focused the majority of the TESSERAE prototypes and ConOps development on the buckminsterfullerene structure self-assembling shell, we also explore a volumetric application of autonomous self-assembly, where pre-fabricated nodes (essentially small, self-contained modules) join together at reconfigurable bonding joints. For this approach, we have focused our initial work on the truncated octahedron—a geometry which is optimized for multi-unit packing and has been previously explored for use in space habitats.⁸⁷ Each module constitutes a “Cell,” with multiple Cells accreting into various configurations of macro-space stations (Figure 6-26). In an improvement upon closed cylinders and ellipsoid or spherical inflatable habitats, the TESSERAE Cell modules can be docked and densely packed into a crystalline-like megastructure to create multi-part, decentralized space stations. Not only does this enable on-demand volume expansions and agile operation needs, but this model also offers a safety-through-redundancy and separation approach to constructing larger microgravity space cities. Decentralized space station concepts offer the ability to pop modules off in an emergency as escape pods¹⁹, or with greater intentionality and forethought, as a transit module to a different orbit. Creating a space station from crystalline-packing principles, while maintaining bonding reversibility, creates an opportunity for both dense and sparse module arrays. Nodes can stay condensed into structures where most sides of a module are contiguous with another module, or nodes can grow in chains and branches, like hydrocarbons with many different branching bonding sites or amino acid molecules with different functional “groups” and zones. The self-assembling and self-disassembling capabilities of the TESSERAE approach offer the ability to adapt to changing priorities and reconfigure the activity of the space station entirely.

This section builds extensively on the generative algorithm simulations with truncated octahedra, first introduced in Chapter 5, Section 5.2. We explored how certain fitness constraints applied to the accreting Cell structures (e.g., maximize surface area, prioritize or deprioritize branches, tune the percentage of exposed faces that can bond with another unit) affect the ultimate morphology of the multi-unit station. In Section 6.2.1, we discuss the promise of plesiohedrons as a design primitive and base unit for space architecture. Working within the cell and tissue metaphor, in Section 6.2.2, we develop the concept of a minimum viable unit (MVU) of space architecture—much like the organelles of a cell, what are the subsystems of a single TESSERAE Cell that will define a self-sustaining, but also easily stacked and replicated, unit for space exploration? In Section 6.2.3, we discuss the wide applicability of volumetric self-assembly to other geometries and even organic units where each node is a custom shape (rather than a repeated, regular geometric solid). Section 6.2.4 compares this Cell model with the TESSERAE Shell model presented previously and other conceptions of near-term realizable space architecture, covering both advantages and limitations of our approach. Our discussion of TESSERAE Cell ConOps then concludes with a summary of next steps.

¹⁹ Inspired by the Arklets in Neal Stephenson’s *Seveneves*.

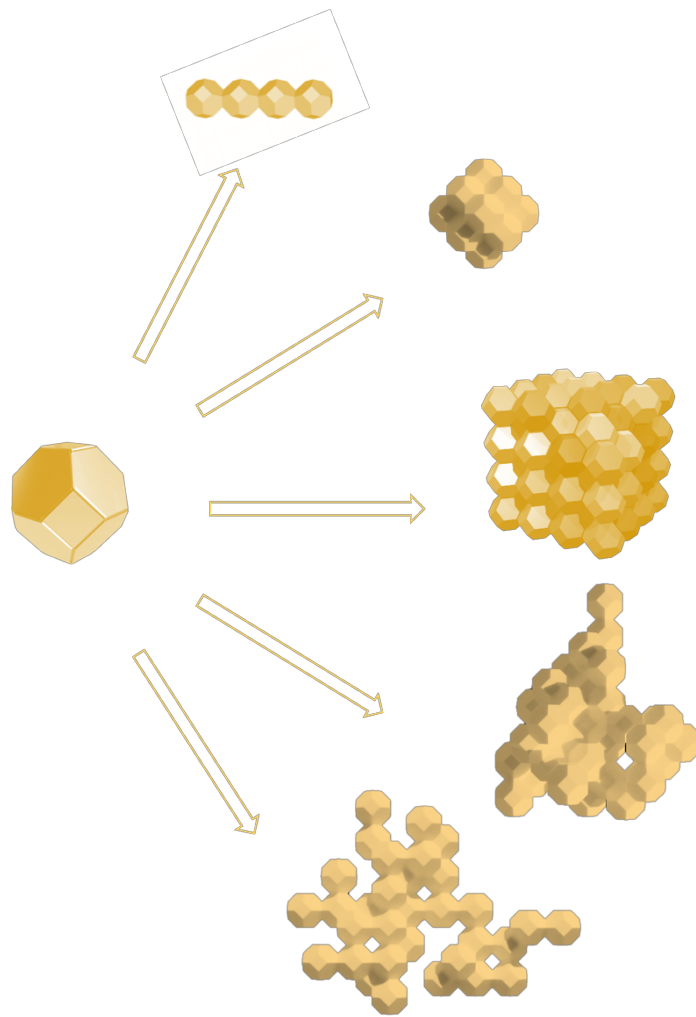


Figure 6-26. TESSERAE Cell base module, with an indefinite range of multi-nodule configurations and associated mission ConOps.

6.2.1 Plesiohedrons and Packing: Crystalline Space Station Mega-Structures

In addition to the geometric representation of the shell surface, we are interested in solid module geometries that can be densely packed in crystalline-like arrangements. The plesiohedron class of solids (e.g., truncated octahedrons, cubes, hexagonal prisms) are able to be stacked such that they completely fill 3D Euclidean space, with no overlaps and no gaps (see Figure 6-27 for an example with the truncated octahedron shape). For both our lunar and MOSAIC concepts, we are building on the notion of plesiohedron solids to propose modular space stations that are “energy favorable” from a self-assembly standpoint and simultaneously packing-volume efficient. These modules can be packed outward in three dimensions to grow an on-demand, radial, modular space station. This decentralized approach to space station design could enable entirely new mission ConOps, where TESSERAE space station modules can separate for escape pod use, or dynamically reconfigure into a new space station arrangement on-demand.

Our use of plesiohedrons also facilitates the indeterminate growth goals from our design theory (Chapter 3). With standard bonding sites that can always accept a new unit of this geometry, we create a matrix structure that can grow and expand incrementally over decades. Rather than requiring a single, massive budget allocation at the beginning of the project (often infeasible in today’s political climate, with many other worthy and competing priorities for national expenditures), we can still achieve large space station concepts by facilitating this kind of incremental, space-packing addition over decades. The following section explores how to achieve resource allocation across many connected units, for holistic space station function out of many plesiohedrons.

When selecting the first plesiohedron to analyze in detail for a mission ConOps, we chose the truncated octahedron for three primary reasons:

- Prevalence of bonding faces (eight hexagons, six squares) to facilitate growth in many directions;
- Closer to a spherical approximation for optimizing volume for a given surface area;
- Use of hexagon faces that could be prospectively joined with the TESSERAE Shell buckyball faces in the future, for a hybrid space station using both concepts.

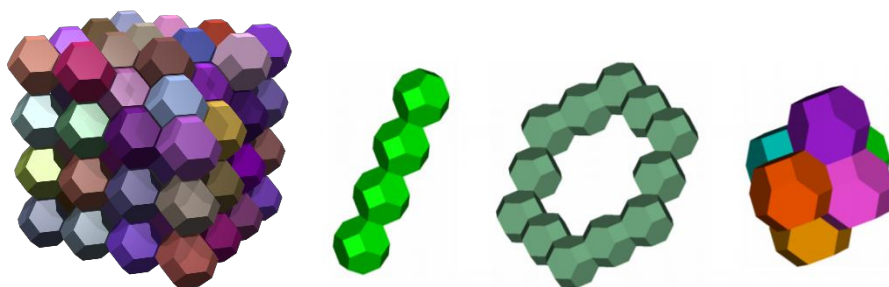


Figure 6-27. Left to Right: Densely packed truncated octahedrons, illustrative of efficient space station module packing for future mega-structure configurations (block image, also known as the Kelvin structure from its application to foam optimizations and bubble packing, courtesy of Andrew Kepert, Creative Commons); Alternative arrangement of truncated octahedra for space stations, image from de Weck et al, 2005.⁸⁷

6.2.2 Defining the Cell MVU: From “Minimum Viable Unit” to Station

For the TESSERAE Cell to offer near-term practicality as a building block of a space habitat, we must consider how many of the critical space station functions could be achieved within a common core module or “minimum viable unit” (MVU). Initially, space station modules must be architected with the hardware, fluid, and electrical systems to support many mission needs (ECLSS; crew rest, eating and exercise; mission control; scientific investigations; etc.). While a single module may never service all such needs at once, prioritizing a generalizable service infrastructure will assist with retrofitting modules over anticipated decades of use. In the years to come, when a certain feasibility and abundance of activity in space has been achieved, we also consider the opportunity for the Cell nodes to supply customized chambers, where an entire node could be dedicated to a more permanent galley, larger personal sleeping quarters, or even a modest arboretum and agricultural production unit. Drawing on ISS technical specs,²²⁰ the delineation of the station’s primary sub-systems²²¹ and the industry stalwart “SMAD: Space Mission Analysis and Design,”²²² we identify the core functionalities and select a subset for inclusion in a prospective Cell demonstration mission (Figure 6-28).

With the MVU subsystems, we aim to design a platform akin to a multi-purpose office building that contains certain common infrastructure throughout the structure, while still allowing for customization by each “tenant.” Each Cell unit should have certain standard tie-ins for ECLSS, storage, crew use, etc. that can be remixed and used differently by different inhabitants and across a range of module functions. These tie-ins should exist within paneling on the interior sides of the module, while preserving as much unobstructed interior volume as possible. There are many ways of envisioning how to subdivide the structure to accommodate interior use cases within the volume boundaries of the truncated octahedron. One might extend the square and hexagon faces into prisms that extend into the center of the structure, intersecting at points that define the limits of sub-chambers. Alternatively, much as we have with the TESSERAE Shell buckyball, space designers could approach filling the TESSERAE Cells with concentric, functional chambers and ad-hoc operation areas like the organelles of living cells (Figure 6-29).

	Subsystem	Included in Cell 1.0 MVU (Yes/No)	Details & Justification
Exterior	Structure	Y	Based on stuffed Whipple Shield initially, until advanced materials are tested (ISS flight heritage)
	Attitude Control	Y/N	Simplified CMGs (ISS flight heritage), not all units
	Orbital Nav & Propulsion	N	Likely relying on docking with existing station for v1 test, or passive orbital test
	Docking & Berthing	Y	One test berthing port with airlock to demonstrate docking functionality
	Computing & Comms 1. Habitat monitoring and workstations 2. Inter-station comms 3. Ground uplink/downlink	1. Y 2. Y 3. Y	Basic comms required for a useful demonstration; significant opportunity noted for use of modern computing architectures and even direct tech transfer.
	Telemetry & Sensing	Y	Native with the TESSERAЕ responsive sensing platform and autonomous self-assembly control algorithm
	External Robotic Arms	Tentative	Depending on launch mass constraints, we may augment Cell with robotic arm extension from deployable compartment. When closed would still maintain truncated octahedron flat face profile.
	External Thermal Radiators	N	Small, single-volume modules like Salyut and Skylab were able to avoid the large, dedicated thermal arrays used in the ISS. When multiple Cells are docked together in a future multi-module demonstration, we will need to upgrade to thermal radiators.
	Electrical Power System	Y	Required for many subsystems; surface area of solar panels to be determined based on downstream loads
	Active & Passive Radiation Protection 1. Active: EM-generated fields 2. Passive: shell material, water walls, etc.	1. Tentative 2. Y	See below discussion of EPM-generated magnetic field for limited radiation protection. Best practices will be used in shell design for passive radiation protection
Interior	ECLSS 1. Breathable air and gas handling (including oxygen generation, particle filter, humidity management, ventilation, etc.) 2. Potable water (including reclamation of waste water) 3. Internal temperature management 4. Maintain total cabin pressure 5. Detect and suppress fire	1. Y	Selection of baseline required functionality drawn from ISS ECLSS (Environmental Control and Life Support System). Subsystems will be included, but scoped down to serve a single cabin volume. Each MVU should be self-contained and not reliant on other docked modules for ECLSS stability.
		2. Y	
		3. Y	
		4. Y	
		5. Y	
	Agriculture/Food Generation	N	While of great interest for future missions, pre-prepared food will be sent for v1 test.
	Waste Management & Sanitation 1. Human waste capture/recycling 2. Alternate trash storage 3. sanitation (e.g., mitigation for molds)	1. Y	Again, selection of baseline required functionality drawn from ISS flight heritage. While mold and sanitation control could reasonably be deferred to a subsequent mission, we are keenly interested in how to optimize the “microbiome” of the station and will include monitoring and mitigation systems for v1 test.
		2. Y	
		3. Y	
	Crew Facilities 1. Sleep 2. Exercise 3. Galley 4. Entertainment	1. Y	Sleeping and galley facilities are a basic requirement. Limited exercise (e.g., isoband) may be supported, unlikely an erg or treadmill would make inclusion for v1 test. Entertainment considerations to be added at a later date.
2. Tentative			
3. Y			
4. N			
Ground	Science Facilities	Y	Limited – proof of concept
	Cargo Storage & Processing	Y	Limited – proof of concept
	Ground: Integrated Mission Control	Y	Mandatory for integrated, observable operations

Figure 6-28. Detailed listing of ISS subsystems, with particular selection chosen for inclusion in TESSERAЕ MVU definition and discussion on justification.

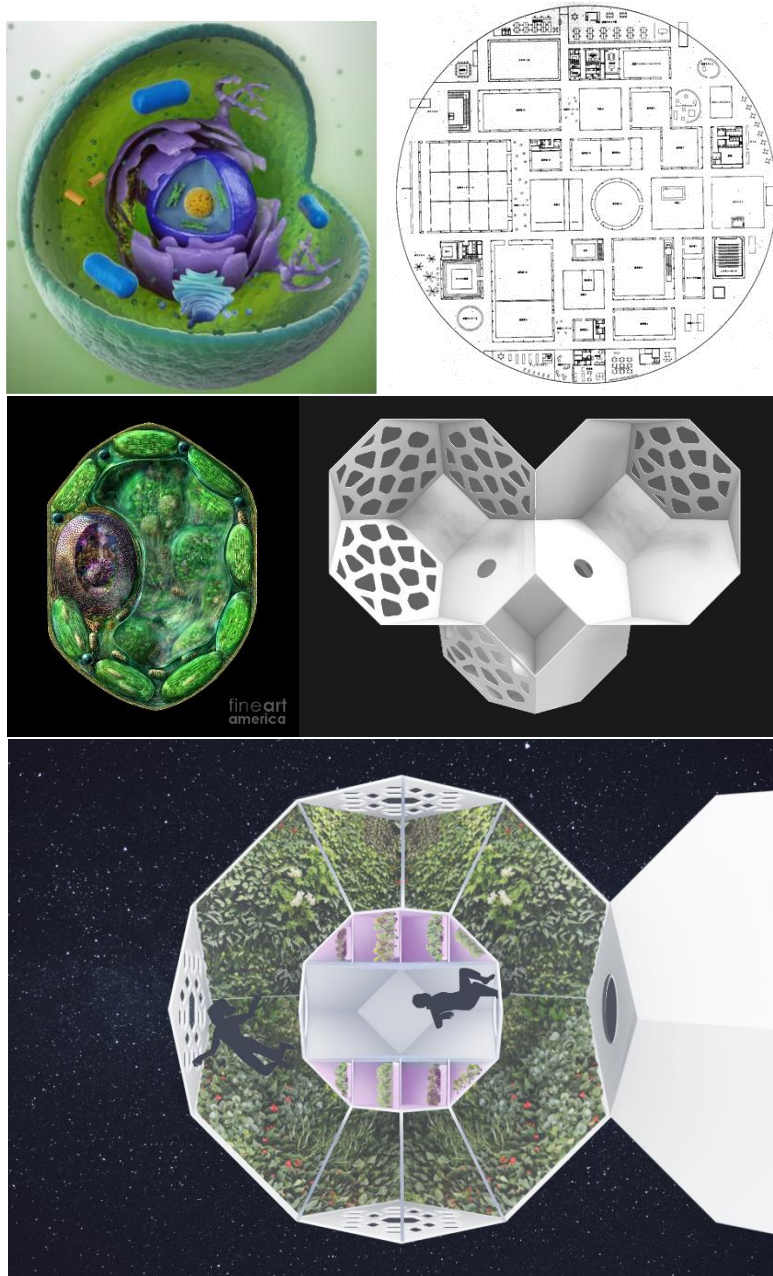


Figure 6-29. Top to Bottom, Left to Right: Artist's render of a living animal cell with nested, self-similar functional zones, or organelles (image credit: Andrzej Wojcicki/ Getty Images); The SANAA Museum of the 21st century plan, showing an alternative allocation of interior space with no particular regard to the nature of the shell; Artist's render of a plant cell (fineart America); Architectural render of several TESSERAE Cell nodes; a TESSERAE Cell node with nested functional areas like organelles (artist's render courtesy of Sana Sharma).

While still under extensive research and development in the broader space industry,^{223,224} cooled superconducting magnets (and other CERN-modeled variants¹³²) have been proposed for active radiation shielding of modules. Neither the TESSERAE Shell tiles nor the Cell nodes currently employ magnets of sufficient size or strength to conceive of using them as a field-generation radiation buffer, but we do note the potential to integrate with larger, sufficiently strong magnets in the future. These magnets could do double duty in creative ways to assist with field generation. Care would have to be taken to limit field strength in the crew cabin to the 2T ceiling recommend by the World Health Organization.²²⁵

While we can readily envision and plan for the geometric packing and even the docking approach (discussed below) to realize multi-unit stations, it is another matter entirely to plan for the integration of shared resources across a mega-structure of many, crystalline-packed TESSERAE nodes. As noted in Geoffrey West's *Scale*,¹ this presupposes that other constituent resource systems (e.g., ECLSS and air purification, water generation, communications) can scale as well through the dense or branch-like amalgam of nodes. From here, we can ask questions like what are the "capillaries" of space ships? What is the maximum reach and physical separation cap of a pipe network of "supply," whether this be electricity or other critical operating supplies (e.g., air to breath, radiative and conductive heat transfer and dissipation)? To do so, we consider three approaches in future work, for a trade study of TESSERAE Cell feasibility:

- The simplest, where each module must be self-sufficient and maintain its own environment, with only limited resource sharing between nodes facilitated by manual, human or robotic occupant transfer;
- One where the plesiohedrons modules include tie-ins connecting fully decentralized resource "pipes" across bonding faces, likely embedded in docking interfaces with valve systems;
- One where a common resource "bank" is established at a central or nexus node of the structure and plesiohedrons can accrete to this, growing up to a maximum distance X (as a function of module diameter) away from the bank before distribution of the resources is strained and placement of another central node is required (see Figure 6-30 for an example of natural, indeterminate growth systems taking this latter approach).



Figure 6-30. Umbrella mushrooms growing incrementally, unit by unit, on a common resource bank of tree bark. Here, the size of the resource bank far outstretches the size of the symbiotic nodes attached to it; for the TESSERAE system, we would expect the sizes to be more similar between node and bank, but the principle remains the same. Image credit: Fern Mock, Pinterest.

In addition to the considerations above, we make the following assumptions in the renders shown below:

- Maximum window diameter should be kept to 80cm (near-term) for consistency with the flight heritage and radiation-mitigation concerns of the ISS Cupola,²²⁶ with the ability to deploy a radiation cover for the window during periods of peak threat like solar storms or coronal mass ejections.
- Both hexagon and square faces can support inter-module docking connections (Figure 6-31). Certain nexus nodes or “spacelocked” nodes (i.e., fully surrounded by other structures) may be augmented in the future with multiple docking interfaces to support connections on all faces and allow interior transit to many other modules. External or more exposed nodes of the crystalline arrangement may feature only a single such interior transit docking interface. A critical feature of this MVU approach is the interoperability and interchangeability with other models. For this, we build on the early work of Baily et al.,²²⁷ Harwood et al.,²²⁸ and Abbot et al.²²⁹ for standardization of interfaces, docking systems and reconfigurable spacecraft, respectively (credit to MIT Systems Engineering Laboratory²³⁰ for the compilation of this particular literature review). Furthermore, decades of ISS interface design exchange and collaboration have led to the International Docking System Standard (IDSS), which guides development of the NASA/Boeing-developed and ISS-deployed International Docking Adaptor (IDA). We intend to base the interoperable docking of multiple TESSERAE Cell nodes on these historical examples, with an eye to recessing as much of the docking hardware as possible to keep to the external profile of the truncated octahedron for dense multi-module packing. Until near-flush mating surfaces can be developed, we anticipate a consistent width of vacuum gap around most of the Cell nodes due to the docking protrusions. The renders below simplify this mating for visual communication purposes and depict a future flush mating surface.
- Exterior, non-window and non-docking faces of the Cell node should be covered with solar panels where feasible.
- A certain benefit will be experienced by “spacelocked” nodes, as the nodes that are entirely encasing them provide a degree of added radiation protection. This leads us to consider placing sensitive research and areas where the crew will spend most of their time closer to the interior of 3D agglomerations. Note that not all TESSERAE Cell stations will feature 3D depth of stacked nodes, however, as linear-axis and 2D station configurations may dominate until resources can provide for module counts in the 10-15 range (14 modules being the minimum for fully encasing a 15th central node).

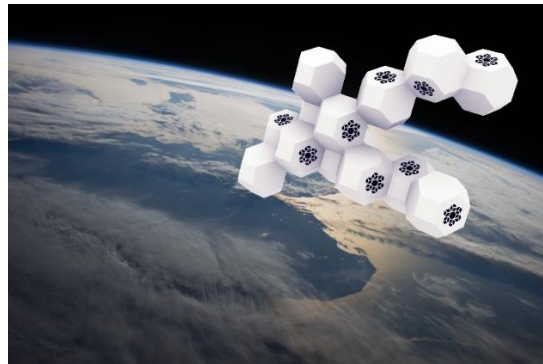


Figure 6-31. Showing prospective TESSERAE Cell station, with nodes assembled in orbit. Artist's render courtesy of Sana Sharma.

As modules accrete and the station grows in size, we anticipate a zone-based growth model, akin to the way that cells accrete and self-organize for tissue differentiation in morphogenesis. Figure 6-32 shows an evolving snapshot of color-coded module accretion by functional zone. In this way, organic, incremental growth of the structure over decades can keep to an organizational principle governed by the human needs and evolving use priorities (e.g. if this particular station becomes a science center, perhaps that zone grows more quickly than the others, around a seed science node with the core resource offerings; alternatively, a station that evolves into a space hotel or transit depot may grow the crew and visitor quarters zone more extensively).

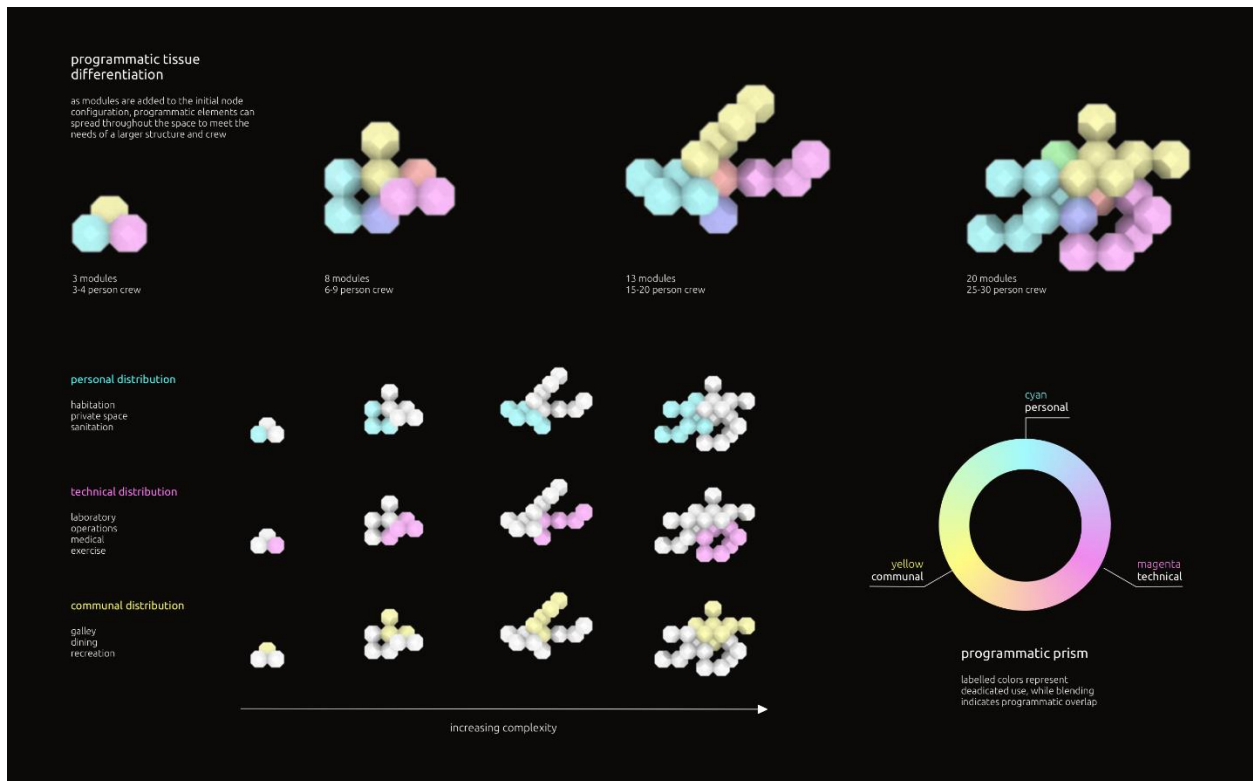


Figure 6-32. Functional zone definition given programmatic needs of the crew, evolving as the station accretes new nodes and expands over time. We tie these programmatic plans to the generative output from the simulation results in Chapter 5, giving a way to connect the morphogenesis tissue differentiation concept to the practical realities of inhabiting a station. Yellow indicates communal space; Cyan indicates private or personal spaces; Magenta indicates technical chambers (e.g., science labs or command centers). Many further categories could be defined and tracked in a similar growth pattern—we choose these three initial categories to align with near-term space habitation priorities. Graphic design courtesy of Sana Sharma.

With the 14 docking faces available on a truncated octahedron, a single “seed” node can dock with several distinct groupings of multiple modules in the next growth generation (say, five modules for “crew quarters,” five for “communal use and facilities,” five for “science operations”). Taking an initial zone size set at five modules, an exponential curve defines the maximum cap of possible bonding faces available for that zone after each generation addition. We start with the theoretical upper ceiling of 13 bonding faces per additional module, as if the additional modules bond only at one site; in practice, we expect less distinct bonding faces available to each generation as modules are likely to bond to neighbors in the same generation, thus reducing their available sites for the subsequent generation. Figure 6-33 presents the theoretical maximum bonding sites²⁰ after four generations of growth, ranging from initial zone group sizes of two modules up to five modules. This shows that the exponentially growing count of available bonding faces in a TESSERAE Cell station will quickly outpace the space industry’s *current* capacity for building and shipping new modules—in essence, we have plenty of room to grow.

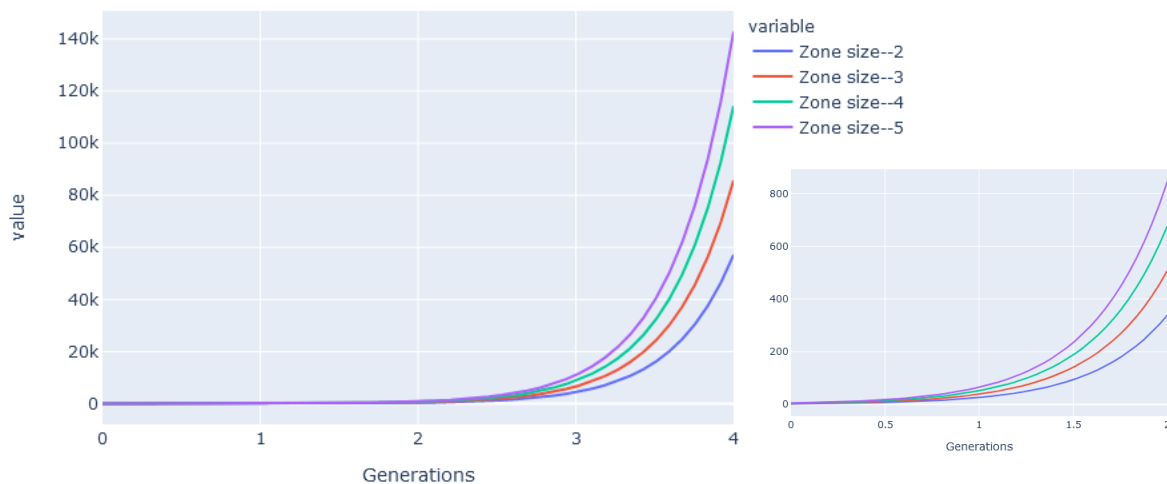


Figure 6-33. Calculated “value” of the count of bonding faces (y-axis) available after increasing generations of module additions (x-axis), predicated on initial zone group size (color series). Inset on the right shows the rapid growth after only two generations. Curve defined by:

$$f(x) = Z * 13^x$$

where Z is initial zone group size

where x is the generation iteration

²⁰ This simplified model does not consider intersections and conflicting growth after many generations.

Assuming a more spatially condensed model (Figure 6-34), where each generation of new zone additions remains densely packed and consumes around half of each nodes' bonding sites, seven bonding sites remain available for the next round. This changes the model as follows, still produces an abundance of bonding sites for station growth:

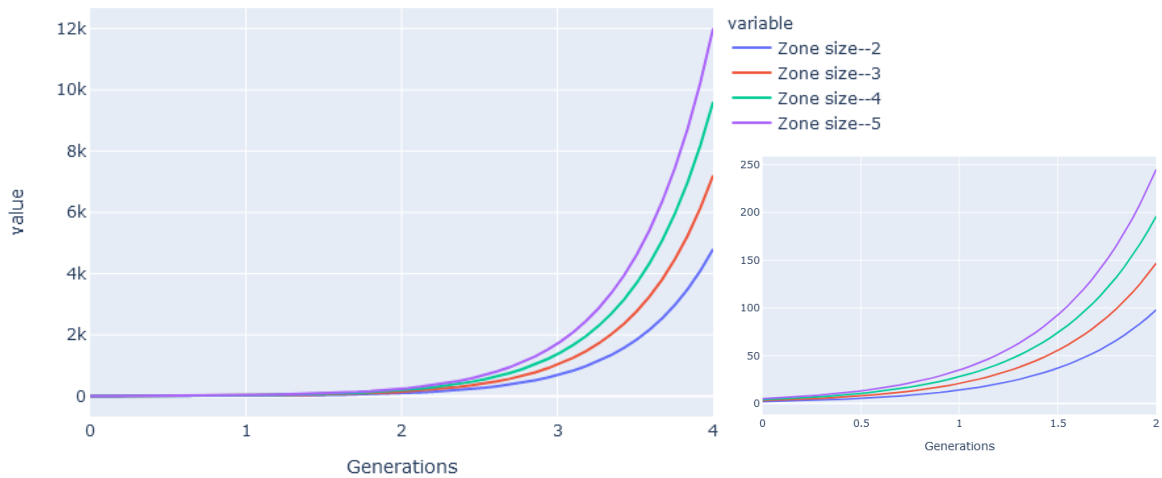


Figure 6-34. Calculated “value” of the count of bonding faces (y-axis) available after increasing generations of module additions (x-axis), predicated on initial zone group size (color series). Inset on the right shows the rapid growth after only two generations. Curve defined by:

$$f(x) = Z * 7^x$$

where Z is initial zone group size

where x is the generation iteration

6.2.3 Extensibility to Other Geometries

Our principle of segmentation and modular accretion for the TESSERAE Cell nodes can be applied to many other shapes (Figure 6-35). As discussed in Chapters 3 and explored briefly in Chapter 4, the self-similarity of fractals provides a promising pattern on which to base iterative growth, as does the geometric repeatability of triply periodic gyroids (e.g., the Schwarz P-structure or G node shown below) and even entirely curvilinear nesting shapes (seen in Greg Lynn’s “blob” structure). Shapes with negative space, like the triply periodic gyroids, could also be used as scaffolds—much as they are in tissue engineering¹⁶¹—to support accreting modules and guide the overall shape and character of a space station. In particular, gyroids of this nature constitute a mathematically defined “minimal surface” of practical benefit to aerospace applications, with minimum surface area material required for a given topology.

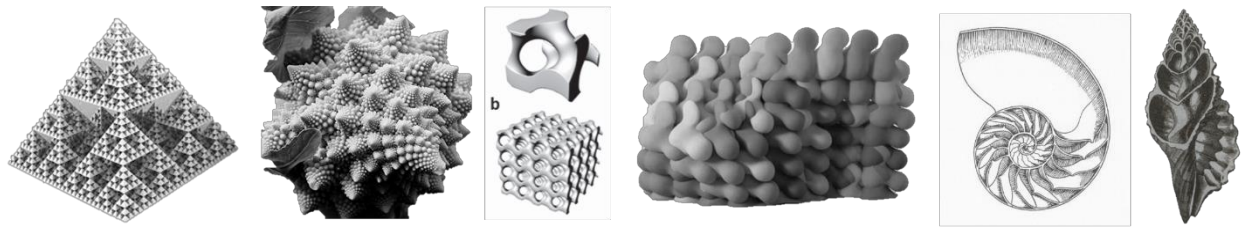


Figure 6-35. A range of forms (see Chapter 4, Section 4.2.2) showing potential focus areas for TESSERAE Cell architecture, from fractals and patterns in nature, to triply periodic gyroids, to the nesting structures of Greg Lynn,⁷² to sea shells.

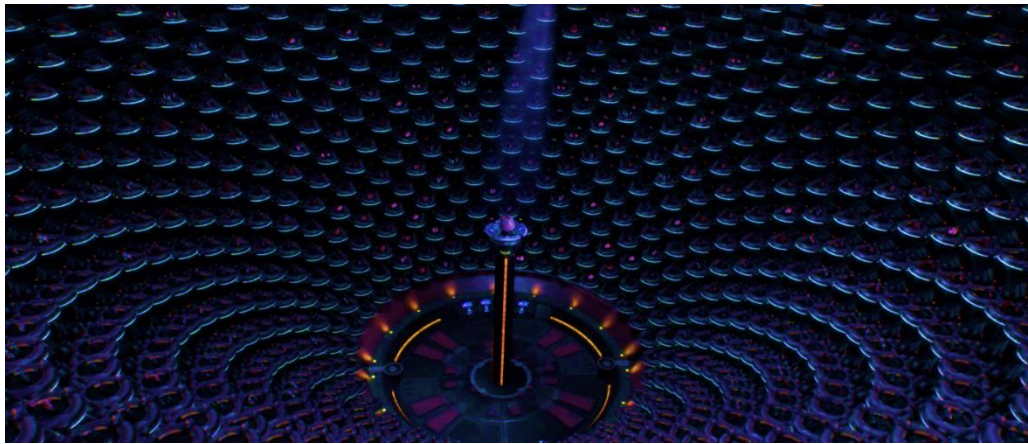


Figure 6-36. An example of parastichy rendered in the Sci Fi universe of Star Wars: the galactic senate chamber.²³¹

These shapes all benefit from constant size base-units, out of which many complex, hierarchical structures can be formed. On the other end of the spectrum, we have irregular organic shapes, like nautilus shells or spiral univalves that still offer a natural subdivision into different chambers. In several cases, these forms offer natural docking geometries and, from the embedded logic of their form, a guide to future growth that could help space planners and future inhabitants achieve a long-term structural goal (rather than say, a random and more opportunist barnacle-like accretion over time).

Through these explorations, we are in search of macrostructures with predictable, even if irregular, base units that facilitate designing space architecture with *centuries of additions in mind*. That means many docking ports in three dimensions, not just in two axes or at one juncture point. In this regard, we can look to examples from human history, where a product of human ingenuity has grown in fits and starts over many generations, but still produces a cohesive structure that is a recognized as a “whole”—the *city*. From modular, dense, desert habitation like the Puebloan hillside dwellings, to modern cities with grid planning, we see incremental, self-similar growth that integrates with existing structures to evolve communities of habitation over centuries. In many metropolises around the world, only the 2D ground surface is fully explored, with the full extent of reaching into 3D often understandably regulated (e.g., to preserve historical character of an old town or central quarter) or dependent on economic status (e.g., feasibility of developing large skyscrapers). When planning the foundation of microgravity space cities, we have an opportunity to think radially from the start, as structures evolve with a new degree of freedom. We have a responsibility to consider the long time horizons inherent to space travel and design patterns of growth that can be self-sustaining. And finally, we can embrace a design challenge—to harness the unique flows of energy in the space environment for architecture that has a

movement (incident photons give movement through light sails, magnetic fields resisting the pressure of a solar wind, station-keeping and attitude control for orbit maintenance) and a rhythm all its own.

6.2.4 Summary: TESSERAE Cell ConOps

When compared with the TESSERAE Shell model, the Cell model offers the benefit of volumetric self-assembly—a more direct approach to habitation space that does not require wait time in orbit for a shell to form. Modules can be prefabricated on the ground, pre-configured on the inside with subsystems and furniture as needed, and self-assembled rapidly in orbit from well-known principles of magnetic docking coupled with the self-aligning joints prototyped and discussed in Chapter 4. This removal of the need for extensive EPM corrective activity will reduce overall system power consumption on-orbit and time to assembly.

The Cell approach creates two main limitations however—the loss of the flat-pack advantage (each Cell module is now constrained by the dimensions of the largest payload fairing available and will not be able to as efficiently fill the fairing volume), and the lack of large, open-area chambers facilitated by shell tiles that create an unconstrained interior volume (e.g., the buckyball). The Cell unit can multi-pack to create a large overall total volume, but the interior experience of this volume will be dominated by walls and segmentation between units. In the near term, this limitation has a silver-lining, as decentralized, small volumes create a safer ConOps where zones can be quickly sealed off during off-nominal events, potentially sparing the other docked modules in a station in an emergency situation. In future work, we will explore a hybrid model with a TESSERAE Shell module as the gathering center point, and TESSERAE Cell nodes accreted on the outside as functional zones. Further, we could merge the two concepts entirely: self-assemble multiple plesiohedron volumetric units from flat-pack shell tiles, and then self-assemble the resulting modules into a crystalline-packed space station.

In summary, we have explored the promise of plesiohedrons' dense packing for future space stations and defined the constituent sub-systems for a TESSERAE Cell MVU. We propose a plan for interoperability and growth curves towards a TESSERAE Cell station. Illustrative renders suggest just a few of the many ways to clad and inhabit these spaces and our discussion of the extensibility to other geometries and irregular, organic shapes maps a large parameter space for further study.

6.3 Integration with NASA mission priorities

In Section 6.3, we consider how the TESSERAE platform contributions map to existing NASA priorities for deep space exploration and how the technology could integrate with near-term missions to the Moon and later to Mars. We also present the intermediate, spin-off concepts associated with certain TESSERAE sub-systems that could contribute to aerospace technology development in other areas and wider benefits to Earth-bound citizens.

6.3.1 TESSERAE Alignment with NASA Strategic Objectives and Roadmaps

Our mission concept directly addresses key priorities for space technology development (STMD) and human exploration (HEOMD and AES), in addition to science operations (SMD) via payloads on TESSERAE modules. Our mission concept described in Section 6.1.1 enables a human-led, hybrid orbit-and-surface operation, supporting NASA’s strategic plan for both returning to the Moon and pushing out to Mars. The engineering contributions and mission concept chosen for this thesis explicitly address Strategic Objective 2.2 in NASA’s 2018 Strategic Plan (“Conduct Exploration in Deep Space, Including to the Surface of the Moon”¹⁸⁰) by developing a new space habitat that will “Extend and Sustain Human Presence and Activities in Space.”²³² We will focus our next phase technology demonstration missions towards supporting mission technology contributions for Gateway and NASA’s Plan for Sustained Lunar Exploration and Development.¹⁷⁹

Though we focus initially on the lunar exploration mission concept, TESSERAE could also support the emerging space tourism economy by supplying scalable, reconfigurable, and affordable habitation space in LEO, and thus also contribute meaningfully to Strategic Objective 2.1 (“Lay the Foundation for America to Maintain a Constant Human Presence in Low Earth Orbit Enabled by a Commercial Market”¹⁸⁰). Our work on TESSERAE focuses primarily on the creation of the buckyball shell, volumetric modules, and accompanying simulation-informed mission architecture, as an extensible platform for multifunctional use in orbit, with reusability for surface operations as well. We do not intend to proscribe a particular habitat function—rather, we aim to make TESSERAE applicable and adaptable for LEO space tourism, lunar orbit in conjunction with the Lunar Gateway, Mars orbit to support on-surface missions, etc.

By assessing mixed-population robot swarms on an inspection target of self-assembling, simulated-structure shells (see Section 6.1.1), we are also advancing progress towards an integrated program of autonomy and technological self-sufficiency for orbiting missions—from the architecture itself to the host of symbiotic robots performing critical life cycle maintenance. This work will help us build towards “trusted autonomy,” a key focus of the Science and Technology Partnership Forum guiding autonomous systems development for lunar missions.²³³

6.3.2 Extensibility and Wider Benefits

While we aim for a habitation-ready deployment in the future, we also note research milestones along the way that will contribute scientific and engineering benefits to other areas of the aerospace field: a novel sensor and communication architecture design applicable to self-assembling CubeSat constellations (a rapidly growing market); a swarm dynamics protocol and modeling for drone/robotics spinoffs; and a new paradigm for in-orbit, modular, autonomous space structures independent of function (with the promise to revolutionize in-space logistics, Section 6.4). Should our full-scale structure succeed, we anticipate a positive impact on the national economy, as our habitation module could help to enable the first significant waves of space tourism and lunar/Mars missions in collaboration with NASA, ESA, SpaceX, Blue Origin, and others. Finally, we anticipate that the architectural design attraction of “geodesic domes in space,” our reference to ancient history

(Roman “tesserae,” “mosaic”), and our homage to modernity’s modularity fascination will “Inspire and Engage the Public in Aeronautics, Space, and Science” (per NASA strategic objective 3.3).¹⁸⁰

We aim to answer the call for visionary ideas that would transform NASA missions with radical breakthroughs, while also benefitting the nation at large; we have thus already begun exploring the TESSERAE concept as a modular, low-cost, easily deployed Earth architecture for areas torn by natural disasters to effectively “Develop and Transfer Revolutionary Technologies to Enable Exploration Capabilities for NASA *and* the Nation” (Strategic Objective 3.1).¹⁸⁰ This work follows in the long tradition of NASA spin-offs coming back down to Earth to benefit a broader population, drawing on the analogs between resource-constrained environments in orbit and on the surface of our planet.

6.4 Applications Beyond Habitats

This research program aims to one-day realize self-assembling space habitats in orbit around Earth, the Moon, and Mars. While we focus on this north star goal, we note a natural extensibility to other microgravity self-assembly contexts, including re-purposing the key technical contributions for autonomous self-assembly of satellites, telescopes or parabolic mirrors, and other in-space infrastructure for space exploration.

6.4.1 Storage Chambers, Space Ports & Logistics Depots

The TESSERAE buckyball Shell and Cell modules can just as easily (and in some cases, with significantly less resource expenditure on ECLSS) be used to store cargo, shipments, and in-space infrastructure as a construction or logistics depot, as speculatively shown in Figure 6-37. With the inclusion of the interoperable docking (Section 6.2.2), large open-volume TESSERAE nodes could serve as multi-access space ports, facilitating re-supply and trade in orbit out of a single large chamber where many visiting spacecraft can berth and access centrally stored resources. The fundamental reconfigurability of the TESSERAE system enables agile retrofitting for evolving logistics needs. We can also envision a recursive functionality, where completed TESSERAE stations include storage of efficiently packed replacement TESSERAE tiles for repair and exchange of tile function.



Figure 6-37. Artist’s render of TESSERAE logistic and storage concept, at scale, in orbit around Mars for a prospective MOSAIC (Mars Orbiting Self-Assembling Interlocking Chambers) mission. Image courtesy of TU Dortmund Fraunhofer Institute, for TESSERAE.

6.4.2. Parabolic Mirrors

Of great interest to the space industry in the near-term, for both astronomy and reconnaissance, parabolic mirrors larger than the largest dimension of a rocket payload fairing have long tested aerospace engineering ingenuity. Teams working on massive telescopes like the JWST (James Webb Space Telescope)²³⁴ are forced to engineer creative origami ConOps to achieve full functionality in orbit, risking tears and failed deploys (like the Skylab solar panel array failure²³⁵). By slightly modifying the TESSERAE hexagon tile geometry to achieve a segmentation of the curvature of circular paraboloids and applying the highly polished mirror surface, we create a unit ready-made for self-assembly of parabolic mirrors. Further work would need to be undertaken in precise jointing design to extreme tolerances (to create a near-unibody mirror out of separate tiles), but the underlying principle of sensor-guided, autonomous self-assembly of shells in orbit lends itself naturally to this application. Furthermore, TESSERAE's reconfigurability enables a modular repair paradigm for parabolic mirrors, should any single unit suffer from a focusing failure like the early days of Hubble.²³⁶

While lower Young's modulus material gradients are planned for the habitat tile edges, to absorb the energy in tile collisions, a refinement of the TESSERAE docking sequence could ensure smooth, safer bonding between mirrored tiles in the expected case of fragile, single-material, rigid units. This modification relies on functionality already embedded in the TESSERAE sensing suite and control actuation logic—the ability to dynamically buffer tile collisions through selective use of the EPM repulsion functionality (discussed in detail in Chapter 4).

In addition to entirely self-assembled parabolic mirrors, we note an opportunity to collaborate with existing research at MIT and NASA Ames, to combine a self-assembled parabolic mirror platform with deformable mirror segment movement for wavefront control and fine tuning the directionality of collimated beams. In concert with TESSERAE self-assembly, the lattice infrastructure construction postulated by Cheung, et al.²³⁷ in Figure 6-38 could facilitate the type of piston, tip and tilt motion used in JWST and the European ELT (Extremely Large Telescope).²³⁸ Together with Sergio Pellegrino's work at Caltech-JPL on self-assembly of other subsystems of modular telescopes,²³⁹ we can readily envision an autonomous, self-assembling mega-telescope in orbit.

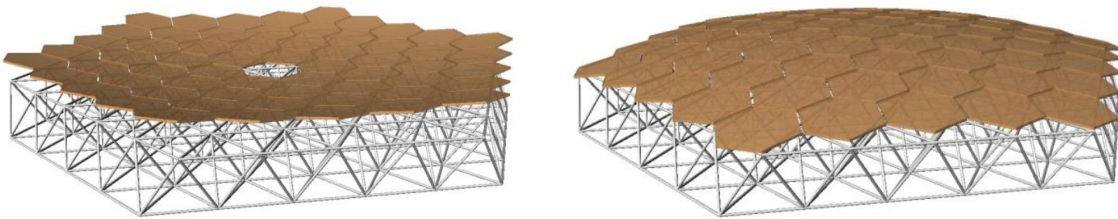


Figure 6-38. Cheung et al. present hierarchical assembly of space structures, applied to parabolic mirrors.

Finally, through coordination with the EPM architecture already supported as a TESSERAE subsystem, we may also be able to explore supporting ferromagnetic fluid mirrors, where certain passive and active induced magnetic fields create smooth “bubble” surfaces out of highly reflective ferrofluid.^{240, 241, 242} Research would need to be undertaken to plan for fluid containment and protection against outgassing (depending on the fluid suspension) in the vacuum.

6.4.3 Satellites

As space launch costs drop and the feasibility of “small-satellite” distributed sensing and imaging improves, the space industry can now support burgeoning interest in satellite swarms across academic, government, and industry labs. Many corporate proposals already explore satellite constellations as the backbone of a global, space-based Internet service, including OneWeb²⁴³ and Space X’s Starlink,²⁴⁴ or for extensive imagery analysis of Earth’s surface, like Planet Labs.²⁴⁵ Government programs, like DARPA’s BlackJack,²⁴⁶ aim to create dynamic communications networks in LEO to supplement reliance on expensive, monolithic GEO satellites. Into this mix, smaller companies like Loft Orbital²⁴⁷ and Open Cosmos²⁴⁸ are helping users deploy custom payloads on a standardized, modular platform, and use software to remotely operate missions once in orbit.²⁴⁹

While these proposals all posit multi-unit satellite “constellations” in orbit, each satellite unit is usually assumed to fly separately (often time-shifted). With TESSERAE’s magnetic docking and sensor-mediated, autonomous self-assembly platform, individual satellite units could be brought together for larger, coordinated purposes—from distributed aperture imaging to achieving modular, re-mixable satellite structures larger than the dimensions of any individual rocket payload fairing (industry examples shown in Figure 6-39). Through adapted use of the TESSERAE EPMS and control algorithm, satellite units could either be brought into direct docking contact or kept at a fixed distance in an array (building on inter-satellite coulomb forces explored in ESA reports⁵⁵).

Research work tangential to this thesis, but emerging from our lab at MIT, has already supervised early stage systems engineering for a rentable, shared-use satellite constellation in orbit (BlockSat²⁵⁰), bringing space assets into the domain of on-demand services like Cloud Computing; we anticipate merging in the hardware and software functionality of TESSERAE to enable self-assembling satellite clusters in LEO and beyond.



Figure 6-39. Related robotic, on-orbit assembly plans with which the TESSERAE Platform could partner. Left—NASA’s 2017 conception of a modular, self-assembling satellite. ²⁵¹ Right—Made in Space’s Archinaut system for additive manufacturing and robotic assembly on-orbit (image credit: MIS).²⁵²

6.5 Extensions of the TESSERAE Paradigm: From Modularity to Continuity

While the primary contributions of the TESSERAE thesis focus on modular self-assembly, in fulfilling the full promise of our new “growth” based design theory, we note an opportunity to extend the TESSERAE paradigm to continuous, rather than solely discrete-part, manufacturing. Section 6.5.1 (Extrusion) briefly describes our preliminary work in these areas and future applications of the *self-aware self-assembly* approach.

6.5.1 Extrusion & the Space Cocoon

Drawing on inspiration from creatures that “self-assemble,” weave, and spin their own homes out of 1D materials, we are pursuing work for a Space Cocoon. This model of self-aware self-assembly relies on a continuous injection of semi-malleable material filament from an extrusion unit (Figure 6-40). Thoughtful design of the extrusion nozzle can produce variably-curved radii for a compound, coiling structure in either a straight-walled cylinder, a sphere, or intermediate variants like an ellipsoid. Much like a caterpillar or larvae spinning a silky cocoon, the material choice for this extrusion must self-bond or be welded (electron beam welding is under consideration for metal materials, due to the benefit of the native space vacuum) at each additional 2D ring layer and depth of overlay, in order to create a closed surface and properly volume-enclosing topology.

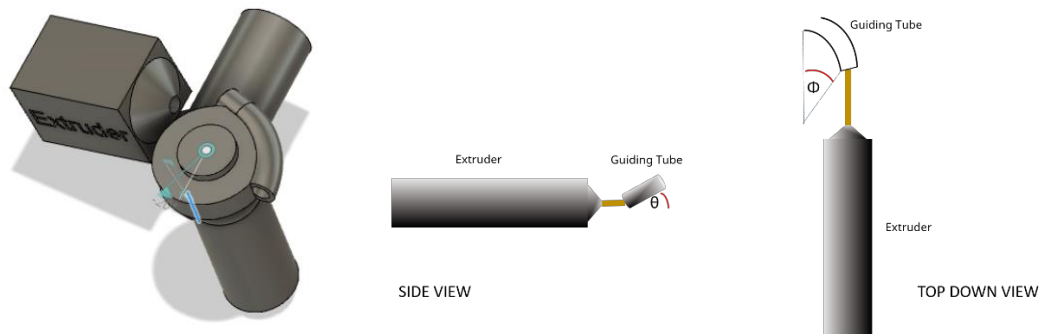


Figure 6-40. Extrusion mechanism with selectively curved guide tube. Two angles (theta, phi) define the angle of the extruded structure relative to the extruding nozzle primary axis and the radius of curvature of each coil rung, respectively. CAD rendering courtesy of MIT UROP Peter Williams.



Figure 6-41. Sample extrusion model process with bonded coils.

Several other mechanisms can be considered for mediating extrusion of the Space Cocoon, including a fixed plate on one or both “tails” of the extruded structure that revolves around its z-axis to twist the filament into overlapping rings. Horizontal travel in the z-axis could be used to form a more compact or looser cocoon, as a technique for compression during assembly. Alternatively, the extrusion apparatus could be made to spin, imparting variable, controllable angular velocity to the extruded material and shape the extent of curvature of each ring that way.

We have applied for NASA SpaceTech-REDDI funding to test a proof-of-concept nozzle and extrusion device for this concept on a 2021 Blue Origin suborbital flight. This approach builds on prior research in microgravity 3D printing²⁵³ and in-space extrusion manufacturing,^{254, 255} improving upon these designs by positing a free-floating system (rather than a containment chamber) and curvilinear compound surface topologies rather than simply open lattices and beams. The broader possibilities for creating complex topologies out of primarily 1D materials^{256, 257, 21} suggests a wide area of application for this technique. The Space Cocoon would benefit from future developments around in-situ resource utilization, where the feedstock for extrusion could be mined and processed from asteroids or other in-space resources; until then, the feedstock would need to be manufactured on the ground and shipped in condensed rolls to the assembly location in orbit. This concept brings 1D materials into the TESSERAE portfolio, thus completing a full suite of options for self-assembly across scales and dimensions: 1D (extrusion from filament into closed-surface topologies), 2D (TESSERAE Shell tiles that join together into a buckyball volume), and 3D (volumetric TESSERAE Cell modules that accrete into a multi-unit packed station).

6.6 Aerospace Mission Architectures Conclusion

Through the TESSERAE research, we aim to create a new paradigm for space architecture that can support a growing human presence in space and respond with agility to evolving mission needs. We aim to avoid reliance on elusive congressional budgets in the future, instead leveraging self-assembly, efficiently designed quasi-stochastic processes for energy and resource conservation, and clever geometries to enable sustainable, indeterminate growth. This chapter presented the TESSERAE Shell and Cell concepts in detail, offering systems engineering mission architecture and feasibility analyses for contextualizing the proposed space structures in realistic aerospace deployments steps and ConOps. We assess the applicability to NASA’s current deep space exploration mission priorities and highlight TESSERAE’s integrated planning for autonomous operation from construction to in-situ servicing and maintenance.

Throughout the robustness and redundancy planning for the TESSERAE Shell and Cell construction, we are compelled to consider adaptations of these mission ConOps for resource-constrained environments on Earth in the face of climate change. We accept and embrace our responsibility for the technologies we develop to benefit life on Earth broadly—and not simply the future microgravity city inhabitants for which we eagerly and speculatively design. We look forward to expanding and adapting the TESSERAE portfolio for a cross-over space and Earth application, focusing on shelter resilience and quick-deploy, robust, reconfigurable architecture.

Our immediate next steps for the in-space TESSERAE mission architecture development will couple closely with the prototype and hardware development in Chapter 4. We aim to progress from production of macroscale tiles (with all self-assembly subsystems integrated), to an on-orbit self-assembly demonstration mission at scale, to partnerships with NASA or space industry partners that can support the extensive engineering required to develop and integrate the many habitat-class subsystems identified in Section 6.2.2 (particularly Figure 6-28—summary chart from ISS systems defining the TESSERAE Cell MVU). We look forward to expanding the

possibility for TESSERAE habitats in the coming years and decades. As related and interdependent technologies in the aerospace engineering and space architecture ecosystem advance beyond our current survivalist mode, we hope to contribute to a period where we can truly delight humans in orbit as master architects aspire to do on Earth today.

With the TESSERAE portfolio, we hope to ignite a new era in the trajectory of space architecture. We look ahead, to the technology needs of the next 10-30 years, to support lunar and martian on-surface operations and to enable the first significant waves of humans transiting and living in microgravity. The ease with which we can deploy, reconfigure, and adapt our habitats will directly impact the success of space missions—from lowering costs, to improving safety via fewer astronaut EVAs, to enabling agile and rapid infrastructure response for operation needs, to finally realizing the beloved megastructures of science fiction. **TESSERAE offers an unprecedented degree of mission flexibility and autonomy—crucial benefits when humans are deployed far away from Earth and space stations cannot be serviced in the way we approach ISS ConOps.** We look forward to active, continuing work across several planned technology demonstration missions and a suite of novel technologies to bring innovation to space structures development in the near term, while also shaping a bold vision for human life and work in orbit—wherever our orbits may be.

7. Conclusion

Chapter 7

“We, all of us, are what happens when a primordial mixture of hydrogen and helium evolves for so long that it begins to ask where it came from...”

– Dr. Jill Tarter

...and where it can go next.

This thesis explored quasi-stochastic, self-aware self-assembly across four primary contribution domains: a novel design theory for space architecture, proof-of-concept development in hardware and software that was tested in the space environment, simulation modeling to translate the hardware concepts to assembly dynamics in orbit at human habitation scale, and finally, a detailed review of feasibility and prospective concepts of operations planning for a near-term, crewed aerospace mission.

The design theory drew heavily from nature, with the principles of indeterminate growth in the plant world influencing all aspects of the thesis—from the design of self-assembling nodes that accrete together like cadherins drawing cells together into tissue, to the division of a space habitat into cellular organelles that define the programmatic use by humans. The reliance on biomimicry extends well beyond that of a metaphor, instead directly guiding technology development choices that are reflected in our overall hardware, controls approach, and mission architecture. The hardware development created an extensible platform with which to test quasi-stochastic self-assembly in microgravity, maturing over four generations of iterative prototyping and four major flight opportunities, culminating in 30 days in orbit. Through the logic embedded in the physicality of the base units (both shape and magnet jointing), and the sensing and control software embedded within each node, we have created a hybrid “algorithm for self-assembly” out of bits and atoms in the space environment. Our simulation models help us build a bridge from the lab hardware development to space structures implementation at scale, elucidating opportunities for optimizations that will make the ultimate realization of such space habitats both timely and realistic, while preserving adaptability. Having proved the convergent nature of our quasi-stochastic system and the associated energy, reconfigurability, and performance benefits, we also showed ways to layer more control back into the system, creating a gradient of stochastic to deterministically-guided self-assembly. This gives us a suite of design options in the future and the ability to tune the TESSERAE platform to the space architect’s particular scenario—all architecture should be responsive to its environment and to the needs of its inhabitants.

The TESSERAE project serves a dual mission—to both reimagine the future of space architecture through growth paradigms and “self-aware self-assembly” writ-large, and to realize near-term, practical incarnations of

these concepts as space habitats. The TESSERAE nodes described in this thesis are one example of a proof-of-concept model platform by which we can achieve discrete, guided self-assembly, in the category of programmable matter at space scale. Our continuing and future work explores both discrete and continuous, guided and unguided self-assembly: discrete, in the model of crystal growth or accretion chemistry, and continuous in the model of extrusion and inflation—though these types of continuous self-assembly generally require an in-situ feedstock and explicit in-situ resource utilization (ISRU). Our hope, through this work, is to suggest a compelling model for indeterminate growth of space architecture. We aim to design, test, and deploy modules that can grow, stack, and expand throughout the expansive physical scales and long-duration time scales associated with space exploration, rather than only across the short time scales known to scoped funding programs at the mercy of changing political winds. It is through such a paradigm that we can conceive of creating humanity’s first space monuments, microgravity concert halls, and orbiting cathedrals. This thesis has discussed a design theory for “growing” space architecture through agentless and swarm-inspired self-assembly, presented a condensed literature review of the giants on whose shoulders we stand, offered a view into our prototype engineering and space environment testing, and closed with our mission ConOps and interior design work to adapt our structures to the real constraints of human habitation.

We note a natural extensibility to multiple microgravity and surface exploration environments and we aim to develop TESSERAE as an extensible platform for decades—maybe even centuries—of space exploration. After all, our own Earth self-assembled due to gravity and planetary accretion. We welcome the daunting realities and harsh design constraints of the environment in which we will be operating, we accept the challenge of securing funding for a project like TESSERAE over the 10 years it may take to develop the first human-ready, space-ready deployment, and we embrace the long road ahead of us for the many further technology demonstration missions necessary to fully execute this concept—because anything we can do to help realize the future of interplanetary civilization for humanity is worth it.

And if you’re left asking why—why space habitats, why space exploration at all—we venture out into the near-Earth cocoon of low Earth orbit, into the near reaches of our solar system, and perhaps one day even further into our galaxy, to expand our spheres of self-awareness. To boldly go where no one has gone before, yes, but also as part of our uniquely human search for new knowledge and to better understand our place in the Cosmos. As Bill Anders famously observed, looking back at the Earth from his Apollo 8 capsule:

*“We came all this way to explore the Moon,
and the most important thing is that we discovered the Earth.”*

Appendix: the MIT Space Exploration Initiative

“Make it So” – Captain Jean-Luc Picard

The public grand opening of Space draws near. The dropping costs of space launches, proliferation of new plans for commercial space stations, and a rush of deep space mission planning all enable a new mode of engagement in low Earth orbit and beyond. What was once an exclusive, expensive, and narrowly serious pursuit is now evolving to include a vast array of possibilities. New ventures in space will impact everyday life on Earth, with the potential to unify us independent of boundaries, cultures, and economies; these new ventures are opportunities to look beyond near-term interests to global and interplanetary opportunities as we enter the New Space Age.

With humanity on the cusp of interplanetary civilization, we are actively building the technologies, tools, and human experiences of our sci-fi space future. The Space Exploration Initiative, founded out of MIT Media Lab, champions the freedom and ingenuity to explore risky, creative, next-generation projects that would not be explored elsewhere, with the capacity to pull in key industry collaborators with deep expertise. This opportunity to design, build, and deploy our interplanetary lives beckons to us—our collective creativity strives to bring science fiction to life.

We build on the spirit of the Media Lab, uniting artists, scientists, engineers, and designers to build a real-life *Starfleet Academy* (inspired by the iconic institution from Star Trek). We are creating space technologies that envision a bold and culturally rich “new space age,” from astro-bacteria wearables, to dynamically rentable and multi-functional space satellite constellations, to musical instruments for our space voyages, to self-assembling autonomous space habitats, to advanced reduced-gravity agriculture, and 3D bio-printing. Our goal is to invent, create, and deploy ideas that seem exotic and impossible today, but could be commonplace in ten years. The philosophy of democratizing access to space exploration—bringing moonshots and starshots into the purview of hackers and makers—courses through our work and guides both our research platform and our extensive STEAM outreach efforts. The Space Exploration Initiative supports: 40+ research projects and over 20 PIs at MIT; a cadence of regular parabolic flights, suborbital, and orbital launch research deployments; and an annual flagship event connecting space visionaries of all disciplines (“Beyond the Cradle”).

To learn more: explore-space.media.mit.edu

I founded the MIT Media Lab's Space Exploration Initiative (SEI) in 2016. The SEI began as a grass-roots effort bringing graduate students together to prototype and realize our sci-fi space future. I have since grown the team to 50+ students, staff, and faculty with a global network of collaborators, astronaut advisors, and senior leaders in the space industry. We work closely with and serve PIs and researchers in departments across MIT, including AeroAstro, EAPS, Architecture, Sloan, and others, and have collaborated on outreach projects with MIT's Lincoln Laboratory. The SEI aspires to function as a launchpad for innovative space research, engineering, design, and art across MIT, while exploring both deep-space and Earth-conscious projects. Below, you'll find a selection of our milestone highlights and a view into the exceptional team behind this endeavor over the last four years. We're just getting started and look forward to the years ahead!



Figure 0-1. The SEI's first parabolic flight in 2017.

We charter the full plane and fly 25 researchers, with 12-15 research projects depending on the year.



Figure 0-2. Photos from 2017 and 2019 flights, showing left to right: co-creator of Telemetron, Nicole L'huillier; SEI advisor Joe Paradiso; SEI Research Affiliate and ret. NASA Astronaut Cady Coleman with Juliet Wanyiri working on her Space Enabled cubesat propellant experiment. Images courtesy of Steve Boxall.



Figure 0-3. The SEI sent six payloads into space with Blue Origin on their New Shepard suborbital rocket in May 2019. This deployment marked the Media Lab's first ever rocket launch.



Figure 0-4. A research showcase in the fall of 2019 at the Media Lab shows the breadth of the SEI portfolio, from an August 2019 parabolic flight, to the Blue Origin launch, to projects funded by NASA-supported TRISH (Translational Research Institute for Space Health).



Figure 0-5. A shot of the SpaceX Dragon capsule that delivered five SEI payloads to the International Space Station in March 2020.

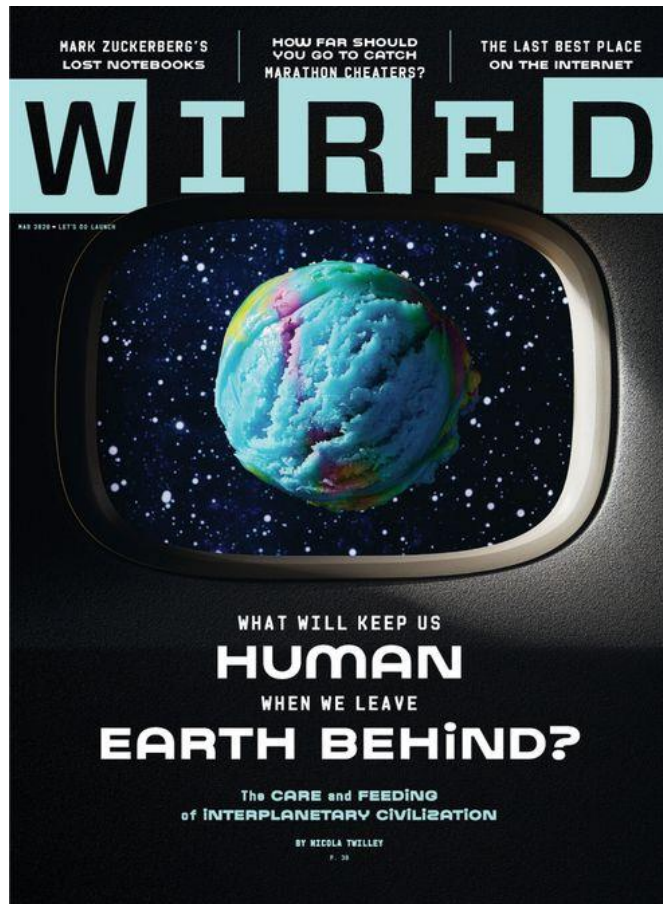


Figure 0-6. SEI space gastronomy research, led by Maggie Coblentz, was featured on the cover of WIRED in March 2020.

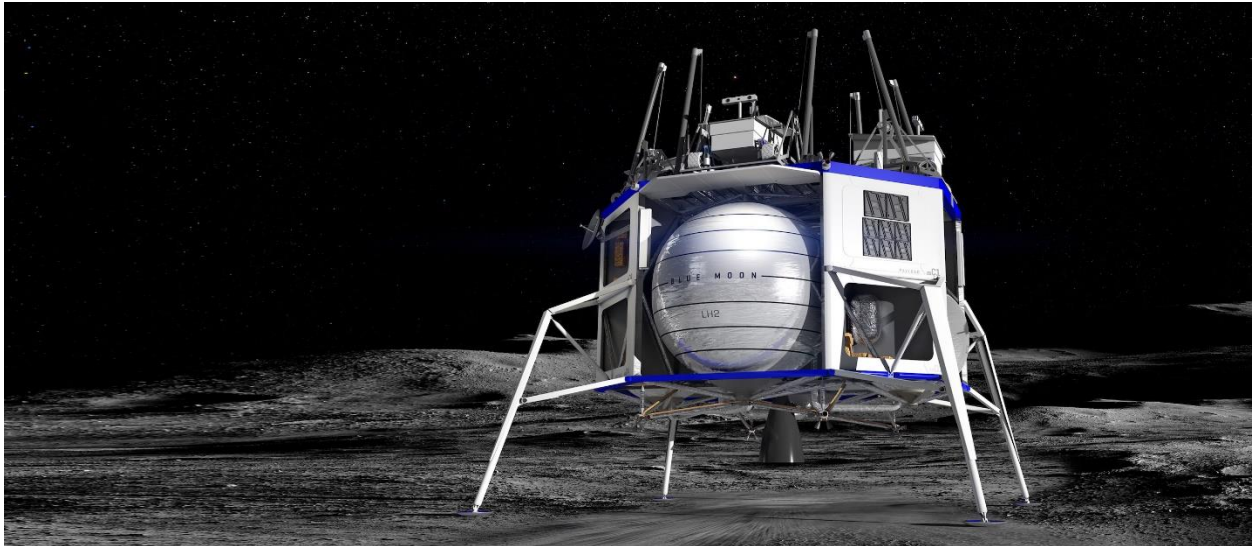


Figure 0-7. The SEI is working towards a lunar surface mission under an MIT MOU with Blue Origin for their Blue Moon Mission in 2024. In 2019, we celebrated the 50th anniversary of the Apollo 11 moon landing, as we look towards the future of interplanetary civilization.



Figure 0-8. A selection of highlights from our annual, flagship event *Beyond the Cradle* (an homage to Konstantin Tsiolkovsky's quote: "Earth is the cradle of humanity, but one cannot remain in the cradle forever."). We gather over 60 leading visionaries—from astronauts to CEOs, from science fiction writers and Hollywood producers to JPL scientists—to co-design the future of life in space together.



THANK YOU: SPACE EXPLORATION INITIATIVE TEAM
 50+ GRADUATE STUDENTS, STAFF, FACULTY, AND ASTRONAUTS



Figure 0-9. Top: The SEI team through the early years (2016, 2017, 2019). Bottom: Current staff, advisors, and selection of our broader community members.



Figure 0-10. The Space Exploration Initiative brings people together in service of humanity’s opportunity to explore our cosmos. Joining Margaret Hamilton on the anniversary of the Apollo 11 moon landing, in the great company of Erika Wagner, Dava Newman, and Jessy Kate Schingler (Top), we are reminded both of the promise of space exploration and our responsibility to Earth’s citizens (Bottom: Iconic Earthrise photo, NASA). As Margaret has noted, reflecting on her time contributing to the Apollo Guidance Computer: “Looking back, we were the luckiest people in the world. There was no choice but to be pioneers; no time to be beginners.”

We stand on the shoulders of giants.

Bibliography

-
- ¹ West, Geoffrey. *Scale: the universal laws of growth, innovation, sustainability, and the pace of life in organisms, cities, economies, and companies*. Penguin, 2017.
- ² Mandelbrot, Benoit B. *The fractal geometry of nature*. Vol. 1. New York: WH freeman, 1982.
- ³ Thompson, Darcy Wentworth. *On growth and form*. (1917). [Page numbers from Cambridge University Press, 1942 edition].
- ⁴ Hillis, Danny. "The enlightenment is dead, long live the entanglement." *Journal of Design and Science* (2016).
- ⁵ The Long Now Foundation. [Online] Accessed 5 August 2020. Available: <http://longnow.org/>
- ⁶ Oxman, Neri. "Material-based design computation." PhD diss., Massachusetts Institute of Technology, 2010.
- ⁷ Oxman, Neri. "Templating design for biology and biology for design." *Architectural Design* 85, no. 5 (2015): 100-107.
- ⁸ T. McNulty. Adapting Biomimicry for Designing Aerospace Materials. Lecture Presentation. NASA NIEA, 2017.
- ⁹ Keating, Steven John. "From bacteria to buildings: additive manufacturing outside the box." PhD diss., Massachusetts Institute of Technology, 2016.
- ¹⁰ Grzybowski, Bartosz A., Adam Winkleman, Jason A. Wiles, Yisroel Brumer, and George M. Whitesides. "Electrostatic self-assembly of macroscopic crystals using contact electrification." *Nature materials* 2, no. 4 (2003): 241.
- ¹¹ Bowden, Ned, Andreas Terfort, Jeff Carbeck, and George M. Whitesides. "Self-assembly of mesoscale objects into ordered two-dimensional arrays." *Science* 276, no. 5310 (1997): 233-235.
- ¹² Whitesides, George M., and Mila Boncheva. "Beyond molecules: Self-assembly of mesoscopic and macroscopic components." *Proceedings of the National Academy of Sciences* 99, no. 8 (2002): 4769-4774.
- ¹³ Whitesides, George M., and Bartosz Grzybowski. "Self-assembly at all scales." *Science* 295, no. 5564 (2002): 2418-2421.
- ¹⁴ Hachohen, Adar, Iddo Hanneil, Yasha Nikulshin, Shuki Wolfus, Almogit Abu-Horowitz, and Ido Bachelet. "Meshing complex macro-scale objects into self-assembling bricks." *Scientific reports* 5 (2015): 12257.
- ¹⁵ Domingos, Jorge LC, François M. Peeters, and W. P. Ferreira. "Self-assembly of rigid magnetic rods consisting of single dipolar beads in two dimensions." *Physical Review E* 96, no. 1 (2017): 012603.
- ¹⁶ Falvello, A. and Tibbits, S. (2013) "Biomolecular, Chiral and Irregular Self-Assemblies," *In Proceedings of the Association for Computer Aided Design in Architecture 2013: Adaptive Architecture*, Waterloo, Canada.
- ¹⁷ Tibbits, Skylar, and Kenny Cheung. "Programmable materials for architectural assembly and automation." *Assembly Automation* 32, no. 3 (2012): 216-225.

-
- ¹⁸ Biased Chains. MIT Self-assembly Lab. [Online] Accessed 25 May 2017. <http://www.selfassemblylab.net/BiasedChains.php>
- ¹⁹ Erik D. Demaine, Sándor Fekete, Christian Scheffer, and Arne Schmidt, “New Geometric Algorithms for Fully Connected Staged Self-Assembly”, *Theoretical Computer Science*, volume 671, April 2017, pages 4–18.
- ²⁰ Erik D. Demaine, Sarah Eisenstat, Mashhood Ishaque, and Andrew Winslow, “One-Dimensional Staged Self-Assembly”, *Natural Computing*, volume 12, number 2, 2013, pages 247–258.
- ²¹ Cheung, Kenneth C., Erik D. Demaine, Jonathan R. Bachrach, and Saul Griffith. "Programmable assembly with universally foldable strings (moteins)." *IEEE Transactions on Robotics* 27, no. 4 (2011): 718-729.
- ²² Haghghat, Bahar, Emmanuel Droz, and Alcherio Martinoli. "Lily: A miniature floating robotic platform for programmable stochastic self-assembly." In *Robotics and Automation (ICRA), 2015 IEEE International Conference on*, pp. 1941-1948. IEEE, 2015.
- ²³ Gilpin, Kyle, Ara Knaian, and Daniela Rus. "Robot pebbles: One centimeter modules for programmable matter through self-disassembly." In *Robotics and Automation (ICRA), 2010 IEEE International Conference on*, pp. 2485-2492. IEEE, 2010.
- ²⁴ Bonabeau, Eric, Directeur de Recherches Du Fnrs Marco, Marco Dorigo, and Guy Theraulaz. *Swarm intelligence: from natural to artificial systems*. No. 1. Oxford university press, 1999.
- ²⁵ Hoff, Nicholas R., Amelia Sagoff, Robert J. Wood, and Radhika Nagpal. "Two foraging algorithms for robot swarms using only local communication." In *2010 IEEE International Conference on Robotics and Biomimetics*, pp. 123-130. IEEE, 2010.
- ²⁶ Rubenstein, Michael, Alejandro Cornejo, and Radhika Nagpal. "Programmable self-assembly in a thousand-robot swarm." *Science* 345, no. 6198 (2014): 795-799.
- ²⁷ Thalamy, Pierre, Benoît Piranda, and Julien Bourgeois. "A survey of autonomous self-reconfiguration methods for robot-based programmable matter." *Robotics and Autonomous Systems* 120 (2019): 103242.
- ²⁸ Knaian, A.N. “Electropermanent magnetic connectors and actuators: devices and their application in programmable matter.” Doctoral dissertation, Massachusetts Institute of Technology, 2010.
- ²⁹ Gershenfeld, Neil. “Programmable Surfaces.” MASSACHUSETTS INST OF TECH CAMBRIDGE CAMBRIDGE United States, 2014.
- ³⁰ E. Hawkes, B. An, N. M. Benbernou, H. Tanaka, S. Kim, E. D. Demaine, D. Rus, and R. J. Wood, “Programmable matter by folding”, *Proceedings of the National Academy of Sciences of the United States of America*, volume 107, number 28, 2010, pages 12441–12445.
- ³¹ Feynman, Richard P. "There's plenty of room at the bottom." *California Institute of Technology, Engineering and Science magazine* (1960).
- ³² Drexler, K. Eric. *Nanosystems: molecular machinery, manufacturing, and computation*. John Wiley & Sons, Inc., 1992.
- ³³ Stephenson, Neal. *The Diamond Age*. Penguin UK, 1998.
- ³⁴ Bobrow, Jonathan. “AutomaTiles: tangible cellular automata for playful engagement with systems thinking.” PhD Dissertation, Massachusetts Institute of Technology, 2016.

-
- ³⁵ “Responsive Environments” Group, PI Joe Paradiso, at the MIT Media Lab. [Online] Accessed 5 August 2020. Available: resenv.media.mit.edu
- ³⁶ Lifton, Joshua, Deva Seetharam, Michael Broxton, and Joseph Paradiso. "Pushpin computing system overview: A platform for distributed, embedded, ubiquitous sensor networks." In *International Conference on Pervasive Computing*, pp. 139-151. Springer, Berlin, Heidelberg, 2002.
- ³⁷ Lifton, Joshua, Michael Broxton, and Joseph A. Paradiso. "Distributed sensor networks as sensate skin." [Tribble] In *SENSORS*, 2003 IEEE, vol. 2, pp. 743-747.
- ³⁸ Paradiso, J.A., Lifton, J., and Broxton, M., “Sensate Media - Multimodal Electronic Skins as Dense Sensor Networks,” *BT Technology Journal*, 22(4), October 2004, pp. 32-44.
- ³⁹ Mayton, Brian, Gershon Dublon, Spencer Russell, Evan F. Lynch, Don Derek Haddad, Vasant Ramasubramanian, Clement Duhart, Glorianna Davenport, and Joseph A. Paradiso. "The networked sensory landscape: Capturing and experiencing ecological change across scales." *Presence: Teleoperators and Virtual Environments* 26, no. 2 (2017): 182-209.
- ⁴⁰ Permanent Electromagnets. APW. [Online] Accessed 29 July 2020. Available: <https://apwelectromagnets.com/permanent-electromagnets/>
- ⁴¹ Permanent Electromagnets – 63mm.” APW. [Online] Accessed 10 October 2018. Available: <https://apwelectromagnets.com/files/attachments/505/EML63mm-xx.pdf>
- ⁴² Permanent Electromagnets.” Magma Magnets. [Online] Accessed 10 October 2018. Available: <http://www.magmamagnets.com/electromagnets-solenoids/permanent-electromagnets/>
- ⁴³ Polymagnet. [Online] Accessed 29 July 2019. Available: <http://www.polymagnet.com/>
- ⁴⁴ Cheung, Kenneth C and Neil Gershenfeld. “Reversibly assembled cellular composite materials.” *Science* 341, no. 6151 (2013): 1219-1221.
- ⁴⁵ Langford, Will, Amanda Ghassaei, and Neil Gershenfeld. “Automated Assembly of Electronic Digital Materials.” In *ASME 2016 11th International Manufacturing Science and Engineering Conference*, pp. V002T01A013-V002T01A013. American Society of Mechanical Engineers, 2016.
- ⁴⁶ Nadya Peek, Rehmi Post, and Neil Gershenfeld, Functional Digital Materials for Electromagnetic Structures and Circuits, *Progress In Electromagnetics Research Symposium (PIERS)*, pp. 721-722 (2012).
- ⁴⁷ Langford, Will, Amanda Ghassaei, Ben Jenett, and Neil Gershenfeld. "Hierarchical assembly of a self-replicating spacecraft." In *Aerospace Conference, 2017 IEEE*, pp. 1-10.
- ⁴⁸ Jenett, Benjamin, Christine Gregg, Daniel Cellucci, and Kenneth Cheung. "Design of multifunctional hierarchical space structures." In *Aerospace Conference, 2017 IEEE*, pp. 1-10.
- ⁴⁹ Otero, Alvar Saenz, Allen Chen, David W. Miller, and Mark Hilstad. "SPHERES: Development of an ISS laboratory for formation flight and docking research." In *Proceedings, IEEE Aerospace Conference*, vol. 1, pp. 1-1. IEEE, 2002.
- ⁵⁰ Howard, N. and Nguyen, H.D., National Aeronautics and Space Administration (NASA), 2010. Magnetic capture docking mechanism. U.S. Patent 7,815,149.
- ⁵¹ Jing Pei, Luke Murchison, Victor Stewart, James Rosenthal, Drew Sellers, Mark Banchy, Adam BenShabat, Ryan Elandt, David Elliott, and Adam K. Weber. "Autonomous Rendezvous and Docking of

Two 3U Cubesats Using a Novel Permanent-Magnet Docking Mechanism", *54th AIAA Aerospace Sciences Meeting, AIAA SciTech Forum*, (AIAA 2016-1465).

⁵² Kong, Edmund Mun Choong. "Spacecraft formation flight exploiting potential fields." PhD diss., Massachusetts Institute of Technology, 2002.

⁵³ Gettliffe, Gwendolyn Vines. "Stability analysis of electromagnetically supported large space structures." PhD diss., Massachusetts Institute of Technology, 2015.

⁵⁴ NISSER, Martin, Dario IZZO, and Andreas BORGGRAEFE. "An Electromagnetically Actuated, Self-Reconfigurable Space Structure." *JSASS Aerospace Tech.* Japan 14 (2017): 1-9.

⁵⁵ Pettazzi, Lorenzo and Hans Kruger, Stephan Theil, Dario Izzo. "Electrostatic Forces for swarm satellite navigation and reconfiguration." ESA final report, 2008.

⁵⁶ Oung, Raymond, and Raffaello D'Andrea. "The distributed flight array." *Mechatronics* 21, no. 6 (2011): 908-917.

⁵⁷ [SELECT CHAPTERS] Bekey, Ivan. *Advanced space system concepts and technologies: 2010-2030+*. AIAA, 2003.

⁵⁸ Minovitch, Michael A. Inflatable core orbital construction method and space station. U.S. Patent 4,730,797, issued March 15, 1988.

⁵⁹ Massey, Jonathan (2012). "Buckminster Fuller's Reflexive Modernism". *Design and Culture*. 4 (3): 325–344.

⁶⁰ Aldersey-Williams, Hugh. *The most beautiful molecule: The discovery of the buckyball*. John Wiley & Sons Incorporated, 1995.

⁶¹ Baldwin, J. "Dymaxion House." Buckminster Fuller Institute. [Online] Accessed 29 July 2020 Available: <https://www.bfi.org/about-fuller/big-ideas/dymaxion-world/dymaxion-house>.

⁶² Fuller, R. Buckminster. *Operating manual for spaceship earth*. Estate of R. Buckminster Fuller, 2008.

⁶³ Buckminster, Fuller Richard. "Laminar geodesic dome." U.S. Patent 3,203,144, issued August 31, 1965.

⁶⁴ Blackburn, Simon. "Structuralism." (2008).

⁶⁵ Foucault, Michel, and Neil Leach. "Rethinking architecture: A reader in cultural theory." (1997): 330.

⁶⁶ Koolhaas, Rem; Obrist, Hans U (2011), *Project Japan Metabolism Talks...*, London: Taschen

⁶⁷ Dadkhah, Negin, Hadi Safaeipour, and Gholamhossein Memarian. "Traditional Complex Modularity in Islamic and Persian Architecture: Interpretations in Muqarnas and Patkâné Crafts, Focusing on their Prefabricated Essence." In *Proceedings of 2012 ACSA FALL CONFERENCE—Offsite: Theory And Practice Of Architectural Production* (Temple University, Philadelphia, PA, 27–29 September 2012).

⁶⁸ Pope, Arthur Upham. "Persian architecture." George Braziller. Inc, New York (1965).

⁶⁹ Schindler House. MAK Center for Art, Architecture, Los Angeles. [Online] Accessed 29 July 2020. Available: <https://makcenter.org/sites/schindler-house/>

⁷⁰ Umberto Eco. *Opera Aperta* (Open Work), 1962

⁷¹ Gibson, Lorna J., and Michael F. Ashby. *Cellular solids: structure and properties*. Cambridge university press, 1999.

-
- ⁷² Lynn, Greg. "Outside the terrestrial sphere Greg Lynn FORM: NOAH (new outer atmospheric habitat) and new city." *Architectural Design* 84, no. 6 (2014): 82-89.
- ⁷³ Julia Koerner's Space Collective (Greg Lynn studio). [Online] Accessed 29 July 2020. Available: <https://www.juliakoerner.com/architecture-space-collective>
- ⁷⁴ Oxman, Neri. "Towards a material ecology." In *32nd Annual Conference of the Association for Computer Aided Design in Architecture (ACADIA)*, San Francisco. 2012.
- ⁷⁵ Kellert, Stephen R., and Edward O. Wilson, eds. "*The biophilia hypothesis.*" Island Press, 1993.
- ⁷⁶ McNulty, T., D. Bhate, A. Zhang, M. A. Kiser, L. Ferry, A. Suder, S. A. Bhattacharya, and P. Boradkar. "Framework for the Design of Biomimetic Cellular Materials for Additive Manufacturing." In *Proceedings of the 2017 Annual International Solid Freeform Fabrication Symposium, Austin, TX, USA*, pp. 7-9. 2017.
- ⁷⁷ Tsiolkovsky, Konstantin. "*Speculations between Earth and Sky.*" Moscow. 1895.
- ⁷⁸ Nixon, David. "*International Space Station: Architecture Beyond Earth.*" Circa Press, 2016.
- ⁷⁹ J. J. Watson, T. J. Collins, and H. G. Bush, "A history of astronaut construction of large space structures at NASA Langley Research Center," in *Aerospace Conference Proceedings, International Conference on*, IEEE 2002, vol. 7, pp. 7
- ⁸⁰ Aguirre, E., "Prof Awarded NASA Grant to Develop Building Blocks for Use in Space Missions," UMASS Lowell, 2015. [Online] Accessed 23 November 2017. Available: <https://www.uml.edu/Research/news/Hansen-NASA-grant.aspx>.
- ⁸¹ "Bigelow Expandable Activities Module (BEAM)," Bigelow Aerospace and NASA, [Online] Accessed 10 October 2018. Available: <https://www.nasa.gov/content/bigelow-expandable-activity-module>.
- ⁸² "B330: XBASE." Bigelow Aerospace. [Online] Accessed 30 July 2020. Available: <https://bigelowaerospace.com/pages/b330/>
- ⁸³ "James Webb Space Telescope." NASA. [Online] Accessed December 9, 2018. Available: <https://jwst.nasa.gov/newtechnology.html>
- ⁸⁴ "Starshade." NASA JPL. [Online] Accessed December 9, 2018. Available: <https://science.jpl.nasa.gov/projects/Starshade/>
- ⁸⁵ Pehrson, Nathan A., and Jeremy Banik. "Folding Approaches for Tensioned Precision Planar Shell Structures." In *2018 ALAA Spacecraft Structures Conference*, p. 1439. 2018.
- ⁸⁶ Trotti, G. "Rice University Space Station Study: An Investigation of the Needs and the Design of an Orbiting Space Station with Growth Capabilities," 1976.
- ⁸⁷ de Weck, Olivier, William Nadir, Justin Wong, Gergana Bounova, and Thomas Coffee. "Modular structures for manned space exploration: The truncated octahedron as a building block." In *1st Space Exploration Conference: Continuing the Voyage of Discovery*, p. 2764. 2005.
- ⁸⁸ Frisina, W., "Close-Pack Modules for Manned Space Structures," *Journal of Spacecraft and Rockets*, Vol. 22, No. 5, 1985, pp. 583–584.
- ⁸⁹ Frisina, W., "Modular Spacecraft," *Journal of Aerospace Engineering*, Vol. 7, No. 4, October 1994, pp. 411–416.

-
- ⁹⁰ Baily, S., Nelson, R. R., and Stewart, W. B., "Interface Standards for Spacecraft As a Means of Enhancing On-Orbit Servicing," *Proceedings of the 18th Annual Electronics and Aerospace Systems Conference, Piscataway, New Jersey*, 1985, pp. 351–355.
- ⁹¹ Harwood, O. P. and Ridenoure, R. W., "A Universal Orbital Docking and Berthing System," *The Case for Mars IV: The International Exploration of Mars, Mission Strategy and Architectures*, edited by T. R. Meyer, Vol. 89, American Astronautical Society, San Diego, California, 1990, pp. 613–630.
- ⁹² Abbott, R. and Aceves, M., "Self-engaging Connector System for Robotic Outposts and Reconfigurable Spacecraft," *Proceedings of the 2002 IEEE Aerospace Conference*, Vol. 5, Piscataway, New Jersey, 2002, pp. 2165–2170.
- ⁹³ Saleh, J.H., Hastings, D.E., and D.J. Newman, "Flexibility in System Design and Implications for Aerospace Systems," *Acta Astronautica*, vol. 53, pp 927-944, 2003.
- ⁹⁴ Parkinson, R. C., "Why space is expensive - operational/economic aspects of space transport," *Journal of Aerospace Engineering*, Vol. 205, No. G1, 1991, pp. 45–52
- ⁹⁵ Kugler, Justin, Juliana Cherston, Eric R. Joyce, Paul Shestople, and Michael P. Snyder. "Applications for the Archinaut In Space Manufacturing and Assembly Capability." In *ALAA SPACE and Astronautics Forum and Exposition*, p. 5365. 2017.
- ⁹⁶ Lunar Orbital Platform – Gateway. NASA. [Online] Accessed 30 July 2020. Available: <https://www.nasa.gov/feature/deep-space-gateway-to-open-opportunities-for-distant-destinations/>
- ⁹⁷ Axiom Commercial Space Station. Axiom Space. [Online] Accessed 30 July 2020. Available: <https://www.axiomspace.com/axiom-station>
- ⁹⁸ Adams, Constance M. "Defining the human domain: the process of architectural integration in long-duration space facilities." *SAE transactions* (1998): 992-999.
- ⁹⁹ Sherwood, Brent. "Lunar architecture and urbanism." *SAE transactions* (2005): 354-361.
- ¹⁰⁰ Leach, Neil, ed. *Space architecture: The new frontier for design research*. John Wiley & Sons, 2014.
- ¹⁰¹ Jordan, Nicole C., Joseph H. Saleh, and Dava J. Newman. "The extravehicular mobility unit: A review of environment, requirements, and design changes in the US spacesuit." *Acta Astronautica* 59, no. 12 (2006): 1135-1145.
- ¹⁰² Newman, Dava, Jeff Hoffman, Kristen Bethke, Joaquin Blaya, Christopher Carr, and Bradley Pitts. "Astronaut bio-suit system for exploration class missions." NIAC Phase II Final Report (2005).
- ¹⁰³ Newman, Dava J., Marita Canina, and Guillermo L. Trotti. "Revolutionary Design for Astronaut Exploration—Beyond the Bio-Suit System." In *AIP Conference Proceedings*, vol. 880, no. 1, pp. 975-986. American Institute of Physics, 2007.
- ¹⁰⁴ C Paige, DJ Newman, SJH Lombrado. An Integrated Innovative 3D Radiation Protection Fabric for Advanced Spacesuits and Systems. *IEEE Aerospace Conference*, 2020.
- ¹⁰⁵ Cherston, Juliana, David Veysset, Yuchen Sun, Hajime Yano, Keith A. Nelson, Shobha Murari, and Joseph A. Paradiso. "Large-area electronic skins in space: vision and preflight characterization for first aerospace piezoelectric e-textile." In *Sensors and Smart Structures Technologies for Civil, Mechanical, and Aerospace Systems 2020*, vol. 11379, p. 113791Q. International Society for Optics and Photonics, 2020.

-
- ¹⁰⁶ Bannova, Olga. "Terrestrial Analog Selection Considerations for Planetary Surface Facility Planning and Operations." *Lunar Settlements* (2010): 375-386.
- ¹⁰⁷ Lim, Darlene SS, Andrew FJ Abercromby, Shannon E. Kobs Nawotniak, David S. Lees, Michael J. Miller, Allyson L. Brady, Matthew J. Miller et al. "The BASALT research program: designing and developing mission elements in support of human scientific exploration of Mars." *Astrobiology* 19, no. 3 (2019): 245-259.
- ¹⁰⁸ Guillermo Trotti, Trotti & Associates, Inc., Extreme eXPeditionary Architecture: Mobile, Adaptable Systems for Space and Earth Exploration. NASA NIAC, 2009.
- ¹⁰⁹ Siddiqi, Asif A. "The Almaz Space Station Complex-A History, 1964-1992 Part 1 1964-1976." *Journal of the British Interplanetary Society* 54 (2001): 389-416.
- ¹¹⁰ Harvey, Brian. "China in space: The great leap forward." Springer Science & Business Media, 2013.
- ¹¹¹ Compton, William David, Charles D. Benson, and Paul Dickson. "Living and Working in Space: A NASA history of Skylab." Courier Corporation, 2011.
- ¹¹² Morgan, Clay. "Shuttle-Mir: The United States and Russia Share History's Highest Stage." (2001).
- ¹¹³ [Stanford Torus] Space Settlement: A Design Study. NASA report, 1975. Available: https://settlement.arc.nasa.gov/75SummerStudy/Table_of_Contents1.html
- ¹¹⁴ O'Neill, Gerard K. "The High Frontier: Human Colonies in Space", third edition. Apogee Books, 2000.
- ¹¹⁵ Orion Spacecraft. NASA. [Online] Accessed 30 July 2010. Available: <https://www.nasa.gov/exploration/systems/orion/index.html>
- ¹¹⁶ Smith, Eric, and Harold J. Morowitz. "The origin and nature of life on earth: the emergence of the fourth geosphere." Cambridge University Press, 2016.
- ¹¹⁷ Mandelbrot, Benoit B., and Michael Frame. "Fractals." *Encyclopedia of physical science and technology* 5 (1987): 579-593.
- ¹¹⁸ "About Ise Jingu." Ise Jingu. [Online] Accessed 5 August 2020. Available: <https://www.isejingu.or.jp/en/about/index.html>
- ¹¹⁹ Ekblaw, Ariel, Anastasia Prosina, Dava Newman, and Joseph Paradiso. "Space Habitat Reconfigurability: TESSERA platform for self-aware assembly." 30th IAA SYMPOSIUM ON SPACE AND SOCIETY (Space Architecture: Habitats, Habitability, and Bases). *Proceedings of the IAF International Astronautical Congress* 2019.
- ¹²⁰ Sancar, Aziz. "Mechanisms of DNA excision repair." *Science* 266, no. 5193 (1994): 1954.
- ¹²¹ International Space Station Transition Report. NASA. 2018 [Online] Accessed 5 August 2020. Available: https://www.nasa.gov/sites/default/files/atoms/files/iss_transition_report_180330.pdf
- ¹²² "Indeterminate Growth." Merriam-Webster. [Online] Accessed 25 July 2020. Available: <https://www.merriam-webster.com/dictionary/indeterminate%20growth>
- ¹²³ Saleh, Joseph H., Daniel E. Hastings, and Dava J. Newman. "Spacecraft design lifetime." *Journal of Spacecraft and Rockets* 39, no. 2 (2002): 244-257.
- ¹²⁴ Jeremijenko, Natalie. "Tree Logic." Mass MOCA Exhibition. [Online] Accessed 5 August 2020. Available: <https://massmoca.org/event/natalie-jeremijenko/>

-
- ¹²⁵ Rian, Iasef Md, and Mario Sassone. "Tree-inspired dendriforms and fractal-like branching structures in architecture: A brief historical overview." *Frontiers of Architectural Research* 3, no. 3 (2014): 298-323.
- ¹²⁶ Johansen, John M. *Nanoarchitecture: a new species of architecture*. Princeton Architectural Press, 2002.
- ¹²⁷ Pearce, Peter. *Structure in Nature is a Strategy for Design*. MIT press, 1990.
- ¹²⁸ Seidel, Ronald, Michael Blumer, Paul Zaslansky, David Knötel, Daniel R. Huber, James C. Weaver, Peter Fratzl, Sidney Omelon, Luca Bertinetti, and Mason N. Dean. "Ultrastructural, material and crystallographic description of endophytic masses—A possible damage response in shark and ray tessellated calcified cartilage." *Journal of Structural Biology* 198, no. 1 (2017): 5-18.
- ¹²⁹ Latour, Bruno. "Why has critique run out of steam? From matters of fact to matters of concern." *Critical inquiry* 30, no. 2 (2004): 225-248. Available: <http://www.bruno-latour.fr/sites/default/files/89-CRITICAL-INQUIRY-GB.pdf>
- ¹³⁰ Lissauer, Jack J. "Timescales for planetary accretion and the structure of the protoplanetary disk." *Icarus* 69, no. 2 (1987): 249-265.
- ¹³¹ Sulleyman, Aatif. "World's First Fully Rotational Skyscraper Allows Residents To Control How Much Their Apartments Spin." Independent UK. [Online] Accessed 5 August 2020. Available: <https://www.independent.co.uk/life-style/gadgets-and-tech/news/dubai-rotating-skyscraper-dynamic-tower-hotel-building-a7585981.html>
- ¹³² "A Superconducting Shield to Protect Astronauts." CERN. [Online] Accessed 5 August 2020. Available: <http://cds.cern.ch/journal/CERNBulletin/2015/32/News%20Articles/2038160?ln=en>
- ¹³³ "Principles of Awareness". MIT Media Lab Course 2017, 2018, 2019. [Online] Accessed 5 August 2020. Available: <https://www.media.mit.edu/courses/awareness-2017/> OR <https://awareness.pubpub.org/>
- ¹³⁴ Johnson, Holbrow (1977). "Space Settlements: A Design Study". National Aeronautics and Space Administration.
- ¹³⁵ Benford, Gregory, and Arthur C. Clarke. *Beyond the Fall of Night*. New York: Putnam (1990).
- ¹³⁶ Marcus Vitruvius Pollio. *The Ten Books of Architecture* (Book 1, Chapter 3). The translated terminology "commodity, firmness and delight" is by Henry Wooten in his 1624 Principles of Architecture.
- ¹³⁷ Sushida, Takamichi, and Yoshikazu Yamagishi. "Geometrical study of phyllotactic patterns by Bernoulli spiral lattices." *Development, Growth & Differentiation* 59, no. 5 (2017): 379-387.
- ¹³⁸ Coldea, Radu, D. A. Tennant, E. M. Wheeler, E. Wawrzynska, D. Prabhakaran, M. Telling, K. Habicht, P. Smeibidl, and K. Kiefer. "Quantum criticality in an Ising chain: experimental evidence for emergent E8 symmetry." *Science* 327, no. 5962 (2010): 177-180.
- ¹³⁹ Pacioli, Luca. *Divina Proportione*. Milan, 1498.
- ¹⁴⁰ Weyl, Hermann. *Symmetry*. Princeton, 1952
- ¹⁴¹ Haeckel, Ernst, *Kunstformen der Natur*, 1904. Dover reprint as Artforms in Nature, 1974.
- ¹⁴² Łukowiak, Magdalena. "Late Eocene siliceous sponge fauna of southern Australia: reconstruction based on loose spicules record." *Zootaxa* 3917, no. 1 (2015): 1-65.

-
- ¹⁴³ “The Beautiful Wonders of Persian Architecture from 5 Cities in Iran. [Online]. Accessed 25 July 2020. Available: <https://www.arch2o.com/beautiful-wonders-persian-architecture-5-cities-iran/>
- ¹⁴⁴ Evans, Dylan W., David John Roberts, and David Neville Thomas. *Ernst Haeckel: Art Forms from the Abyss: Images from the HMS Challenger Expedition*. Prestel, 2015.
- ¹⁴⁵ Solar Egg/ Bigert and Bogström. Arch Daily. 2017. [Online] Accessed 5 August 2020. Available: <https://www.archdaily.com/881832/solar-egg-bigert-and-bergstrom>
- ¹⁴⁶ Ekblaw, Ariel, and Joseph Paradiso. "Self-Assembling Space Structures: Buckminsterfullerene Sensor Nodes." In *2018 ALAA SciTech/AHS Adaptive Structures Conference*, (p. 0565). 2018.
- ¹⁴⁷ Ekblaw, Ariel, and Joseph Paradiso. "TESSERAE: Self-Assembling Shell Structures for Space Exploration." In *Proceedings of the Annual Symposium of the International Association of Shell and Spatial Structures (IASS): Extraplanetary Architecture*, p. 317. 2018.
- ¹⁴⁸ Ekblaw, Ariel, and Joseph Paradiso., "Self-assembling Space Architecture: tessellated shell structures for space habitats," In *ALAA Scitech 2019 Forum, Smart/Adaptable Deployable Structures*, (p. 0481). 2019.
- ¹⁴⁹ Ekblaw, Ariel, and Joseph Paradiso. "Self-Assembling Space Habitats: TESSERAE design and mission architecture." In *2019 IEEE Aerospace Conference*, pp. 1-11. IEEE, 2019.
- ¹⁵⁰ Montreal Biosphere, Environment Museum. Parc Jean-Drapeau. [Online] Accessed 5 August 2020. Available: <https://www.parcjeandrapeau.com/en/biosphere-environment-museum-montreal/>
- ¹⁵¹ Epcot Spaceship Earth. Disney. [Online] Accessed 5 August 2020. Available: <https://disneyworld.disney.go.com/destinations/epcot/>
- ¹⁵² IXOLAR High Efficiency SolarBIT. IXYS. [Online] Accessed 25 May 2017. Available: http://ixapps.ixys.com/DataSheet/KXOB22-01X8F__Nov16.pdf
- ¹⁵³ Technical Documents: Ultra Low Power Harvester Power Management IC with Boost Charger, and Nanopower Buck Converter. Texas Instruments. [Online] Accessed 25 May 2017. Available: <http://www.ti.com/product/BQ25570/technicaldocuments>
- ¹⁵⁴ Adopted Specifications. Bluetooth Special Interest Group. [Online] Accessed 25 May 2017. Available: <https://www.bluetooth.com/specifications/adopted-specifications>
- ¹⁵⁵ Evans, Lawrence. An Introduction to Mathematical Optimal Control Theory Version 0.2. UC Berkeley Course. [Online] Accessed 5 August 2020. Available: <https://math.berkeley.edu/~evans/control.course.pdf>
- ¹⁵⁶ Reference Guide to the International Space Station: International Standard Payload Rack. NASA. [Online] Accessed 5 August 2020. Available: https://www.nasa.gov/sites/default/files/atoms/files/np-2015-05-022-jsc_iss_utilization_guide_2015-508c.pdf
- ¹⁵⁷ Coronavirus (COVID-19). CDC. [Online] Accessed 5 August 2020. Available: <https://www.cdc.gov/coronavirus/2019-ncov/index.html>
- ¹⁵⁸ “Polymagnets.” Correlated Magnetics. [Online] Accessed 5 August 2020. Available: <https://www.cdc.gov/coronavirus/2019-ncov/index.html>
- ¹⁵⁹ Bishop Airlock. NanoRacks. [Online] Accessed 5 August 2020. Available: <https://nanoracks.com/bishop-airlock/>

-
- ¹⁶⁰ TILE: Tile Ionic Liquid Electrospray. Acciom. [Online] Accessed 5 August 2020. Available: <https://www.accion-systems.com/tile>
- ¹⁶¹ Blanquer, Sébastien BG, Maïke Werner, Markus Hannula, Shahriar Sharifi, Guillaume PR Lajoïnie, David Eglin, Jari Hyttinen, André A. Poot, and Dirk W. Grijpma. "Surface curvature in triply-periodic minimal surface architectures as a distinct design parameter in preparing advanced tissue engineering scaffolds." *Biofabrication* 9, no. 2 (2017): 025001.
- ¹⁶² Blob Wall. Greg Lynn. [Online] Accessed 5 August 2020. Available: <https://inhabitat.com/blobwall-the-brick-reinterpreted/>
- ¹⁶³ Space Collective. Julia Korner. [Online] Accessed 5 August 2020. Available: <https://www.juliakoerner.com/architecture-space-collective>
- ¹⁶⁴ "WeBots." Cyberbotics. [Online] Accessed 10 August 2020. Available: <https://www.cyberbotics.com/>
- ¹⁶⁵ "Unity Real Time Development Platform." Unity. [Online] Accessed 10 August 2020. Available: <https://unity.com/>
- ¹⁶⁶ "Simulink Simulation and Model-Based Design." MathWorks. [Online] Accessed 10 August 2020. Available: <https://www.mathworks.com/products/simulink.html>
- ¹⁶⁷ Drumwright, Evan, John Hsu, Nathan Koenig, and Dylan Shell. "Extending open dynamics engine for robotics simulation." In *International Conference on Simulation, Modeling, and Programming for Autonomous Robots*, pp. 38-50. Springer, Berlin, Heidelberg, 2010.
- ¹⁶⁸ "International Geomagnetic Reference Field." IAGA Division V-MOD. [Online] Accessed 11 August 2020. Available: <https://www.ngdc.noaa.gov/IAGA/vmod/igrf.html>
- ¹⁶⁹ "How Powerful is the Magnetic Field of the Earth in Space?" NASA. [Online] Accessed 11 August 2020. Available: <https://image.gsfc.nasa.gov/poetry/ask/a10015.html>
- ¹⁷⁰ Synchronous versus Asynchronous Controllers. Cyberbotics. [Online] Accessed 11 August 2020. Available: <https://cyberbotics.com/doc/reference/robot#synchronous-versus-asynchronous-controllers>
- ¹⁷¹ "Generative Design." AUTODESK. [Online] Accessed 12 August 2020. Available: <https://www.autodesk.com/solutions/generative-design>
- ¹⁷² Matejka, Justin, Michael Glueck, Erin Bradner, Ali Hashemi, Tovi Grossman, and George Fitzmaurice. "Dream lens: Exploration and visualization of large-scale generative design datasets." In *Proceedings of the 2018 CHI Conference on Human Factors in Computing Systems*, pp. 1-12. 2018.
- ¹⁷³ "Generative Design at the Intersection of Art, Science and Technology." Deskriptiv. [Online] Accessed 12 August 2020. Available: <https://deskriptiv.com/>
- ¹⁷⁴ Jones, Harry. "The Recent Large Reduction in Space Launch Cost." 48th *International Conference on Environmental Systems*, 2018.
- ¹⁷⁵ 2018 Global Space Technology. Bryce Space and Technology. [Online] Accessed 5 August 2020. Available: https://brycotech.com/downloads/2018_Global_Space_Economy.pdf
- ¹⁷⁶ NextSTEP-2 Appendix I: Commercial Destination Development in Low Earth Orbit using the International Space Station. NASA. [Online] Accessed 5 August 2020. Available:

https://www.fbo.gov/index?s=opportunity&mode=form&tab=core&id=86d28a489edcc585145a0e0da2caadc&_cview=0

¹⁷⁷ NASA Selects First Commercial Moon Landing Services for Artemis Program. NASA. May 31 2019. [Online] Accessed 5 August 2020. Available: <https://www.nasa.gov/press-release/nasa-selects-first-commercial-moon-landing-services-for-artemis-program>

¹⁷⁸ "Reusability: The Key to Making Human Life Multi-Planetary," and "Falcon 9 Heavy" SpaceX, 2015. [Online] Available: <http://www.spacex.com/news/2013/03/31/reusability-key-making-human-life-multi-planetary> and <http://www.spacex.com/falcon-heavy> [Accessed: Accessed 26 April 2018].

¹⁷⁹ NASA's Plan for Sustained Lunar Exploration and Development. April 2020. [Online] Accessed 5 August 2020. Available: https://www.nasa.gov/sites/default/files/atoms/files/a_sustained_lunar_presence_nspc_report4220final.pdf

¹⁸⁰ "NASA Strategic Plan 2018." NASA. [Online] Accessed 11 November 2018. Available: https://www.nasa.gov/sites/default/files/atoms/files/nasa_2018_strategic_plan.pdf

¹⁸¹ "NASA's Lunar Outpost will Extend Human Presence in Deep Space." NASA. [Online] Accessed 11 November 2018. Available: <https://www.nasa.gov/feature/nasa-s-lunar-outpost-will-extend-human-presence-in-deep-space>

¹⁸² Minovitch, Michael A. *Inflatable core orbital construction method and space station*. U.S. Patent 4,730,797, issued March 15, 1988.

¹⁸³ Howard, N. and Nguyen, H.D., National Aeronautics and Space Administration (NASA), 2010. *Magnetic capture docking mechanism*. U.S. Patent 7,815,149.

¹⁸⁴ Jing Pei, Luke Murchison, Victor Stewart, James Rosenthal, Drew Sellers, Mark Banchy, Adam BenShabat, Ryan Elandt, David Elliott, and Adam K. Weber. "Autonomous Rendezvous and Docking of Two 3U Cubesats Using a Novel Permanent-Magnet Docking Mechanism", *54th AIAA Aerospace Sciences Meeting, AIAA SciTech Forum*, (AIAA 2016-1465).

¹⁸⁵ Kong, Edmund Mun Choong. "Spacecraft formation flight exploiting potential fields." PhD diss., Massachusetts Institute of Technology, 2002.

¹⁸⁶ Gettliffe, Gwendolyn Vines. "Stability analysis of electromagnetically supported large space structures." PhD diss., Massachusetts Institute of Technology, 2015.

¹⁸⁷ Garcia, Mark. "Beam Expanded to Full Size." NASA Space Station Blog, May 28, 2016. [Online] Accessed 10 October 2018. Available: <https://blogs.nasa.gov/spacestation/2016/05/28/beam-expanded-to-full-size/>

¹⁸⁸ Ashby, Michael F. "Overview No. 80: On the engineering properties of materials." *Acta metallurgica* 37, no. 5 (1989): 1273-1293.

¹⁸⁹ Falcon Heavy. SpaceX. [Online] Accessed 5 August 2020. Available: <https://www.spacex.com/vehicles/falcon-heavy/>

¹⁹⁰ Falcon Heavy. SpaceX. [Online] Accessed 5 August 2020. Available: <https://www.spacex.com/vehicles/starship/>

¹⁹¹ New Glenn. Blue Origin. [Online] Accessed 5 August 2020. Available: <https://www.blueorigin.com/new-glenn/>

-
- ¹⁹² Space Launch System. NASA. [Online] Accessed 5 August 2020. Available: <https://www.nasa.gov/exploration/systems/sls/index.html>
- ¹⁹³ Protecting the space station from meteoroids and orbital debris. National Research Council (US). Committee on International Space Station Meteoroid/Debris Risk Management. *National Academies Press*, 1997.
- ¹⁹⁴ "Facts and Figures: Space Station at Completion," NASA, [Online] Accessed 26 April 2018. Available: <https://www.nasa.gov/feature/facts-and-figures>
- ¹⁹⁵ Lin, Zhongjie. *Kenzo Tange and the Metabolist movement: urban utopias of modern Japan*. Routledge, 2010.
- ¹⁹⁶ Howe, A. Scott, Raul Polit-Casillas, David L. Akin, Katherine McBryan, and Christopher Carlsen. "Random Access Frame (RAF) System Neutral Buoyancy Evaluations." 45th *International Conference on Environmental Systems*, 2015.
- ¹⁹⁷ Jet Propulsion Laboratory Vision. JPL. [Online] Accessed 5 August 2020. Available: <https://www.jpl.nasa.gov/about/strategic-implementation-plan/vision/>
- ¹⁹⁸ Figueroa, Fernando, Mark Walker, and Lauren W. Underwood. "NASA Platform for Autonomous Systems (NPAS)." In *ALAA Scitech 2019 Forum*, p. 1963. 2019. Accessed 17 May 2020. Available online: <https://ntrs.nasa.gov/search.jsp?R=20180007990>
- ¹⁹⁹ Abdel-Rahman, Amira, Aaron T. Becker, Daniel E. Biediger, Kenneth C. Cheung, Sándor P. Fekete, Neil A. Gershenfeld, Sabrina Hugo et al. "Space Ants: Constructing and Reconfiguring Large-Scale Structures with Finite Automata (Media Exposition)." In *36th International Symposium on Computational Geometry (SoCG 2020)*. Schloss Dagstuhl-Leibniz-Zentrum für Informatik, 2020.
- ²⁰⁰ Saleh, Joseph H., Elisabeth S. Lamassoure, Daniel E. Hastings, and Dava J. Newman. "Flexibility and the value of on-orbit servicing: New customer-centric perspective." *Journal of Spacecraft and Rockets* 40, no. 2 (2003): 279-291.
- ²⁰¹ "Working Toward an Autonomous Future Starts Now for NASA, Partners." NASA, April 2020. Accessed 17 May 2020. Available Online: <https://www.nasa.gov/offices/oct/working-toward-an-autonomous-future-starts-now-for-nasa-partners.html>
- ²⁰² Dementyev, Artem. "Dynamic wearable technology: designing and deploying small climbing robots for sensing and actuation on the human body." PhD diss., Massachusetts Institute of Technology, 2019.
- ²⁰³ Destefanis, R., E. Amerio, M. Briccarello, M. Belluco, M. Faraud, E. Tracino, and C. Lobascio. "Space environment characterisation of Kevlar®: good for bullets, debris and radiation too." *Universal Journal of Aeronautical & Aerospace Sciences* 2 (2014): 80-113.
- ²⁰⁴ "Mars." SpaceX. [Online] Accessed 10 October 2018. Available: <https://www.spacex.com/mars>
- ²⁰⁵ McLaughlin, Richard J., and William H. Warr. The Common Berthing Mechanism (CBM) for International Space Station. No. 2001-01-2435. *SAE Technical Paper*, 2001.
- ²⁰⁶ "Swivel and Pull Clamps," Roemheld, [Online] Accessed 26 April 2018. Available: https://www.roemheld-gruppe.de/shop/en/5-2640-swivel-and-pull-clamps.html?contact=product_all
- ²⁰⁷ "About the Space Station Solar Arrays." NASA. [Online] Accessed 10 October 2018. Available: https://www.nasa.gov/mission_pages/station/structure/elements/solar_arrays-about.html

-
- ²⁰⁸ Kraemer, Daniel, Bed Poudel, Hsien-Ping Feng, J. Christopher Caylor, Bo Yu, Xiao Yan, Yi Ma et al. "High-performance flat-panel solar thermoelectric generators with high thermal concentration." *Nature materials* 10, no. 7 (2011): 532.
- ²⁰⁹ Permanent Electromagnets." Magma Magnets. [Online] Accessed 10 October 2018. Available: <http://www.magmamagnets.com/electromagnets-solenoids/permanent-electromagnets/>
- ²¹⁰ Permanent Electromagnets." APW. [Online] Accessed 10 October 2018. Available: <https://apwelectromagnets.com/files/attachments/505/EML63mm-xx.pdf>
- ²¹¹ Ward, Peter, and Dikai Liu. "Design of a high capacity electro permanent magnetic adhesion for climbing robots." In *Robotics and Biomimetics (ROBIO), 2012 IEEE International Conference on*, pp. 217-222. IEEE, 2012.
- ²¹² "Space Shuttle Orbital Docking System." NASA. [Online] Accessed 10 October 2018. Available: https://www.nasa.gov/pdf/593865main_AP_ST_Phys_ShuttleODS.pdf
- ²¹³ "Columbus Fact Sheet: European research laboratory." ESA. [Online] Accessed 10 October 2018. Available: <http://wsn.spaceflight.esa.int/docs/Factsheets/2%20Columbus%20LR.pdf>
- ²¹⁴ Destiny Laboratory." NASA [Online] Accessed 10 October 2018. Available: https://www.nasa.gov/mission_pages/station/structure/elements/destiny.html
- ²¹⁵ "Bigelow Expandable Activities Module (BEAM)," Bigelow Aerospace and NASA, [Online] Accessed 10 October 2018. Available: <https://www.nasa.gov/content/bigelow-expandable-activity-module>.
- ²¹⁶ Hoberman, Charles. "Reversibly expandable doubly-curved truss structure." U.S. Patent 4,942,700, issued July 24, 1990.
- ²¹⁷ Overvelde, Johannes TB, Twan A. De Jong, Yanina Shevchenko, Sergio A. Becerra, George M. Whitesides, James C. Weaver, Chuck Hoberman, and Katia Bertoldi. "A three-dimensional actuated origami-inspired transformable metamaterial with multiple degrees of freedom." *Nature communications* 7 (2016): 10929.
- ²¹⁸ "Create a Torus with a Hexagonal Mesh for 3D-printing." Mathematica Stack Exchange. [Online] Accessed December 9, 2018. Available: <https://mathematica.stackexchange.com/questions/39879/create-a-torus-with-a-hexagonal-mesh-for-3d-printing>
- ²¹⁹ Sullivan, John M. "Conformal tiling on a torus." *Proc. Bridges, Coimbra* (2011): 593-596.
- ²²⁰ Lueders, Kathryn L. "ISS Crew Transportation and Services Requirements Document." (2015). Available: <https://ntrs.nasa.gov/citations/20170001943>
- ²²¹ International Space Station Flight Systems. NASA. [Online] Accessed 5 August 2020. Available: https://www.nasa.gov/pdf/167129main_Systems.pdf
- ²²² Larson, Wiley J., and James Richard Wertz. *Space mission analysis and design* [Select Chapters]. No. DOE/NE/32145--T1. Microcosm, Inc., Torrance, CA (US), 1992.
- ²²³ Slough, John. "Spacecraft Scale Magnetospheric Protection from Galactic Cosmic Radiation." NASA. [Online] Accessed 5 August 2020. Available: https://www.nasa.gov/directorates/spacetech/niac/2018_Phase_I_Phase_II/Spacecraft_Scale_Magnetospheric_Protection_from_Galactic_Cosmic_Radiation/
- ²²⁴ Davies, Francis, et al. "Magnet Architectures and Active Radiation Shielding Study (MAARSS) Final Report for NASA Innovative Advanced Concepts Phase II." NASA. [Online] Accessed 5 August 2020.

Available: https://www.nasa.gov/sites/default/files/atoms/files/niac_2012_phaseii_westover_radiationprotectionandarchitecture_tagged.pdf

²²⁵ “Electromagnetic Fields: EMF”. World Health Organization. [Online] Accessed 5 August 2020. Available: <https://www.who.int/peh-emf/publications/facts/fs299/en/#:~:text=For%20occupational%20exposure%2C%20present%20limits,ceiling%20value%20of%202%20T>.

²²⁶ ESA’s Room with a View. ESA. [Online] Accessed 5 August 2020. Available: http://www.esa.int/esapub/bulletin/bulletin137/bul137h_deloo.pdf

²²⁷ Baily, S., Nelson, R. R., and Stewart, W. B., “Interface Standards for Spacecraft As a Means of Enhancing On-Orbit Servicing,” *Proceedings of the 18th Annual Electronics and Aerospace Systems Conference, Piscataway, New Jersey*, 1985, pp. 351–355.

²²⁸ Harwood, O. P. and Ridenoure, R. W., “A Universal Orbital Docking and Berthing System,” *The Case for Mars IV: The International Exploration of Mars, Mission Strategy and Architectures*, edited by T. R. Meyer, Vol. 89, *American Astronautical Society*, San Diego, California, 1990, pp. 613–630.

²²⁹ Abbott, R. and Aceves, M., “Self-engaging Connector System for Robotic Outposts and Reconfigurable Spacecraft,” *Proceedings of the 2002 IEEE Aerospace Conference*, Vol. 5, Piscataway, New Jersey, 2002, pp. 2165–2170.

²³⁰ MIT Engineering Systems Laboratory. Department of Aeronautics and Astronautics. <https://systems.mit.edu/>

²³¹ Lucas, George, Rodolfo Damaggio, and Al Williamson. *Star Wars, episode I: The phantom menace*. Dark Horse Comics, 1999.

²³² “NASA Strategic Space Technology Investment Plan.” NASA. August 2017. [Online] Accessed 23 November 2017. https://www.nasa.gov/sites/default/files/atoms/files/2017-8-1_stip_final-508ed.pdf

²³³ “Working Toward an Autonomous Future Starts Now for NASA, Partners.” NASA, April 2020. Accessed 17 May 2020. Available Online: <https://www.nasa.gov/offices/oct/working-toward-an-autonomous-future-starts-now-for-nasa-partners.html>

²³⁴ James Webb Space Telescope. NASA. [Online] Accessed 5 August 2020. Available: <https://www.jwst.nasa.gov/>

²³⁵ SkyLab 2: First Repair Spacewalk. NASA [Online] Accessed 5 August 2020. Available: <https://www.nasa.gov/feature/skylab-2-first-repair-spacewalk>

²³⁶ Hubble’s Mirror Flaw. NASA [Online] Accessed 5 August 2020. Available: <https://www.nasa.gov/content/hubbles-mirror-flaw>

²³⁷ Jenett, Benjamin, Christine Gregg, Daniel Cellucci, and Kenneth Cheung. "Design of multifunctional hierarchical space structures." In *Aerospace Conference*, 2017 IEEE, pp. 1-10. IEEE, 2017.

²³⁸ ESO’s Extremely Large Telescope. ESO. [Online] Accessed 5 August 2020. Available: <https://www.eso.org/public/usa/teles-instr/elt/>

²³⁹ Lee, Nicolas N., Joel W. Burdick, Paul Backes, Sergio Pellegrino, Kristina Hogstrom, Christine Fuller, Brett Kennedy et al. "Architecture for in-space robotic assembly of a modular space telescope." *Journal of Astronomical Telescopes, Instruments, and Systems* 2, no. 4 (2016): 041207.

-
- ²⁴⁰ Laird, Phil R., Rosangela Bergamasco, Vincent Bérubé, Ermanno F. Borra, Julie Gingras, Anna-Marie R. Ritcey, Myriam Rioux et al. "Ferrofluid-based deformable mirrors: a new approach to adaptive optics using liquid mirrors." In *Adaptive Optical System Technologies II*, vol. 4839, pp. 733-740. International Society for Optics and Photonics, 2003.
- ²⁴¹ Laird, Philip, Nicolas Caron, Myriam Rioux, Ermanno F. Borra, and A. Ritcey. "Ferrofluidic adaptive mirrors." *Applied optics* 45, no. 15 (2006): 3495-3500.
- ²⁴² Brousseau, D., Borra, E.F. and Thibault, S., 2007. Wavefront correction with a 37-actuator ferrofluid deformable mirror. *Optics express*, 15(26), pp.18190-18199.
- ²⁴³ OneWeb. [Online] Accessed 5 August 2020. Available: <https://www.oneweb.world/>
- ²⁴⁴ "Starlink Microsat Experiment Purposes". FCC. [Online] Accessed 5 August 2020. Available: <https://apps.fcc.gov/els/GetAtt.html?id=185534>.
- ²⁴⁵ Planet Labs. [Online] Accessed 5 August 2020. Available: <https://www.planet.com/>
- ²⁴⁶ BlackJack Program. DARPA. [Online] Accessed 5 August 2020. Available: <https://www.darpa.mil/program/blackjack>
- ²⁴⁷ Loft Orbital. [Online] Accessed 5 August 2020. Available: <https://www.loftorbital.com/>
- ²⁴⁸ Open Cosmos. [Online] Accessed 5 August 2020. Available: <https://www.open-cosmos.com/>
- ²⁴⁹ Yoo, Making Space Simple. Apogeo Spatial (blog). 18 August 2018. [Online] Available: <http://apogeospacial.com/making-space-simple/>
- ²⁵⁰ Ekblaw, Ariel, Raghav Chawla, Mehak Sarang, Griffin Cleverly and Joseph Paradiso. "BlockSat: On-Demand Access to Shared-Use Satellite Constellations." 26th IAA SYMPOSIUM ON SMALL SATELLITE MISSIONS (Small Satellite Operations). Proceedings of the IAF International Astronautical Congress 2019.
- ²⁵¹ NASA's Dragonfly Project Demonstrates Robotic Satellite Assembly Critical to Future Space Infrastructure Development. NASA. 13 September 2017. [Online] Available: https://www.nasa.gov/mission_pages/tdm/irma/nasas-dragonfly-project-demonstrates-robotic-satellite-assembly-critical-to-future-space.html
- ²⁵² Archinaut. Made in Space. [Online] Accessed 5 August 2020. Available: <https://madeinspace.us/capabilities-and-technology/archinaut/>
- ²⁵³ Advanced Manufacturing Facility. Made in Space. [Online] Accessed 5 August 2020. Available: <https://madeinspace.us/capabilities-and-technology/additive-manufacturing-facility/>
- ²⁵⁴ Vulcan. Made in Space. [Online] Accessed 5 August 2020. Available: <https://madeinspace.us/capabilities-and-technology/vulcan/>
- ²⁵⁵ Snyder, Michael, Jason Dunn, and Eddie Gonzalez. "The effects of microgravity on extrusion based additive manufacturing." In *ALAA SPACE 2013 Conference and Exposition*, p. 5439. 2013.
- ²⁵⁶ Erik D. Demaine, Sándor Fekete, Christian Scheffer, and Arne Schmidt, "New Geometric Algorithms for Fully Connected Staged Self-Assembly", *Theoretical Computer Science*, volume 671, April 2017, pages 4–18.
- ²⁵⁷ Erik D. Demaine, Sarah Eisenstat, Mashhood Ishaque, and Andrew Winslow, "One-Dimensional Staged Self-Assembly", *Natural Computing*, volume 12, number 2, 2013, pages 247–258.